SENSITIVITY STUDIES ON A LIMITED
AREA MESOSCALE MODEL: AN EXAMINATION
OF LATERAL BOUNDARY PLACEMENT,
GRID RESOLUTION AND NESTING TYPE

THESIS

Robert A. Stenger, Captain, USAF

AFIT/GM/ENP/00M-13

DEPARTMENT OF THE AIR FORCE
AIR UNIVERSITY

AIR FORCE INSTITUTE OF TECHNOLOGY

Wright-Patterson Air Force Base, Ohio

AFIT/GM/ENP/00M-13

SENSITIVITY STUDIES ON A LIMITED
AREA MESOSCALE MODEL: AN EXAMINATION
OF LATERAL BOUNDARY PLACEMENT,
GRID RESOLUTION AND NESTING TYPE

THESIS
Robert A. Stenger
Captain, USAF

AFIT/GM/ENP/00M-13

20001113 024

The views expressed in this thesis are those of the author and do not reflect the official policy or position of the Department of Defense or the United States Government.

SENSITIVITY STUDIES ON A LIMITED AREA MESOSCALE MODEL: AN EXAMINATION OF LATERAL BOUNDARY PLACEMENT, GRID RESOLUTION AND NESTING TYPE

THESIS

Presented to the Faculty

Department of Engineering Physics

Graduate School of Engineering and Management

Air Force Institute of Technology

Air University

Air Education and Training Command

In Partial Fulfillment of the Requirements for the

Degree of Master of Science in Meteorology

Robert A. Stenger, B.S.
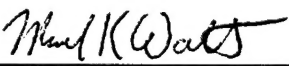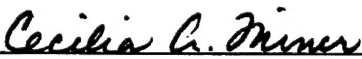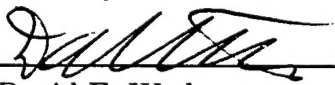
Captain, USAF

March 2000

AFIT/GM/ENP/00M-13

SENSITIVITY STUDIES ON A LIMITED AREA MESOSCALE MODEL: AN EXAMINATION OF LATERAL BOUNDARY PLACEMENT, GRID RESOLUTION AND NESTING TYPE

Robert A. Stenger, B.S.

Captain, USAF

Approved:

_____   3 MAR 2000
Michael K. Walters   Date
Advisory Committee Chairman

_____   3 March 2000
Cecilia A. Miner   Date
Advisory Committee Member

_____   3 Mar 2000
David E. Weeks   Date
Advisory Committee Member

Table of Contents

List of Figures

List of Tables

AFIT/GM/ENP/00M-13

Abstract

With the advances of computer technology in recent years, limited area meso-scale models are being used to produce operational forecasts on a broader scale worldwide than ever before. The past limitations of computational resources have caused previous research efforts to focus more on model physics, thus creating a gap in the number of sensitivity studies conducted on these models. This research is intended to bridge a gap in the apparent paucity of sensitivity studies on the limited area model (LAM). The Pennsylvania State University/National Center for Atmospheric Research Mesoscale Model 5 was utilized to conduct sensitivity studies on lateral boundary placement in regions of strong topography, grid resolution and nesting type. This research has resulted in three significant findings: (1) optimally placing the windward lateral boundary of a LAM with respect to the tallest peaks of a strong orography increases the model's forecast veracity; (2) the paradigm that finer grid resolutions will always produce better forecasts is flawed when there is an absence of strong ageostrophic motions in the troposphere; and (3) two-way nesting will generally produce a more accurate forecast than one-way nesting when significant ageostrophic motions are present in the troposphere.

SENSITIVITY STUDIES ON A LIMITED AREA MESOSCALE MODEL: AN EXAMINATION OF LATERAL BOUNDARY PLACEMENT, GRID RESOLUTION AND NESTING TYPE

I. Introduction

1.1 Motivation

Advances in computer technology over the past two decades have made the use of limited area models (LAMs) increasingly attractive to government, commercial, and educational institutions for both research and operational applications (21: Warner et al. 1997). Unlike its predecessor, the global model, the LAM requires the specification of spatial boundary conditions prior to the time-stepped integration of the model; therefore, the boundary conditions in a LAM are usually obtained from a global model or by data analysis. In general, boundary conditions are defined on the outermost grid points of the model's three-dimensional domain. There are three types of boundaries: the bottom or terrain boundary, the top boundary, and the lateral boundaries (14, 21: Pielke 1984; Warner et al. 1997). Unlike the prescribed and somewhat well-behaved bottom and top boundaries, the lateral boundary conditions (LBCs) are not well behaved and may vary greatly in spatial and temporal aspects (21: Warner et al. 1997). The lateral boundaries are composed of a locus of horizontal grid points along the outermost edges of each layer in the model domain. Figure 1 shows a horizontal depiction of the lateral boundary grid points for a given vertical layer of the model. The LBCs of a LAM cannot be prescribed using physical-process parameterizations alone, since movement of weather systems through the model's three-dimensional domain prohibit the use of fixed parameteri-

1
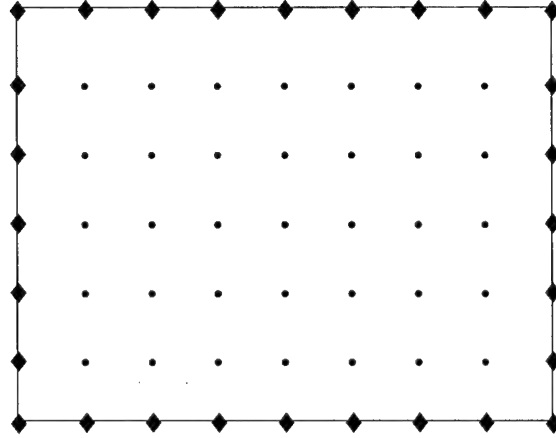
Figure 1   Lateral boundaries.   Schematic is a horizontal depiction of a vertical model level. Diamonds (♦) denote the lateral boundary grid points and dots (•) denote interior grid points.

zations. As such, inaccuracies in the LBCs will introduce an initial error to the LAM domain. Baumhefner and Perkey (3: 1982) found that LBC errors can propagate into the LAM domain at the rate of 20-30 degrees of longitude per day. Fortunately, awareness of the conditions which cause LBC errors can help a modeler minimize their impacts.

1.2   Problem and Objective

It should be recognized that LBC errors are inevitable in all LAM applications; thus, a realistic objective is to understand the nature of the problem and develop methods to mitigate their negative impacts (21: Warner et al. 1997). As such, well-constructed sensitivity studies need to be conducted to quantify the relative importance of various parameters on a LAM solution. Due to high computational costs and past resource limitations, only a handful of studies have been conducted on the placement and size of the LAM domain; the majority of past sensitivity studies have concentrated on honing the physical-process parameterizations. Of the sensitivity studies that focused on placement and size of LAM domains, only the

work of Alpert et al. (1: 1996) is known to have addressed the impacts of horizontal placement of the upstream lateral boundary in reference to significant orography.

The objective of this research was to bridge a gap in the apparent paucity of sensitivity studies on the LAM. Therefore, the following three questions were posed:

- Can forecast veracity be improved by optimally placing the windward lateral boundary of a limited area mesoscale model with respect to strong topographic features?

- Is the paradigm that finer grid resolution always improves a models forecast correct?

- Do two-way nested model domains produce a superior forecast when compared to one-way nested domains?

With a better understanding of how to best place a nested window of a LAM, a modeler can optimize the performance of the model to meet the temporal needs of his or her customers. In addition, an enlightened knowledge of whether finer grid resolutions always improve a model's forecast will enable a modeler to better perform a computation cost versus benefits analysis. Finally, assessment of nesting type will help shed light on the apparent split in the modeling community over which method of nesting provides the superior forecast.

1.3 Research Importance

A growing desire to generation longer model runs is stretching the limits of the current knowledge and technology. In the past, the lack of readily available computer resources limited the number of sensitivity studies that were conducted; therefore, much of the past research in numerical weather prediction with mesoscale models has focused on model physics. With the growing desire to produce longer forecasts, current and future research on mesoscale models needs to involve a greater number of sensitivity studies to test/validate the current model physics and configurations.

This research has both a general importance to the modeling community and specific importance to the United States Air Force (USAF). The general importance involves bridging the current gap left by an apparent lack of sensitivity studies on LBC placement relative to known topographic features, evaluating the validity of the paradigm that finer model grid resolution will always produce a more accurate forecast, and determining whether one-way or two-way nesting produces the superior forecast.

The specific value of this research to the USAF involves determining the best model nesting configuration and identifying the need for further sensitivity studies on LBC placement and model usage. The growing mission of the USAF in recent years and advancement of computer technology have led the Air Force Weather Agency (AFWA) to place nested model windows in numerous regions globally with limited knowledge on how placement of the LBCs effect the forecast accuracy. In addition, this research suggests that the usefulness of the high computational cost, finer resolution model grids currently employed by AFWA in tropical regions around the world may provide little or no improvements to the forecast of a lower resolution grid.

1.4   Summary of Results

The first key result of this research is that optimally placing the windward lateral boundary for a two-way nested domain with respect to the tallest peaks of a strong topographic feature can improve forecast accuracy. This implies that a model's forecast veracity can be improved without additional computation expense by shifting the model grid a few degrees of longitude with respect to the topography. The results for one-way nesting were inconclusive as this type of nesting appears to be less affected by boundary placement with respect to the orography.

The second key result of this research is that the paradigm that finer model grid resolutions will always produce better forecasts is flawed in some forecast situ-

ations. When ageostrophic motions are large in the troposphere, a two-way nested high-resolution domain can offer substantial improvement to the accuracy of the geopotential height and temperature forecast fields, thus supporting this paradigm. In contrast, atmospheric conditions which are more geostrophic often cause high-resolution forecasts to become inferior with time when compared to lower resolution. In addition, some meteorological fields, such as wind speed and direction, are sometimes more accurately forecasted with a lower resolution model grid, thus contradicting the paradigm.

The third and final key result of this research is that two-way nesting will generally produce a more accurate forecast than one-way nesting when significant ageostrophic motions are present in the troposphere. The feedback mechanism that is present for two-way nesting appears to be better able to handle the ageostrophic motions which are present during cyclogenesis. In contrast, a short-term forecast of less than 36 hours with no cyclogenesis present will produce less error when one-way nesting is utilized.

1.5 Thesis Organization

In this chapter, the motivation for this research was presented, followed by the problems to be addressed in this document, the importance of this research, and the key results. Chapter 2 will give a detailed background on the causes of LBC errors and ways to minimize their impacts. Model setup, validation, and configuration will be covered in Chapter 3, followed by the research findings in Chapter 4. Lastly, Chapter 5 will provide the conclusions and recommendations resulting from this research, and ideas for future research topics.

II. Subject Background

2.1 Overview

This chapter reviews the subject background necessary to appreciate the importance of lateral boundary condition (LBC) error. The chapter begins by introducing some of the basic modeling terminology used throughout this document. Then, some of the known causes of LBC error in a limited area model (LAM) are covered. Lastly, the techniques that can be employed to minimize the impacts of LBC error in a LAM are explored.

2.2 Terminology

Before discussing the causes of LBC errors and techniques to minimize their effects, some common terminology for numerical weather modeling will be defined. There are two kinds of models used for numerical weather prediction: global models, and LAMs. *Global models* cover a finite depth of the atmosphere for the entire planet (e.g., the entire northern and southern hemisphere); thus, they do not have lateral boundaries. In contrast, *LAMs* cover a "limited area" of the globe which cause them to have artificially produced lateral boundaries on four sides. In addition, global models generally use spectral methods to solve the mathematical equations for the atmosphere, while LAMs commonly employ finite differencing schemes. For more information on spectral methods and finite differencing, the reader is referred to a text on numerical weather prediction, such as Haltiner and Williams (7: 1980) or Pielke (14: 1984).

Since the lateral boundaries introduced in a LAM must be specified in order to solve the elliptic and hyperbolic equations which specify the state of the atmosphere, a LAM must obtain its LBCs from a host model domain or by data analysis. *Host* refers to any model domain, global or limited area, which provides boundary conditions for the smaller LAM nested model domain. *Nested* refers to any

6

model domain which requires the specification of LBCs. Therefore, a low-resolution LAM domain may be nested within a host global model, while performing the duties of a host by providing LBCs for a high-resolution LAM domain nested within its bounds. It is also important to note that the terms *domain, grid,* and *window* are used synonymously throughout this document.

Nesting is further defined as one of two types: one-way, or two-way. *One-way nesting* refers to any nested domain which is parasitic in nature (i.e., the nested domain receives information from its host grid, but does not return any information to its host grid). In contrast, *two-way nesting* refers to any nested domain which is beneficent in nature (i.e., the nested domain both receives information from and returns information to its host grid).

2.3 Causes of Lateral Boundary Condition Errors

This section will illustrate how error is introduced into the LAM by each of the conditions identified in the list below. Warner et al. (21: 1997) identified the following causes of LBC errors:

- Differences in grid resolution between the host and nested windows;

- Erroneous initialization data;

- Inability of longer wavelengths to interact with the model solution in the interior;

- Transient non-meteorological inertia-gravity waves caused by LBC formulation; and

- Differing physical-process parameterizations.

As mentioned previously, the LBC of a LAM must be specified prior to the time-stepped integration of the model domain. In many cases, the LBCs are specified using a global model. Global models generally have lower resolution, or a greater

7

spacing between grid points, than found in a LAM. Figure 2 illustrates how a nested window may interact with its host window. An **X** denotes a grid point that is coincident between the host window and a lateral boundary of the nested window; whereas, a dot (•) denotes those grid points that are representative of the nested window only. It can be seen from Figure 2 that the LBC of the LAM at point
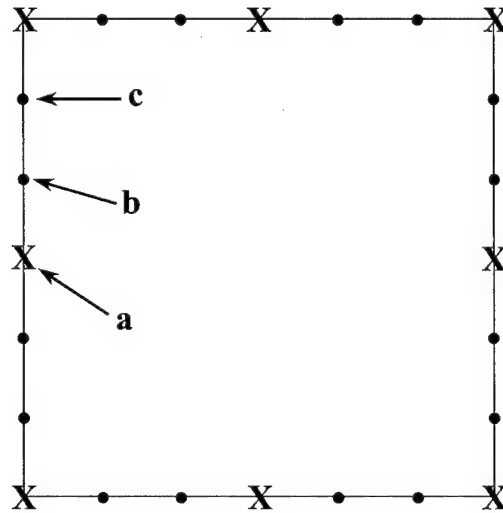
Figure 2   Nested grid points. Schematic represents the interaction of grid points between a host and nested window for a given vertical model layer. An **X** denotes a grid point that is coincident between the host and nested windows. A dot (•) denotes a grid point that is contained in the nested window only.

(a) may be obtained directly from the host grid point, but this is not the case for all the boundary grid points in the LAM. Points (b) and (c) must be interpolated from one or more of the host grid points, denoted by **X**s in Figure 2. This need for interpolation causes LBC errors that result due to varying grid resolution between the host and nested windows (21: Warner et al. 1997). Figure 2 presents a simplistic two-dimensional view of interpolation; whereas, in reality there are also differences in the number of vertical layers between the global model and the LAM. For example, a global model may only have eight vertical layers compared to 24 vertical layers in

8

a LAM; therefore, many grid points in the LAM model will require both horizontal and vertical interpolation.

If both the LAM and the host model supplying LBCs to the LAM have the same grid resolution, errors will still occur in the initial values of the lateral boundaries (21: Warner et al. 1997) because of erroneous initialization data. These errors are due to the limitations of both the observing network and the host model numerics, and cause divergence of the host model output from reality, thus feeding erroneous data to the lateral boundaries of the LAM.

The specified LBCs of a one-way nested model domain determine the "computational-grid-scale variations to the meteorological fields," thus making long wavelength interactions with the interior grid points of the nested grid impossible (21: Warner et al. 1997). Simply stated, a one-way nested domains inability to feed information back to the host grid can ultimately affect the accuracy of the longwave synoptic weather pattern. In addition, the greater grid resolution of the two-way nested domain makes feedback to the host grid cumbersome since small scale features in the nested domain may not be resolvable on the scale of the host grid. This limited interaction between the nested window and its host will negatively impact the evolution of synoptic scale systems in the LAM domain.

The formulation, or way LBCs are specified in the LAM, can lead to the generation of transient non-meteorological inertia-gravity waves along the boundaries of the model. As the numerical solution evolves through the time-stepped integration of the model's mathematical equations, the boundary errors will propagate into the model domain at the speed of the fastest inertia-gravity wave (21: Warner et al. 1997). As stated earlier, Baumhefner and Perkey (3: 1982) found that LBC errors can propagate into the LAM domain at the rate of 20-30 degrees of longitude per day. Even though inertia-gravity waves are not believed to interact strongly with the model domain, Warner et al. (21: 1997) suggested that they can complicate the interpretation of the meteorological solution. For more information on inertia-

gravity waves, the reader is referred to a text on atmospheric dynamics, such as Holton (8: 1992) or Gill (6: 1982).

Lastly, differing physical-process parameterizations introduce boundary errors. Pielke (14: 1984) defined parameterization as the "specification of subgrid scales and source-sink processes using experimental data and simplified fundamental concepts." Surface moisture flux is one example of a physical-process parameterization since this process occurs on scales smaller than the model's grid resolution. These physical-process parameterizations are often different between the host model and the LAM. The differences in parameterization are often necessary due to variations in grid resolution between the models and can lead to spurious gradients that feed back to the LAM domain (21: Warner et al. 1997).

2.4 Techniques to Minimize Lateral Boundary Condition Errors

Now that the sources of LBC error have been identified, how can their impacts be minimized? This section presents ways to minimize the impacts of the LBC errors presented in the previous section. Warner et al. (21: 1997) offered the following suggestions:

- Incorporate the use of a lateral-boundary buffer zone;

- Use a host model that has similar physics and numerics with the limited area model;

- Employ well-tested and effective lateral boundary condition formulations;

- Compensate for lateral boundary condition impacts resulting from the data assimilation preforecast period;

- Account for the importance of local forcing;

- Avoid strong forcing at the lateral boundaries;

- Apply interactive grid nests when possible; and

10

- Perform sensitivity studies to determine lateral boundary influences.

Baumhefner and Perkey (3: 1982) conducted one of the first studies identifying the impacts of LBC errors on the output of a LAM. Since then, other researchers, such as Vukicevic and Paegle (20: 1989) and Alpert et al. (1: 1996), have come to similar conclusions about the impacts of these errors on the LAM domain. Treadon and Petersen (17: 1993) conducted domain size sensitivity experiments and found "decreasing domain size increasingly degraded forecast skill." Warner et al. (21: 1997) synthesized these works and indicated that one solution proposed by many researchers was to remove the LBCs from the area of forecast interest by increasing the LAM domain size. This "buffer zone" is illustrated by the shaded region in Figure 3. In this example, the LBCs have been removed from the area of forecast interest
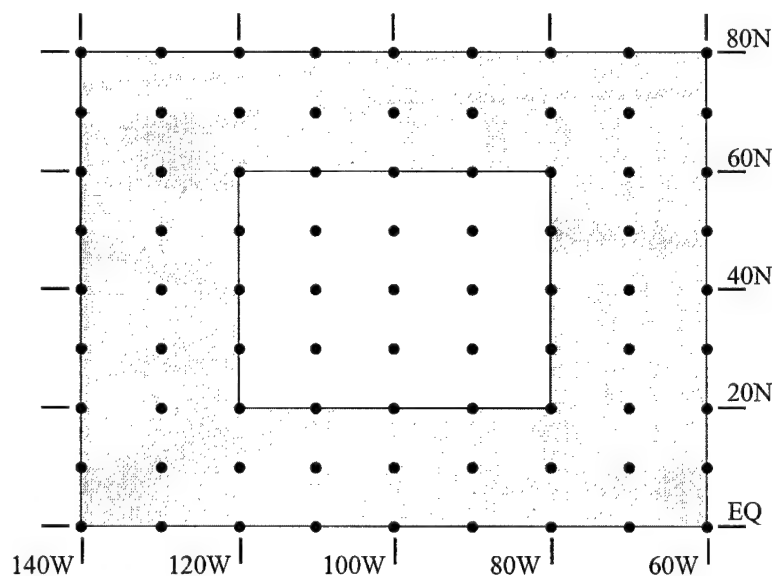
Figure 3   Buffer zone.   Schematic represents a LAM domain size increase of 50 percent on each side. Shaded region denotes an increase of 20 degrees on all sides, unshaded region denotes the area of forecast interest, and dots represent the grid points.

(unshaded) by 20 degrees in all directions based on the findings of Baumhefner and Perkey (3: 1982). While this method delays the effects of LBC errors on the area of forecast interest, there is a high computational cost incurred. This is easily seen

by noting the increased number of grid points (dots), in Figure 3. In general, a 50 percent increase of the LAM domain on each side yields a four-fold increase in the computational cost. This extra computational cost is not always acceptable; thus, other alternatives have been explored.

Differences in model physics between a host global model and a LAM, are rarely avoidable; however, choosing a global model that minimizes the amount of interpolation to the LAM grid points will reduce the amount of LBC error (21: Warner et al. 1997). For example, if a global model has an 80 km grid spacing, then a LAM with 40 km grid spacing will have less interpolation error than a LAM with a 20 km grid spacing. This illustrates the need for multiple nesting since going from an 80 km grid spacing to one with a 20 km spacing is not advisable. In this case, the 20 km grid can be initialized by the 40 km grid which has been initialized by the 80 km global model grid.

Baumhefner and Perkey (3: 1982) studied boundary condition formulations in their evaluation of LBC errors. Their study compared the Perkey-Kreitzberg (PK) scheme to the Williamson-Browning (WB) method. The PK lateral boundary scheme "consists of large-scale time-varying tendencies linearly combined with model-calculated tendencies" (13: Perkey and Kreitzberg 1976). Simply stated, the PK scheme specifies LBCs of the LAM from the exterior host grid only. In contrast, the WB method specifies LBCs in the following two ways: if the synoptic scale winds are directed into the LAM domain, then the LBC are obtained from the host model; if the synoptic scale winds are directed out of the LAM domain, then the LBCs are obtained from the interior grid of the LAM, keeping in mind that the initial set of LBCs must still be obtained from the host model (24: Williamson and Browning 1974). Baumhefner and Perkey (3: 1982) found the WB method produced less error in the LAM domain during the first twelve hours of integration than the PK scheme; however, the errors grew unbounded in the WB method after the first twelve hours. Conversely, the error growth in the PK scheme was fast during the first 24 hours but

stabilized after 48 hours. Using these results, a modeler can determine which LBC scheme best fits the needs of a particular model application.

Zou and Kuo (26: 1996) showed that data assimilation, also called four-dimensional data assimilation (FDDA), enables a LAM to "generate and maintain realistic mesoscale atmospheric features" not resolvable without data assimilation. However, FDDA involves the input of observed data and integration of the model's mathematical equations during a preforecast period which allows LBC errors to propagate toward the interior of the LAM domain prior to the forecast period of interest. This error propagation can be offset by including the LBCs in the FDDA or by increasing the upstream buffer zone discussed earlier (21, 26: Warner et al. 1997; Zou and Kuo 1996).

Strong local forcing mechanisms within the LAM domain will generally decrease the negative effects caused by LBC errors (21: Warner et al. 1997). Vukicevic and Errico (19: 1990) showed in their predictability study that "topography forcing increases the predictability of atmospheric flows." Therefore, if a LAM has strong forcing on the interior domain, the LBC errors are not as large relative to the total error, and the LAM domain size will not need to be increased. For example, mountains in the center of a LAM domain will cause forcing due to orographic lift along the slopes.

Strong forcing on the lateral boundaries can cause numerical problems with the LBC formulations. Therefore, one should avoid placing the lateral boundaries of a LAM directly over these regions (21: Warner et al. 1997). Alpert et al. (1: 1996) indirectly demonstrated this in their study of lee cyclogenesis in the Gulf of Genoa. In the study, the western lateral boundary of the LAM was moved to the west in two degree increments of longitude from the cyclogenesis region in the Gulf of Genoa. The LBCs closest to the cyclogenesis region yielded the second worst result, surpassed only by the LBCs removed by 10 degrees to the west of the orography.

Interactive grid nesting is the two-way interaction of the nested domain with the host model grid, whereas a one-way interaction of the nested domain is a parasitic-type grid (21: Warner et al. 1997). Zhang et al. (25: 1986) found interactive nesting could reduce noise in the LAM output. In a study using a parasitic grid, Vukicevic and Errico (19: 1990) indicated that one-way interaction tended to dampen out errors originating on the boundaries. Consequently, a split in the modeling community exists on whether interactive or parasitic nesting is better. In the author's opinion, more sensitivity studies are required on interactive nesting techniques before a subjective judgment can be forthcoming. The question that must be answered to validate the feasibility of using interactive nesting is whether or not the low-resolution host grid can reasonably resolve the higher resolution data from the nested domain (i.e., the high-resolution data is on a subgrid scale in the host domain).

Lastly, sensitivity studies must be conducted to increase our knowledge of LAMs so the pitfalls described above may be avoided. In addition, Stein and Alpert (15: 1993) have questioned the validity of past sensitivity studies involving quantitative results since they were conducted under an assumption of parameter independence, whereas their proposed "factor separation" method assumes parameter dependence during a sensitivity study. Simply stated, past sensitivity studies did not account for synergism between the parameters responsible for error growth in the model's output. The findings of Stein and Alpert have added to the apparent need for more sensitivity studies in the future.

III. Research Methodology

3.1 Overview

This chapter details the methodology used in this research. The chapter begins with a brief overview of the model used and its characteristics. Then, the model's setup and validation at the Air Force Institute of Technology (AFIT) will be discussed, followed by the specific configuration of the model for this project. The second half of the chapter is devoted to discussing the data sets obtained from outside agencies along with those generated by Fortran programs written by the author. Additionally, an overview of the two case studies used in this research will be given.

3.2 Model

3.2.1 Description. This research was conducted using the Pennsylvania State University (PSU)/National Center for Atmospheric Research (NCAR) Mesoscale Model 5, Version 2, Release 12 modeling system. The model is more commonly referred to as the MM5 modeling system and will be referred to as such for the remainder of this document. The MM5 modeling system consists of four preprocessors (TERRAIN, REGRID, RAWINS/little_r, and INTERP), the main model code (MM5), and a post-processor (GRAPH). For the current research, the Read/Interpolate/Plot (RIP) program, which also requires the availability of the NCAR Graphics software, was substituted for the standard modeling system post-processor. For detailed information about the RIP program, the reader is referred to *A User's Guide to Read/Interpolate/Plot (RIP): A Program for Visualizing PSU/NCAR Mesoscale Model Output* (16: Stoelinga 1997). A general discussion of the MM5 modeling system is forthcoming in this chapter; however, for a more detailed discussion of the MM5 modeling system, the reader is referred to

the *PSU/NCAR Mesoscale Modeling System Tutorial Class Notes and User's Guide: MM5 Modeling System Version II* (12: MMMD/NCAR 1999).

The MM5 modeling system uses sigma coordinates which are the most commonly used vertical coordinate system for a limited area model (LAM). Sigma (σ) is a dimensionless quantity that varies from zero to one and is given by the following relationship of pressures:

$$\sigma = \frac{(p - p_t)}{(p_s - p_t)} \quad , \tag{1}$$

where p is the pressure, p_t is a specified constant top pressure, and p_s is the surface pressure (12: MMMD/NCAR 1999). Figure 4 shows an example of a vertical cross section with 16 sigma levels (K). The lowest level (σ=1.0) is terrain following and corresponds to the bottom boundary of the model. Physical processes along the bottom boundary, such as surface moisture and heat fluxes, can be prescribed using physical process parameterizations in the model. The highest level (σ=0.0) is quasi-horizontal and corresponds to the top boundary of the model. The top layer, often considered the tropopause or higher (set at 100 mb for the current research), acts as a material surface which limits the flux of atmospheric properties across it and can also be parameterized within the model physics (14: Pielke 1984).

The vertical velocity (w) forecasted by the MM5 modeling system is defined at full-sigma levels, whereas the remainder of the forecast variables are defined at the half-sigma levels (12: MMMD/NCAR 1999). The MM5 uses an Arakawa-Lamb B-staggered grid as shown in Figure 5. This method of staggering collocates the eastward velocity component (u), northward velocity component (v), and Coriolis force at the corners, or dot points ($\bullet$). In contrast, the remaining forecast variables are defined in the center of the grid squares as denoted by the cross points ($\mathbf{X}$) in Figure 5 (12: MMMD/NCAR 1999). In addition, it is important to note that
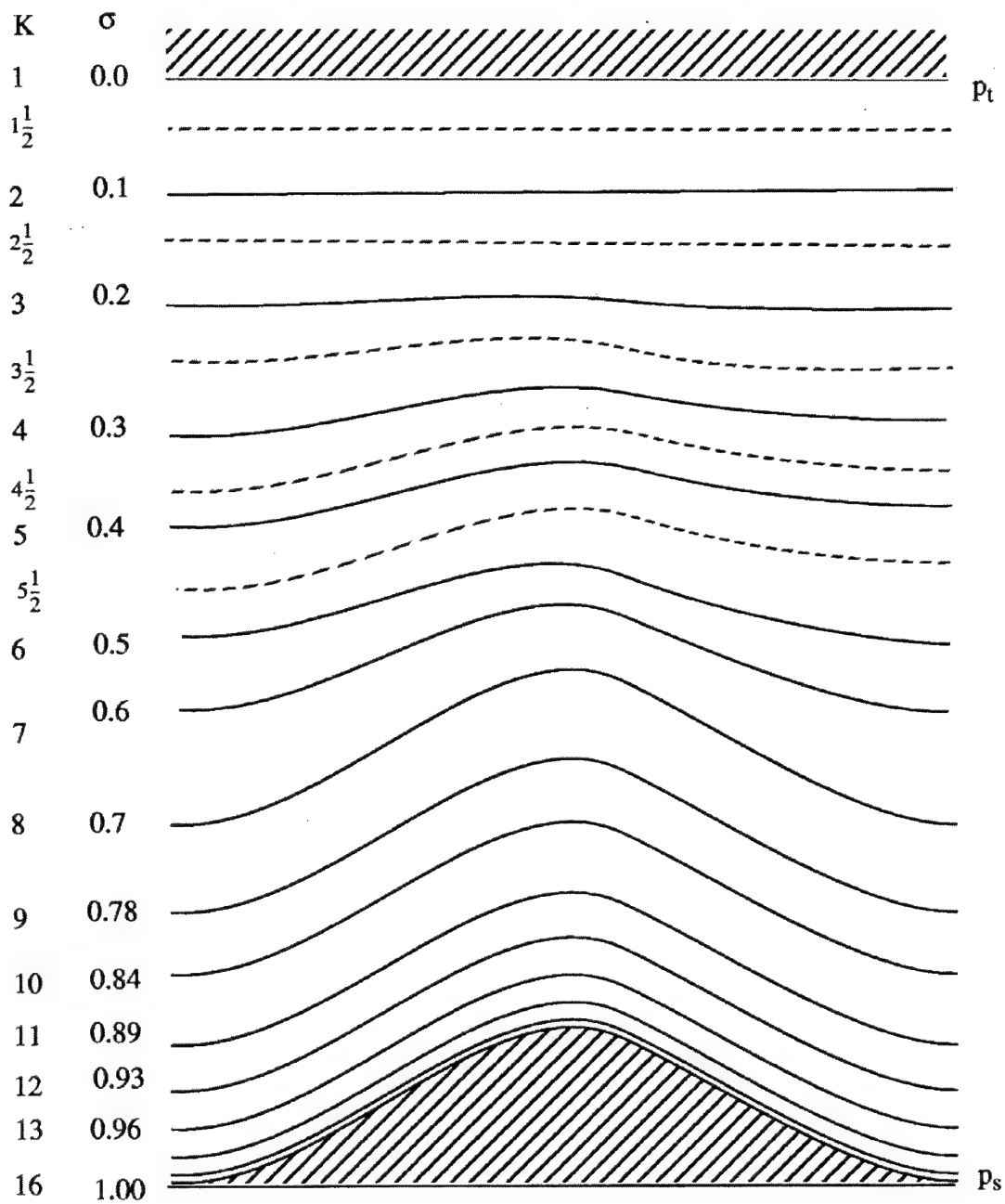
Figure 4   Sigma coordinates.   Schematic representation of the vertical structure of
the model.   This example is for 16 vertical levels as denoted by values of
K. Dashed lines denote half-sigma levels and solid lines denote full-sigma
levels.   Adapted from MMMD/NCAR (12: 1999).
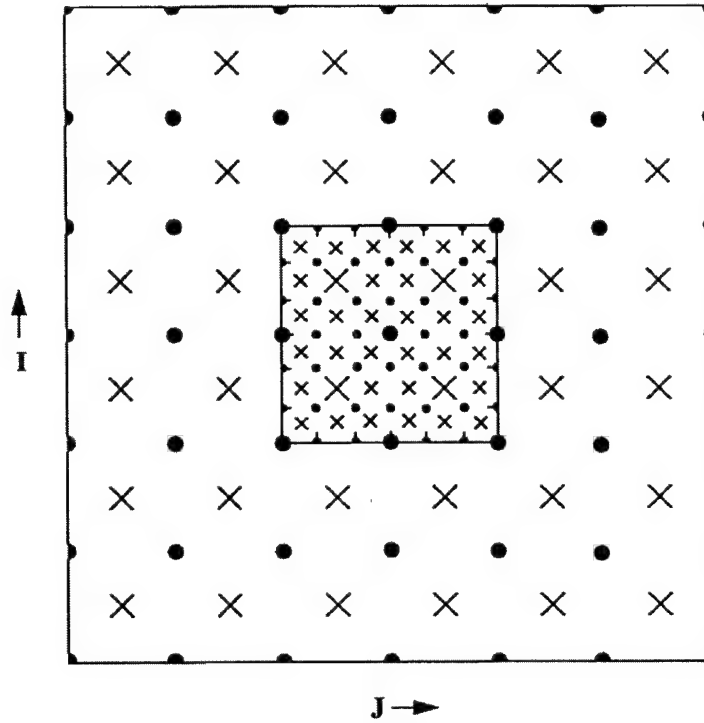
Figure 5   Arakawa-Lamb B-staggered grid. This figure shows the dot point and cross point staggering of the grid used in the MM5 modeling system. The directional wind components and Coriolis force are defined at dot points, while the remaining variables are defined at cross points.   The smaller box in the center represents a nested grid with a 3:1 ratio to the host, or outer, grid. Adapted from MMMD/NCAR (12: 1999).

the I and J directional unit vectors are opposite those found on a typical Cartesian Coordinate System.

3.2.2   Setup and Validation.   Before discussing the configuration of the MM5 modeling system used in this research, it is necessary to discuss the setup and validation of the system at AFIT, since this was the first time the model had been used at this facility.   All of the model preprocessing and post-processing was conducted at the AFIT Weather Lab on a Sun SPARC Ultra II system with twin-processors, while the MM5 code was configured for parallel processing on an IBM

SP2 system at the Major Shared Resource Center on Wright-Patterson Air Force Base in Ohio.

The test case data set used to validate the setup of the MM5 modeling system code at AFIT was the intense weather storm of 12-14 March 1993, often dubbed the "Storm of the Century" (10: Kocin et al. 1995). This case study was convenient for validating the model setup since it is used for the NCAR MM5 Tutorial Workshop and is presented in Chapter 12 of the MM5 User's Guide (12: MMMD/NCAR 1999). For a more detailed discussion of the "Storm of the Century" weather system, the reader is referred to Kocin et al. (10: 1995) and Uccellini et al. (18: 1995).

Figure 6 is a surface pressure chart showing the results of the validation run of the model. This 24 hr forecast field of the nested 30 km resolution grid has a positive pressure bias of 9.55 mb, and the surface pressure center is slightly to the north of the actual system track, denoted by the star ($\bigstar$) in Figure 6. These results are consistent with those generated by other mesoscale and global models, and the MM5 output illustrated in the MM5 User's Guide (12, 18: MMMD/NCAR 1999; Uccellini et al. 1995).

3.2.3   Configuration.   The main focus of this research was to quantify the effects of topographic forcing on the lateral boundaries of the model domain, thus dictating the general design of the experiment. The Rocky Mountains were chosen as the source of topographic forcing due to the availability of data. Figure 7 illustrates the setup of the model domains used in this research. The five domains, labeled A, B, C, D and E, represent the 12 km resolution nested grids that were embedded in the 36 km resolution host grid. The choice of resolution for the host and nested domains was designed to mirror the resolution being used by the Air Force Weather Agency. The host, or outermost, domain was centered at 39°N latitude and 100°W longitude with a size of 112 by 193 (vertical by horizontal) grid points. The shaded region (Domain A) represents the standard size of the nested domains with a size of 145 by
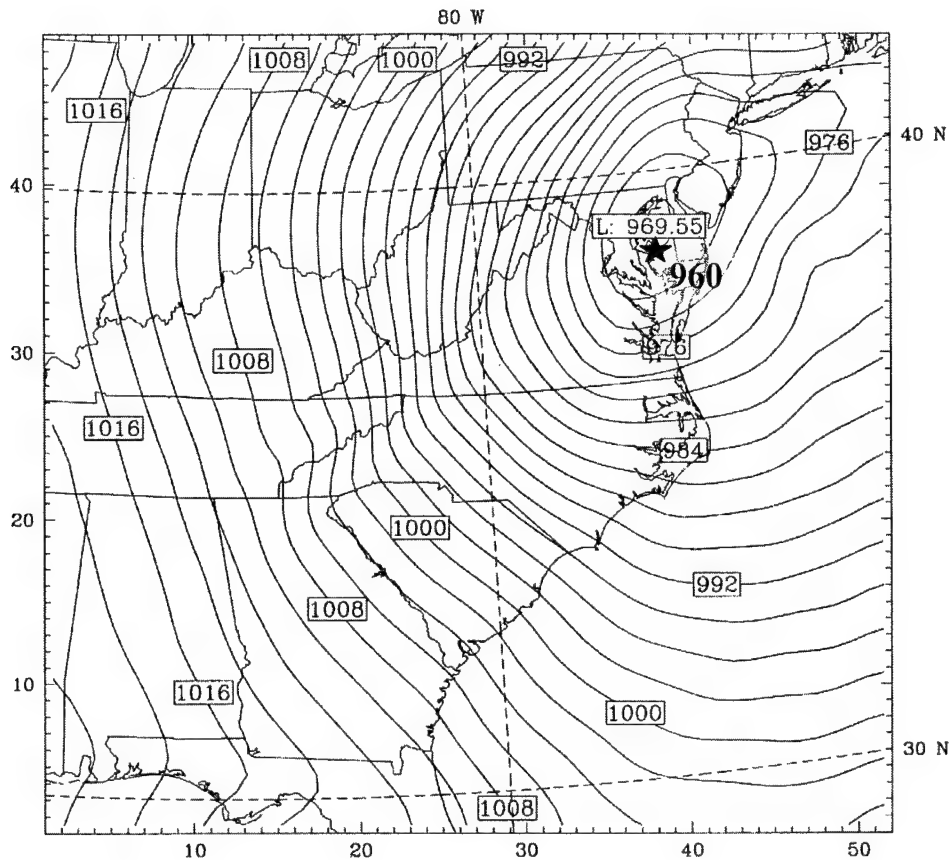
Figure 6   MM5 modeling system validation.   This chart shows the model's 24 hr forecast of sea level pressure.   Contours are plotted in 2 mb intervals. The star (★) represents the observed center of the weather system with a pressure of 960 mb.   The coordinates are labeled in both grid point space and latitude/longitude.

220 grid points.   Domain A had a starting point, or lower left corner, of I=32 and J=90 on the host grid (where I is along the ordinate and J is along the abscissa) and a western boundary along the front range of the Rocky Mountains.   Each successive nested domain, Domains B, C, D, and E, was moved seven J grid points to the west on the host grid, while the I grid point remained constant.   Thus, each successive nested domain was moved in approximately three degree increments to the west of the previous domain and run independently to eliminate any interaction between the
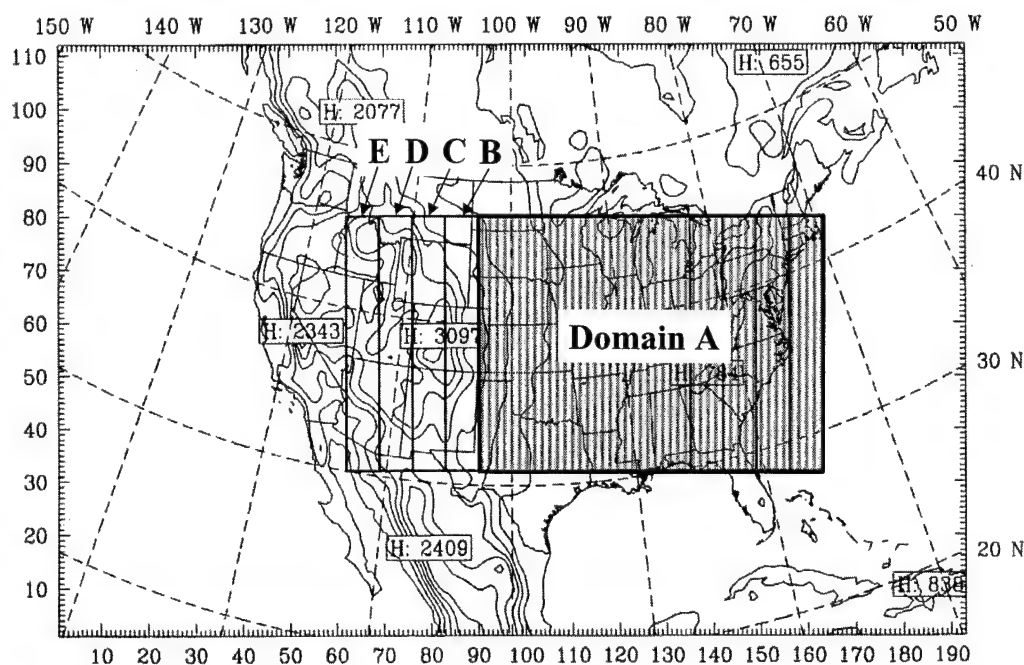
Figure 7   Model domains. This figure illustrates the positions of the five nested domains used to conduct this research. The outer grid (entire picture) was 36 km resolution, while the nested windows were 12 km resolution. The shaded region represents the standard nested domain size used. The contours show terrain height in meters with an interval of 400 m. The coordinates are labeled in both grid point space and latitude/longitude.

various nested grids. This approach of successive domains is similar to that used by Alpert et al. (1: 1996) in their study of lee cyclogenesis in the Gulf of Genoa.

Figure 8 shows a vertical cross-section along the 39°N latitude circle between 100°W and 120°W longitude. The positions of the windward lateral boundary for each of the five nested domains (labeled A to E) are indicated by the vertical dashed lines in this figure. The shaded region in Figure 8 represents the terrain as viewed by the model. From this cross-section, it is evident that the windward boundary of Domain A is downstream from the tallest peak (greater than 3000 meters) of the Rockies, the windward boundary of Domain B is over the tallest peak, and the remaining domains (Domains C through E) are upstream from the tallest peak.
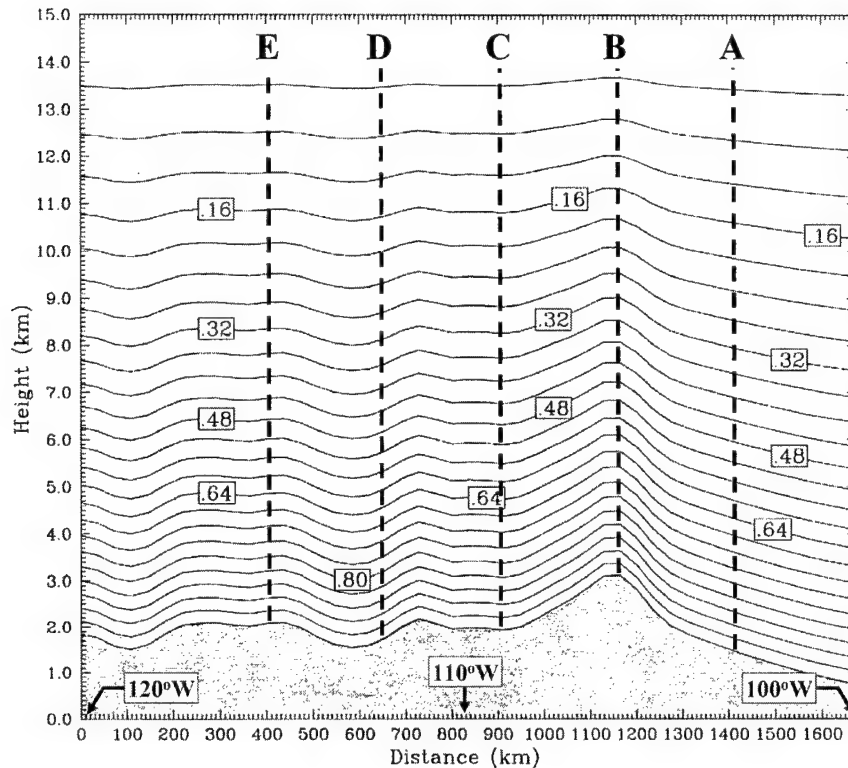
Figure 8   Vertical cross-section of windward lateral boundaries. This figure shows the positions of the windward lateral boundary (vertical dashed lines) with reference to orography at 39°N latitude for each of the five nested domains (labeled A to E) used to conduct this research. The contours show the 24 terrain-following sigma levels that were setup in the model's configuration. The shaded region represents the terrain as viewed by the model. The coordinates are labeled in kilometers with the horizontal axis between 100°W and 120°W longitude.

There were two cases of lee cyclogenesis selected to use in this research: a January and a May case. A description of the selected cases will be presented in the next section. The forecast period for the January and May model runs was set at 120 hours and 144 hours, respectively. The veracity of each domain's output was measured by comparing the 12 hr forecast intervals to the analysis for the same time period. Figure 9 shows the region (shaded) that was used for statistical comparison of the various domains. This region was selected to ensure that verification was conducted over an area common to all domains. The method of statistical verification

22
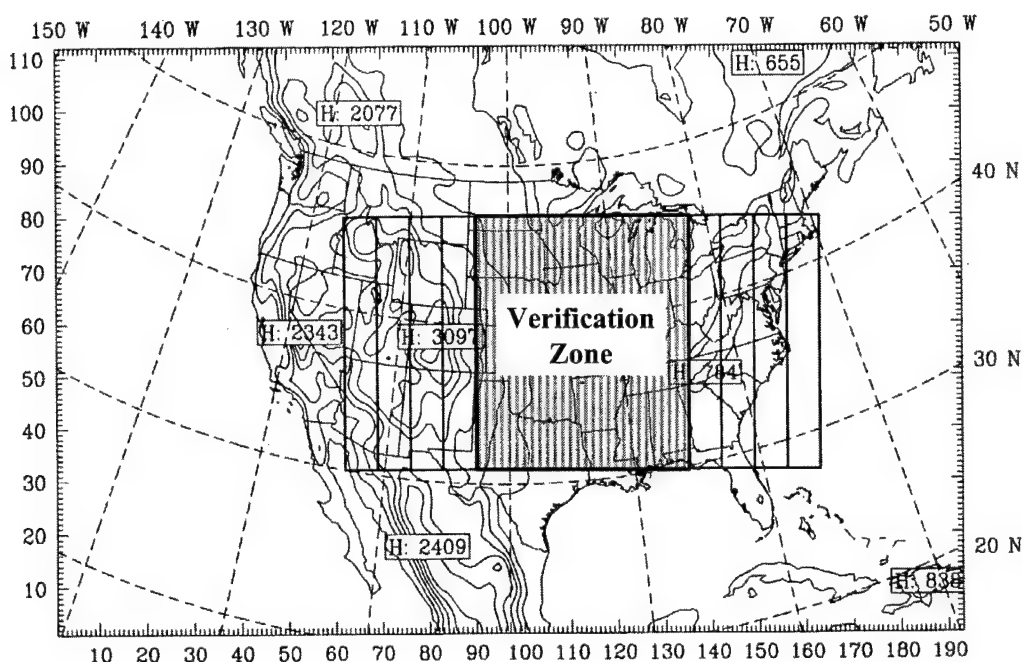
Figure 9   Verification zone. This figure depicts the verification zone where statistical computations were performed for this research. The contours show terrain height in meters with an interval of 400 m. The coordinates are labeled in both grid point space and latitude/longitude.

will be covered in the next chapter. Table 1 lists the 22 model runs conducted for this research. Each two-way nested domain was run independent of the others to ensure that there was no interaction between the various domain placements. The outer domain (denoted as "1" in the table) used in the two-way nested configuration was not used for verification since they were strongly influenced by the two-way interaction and indicated similar results to the higher resolution two-way nested domain over the verification zone. Therefore, the use of the independently run low-resolution outer domain (model runs #1 and #12) ensured that the verification was not biased by the two-way nested interactions.

There were two basic MM5 modeling system configurations used in this research to facilitate answering the question of one-way versus two-way nesting posed earlier. The main difference between the two configurations lies in the fact that two-

Table 1   Model runs conducted for this research

Run #	Case	1 (Outer)	A	B	C	D	E	Nesting Type
		Domain Identity						**Nesting**
Run #	**Case**	**1 (Outer)**	**A**	**B**	**C**	**D**	**E**	**Type**
1	January	■						None
2	January	■ †	■					2-way
3	January	■ †		■				2-way
4	January	■ †			■			2-way
5	January	■ †				■		2-way
6	January	■ †					■	2-way
7	January		■					1-way
8	January			■				1-way
9	January				■			1-way
10	January					■		1-way
11	January						■	1-way
12	May	■						None
13	May	■ †	■					2-way
14	May	■ †		■				2-way
15	May	■ †			■			2-way
16	May	■ †				■		2-way
17	May	■ †					■	2-way
18	May		■					1-way
19	May			■				1-way
20	May				■			1-way
21	May					■		1-way
22	May						■	1-way

† denotes that domain was not used for verification

24
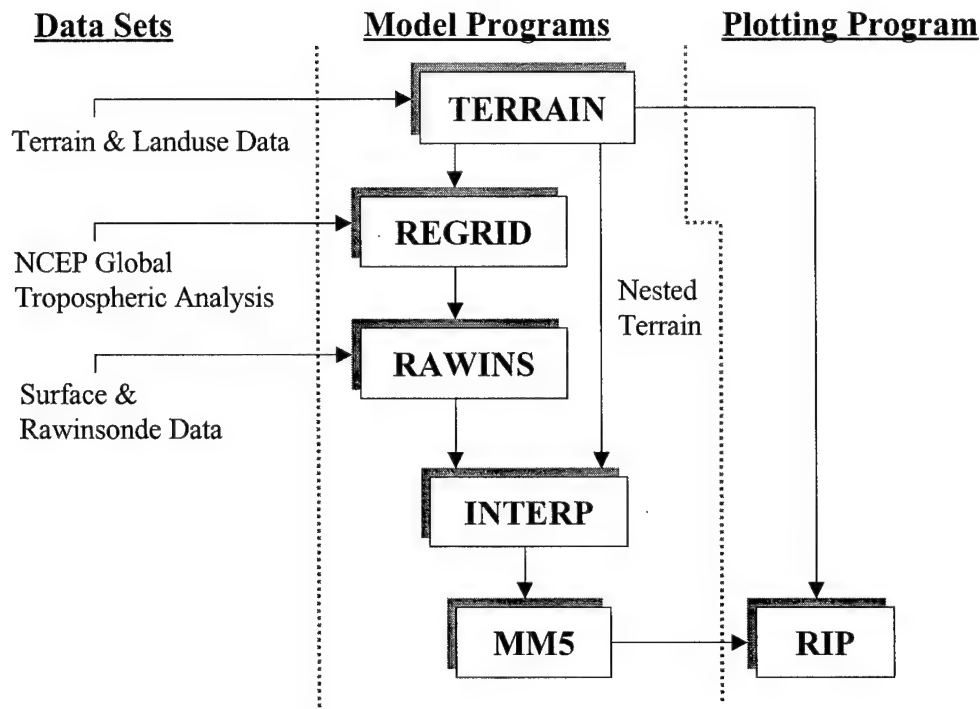
Figure 10   MM5 system configuration for two-way nesting. This flow chart shows the general flow of data through the MM5 modeling system with a two-way nesting configuration. The schematic has three major subdivisions: input data sets, model preprocessing and main programs, and a post-processing program.

way nesting allows the higher resolution grid to feed information back to the host grid. The configuration for two-way nesting, shown in Figure 10, is the simplest of the two configurations. With this configuration, 5 and 10 minute terrain height data from the Geophysical Data Center, and 13 category landuse data from PSU/NCAR was input into the TERRAIN preprocessing program of the MM5 modeling system. The TERRAIN program interpolated this input data to the host and nested domains in this research. Next, the TERRAIN coarse domain output along with the National Center for Environmental Prediction (NCEP) Global Tropospheric Analysis were fed into the REGRID preprocessing program of the MM5 modeling system. The RE-GRID program preformed two operations: reading in the meteorological analysis

(first-guess), and interpolating the analysis to the model grid (12: MMMD/NCAR 1999). Then, output from the REGRID program, for both the coarse and nested domains, was input into the RAWINS preprocessing program of the MM5 modeling system. The RAWINS program was used to enhance the first-guess field (provided by the NCEP Global Tropospheric Analysis) through the input of NCEP ADP Global Upper Air Observations and NCEP ADP Global Surface Observations. The final preprocessor of the MM5 modeling system (INTERP) vertically and horizontally interpolated the output from the RAWINS program and the higher resolution nested data from the TERRAIN program to the sigma coordinates of the model (12: MMMD/NCAR 1999). The INTERP program produced the initial condition and boundary condition files necessary to solve the meteorological equations in the MM5 main model code. For more information on the need for initial and boundary conditions, the reader is referred to a text on numerical weather prediction, such as Pielke (14: 1984), or Haltiner and Williams (7: 1980). Finally, the main code of the MM5 modeling system (MM5) was run using the initial and boundary conditions output from the INTERP program. The MM5 program was configured to run non-hydrostatically, with no four-dimensional data assimilation. The following physics options were used for all domains in this research: the mixed-phase (Reisner) moisture scheme, the Grell cumulus scheme, the medium range forecast (MRF) planetary boundary layer scheme, the cloud atmospheric radiation scheme, the multi-layer soil moisture model, and the no shallow convection option. For more information on the various physical process parameterization schemes available to the MM5 modeling system, the reader is referred to Chapter 9 of the MM5 User's Guide (12: 1999). The MM5 output for both the host and nested domains was plotted using the RIP post-processing program developed by Stoelinga (16: 1997).

Figure 11 shows the more complex configuration used for one-way nesting of the MM5 modeling system. The input data sets were the same for both nesting configurations. The preprocessing for the MM5 modeling system was conducted

Data Sets　　　　　**Model Programs**　　　　**Plotting Program**

```
                                    ┌──────────────┐
Terrain & Landuse Data ────────────▶│   TERRAIN    │──────────────┐
                                    └──────────────┘              │
                                           │                      │
                                           ▼                      │
                                    ┌──────────────┐              │
NCEP Global        ────────────────▶│   REGRID     │              │
Tropospheric Analysis               │(coarse domain only)│   Nested  │
                                    └──────────────┘    Terrain    │
                                           │                      │
                                           ▼                      │
                                    ┌──────────────┐              │
Surface &          ────────────────▶│   RAWINS     │              │
Rawinsonde Data                     │(coarse domain only)│        │
                                    └──────────────┘              │
                                           │                      │
                          ┌────────────────┤                      │
                          ▼                ▼                      ▼
                  ┌──────────────┐   ┌──────────────┐
                  │   INTERP     │──▶│   INTERP     │
                  │(coarse domain only)│ │(back-end job)│
                  └──────────────┘   └──────────────┘
                          │                │
                          ▼                ▼
                  ┌──────────────┐   ┌──────────────┐
                  │    MM5       │   │    MM5       │
                  │(coarse domain )│ │(nested domain)│──┐
                  └──────────────┘   └──────────────┘   │
                          │                         ┌──────────────┐
                          └────────────────────────▶│    RIP       │
                                                     └──────────────┘
```
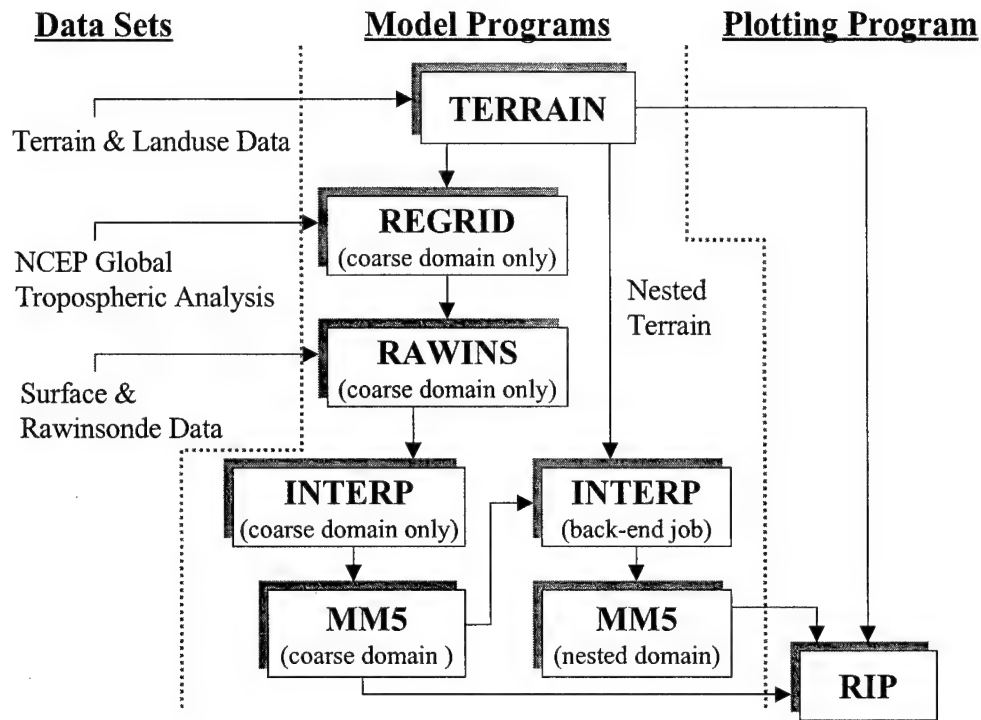
Figure 11　MM5 system configuration for one-way nesting. This flow chart shows the general flow of data through the MM5 modeling system with a one-way nesting configuration. The schematic has three major subdivisions: input data sets, model preprocessing and main programs, and a post-processing program.

in a similar manner as it was for two-way nesting with one exception: only the coarse domain was run through the REGRID, RAWINS, and INTERP programs. The preprocessing on the coarse domain in the INTERP program is referred to as a "front-end job" (12: MMMD/NCAR 1999). Next, the coarse domain initial and boundary conditions from the INTERP program provided the input to a MM5 model run on the coarse domain only. The MM5 main model code physical options were set the same as those mentioned earlier. Then, the coarse output from the MM5 main model code and the higher resolution nested data from the TERRAIN program were input back into the INTERP program to interpolate the initial condition and boundary condition files for the nested domain. The interpolation of the model

output is referred to as a "back-end job" (12: MMMD/NCAR 1999). Finally, the MM5 main model code was run for the nested domain only. Output was generated by the RIP program for both the host and nested domains. With this configuration, the interaction between the host and nested domains was parasitic in nature (i.e., the nested domain receives information from the host domain, but does not return any information to the host domain).

3.3   Research Data

3.3.1   Model Input Data.   The terrain and landuse data sets for the MM5 modeling system were obtained from the anonymous FTP server at the University Corporation for Atmospheric Research. The remaining input data sets, listed in Figures 10 and 11, were retrieved from the Data Support Section, Scientific Computing Division, NCAR. The NCEP Global Tropospheric Analysis consists of the MRF model analysis of surface temperature, geopotential height, upper air temperature, winds, and relative humidity on a 145x37 2.5 degree hemispheric grid. In addition, the ON84 formatted data contains the sea surface temperature and snow cover data. The NCEP ADP Global Upper Air Observations consist of observations from the following data sources: synoptic, profiler, upper air, land, ship, radar, pilot-balloon, aircraft, satellite, and bogus. The NCEP ADP Global Surface Observations are comprised of 3-hourly, and 6-hourly land and ship observations.

Potential case studies for this research were identified by reviewing recent work in the area of numerical weather prediction. First, potential cases were identified as weather scenarios involving cyclogenesis in the lee of the Rocky Mountains which moved across the central Great Plains of the United States. Secondly, potential cases were screened by checking for completeness of the three NCEP data sets mentioned in the last paragraph. Lastly, the data sets were checked for sea surface temperature and snow cover data completeness after being read by the REGRID program of the MM5 modeling system. After screening the data, the following two case studies

Figure 12   Sea level pressure analysis at 0000 UTC 15 January 1995.   This chart
             shows contours of the model's sea level pressure analysis in 2 mb inter-
             vals.   The research verification zone is enclosed by the box.

were identified for use in the current research: 0000 UTC 15 January 1995 to 0000

UTC 20 January 1995, and 0000 UTC 4 May 1995 to 0000 UTC 10 May 1995.   The

January case study was limited to a forecast period of 120 hours due to missing data

at 1200 UTC 20 January 1995 in the NCEP Global Tropospheric Analysis.   The

May case study was used for a 144 hour forecast period, since no data was missing.

      The January case is illustrated in Figures 12 through 20.   The contours provide

sea level pressure analysis in 2 mb intervals at a 12 km grid resolution.   The box in

each figure outlines the verification zone for this research.   The figure coordinates are

labeled in both grid point space and latitude/longitude.   This case study featured

the movement of two low pressure systems through the verification zone.   The first

low pressure system approached the verification zone from the northwest, as shown

by the analysis at 0000 UTC 15 January 1995 in Figure 12.   The pressure dropped

to about 996 mb as the system moved southward over Colorado 24 hours later (see

Figure 13   Sea level pressure analysis at 0000 UTC 16 January 1995.   This chart
shows contours of the model's sea level pressure analysis in 2 mb inter-
vals.   The research verification zone is enclosed by the box.
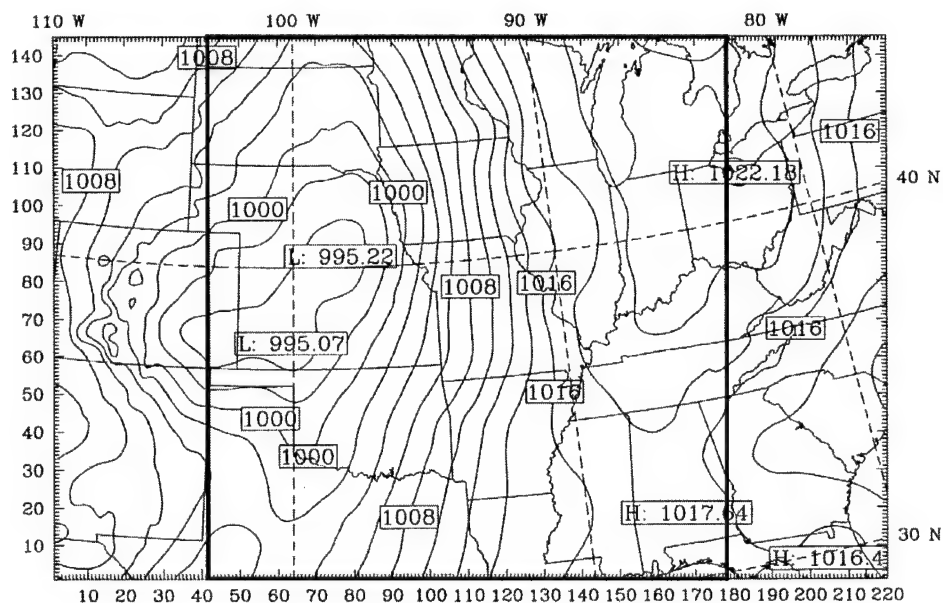
Figure 14   Sea level pressure analysis at 0000 UTC 17 January 1995.   This chart
shows contours of the model's sea level pressure analysis in 2 mb inter-
vals.   The research verification zone is enclosed by the box.
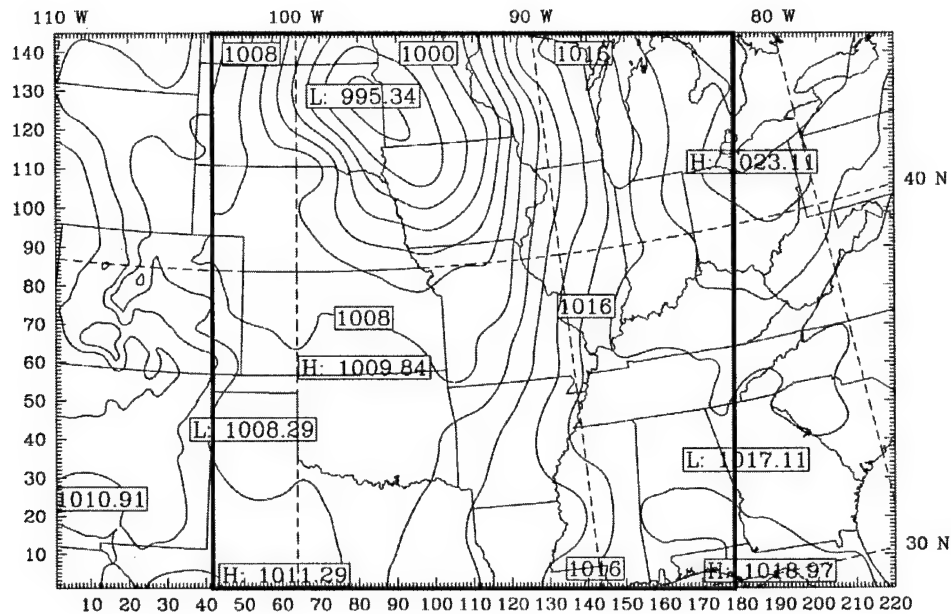
Figure 15   Sea level pressure analysis at 1200 UTC 17 January 1995.   This chart
shows contours of the model's sea level pressure analysis in 2 mb inter-
vals.   The research verification zone is enclosed by the box.
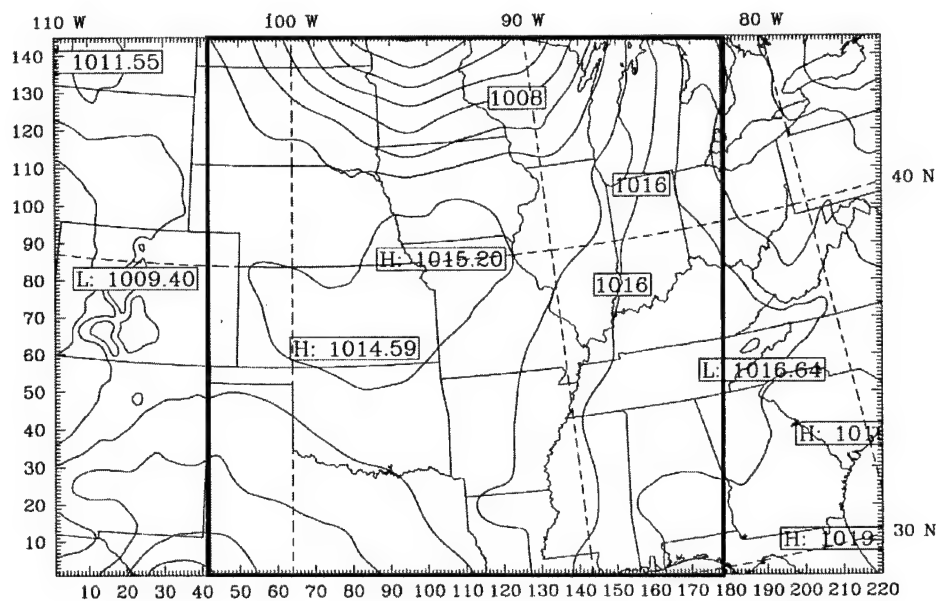
Figure 16   Sea level pressure analysis at 0000 UTC 18 January 1995.   This chart
shows contours of the model's sea level pressure analysis in 2 mb inter-
vals.   The research verification zone is enclosed by the box.
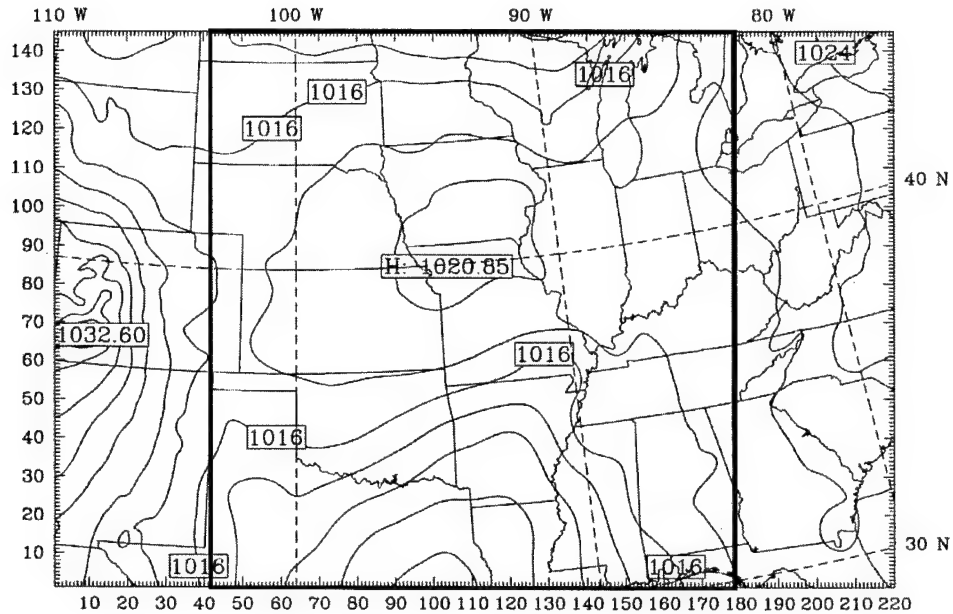
Figure 17   Sea level pressure analysis at 1200 UTC 18 January 1995. This chart shows contours of the model's sea level pressure analysis in 2 mb intervals. The research verification zone is enclosed by the box.
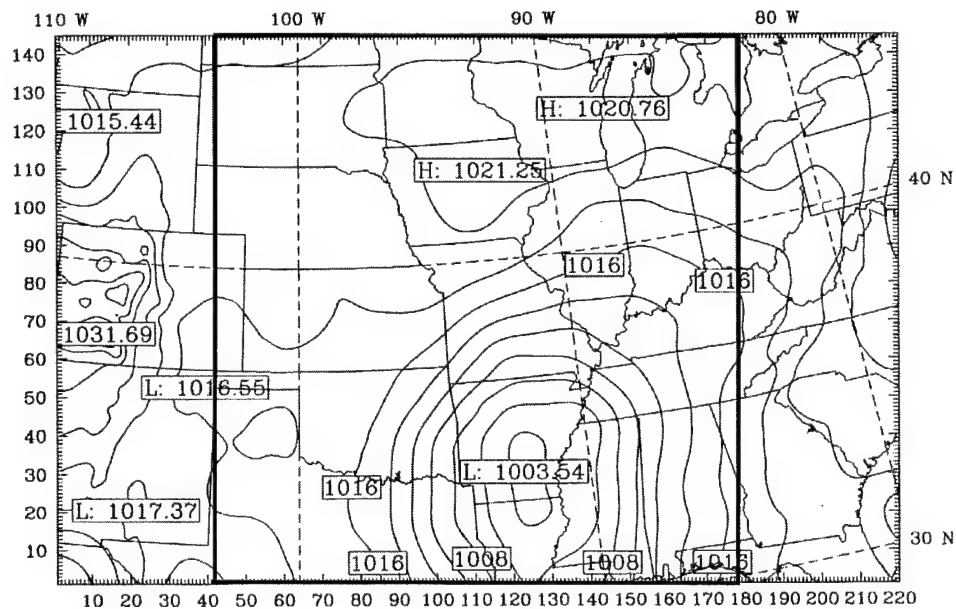
Figure 18   Sea level pressure analysis at 0000 UTC 19 January 1995. This chart shows contours of the model's sea level pressure analysis in 2 mb intervals. The research verification zone is enclosed by the box.
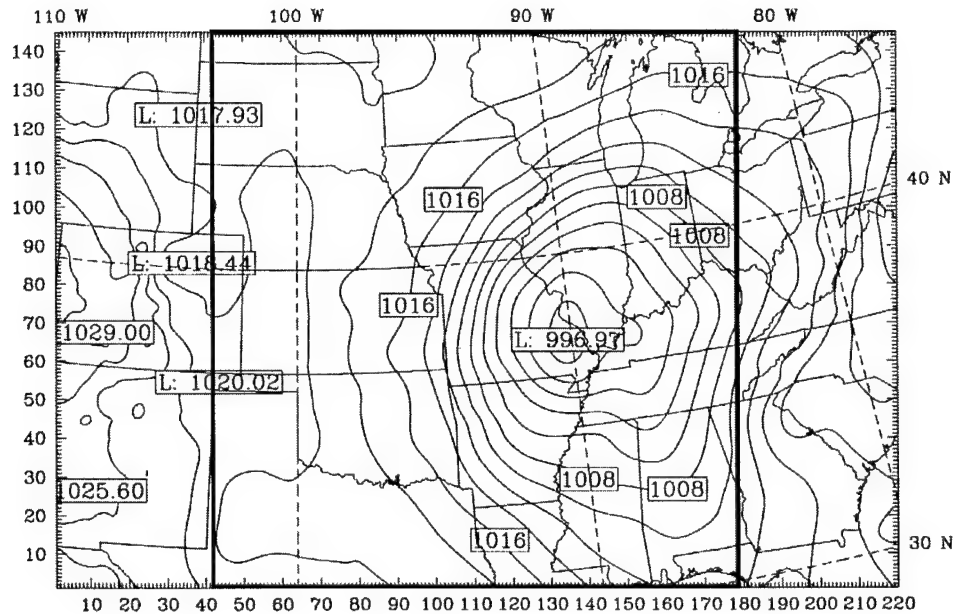
Figure 19   Sea level pressure analysis at 1200 UTC 19 January 1995.   This chart
shows contours of the model's sea level pressure analysis in 2 mb inter-
vals.   The research verification zone is enclosed by the box.
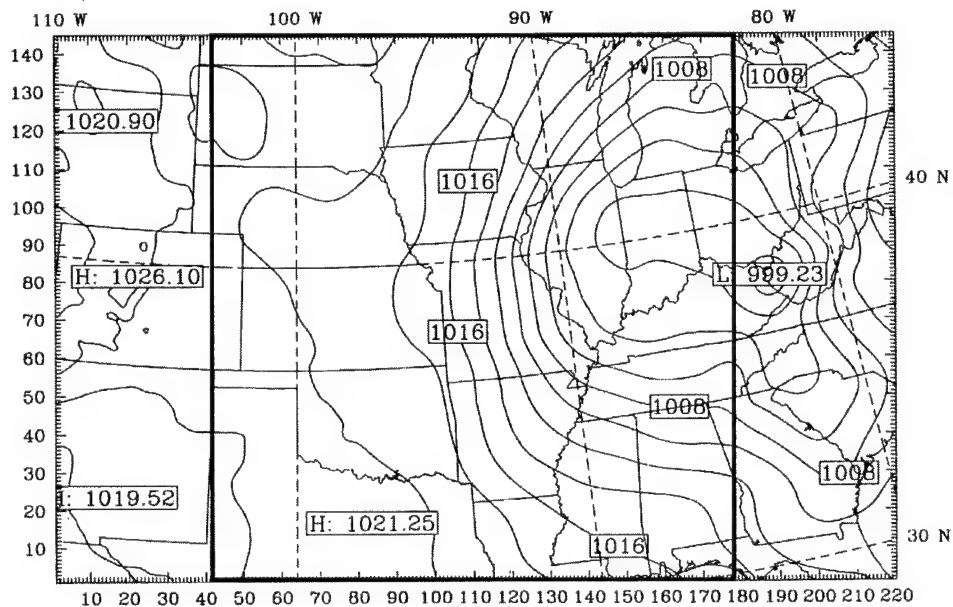
Figure 20   Sea level pressure analysis at 0000 UTC 20 January 1995.   This chart
shows contours of the model's sea level pressure analysis in 2 mb inter-
vals.   The research verification zone is enclosed by the box.

Figure 13). In Figure 14, the analysis at 0000 UTC 17 January 1995 depicted the system reaching a minimum pressure of about 995 mb as it moved eastward into western Kansas. This chart also showed a trough extending into deep southwest Texas and northern Mexico. The low pressure system over Kansas moved quickly to the north-northeast over the next 24 hours as the second low pressure system began to develop over southern Texas, as shown by the analysis in Figures 15 and 16. In Figure 17, the analysis at 1200 UTC 18 January 1995 indicated a strengthening of the second low pressure system as it moved eastward along the southern boundary of the verification zone. By 0000 UTC 19 January 1995, the system was seen moving north-northeast along the Mississippi River Basin and continued to strengthen (see Figure 18). The low pressure system reached a minimum pressure of about 997 mb over southeastern Missouri and southwestern Illinois prior to moving in an eastward direction along the Ohio River Valley and east of the verification zone, as shown by the analysis in Figures 19 and 20. Additional information about the second weather system can be found in Martin (11: 1998).

The May case is illustrated in Figures 21 through 29. The contours provide sea level pressure analysis in 2 mb intervals at a 12 km grid resolution. The box in each figure outlines the verification zone for this research. The figure coordinates are labeled in both grid point space and latitude/longitude. This case study featured the movement of a low pressure system into the verification zone from the southwestern lateral boundary. During the first 72 hours, a weak low pressure trough was seen over the Rocky Mountains and weak low pressure centers formed and moved across the southwestern portion of the verification zone, as shown by the analysis in Figures 21 through 24. The remainder of the verification zone was dominated by a high pressure system. In Figure 25, the analysis at 0000 UTC 8 May 1995 depicted a strong low pressure system along the southwestern lateral boundary over the panhandles of Oklahoma and Texas. The system reached a minimum pressure of about 991 mb as it moved north-northeast over western Kansas, as shown by the analysis in Figure

34

Figure 21   Sea level pressure analysis at 0000 UTC 4 May 1995. This chart shows contours of the model's sea level pressure analysis in 2 mb intervals. The research verification zone is enclosed by the box.

Figure 22   Sea level pressure analysis at 0000 UTC 5 May 1995. This chart shows contours of the model's sea level pressure analysis in 2 mb intervals. The research verification zone is enclosed by the box.

Figure 23   Sea level pressure analysis at 0000 UTC 6 May 1995. This chart shows contours of the model's sea level pressure analysis in 2 mb intervals. The research verification zone is enclosed by the box.
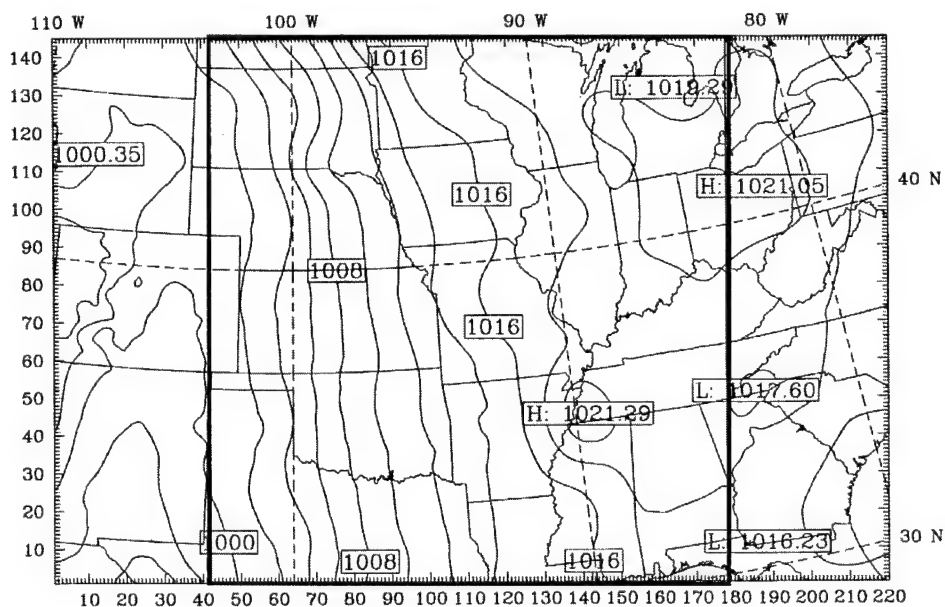
Figure 24   Sea level pressure analysis at 0000 UTC 7 May 1995. This chart shows contours of the model's sea level pressure analysis in 2 mb intervals. The research verification zone is enclosed by the box.
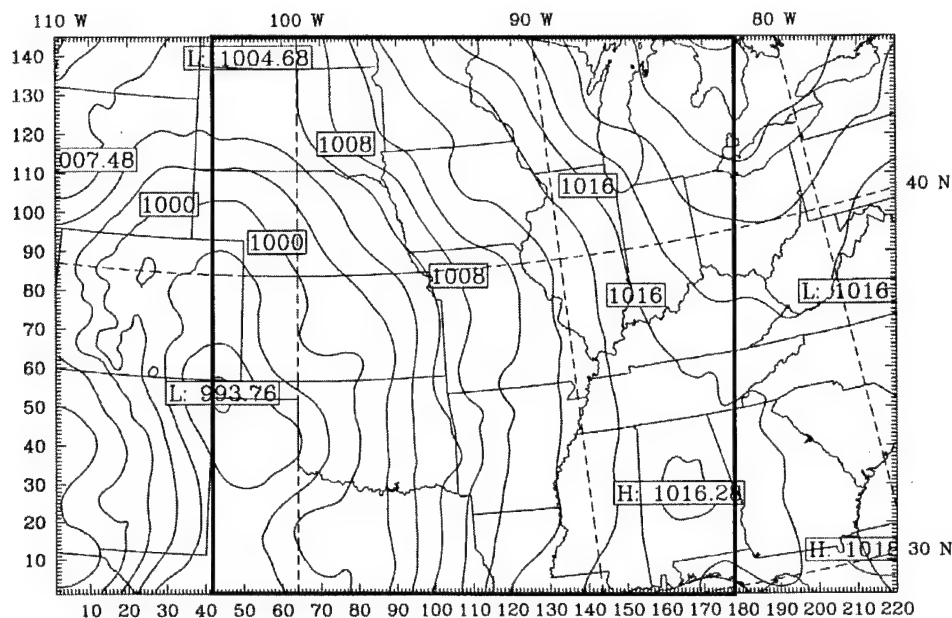
Figure 25   Sea level pressure analysis at 0000 UTC 8 May 1995. This chart shows contours of the model's sea level pressure analysis in 2 mb intervals. The research verification zone is enclosed by the box.
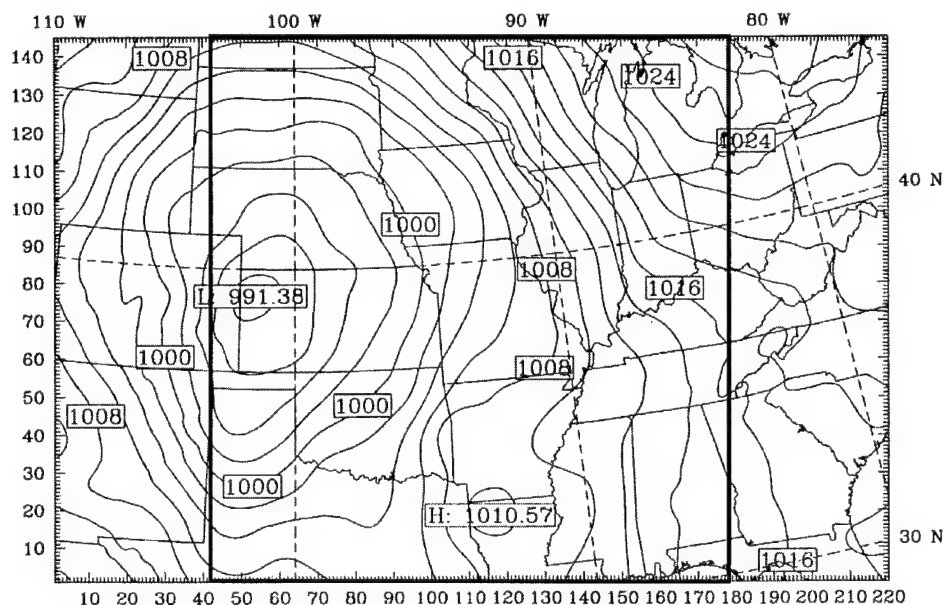
Figure 26   Sea level pressure analysis at 1200 UTC 8 May 1995. This chart shows contours of the model's sea level pressure analysis in 2 mb intervals. The research verification zone is enclosed by the box.
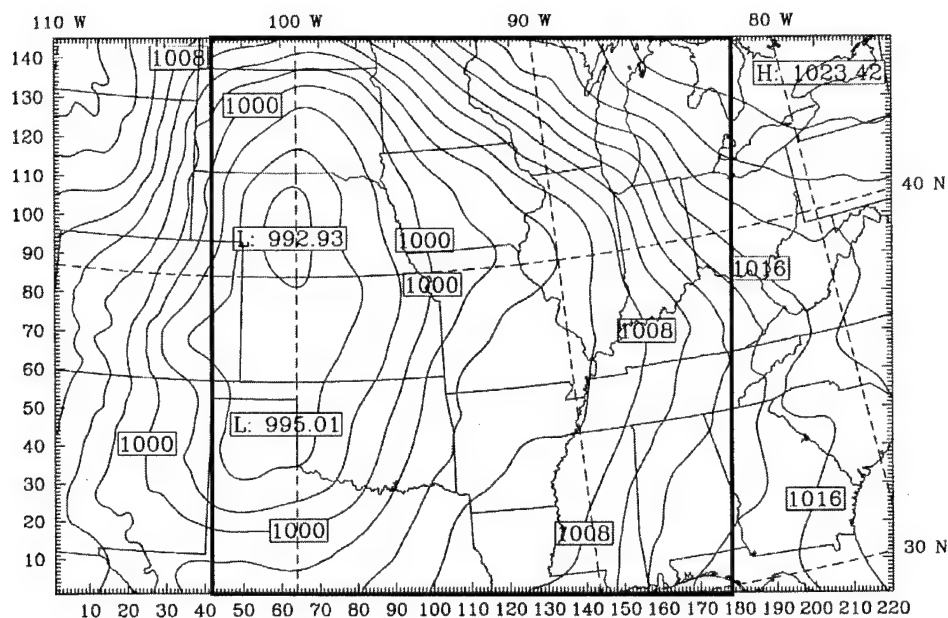
Figure 27   Sea level pressure analysis at 0000 UTC 9 May 1995. This chart shows contours of the model's sea level pressure analysis in 2 mb intervals. The research verification zone is enclosed by the box.
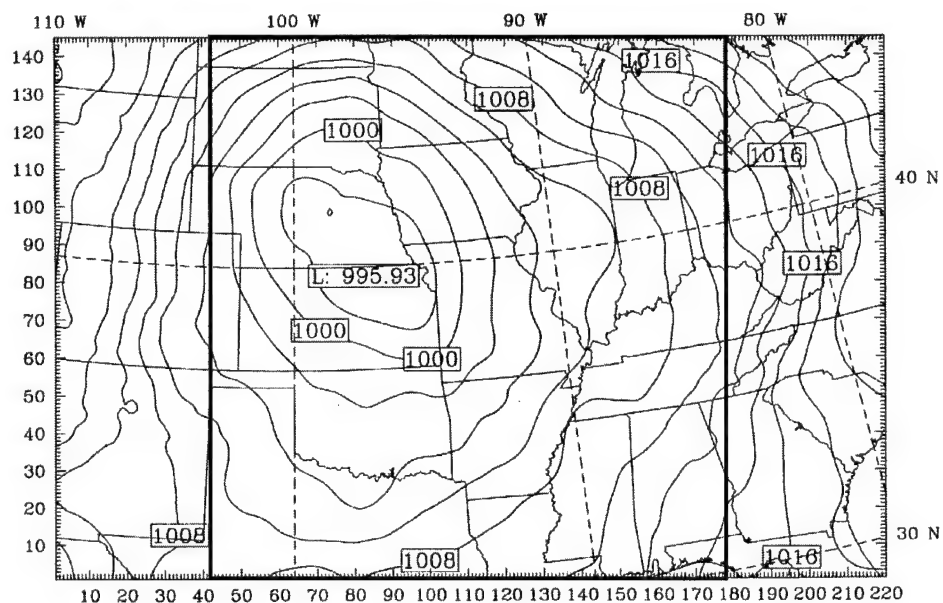
Figure 28   Sea level pressure analysis at 1200 UTC 9 May 1995. This chart shows contours of the model's sea level pressure analysis in 2 mb intervals. The research verification zone is enclosed by the box.
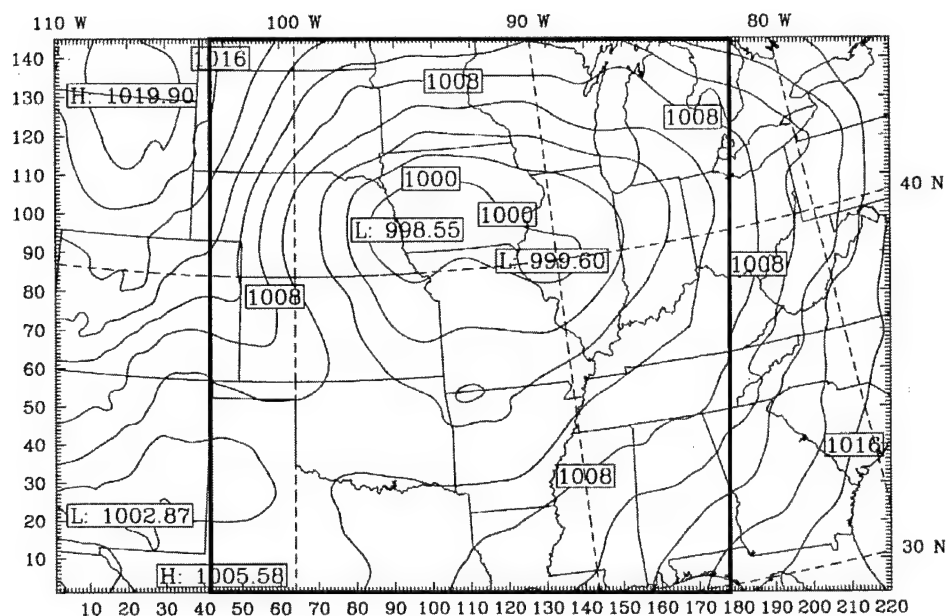
Figure 29   Sea level pressure analysis at 0000 UTC 10 May 1995. This chart shows
contours of the model's sea level pressure analysis in 2 mb intervals. The
research verification zone is enclosed by the box.

26.   Over the next 12 hours, the low pressure system continued to move slowly to
the north-northeast over central Nebraska (see Figure 27). In Figures 28 and 29, the
analysis at 1200 UTC 9 May 1995 and 0000 UTC 10 May 1995 indicated a drift of
the system eastward as it began to slowly fill. At 0000 UTC 10 May 1995, the low
pressure system was centered over Iowa with a trough extending to the southwest
over the panhandle of Texas. Additional information about this weather system can
be found in Atkins et al. (2: 1998).

3.3.2   Rawinsonde Data.   Rawinsonde data corresponding to the case stud-
ies identified for this research was obtained from the Air Force Combat Climatology
Center (AFCCC). Figure 30 shows the 21 locations where 0000 and 1200 UTC
rawinsonde soundings were available to verify against the model forecasts of the
January case study, whereas Figure 31 shows the 21 locations where 0000 and 1200
UTC rawinsonde soundings were available to verify against the model forecasts of
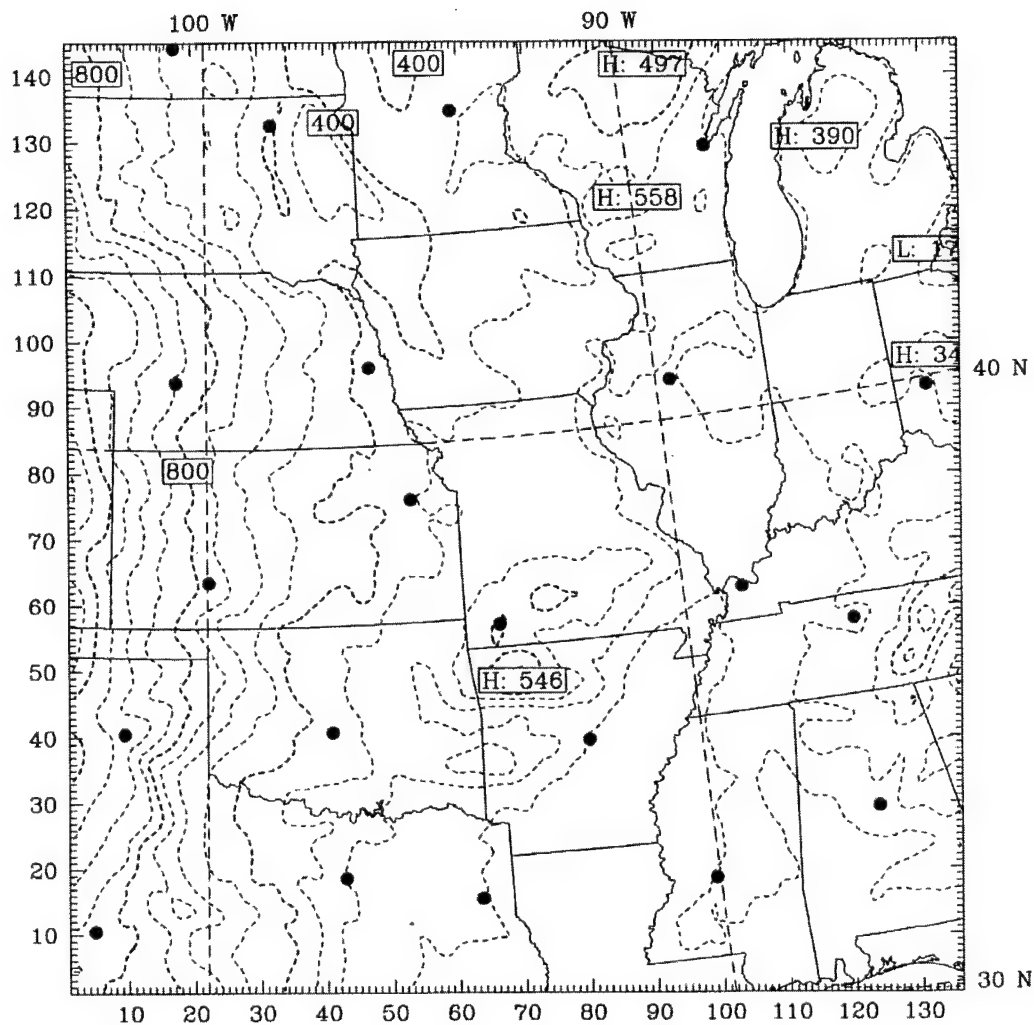
Figure 30   January rawinsonde locations.   This figure shows the rawinsonde sounding locations (•) used to verify the model forecasts of the January case study.   The dashed lines provide the terrain height in 100 m intervals.   The coordinates are labeled in both grid point space and latitude/longitude.

40
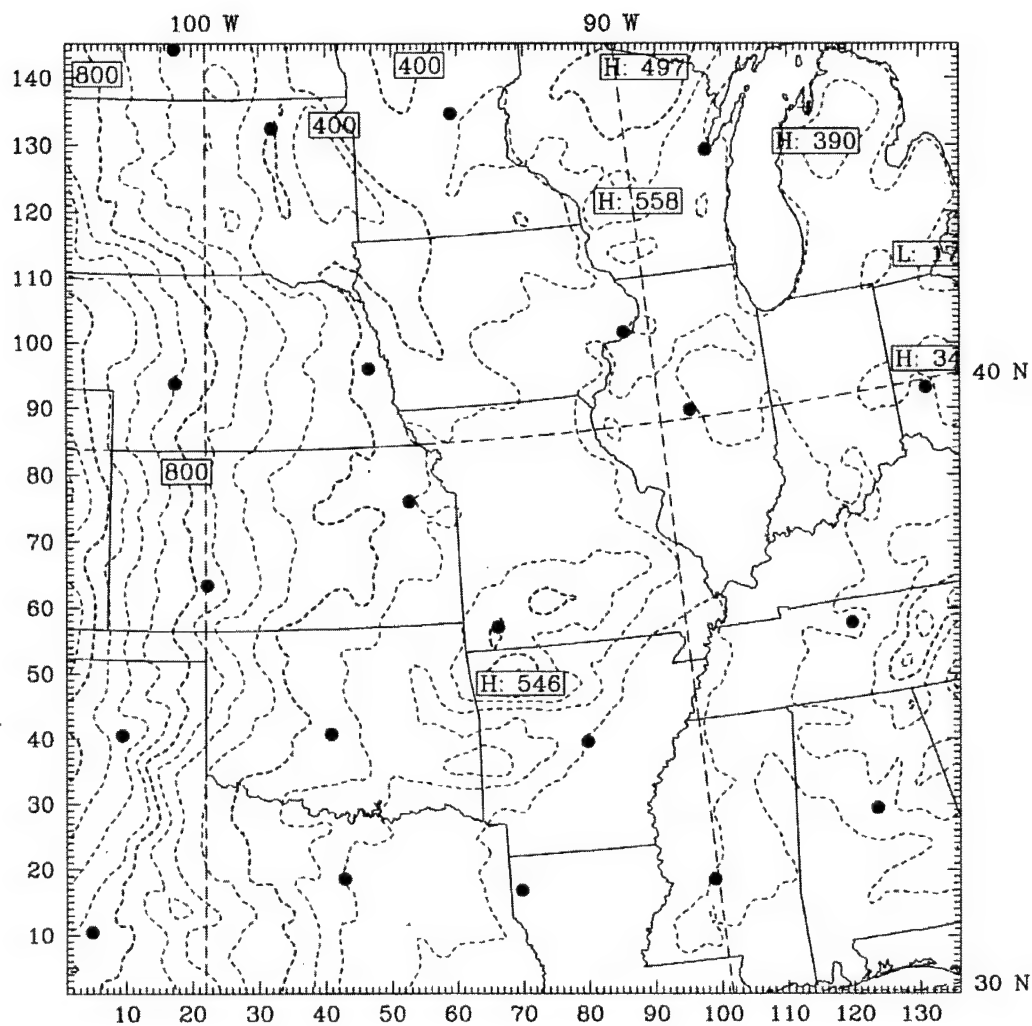
Figure 31   May rawinsonde locations. This figure shows the rawinsonde sounding locations (•) used to verify the model forecasts of the May case study. The dashed lines provide the terrain height in 100 m intervals. The coordinates are labeled in both grid point space and latitude/longitude.

41

the May case study. Although Figure 30 and Figure 31 are similar, some of the rawinsonde launch sites were different between the two cases. The dashed lines in both figures provides the terrain height in 100 meter intervals. A total of 504 rawinsonde soundings were provided by AFCCC of which seven were eliminated due to an asynoptic time or limited data (i.e., fewer than 25 levels in the sounding). A Fortran program was used to log-pressure interpolate missing and bogus data in the remaining 497 rawinsonde soundings over the verification zone. The general formula for log-pressure interpolation is given by

$$
var(k) = var(k-a) + \ln\left\{\frac{prs(k)}{prs(k-a)}\right\} \cdot \left\{\frac{var(k+b)-var(k-a)}{\ln\left[prs(k+b)/prs(k-a)\right]}\right\} \quad , \quad (2)
$$

where $var(k)$ is the missing or bogus value being calculated, $var(k-a)$ and $var(k+b)$ are the values below and above the missing value, a and b are integer constants, and $prs(k)$ represents the atmospheric pressure at a specified vertical level. It should be noted that wind directional computations require a decomposition into u and v wind components prior to calculation of a missing value.

3.3.3   Model Forecast Soundings.   Model soundings were generated in this research using a Fortran program.   The program, read in RIP formatted model output, located the precise grid coordinates for the launch sites where rawinsonde soundings were available, and generated a forecast atmospheric sounding using four-point inverse weighted interpolation of the surrounding grid points. The four-point inverse weighted interpolation was performed using the following formula

$$
var_{site}(k) = \frac{\sum_i \sum_j \left(1/r_{ij} \cdot var(j,i,k)\right)}{\sum_i \sum_j 1/r_{ij}} \quad , \quad (3)
$$

where var_{site} is the forecast variable being calculated at a given site and sigma level (k), r_{ij} represents the distance between the point being calculated and a particular x,y coupled grid point in the domain, and $var(j,i,k)$ represents the surrounding grid

Table 2	Excerpt of a model sounding				
sigma (σ)	p (mb)	hgt (m)	T (K)	u (m/s)	v (m/s)
0.99500000	982.57	232.6	285.77	-2.16	9.18
0.98500001	974.14	305.0	285.58	-2.31	12.09
0.97000003	961.50	414.7	285.23	-2.11	14.45
0.94499999	940.45	600.2	284.66	-1.22	16.66
0.90999997	911.04	866.1	284.26	2.19	18.71
0.87000000	877.52	1179.2	283.28	7.45	17.12
0.82500005	839.84	1544.0	281.87	9.77	13.90
0.77499998	798.00	1966.4	280.45	9.69	10.80
0.72500002	756.12	2408.4	277.92	9.10	8.69
0.67499995	714.11	2872.3	274.71	9.34	9.28

points used in the computation. The method of locating a precise location on the model grid will be discussed in the next chapter. Table 2 is an excerpt from one of the 8064 model soundings generated in this research. The first column contains the model sigma level. The remaining columns provide pressure (p) in millibars, geopotential height (hgt) in meters, temperature (T) in Kelvin, u-component of the wind (u) in meters per second, and v-component of the wind (v) in meters per second, respectively.

3.3.4 Precipitation Data. Precipitation data coinciding with the case studies of this research was provided by AFCCC. The data consisted of 6-hr and 24-hr cumulative totals for sites within the research verification zone. Reporting times for the 24-hr cumulative precipitation were 0000, 0600, 1200, and 1800 UTC. Verification was limited to those stations reporting 24-hr cumulative precipitation at 1200 UTC, since the largest number of reports were found for this reporting time. The sites where precipitation totals were available at 1200 UTC to verify against the January and May case studies are shown in Figures 32 and 33, respectively. Each station represents a location where a report was provided at least once during the verification period; thus, the number of available reports varied from one verification time to another. All verification times, except 1200 UTC 16 January 1995, had

43
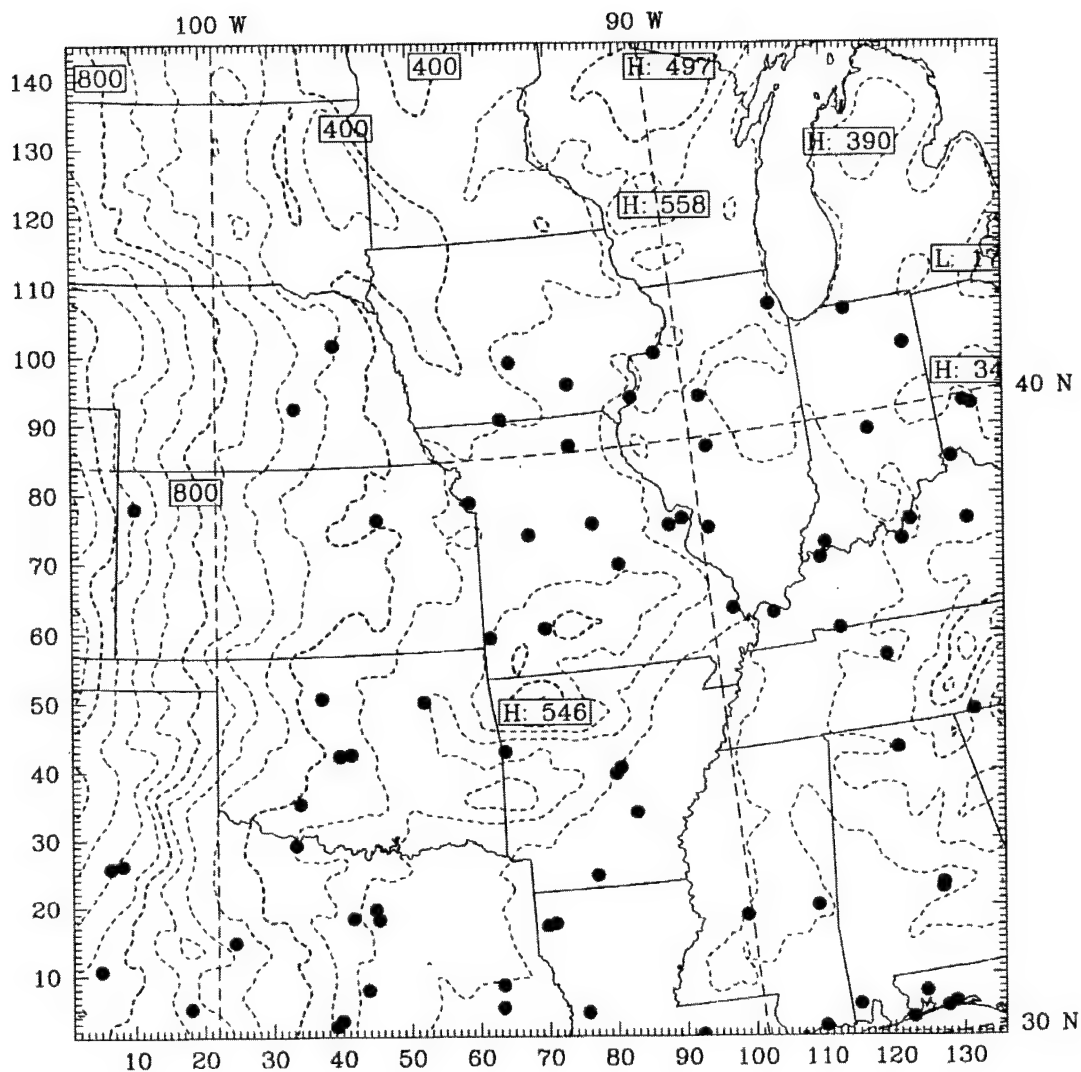
Figure 32   January precipitation reporting sites.   This figure shows the locations
(•) where 24 hr cumulative precipitation was reported at 1200 UTC
and used in this research to verify the model forecasts of the January
case study.   The dashed lines provide the terrain height in 100 m in-
tervals.   The coordinates are labeled in both grid point space and
latitude/longitude.
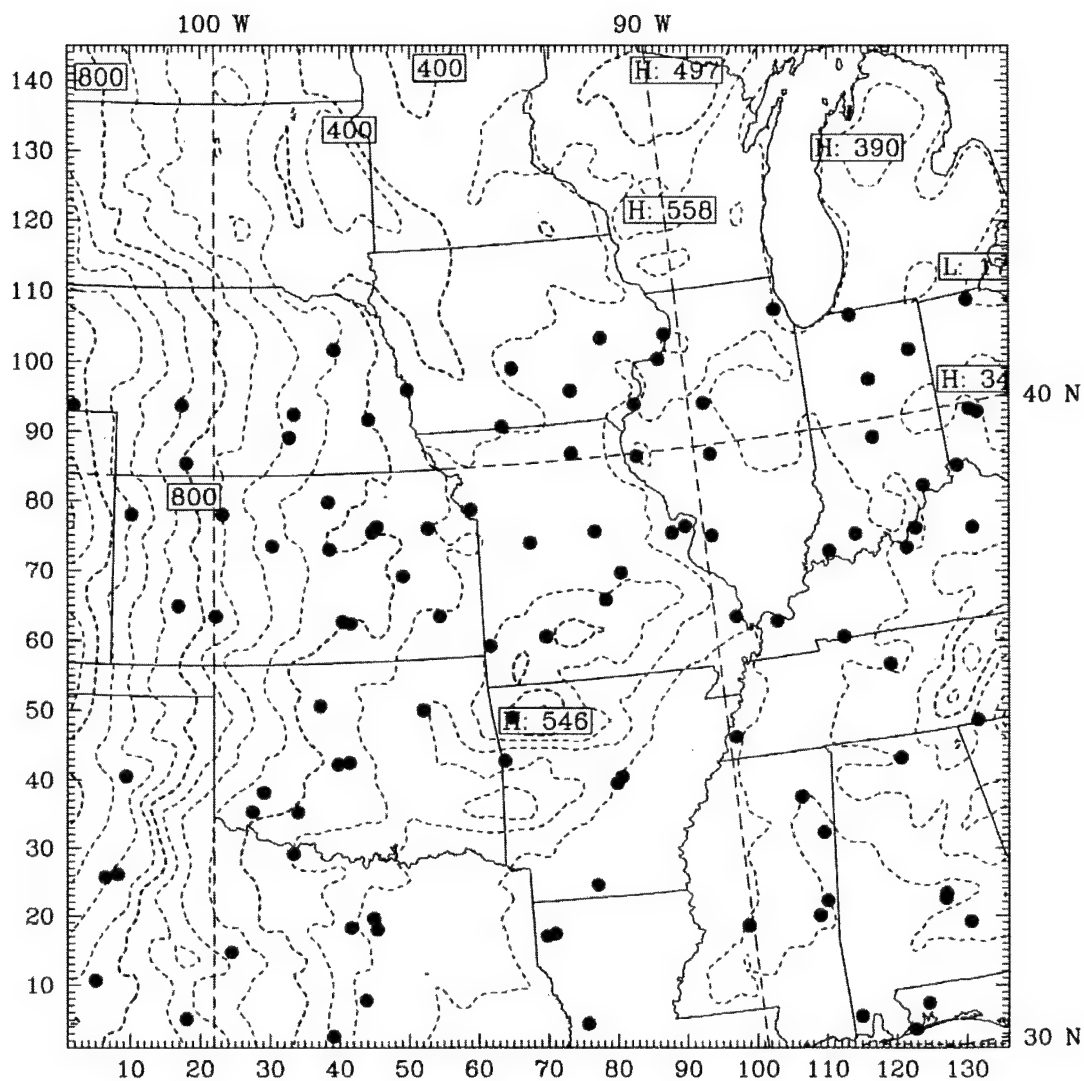
Figure 33   May precipitation reporting sites.   This figure shows the locations (•)
where 24 hr cumulative precipitation was reported at 1200 UTC and
used in this research to verify the model forecasts of the May case study.
The dashed lines provide the terrain height in 100 m intervals.   The
coordinates are labeled in both grid point space and latitude/longitude.

between 22 and 66 observations to verify against. The computations performed on precipitation and described in the next chapter for 1200 UTC 16 January 1995 should be considered suspicious, since the number of available observations was only eight and likely unrepresentative of the true amount of precipitation observed.

IV. Analysis and Results

4.1 Overview

This chapter presents the findings of this research. The chapter begins with a discussion of the root mean square error (RMSE) calculation used to measure the forecast accuracy of the various model nested domains outlined in Chapter 3. Then, the two common methods of employing the RMSE calculation are examined. The final three sections are used to present the findings related to the three questions posed in Chapter 1.

4.2 Root Mean Square Error Calculations

4.2.1 Verification Methods. In the last chapter, the configuration of the MM5 modeling system to conduct the current research and the verification zone were established. The next step was to establish the type of verification to be used in answering the questions posed in Chapter 1. Since the overall forecast accuracy of the MM5 modeling system was not the main focus of this research, the author chose to determine the relative forecast accuracy between various domains by calculating the RMSE of several primary forecast fields. The forecast variables chosen for verification were geopotential height, temperature, wind speed, and wind direction. In addition, RMSE was calculated on the 24 hr cumulative precipitation since it represented a field traditionally assumed to be better forecasted by finer resolution grid models. Simply stated, RMSE is a measure of the absolute distance a predicted variable deviates from the observation. The equation for calculating the RMSE can be found in Pielke (14: 1984) or Wilks (23: 1995) and is given by the following equation

$$RMSE_{var} = \left[\frac{\sum_{k=1}^{K_z} \sum_{s=1}^{S_{xy}} (var_{obs}(s,k) - var_{pred}(s,k))^2}{S_{xy}K_z} \right]^{1/2} , \qquad (4)$$

where var_{obs} is the observed value of the variable, var_{pred} is the predicted value of the variable, S_{xy} is the number of rawinsonde stations, and K_z is the number of grid points in the vertical. Although the predicted value in the RMSE calculation is set as the model's forecast values, the observed value in the calculation has traditionally been considered either the values from the model's analysis field, which coincides with the forecast, or observations from a meteorological observing device (i.e., rawinsonde data). In either case, the observed variable is treated as "truth" and all sources of observational error are neglected. The use of the model's analysis field as the observed variable is referred to as grid-to-grid verification, while the use of rawinsonde data is considered grid-to-station verification. The following paragraphs will discuss these two methods and justify the choice of method for the current research.

4.2.2 Grid-to-Grid Verification. The use of grid-to-grid verification has been commonly used in numerical weather prediction studies throughout the literature. This type of difference calculation is fairly simple to accomplish since many of the points to be compared are coincident in space. However, this method should be used with caution when conducting fine resolution grid modeling studies, such as the current research. White et al. (22: 1999) found that grid-to-grid verification was prone toward a low-resolution grid bias. The 700 mb temperature difference plots in figures 34 through 39 show an example of this bias. Although the error pattern is similar between the low-resolution (36 km) grid in Figure 34 and the higher resolution (12 km) grids in Figures 35 through 39, the magnitudes suggest that the overall error was smallest in the low-resolution grid. In contrast, grid-to-station verification using rawinsonde data for the locations marked by the dots (•) indicated that the low-resolution grid produced the worst forecast when compared to any of the two-way nested, high-resolution grids (as shown in Table 16 of Appendix A). A Fortran program was used to calculate the grid-to-grid differences used to plot the example charts in Figures 34 through 39.
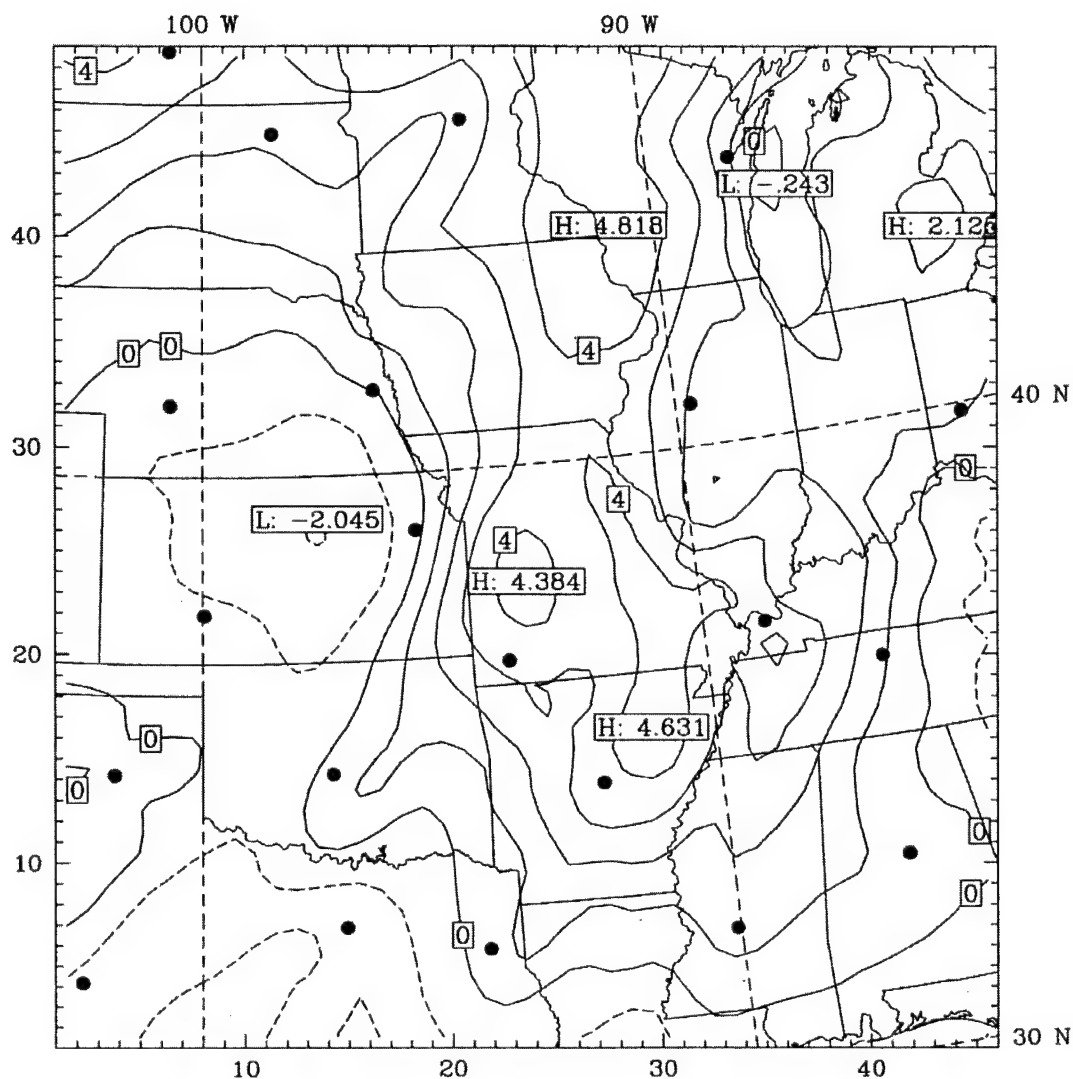
Figure 34   Temperature difference (700 mb) for 84 hr 15 January 1995 forecast outer domain.   This chart shows the temperature difference of the 36 km resolution outer domain between the 84 hr 15 January 1995 model forecast and the model analysis at 1200 UTC 18 January 1995. The contours are in one degree intervals with the solid lines (+ values) representing a warm bias in the forecast field and the dashed lines (- values) representing a cold bias. The dots (•) show the locations used for grid-to-station verification. The coordinates are labeled in both grid point space and latitude/longitude.

49
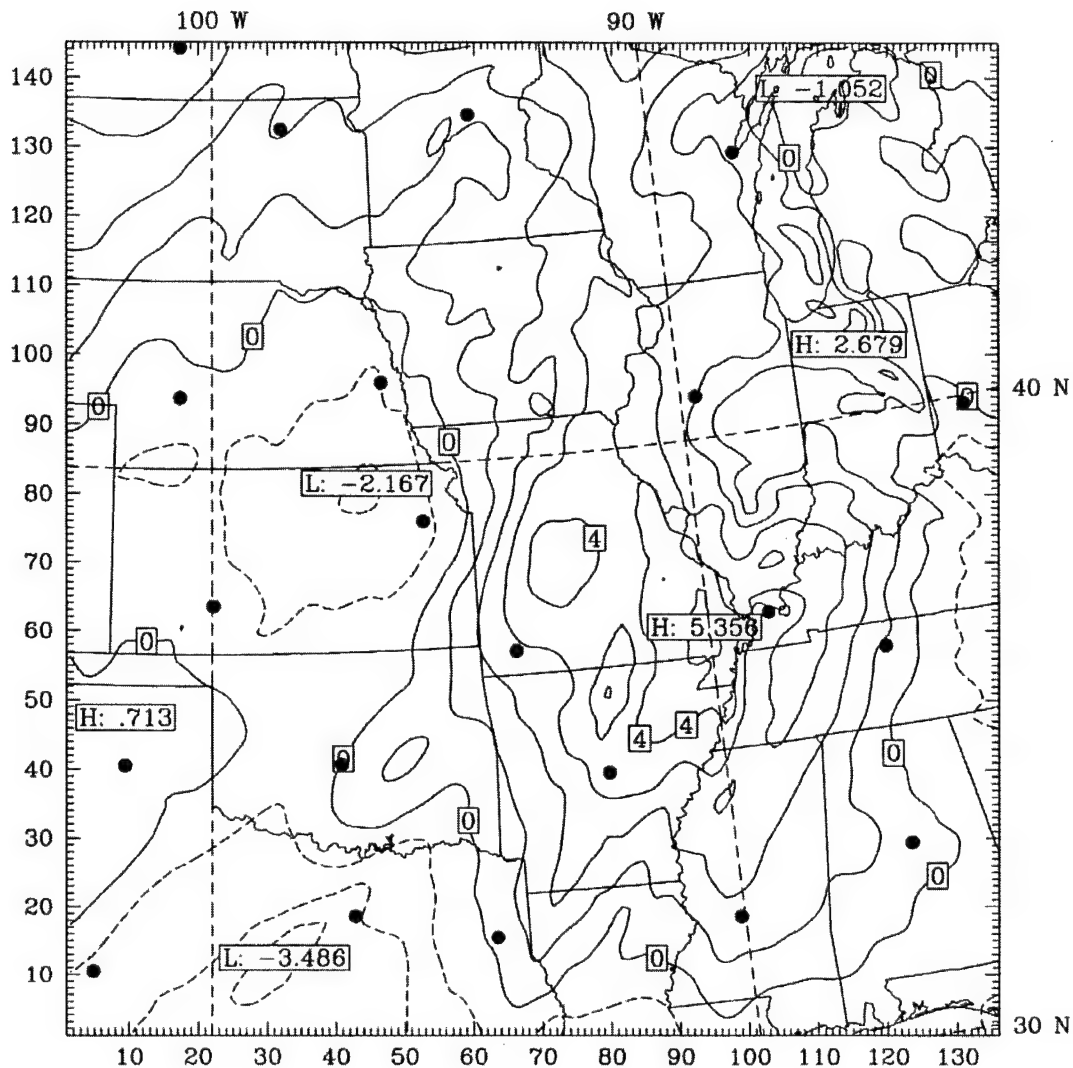
Figure 35   Temperature difference (700 mb) for 84 hr 15 January 1995 forecast two-way nested Domain A. This chart shows the temperature difference of the 12 km resolution two-way nested domain between the 84 hr 15 January 1995 model forecast and the model analysis at 1200 UTC 18 January 1995. The contours are in one degree intervals with the solid lines (+ values) representing a warm bias in the forecast field and the dashed lines (- values) representing a cold bias. The dots (•) show the locations used for grid-to-station verification. The coordinates are labeled in both grid point space and latitude/longitude.
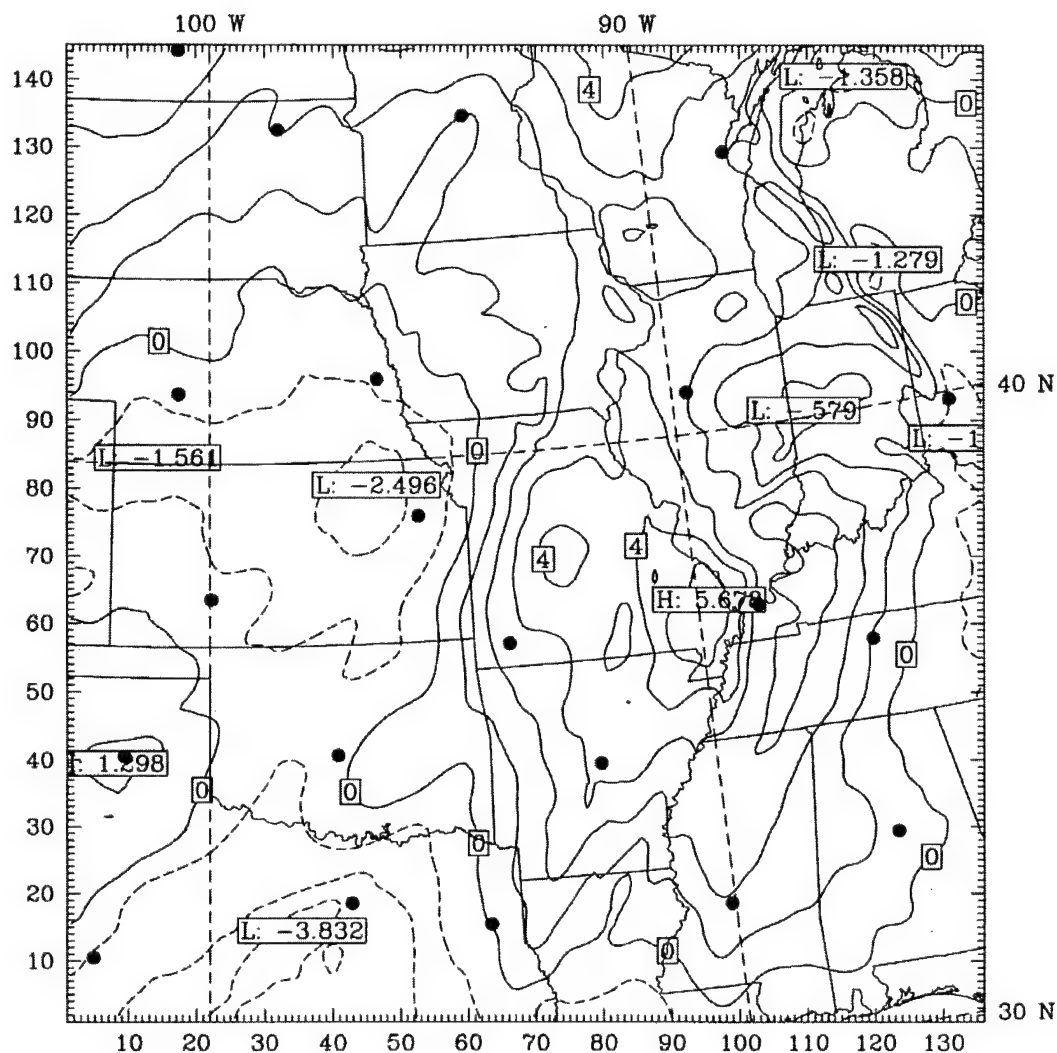
Figure 36   Temperature difference (700 mb) for 84 hr 15 January 1995 forecast two-way nested Domain B. This chart shows the temperature difference of the 12 km resolution two-way nested domain between the 84 hr 15 January 1995 model forecast and the model analysis at 1200 UTC 18 January 1995. The contours are in one degree intervals with the solid lines (+ values) representing a warm bias in the forecast field and the dashed lines (- values) representing a cold bias. The dots (•) show the locations used for grid-to-station verification. The coordinates are labeled in both grid point space and latitude/longitude.

51
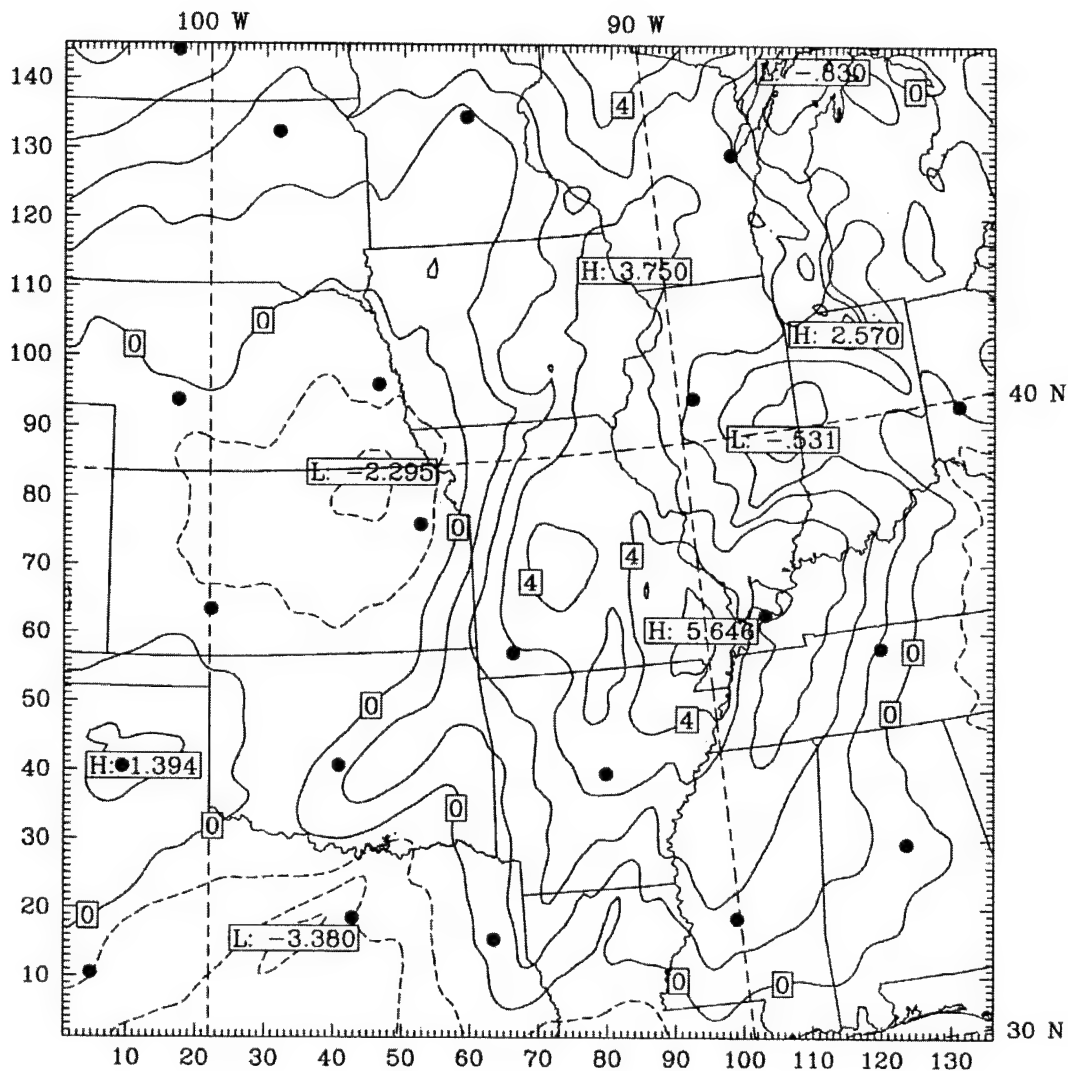
Figure 37   Temperature difference (700 mb) for 84 hr 15 January 1995 forecast two-way nested Domain C. This chart shows the temperature difference of the 12 km resolution two-way nested domain between the 84 hr 15 January 1995 model forecast and the model analysis at 1200 UTC 18 January 1995. The contours are in one degree intervals with the solid lines (+ values) representing a warm bias in the forecast field and the dashed lines (- values) representing a cold bias.   The dots (•) show the locations used for grid-to-station verification. The coordinates are labeled in both grid point space and latitude/longitude.
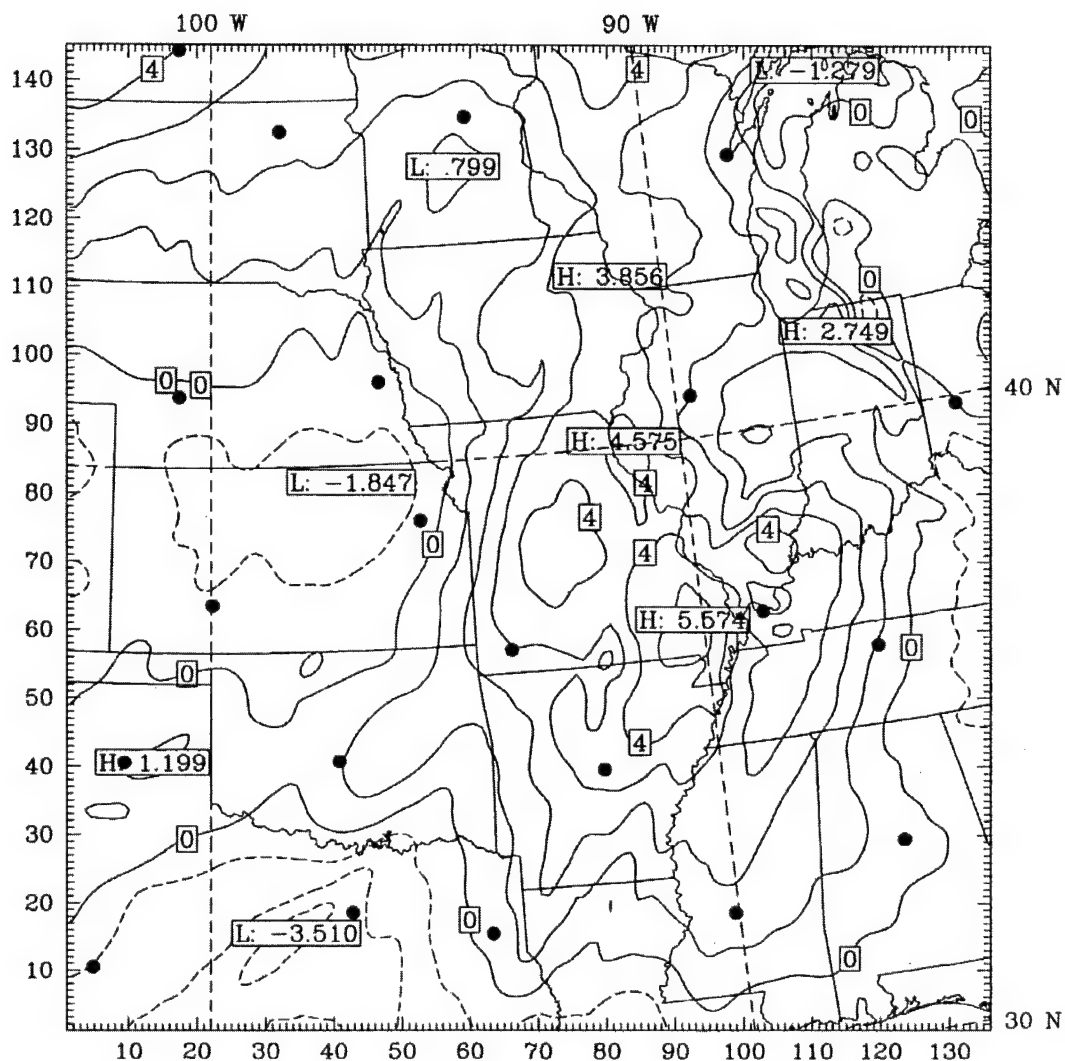
Figure 38   Temperature difference (700 mb) for 84 hr 15 January 1995 forecast
two-way nested Domain D. This chart shows the temperature difference
of the 12 km resolution two-way nested domain between the 84 hr 15
January 1995 model forecast and the model analysis at 1200 UTC 18
January 1995. The contours are in one degree intervals with the solid
lines (+ values) representing a warm bias in the forecast field and the
dashed lines (- values) representing a cold bias. The dots (•) show
the locations used for grid-to-station verification. The coordinates are
labeled in both grid point space and latitude/longitude.
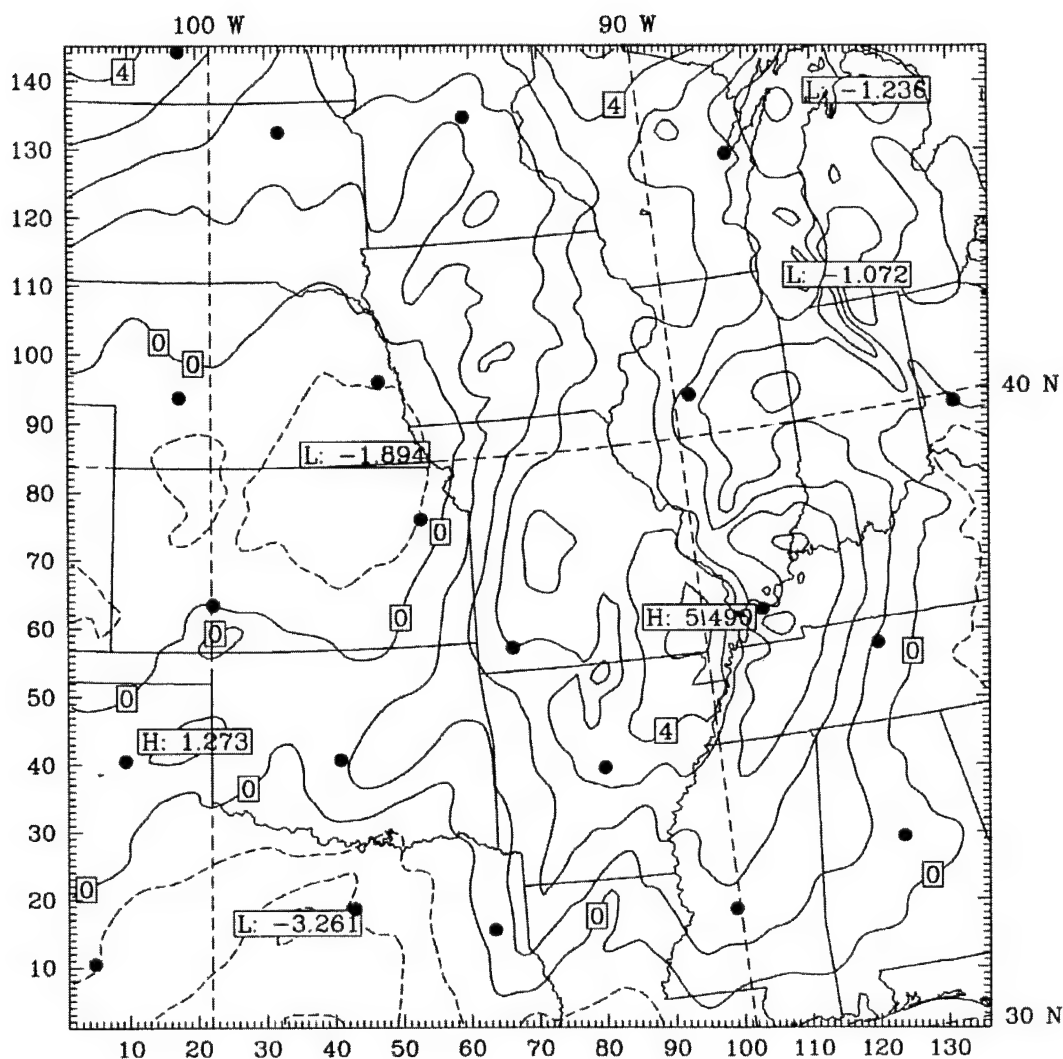
Figure 39   Temperature difference (700 mb) for 84 hr 15 January 1995 forecast
two-way nested Domain E. This chart shows the temperature difference
of the 12 km resolution two-way nested domain between the 84 hr 15
January 1995 model forecast and the model analysis at 1200 UTC 18
January 1995. The contours are in one degree intervals with the solid
lines (+ values) representing a warm bias in the forecast field and the
dashed lines (- values) representing a cold bias. The dots (•) show
the locations used for grid-to-station verification. The coordinates are
labeled in both grid point space and latitude/longitude.

There are two reasons to suspect a low resolution bias in the current research. First, the 2.5 degree gridded data from the medium range forecast (MRF) model used to initialize the MM5 modeling system varies in resolution from 238 km along the southern edge of the verification zone to 190 km along the northern edge. These resolutions are substantially lower than those being forecast by either the 36 km outer domain or 12 km nested domains in this research. A second source of this suspected bias comes from the input of rawinsonde data into the MM5 modeling system. James (9: 1995) reported, "the average distance between adjacent stations is about 700 km" globally. However, the spacing between adjacent launch sites over land in the northern hemisphere is typically smaller. Using Figures 30 and 31 from the last chapter, it can be shown that the average rawinsonde spacing over the verification zone is approximately 250-300 km. Again, the best resolution of the input data is much coarser than those being used in the forecast fields of this research. Since atmospheric waves shorter than the span of three observation points cannot be resolved by the model's analysis field, any verification using the model's analysis field will neglect to accurately account for the development of small-scale features on a fine resolution grid. While grid-to-grid comparisons are useful for quantifying differences between forecast fields, the initialization processes of the model will ultimately influence the rawinsonde observations being used as "truth". Therefore, the use of grid-to-station verification has been chosen for the current research.

4.2.3 Grid-to-Station Verification. Unlike grid-to-grid verification, the points to be compared in grid-to-station verification are rarely coincident. Therefore, the key step in performing this type of verification requires locating the observation point, or rawinsonde launch site, in reference to the model grid. For a discussion on converting map projections to a model grid the reader is referred to Haltiner and Williams (7: 1980) and Djuric (5: 1994). In the current research, a Lambert conical projection was used and the equations to convert latitude/longitude to grid space follow those found in the RIP post-processing code (16: Stoelinga 1997). The

equation to find the grid point in the y-direction is given by

$$riy = riy_c - \frac{r}{\Delta x} - \frac{r_o \left[\tan\left(\frac{\pi}{4} - \frac{\varphi}{2}\right)\right]^{K\cos(K\delta\lambda)}}{\Delta x} \quad , \qquad (5)$$

where riy_c represents the central point of the model grid in the y-direction, r is the radius of the latitude circle, r_o is a constant for the chosen projection, φ is the latitude, $\delta\lambda$ is the change in longitude, Δx is the distance between adjacent model grid points, and K is the cone formed by the Lambert conical projection. A similar equation for finding the grid point in the x-direction is given by

$$rjx = rjx_c + \frac{r_o \left[\tan\left(\frac{\pi}{4} - \frac{\varphi}{2}\right)\right]^{K\sin(K\delta\lambda)}}{\Delta x} \quad , \qquad (6)$$

where rjx_c represents the central point of the model grid in the x-direction. The cone of the Lambert conical projection (K) is given by

$$K = \log_{10}\left\{\frac{\cos\varphi_1}{\cos\varphi_2}\right\} \div \log_{10}\left\{\frac{\tan\left(\frac{\pi}{4} - \frac{\varphi_1}{2}\right)}{\tan\left(\frac{\pi}{4} - \frac{\varphi_2}{2}\right)}\right\} \quad , \qquad (7)$$

where φ_1 and φ_2 are true latitudes (set at 60 and 30 degrees latitude for the current research). The radius of the latitude circle (r) is given by

$$r = r_o \left[\tan\left(\frac{\pi}{4} - \frac{\varphi_c}{2}\right)\right]^K \quad , \qquad (8)$$

where φ_c is the central latitude of the model grid. The constant r_o is given by

$$r_o = a\left\{\frac{\sin\phi}{K\left(\frac{\phi}{2}\right)^K}\right\} \quad , \qquad (9)$$

where a is the mean radius of the earth, and ϕ is the colatitude of the true latitude φ_1 (i.e., $90° - \varphi_1$).

Once the exact locations of the rawinsonde launch sites were found, model soundings were generated as discussed in the last chapter. Then, RMSE verification was calculated using Equation 4, where var_{obs} was represented by the rawinsonde sounding and var_{pred} by the generated model soundings. Log-pressure interpolation was used to ensure the coincidence of vertical levels, and verification was calculated every 25 mb for layers. The rawinsonde sounding was assumed to represent "truth" in these calculations. Therefore, instrument errors were assumed to be negligible. The measurement errors of a radiosonde are reported to be within ±1 K for temperature, ±10 percent for relative humidity, and ±3-5 m/s for wind speeds by Daley (4: 1996) and James (9: 1995). In addition, it was assumed that the rawinsonde remains over the launch site as it ascends through the atmosphere. Although this assumption is unrealistic, the drift of the radiosonde has been in some part accounted for in the model's input data. A Fortran program was used to perform the aforementioned RMSE calculations and the results are found in the tables of Appendices A and B. The method used to verify the 24 hr cumulative precipitation was similar in nature, but required an additional Fortran program to account for the differences in the observational data set and to perform the necessary calculation of the model's 24 hr precipitation (*pcp*) totals. The equation used to calculate the model's 24 hr precipitation totals is given by

$$pcp_{24hr}(s,t) = pcp_{cv}(s,t) + pcp_{cv}(s,t-12) + pcp_{ncv}(s,t) + pcp_{ncv}(s,t-12) , \quad (10)$$

where s is the location of the surface report, t is time in hours, and cv and ncv symbolize convective and non-convective precipitation, respectively. The resulting RMSE calculations for precipitation are found in Appendix C.

4.3 Nested Grid Placement

4.3.1 General Discussion.   As stated in Chapter 1, this research has attempted to answer the question of whether optimally placing of the windward lateral

boundary of a limited area model (LAM) can improve forecast accuracy. This section explored these impacts by employing RMSE calculations on the model configuration discussed in Chapter 3. The meteorological variables that were examined to address the posed question are geopotential height, temperature, wind speed, and wind direction. The statistical plots have been normalized to provide a more meaningful representation of the results. Normalization allows different forecast variables to be directly compared. Additionally, various domains can be compared to determine the improvement or degradation of the model's forecast. The general form of the equation used to normalize the RMSE values is given by

$$RMSE_{norm} = \frac{RMSE_{grid\beta} - RMSE_{grid\alpha}}{RMSE_{grid\alpha}} \quad , \tag{11}$$

where $grid\alpha$ represents the control value (or standard), and $grid\beta$ represents the value to be compared to the set standard of $grid\alpha$.

4.3.2 Findings for Two-way Nesting.

4.3.2.1 General Discussion.   Before delving into the results for two-way nesting, a general description of the statistical plots in this subsection should benefit the reader. The plots in this subsection are standardized with time (in hours) along the abscissa, and RMSE or normalized RMSE along the ordinate. Normalized RMSE is either positive, negative, or zero. The zero line represents the control value which has been chosen as Domain B for each plot. A negative value represents a decrease in the RMSE, or improvement in the model's forecast, and vice versa. Each trace represents the model domain denoted in the key and was generated using the RMSE calculation for each verification time during the forecast period. It should also be noted that the resulting percentages of these normalized plots must be compared to the actual RMSE to quantify the decrease or increase in error (relative to domain B). Statistical plots have been generated for three layers in the atmosphere: 950/150

58

Figure 40   Geopotential height RMSE for the January case over a 950/150 mb layer (two-way nesting). This figure shows the RMSE for the outer domain (36 km) and the five high-resolution (12 km) two-way nested domains for the January case The domains represented by the traces are the Outer Domain (heavy solid), Domain A (heavy dotted), Domain B (dashed), Domain C (solid), Domain D (dotted), and Domain E (dash-dot).

mb, 950/700 mb, and 500/200 mb where verification was computed every 25 mb throughout the layer.

   4.3.2.2   Geopotential Height.   Figure 40 shows January geopotential height RMSE for the outer domain and the five two-way nested domains over a 950/150 mb layer (entire troposphere). This graph indicates that the RMSE generally increased with time as the various nested domain solutions diverged. Figure 40 should be used in conjunction with the next figure to obtain the actual decrease or increase of RMSE relative to Domain B. Figure 41 shows the statistical com-

59
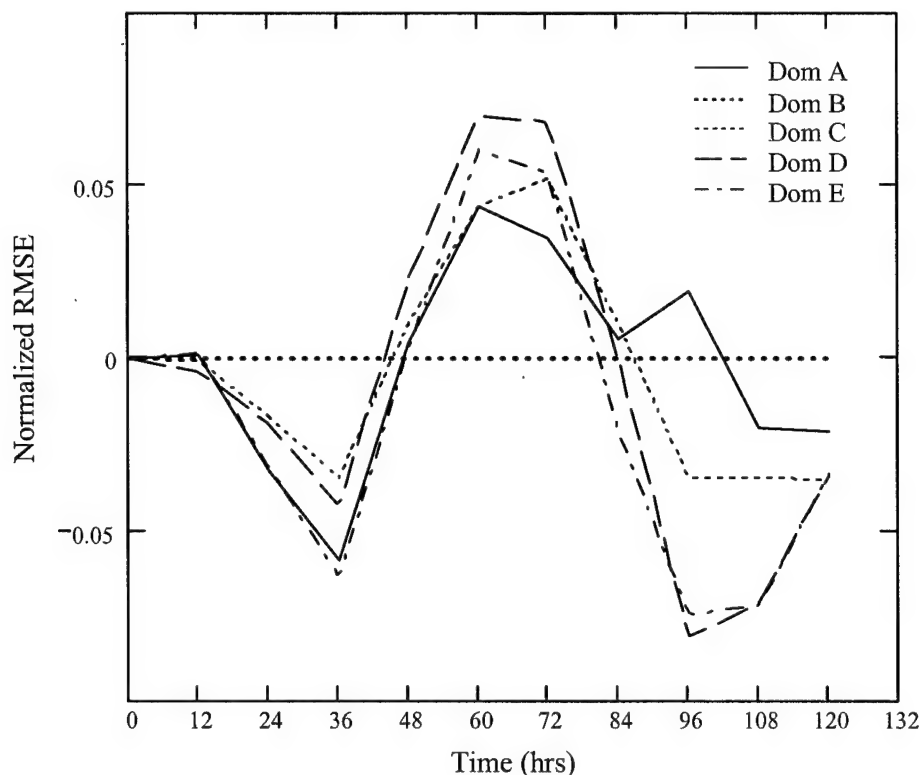
Figure 41   Two-way nested domain placement comparison (geopotential height) for the January case over a 950/150 mb layer. This figure compares the placement of the five high-resolution (12 km) two-way nested domains for the January case using normalized RMSE where the control value is from Domain B. The domains represented by the traces are Domain A (solid), Domain B (heavy dotted), Domain C (dotted), Domain D (dashed), and Domain E (dash-dot).

parison (geopotential height) of the five two-way nested domains for the January case over a 950/150 mb layer (33 verification levels). As seen from the graph, both the downstream (Domain A) and upstream (Domains C to E) domains yielded a forecast improvement relative to Domain B (the control) during the first 48 hours of the forecast period. However, this geopotential height improvement was small (1.5 meters or less), as seen from Figure 40. From the 60 hr to 72 hr forecast, Domain B appeared to produce the best forecast between the time when the first surface cyclone exited the verification zone through the northern boundary and the

Figure 42   Geopotential height RMSE for the May case over a 950/150 mb layer
(two-way nesting). This figure shows the RMSE for the outer domain
(36 km) and the five high-resolution (12 km) two-way nested domains
for the May case The domains represented by the traces are the Outer
Domain (heavy solid), Domain A (heavy dotted), Domain B (dashed),
Domain C (solid), Domain D (dotted), and Domain E (dash-dot).

second cyclone entered through the southern boundary.   After the 84 hr forecast,
the downstream domain yielded a similar solution to Domain B, while the upsteam
domains showed forecast improvement relative to Domain B. The most significant
improvement was yielded by Domains D and E with as much as 8.5 percent improve-
ment in geopotential height.   Similar patterns were seen for the 950/700 mb and
500/200 mb layers.

Figure 42 shows May geopotential height RMSE for the outer domain and the
five two-way nested domains over a 950/150 mb layer. This graph indicates that the

Figure 43   Two-way nested domain placement comparison (geopotential height) for the May case over a 950/150 mb layer. This figure compares the placement of the five high-resolution (12 km) two-way nested domains for the May case using normalized RMSE where the control value is from Domain B. The domains represented by the traces are Domain A (solid), Domain B (heavy dotted), Domain C (dotted), Domain D (dashed), and Domain E (dash-dot).

RMSE increased slowly during the first 84 hours, then more rapidly with time. The solutions of the nested domains began to diverge after 72 hours. Figure 43 shows the statistical comparison (geopotential height) of the five two-way nested domains for the May case over a 950/150 mb layer. This case showed similar results to the January case. As seen from the graph, both the downstream (Domain A) and upstream (Domains C to E) domains yielded a similar forecast relative to Domain B (the control) during the first 72 hours of the forecast period. The similarity of the geopotential height forecasts was also very apparent in Figure 42. Beyond the 72

Figure 44   Temperature RMSE for the January case over a 950/150 mb layer (two-way nesting).   This figure shows the RMSE for the outer domain (36 km) and the five high-resolution (12 km) two-way nested domains for the January case The domains represented by the traces are the Outer Domain (heavy solid), Domain A (heavy dotted), Domain B (dashed), Domain C (solid), Domain D (dotted), and Domain E (dash-dot).

hr forecast, Domain D (windward boundary at 112°W longitude) yielded the most forecast improvement relative to Domain B, while the remaining domains continued to showed a similar solution to Domain B. The most significant improvement was yielded by Domain D with as much as nine percent improvement in geopotential height during the period when the surface cyclone was in the verification zone. Similar patterns were seen for the 950/700 mb and 500/200 mb layers.

4.3.2.3   Temperature.   Figure 44 shows January temperature RMSE for the outer domain and the five two-way nested domains over a 950/150 mb layer.
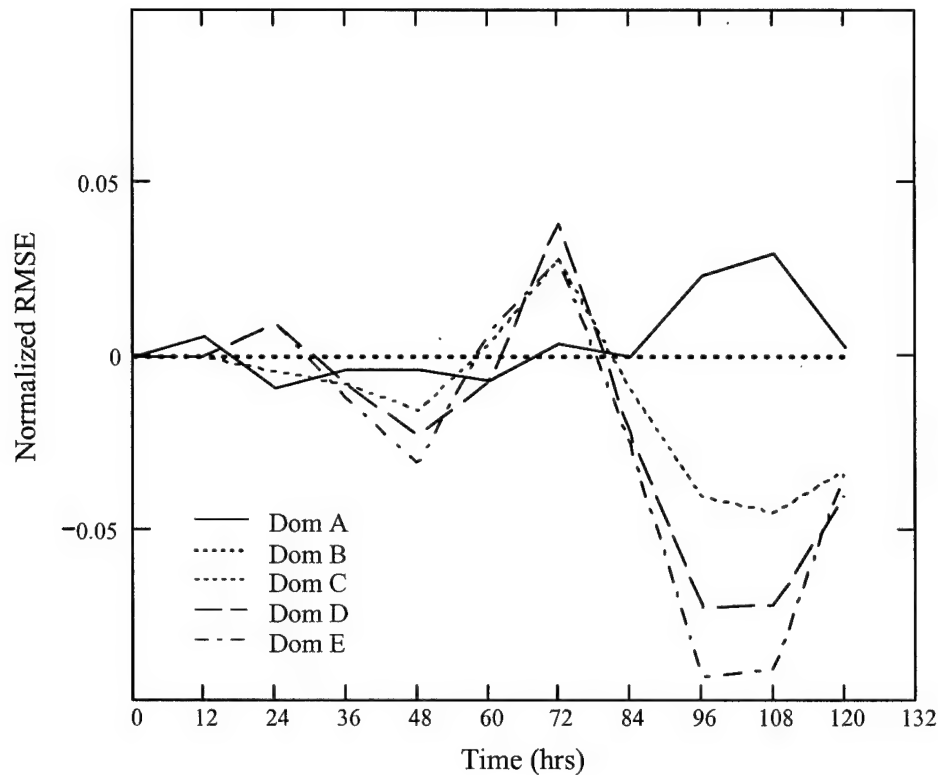
Figure 45   Two-way nested domain placement comparison (temperature) for the
January case over a 950/150 mb layer. This figure compares the place-
ment of the five high-resolution (12 km) two-way nested domains for
the January case using normalized RMSE where the control value is
from Domain B. The domains represented by the traces are Domain
A (solid), Domain B (heavy dotted), Domain C (dotted), Domain D
(dashed), and Domain E (dash-dot).

This graph indicates that the RMSE generally increased with time and the various
nested domain solutions began to diverge after 60 hours.   Figure 45 shows the
statistical comparison (temperature) of the five two-way nested domains for the
January case over a 950/150 mb layer. As seen from the graph, both the downstream
(Domain A) and upstream (Domains C to E) domains yielded a similar forecast
relative to Domain B (the control) during the first 84 hours of the forecast period.
This temperature similarity can also be seen in Figure 44. After the 84 hr forecast,
the downstream domain yielded a similar solution to Domain B, while the upsteam

64

Figure 46   Temperature RMSE for the January case over a 950/700 mb layer (two-way nesting).   This figure shows the RMSE for the outer domain (36 km) and the five high-resolution (12 km) two-way nested domains for the January case The domains represented by the traces are the Outer Domain (heavy solid), Domain A (heavy dotted), Domain B (dashed), Domain C (solid), Domain D (dotted), and Domain E (dash-dot).

domains showed forecast improvement relative to Domain B. Improvement relative to Domain B increased as the windward boundary was moved farther upstream (i.e., Domains C, D and E). Domain E had the most significant improvement with as much as 9.5 percent for temperature.

Figure 46 shows January temperature RMSE for the outer domain and the five two-way nested domains over a 950/700 mb layer (lower troposphere). This graph indicates that the RMSE increased rapidly during the first 36 hours and than leveled off with time. The various nested domain solutions began to diverge after 48 hours.
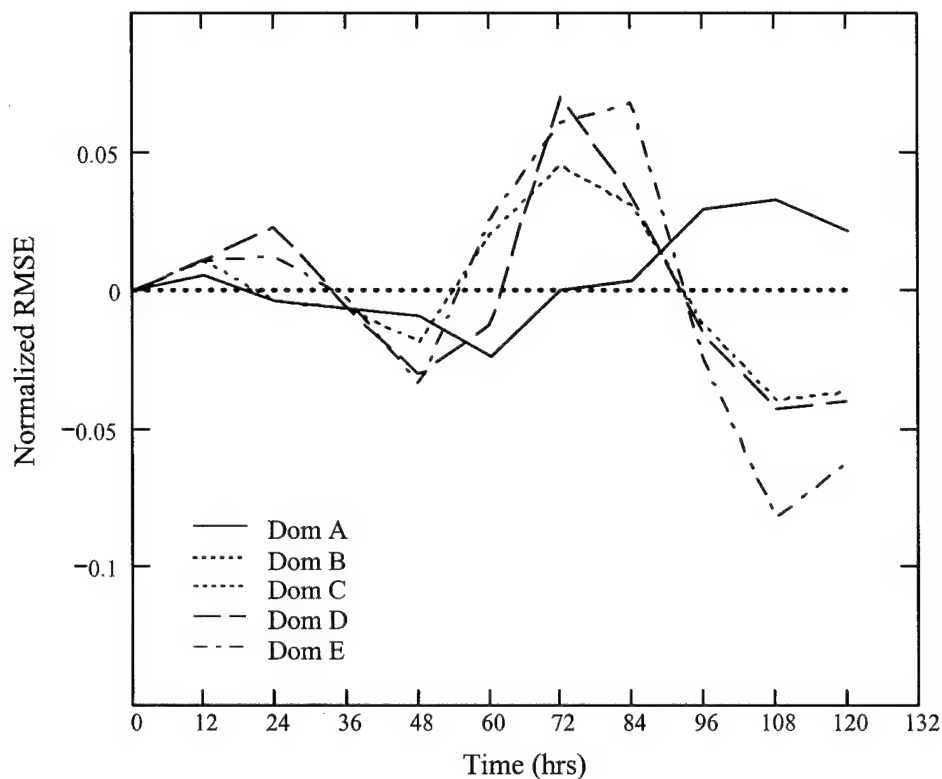
Figure 47   Two-way nested domain placement comparison (temperature) for the January case over a 950/700 mb layer. This figure compares the placement of the five high-resolution (12 km) two-way nested domains for the January case using normalized RMSE where the control value is from Domain B. The domains represented by the traces are Domain A (solid), Domain B (heavy dotted), Domain C (dotted), Domain D (dashed), and Domain E (dash-dot).

Figure 47 shows the statistical comparison (temperature) of the five two-way nested domains for the January case over a 950/700 mb layer (11 verification levels). As seen from the graph, the downstream domain (Domain A) yielded a similar forecast relative to Domain B (the control) throughout the forecast period. The upsteam domains (Domains C to E) showed an oscillator nature with forecast degradation between 60 to 84 hours and forecast improvement beyond 96 hours relative to Domain B. The most significant degradation was as much as 6.5 percent, while the most significant improvement was as much as 8 percent for temperature.

Figure 48   Temperature RMSE for the January case over a 500/200 mb layer (two-way nesting).   This figure shows the RMSE for the outer domain (36 km) and the five high-resolution (12 km) two-way nested domains for the January case The domains represented by the traces are the Outer Domain (heavy solid), Domain A (heavy dotted), Domain B (dashed), Domain C (solid), Domain D (dotted), and Domain E (dash-dot).

Figure 48 shows January temperature RMSE for the outer domain and the five two-way nested domains over a 500/200 mb layer (upper troposphere).   This graph indicates that the RMSE generally increased with time and the various nested domain solutions diverged.   Figure 49 shows the statistical comparison (temperature) of the five two-way nested domains for the January case over a 500/200 mb layer (13 verification levels).   As seen from the graph, the downstream domain (Domain A) yielded a similar forecast relative to Domain B (the control) during the entire forecast period.   The upsteam domains (Domains C to E) generally improved the

Figure 49   Two-way nested domain placement comparison (temperature) for the January case over a 500/200 mb layer. This figure compares the placement of the five high-resolution (12 km) two-way nested domains for the January case using normalized RMSE where the control value is from Domain B. The domains represented by the traces are Domain A (solid), Domain B (heavy dotted), Domain C (dotted), Domain D (dashed), and Domain E (dash-dot).

temperature forecast throughout the entire forecast period relative to Domain B. Improvement relative to Domain B increased as the windward boundary was moved farther upstream (i.e., Domains C, D and E) and was maximized during the two periods when cyclogenesis entered the verification zone. Domains D and E had the most significant improvements with as much as eight and ten percent improvement in temperature, respectively.

Figure 50 shows May temperature RMSE for the outer domain and the five two-way nested domains over a 950/150 mb layer. This graph indicates that the

Figure 50   Temperature RMSE for the May case over a 950/150 mb layer (two-way nesting).   This figure shows the RMSE for the outer domain (36 km) and the five high-resolution (12 km) two-way nested domains for the May case   The domains represented by the traces are the Outer Domain (heavy solid), Domain A (heavy dotted), Domain B (dashed), Domain C (solid), Domain D (dotted), and Domain E (dash-dot).

RMSE generally increased with time and the solutions of the nested domains began to diverge after 48 hours. Figure 51 shows the statistical comparison (temperature) of the five two-way nested domains for the May case over a 950/150 mb layer. This case showed similar results to the January case. As seen from the graph, both the downstream (Domain A) and upstream (Domains C to E) domains yielded a similar forecast relative to Domain B (the control) during the first 48 to 60 hours of the forecast period. The similarity of the temperature forecasts was also apparent in Figure 50. Beyond the 60 hr forecast, Domain D (windward boundary at 112°W

69

Figure 51   Two-way nested domain placement comparison (temperature) for the May case over a 950/150 mb layer. This figure compares the placement of the five high-resolution (12 km) two-way nested domains for the May case using normalized RMSE where the control value is from Domain B. The domains represented by the traces are Domain A (solid), Domain B (heavy dotted), Domain C (dotted), Domain D (dashed), and Domain E (dash-dot).

longitude) yielded the most forecast improvement relative to Domain B. Domains C and D showed forecast improvement from 60 to 108 hours, but showed a similar solution to Domain B after 108 hours. The most significant improvement was yielded by Domain D with as much as 6.5 percent improvement in temperature during the period of maximum cyclogenesis in the verification zone. Similar patterns to those of the January case were seen for the 950/700 mb and 500/200 mb layers.

4.3.2.4   Wind Speed.   Figure 52 shows January wind speed RMSE for

Figure 52   Wind speed RMSE for the January case over a 950/150 mb layer (two-way nesting).   This figure shows the RMSE for the outer domain (36 km) and the five high-resolution (12 km) two-way nested domains for the January case The domains represented by the traces are the Outer Domain (heavy solid), Domain A (heavy dotted), Domain B (dashed), Domain C (solid), Domain D (dotted), and Domain E (dash-dot).

the outer domain and the five two-way nested domains over a 950/150 mb layer. This graph indicates that the RMSE generally increased with time with minimal divergence in the various solutions of the nested domains. Figure 53 shows the statistical comparison (wind speed) of the five two-way nested domains for the January case over a 950/150 mb layer. As seen from the graph, both the downstream (Domain A) and upstream (Domains C to E) domains exhibited an oscillatory nature relative to Domain B (the control) throughout the entire forecast period. The upstream domains showed as much as four percent improvement relative to Domain B

71

Figure 53   Two-way nested domain placement comparison (wind speed) for the January case over a 950/150 mb layer. This figure compares the placement of the five high-resolution (12 km) two-way nested domains for the January case using normalized RMSE where the control value is from Domain B. The domains represented by the traces are Domain A (solid), Domain B (heavy dotted), Domain C (dotted), Domain D (dashed), and Domain E (dash-dot).

during the first 36 hours of the forecast period and beyond 84 hours. In contrast, the upstream domains displayed as much as 3.5 percent degradation relative to Domain B from 48 to 72 hours. The results were inconclusive in showing whether there is an optimal placement of the windward lateral boundary for wind speed. A similar pattern was seen for the 500/200 mb layer.

Figure 54 shows January wind speed RMSE for the outer domain and the five two-way nested domains over a 950/700 mb layer. This graph indicates that the RMSE generally increased with time and had some divergence in the various nested
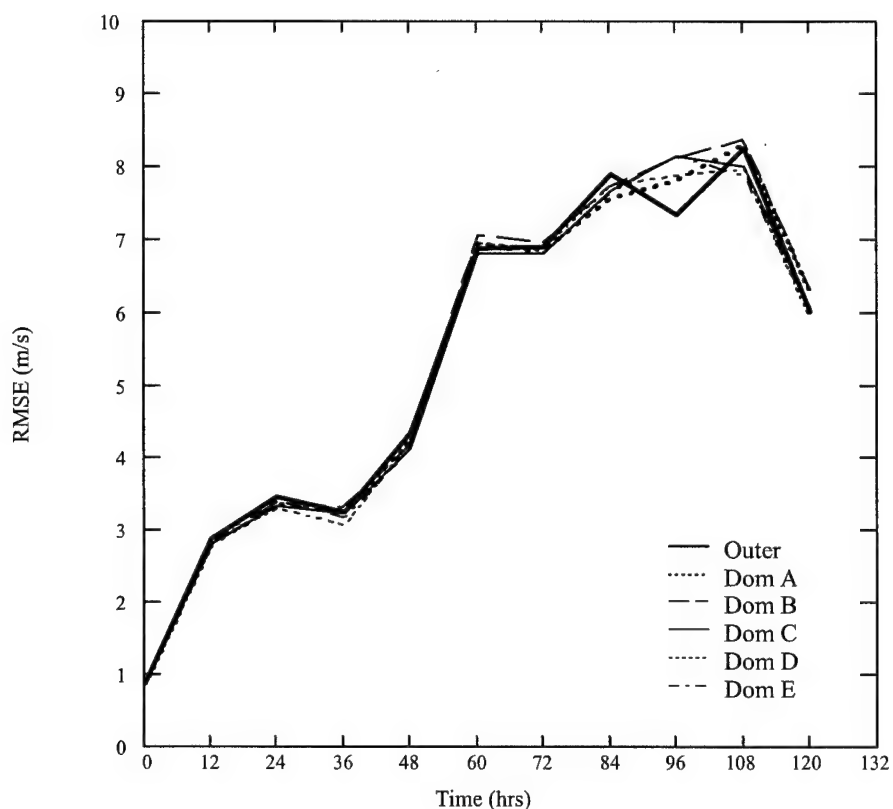
Figure 54   Wind speed RMSE for the January case over a 950/700 mb layer (two-way nesting). This figure shows the RMSE for the outer domain (36 km) and the five high-resolution (12 km) two-way nested domains for the January case The domains represented by the traces are the Outer Domain (heavy solid), Domain A (heavy dotted), Domain B (dashed), Domain C (solid), Domain D (dotted), and Domain E (dash-dot).

domain solutions beyond 72 hours. Figure 55 shows the statistical comparison (wind speed) of the five two-way nested domains for the January case over a 950/700 mb layer. As seen from the graph, both the downstream (Domain A) and upstream (Domains C to E) domains generally yielded marginal forecast improvement relative to Domain B (the control) throughout the entire forecast period. Domains D and E produced the most significant improvements by as much as six to seven percent relative to Domain B for wind speed. The maximum improvements at 36 and 108

Figure 55   Two-way nested domain placement comparison (wind speed) for the January case over a 950/700 mb layer. This figure compares the placement of the five high-resolution (12 km) two-way nested domains for the January case using normalized RMSE where the control value is from Domain B. The domains represented by the traces are Domain A (solid), Domain B (heavy dotted), Domain C (dotted), Domain D (dashed), and Domain E (dash-dot).

hours were loosely correlated with the presence of cyclogenesis in the verification zone.

Figure 56 shows May wind speed RMSE for the outer domain and the five two-way nested domains over a 950/150 mb layer. This graph indicates that the RMSE generally increased with time and the various nested domain solutions began to diverge after about 72 hours. Figure 57 shows the statistical comparison (wind speed) of the five two-way nested domains for the May case over a 950/150 mb layer. This case showed similar results to the January case. As seen from the graph, both

74

Figure 56   Wind speed RMSE for the May case over a 950/150 mb layer (two-way nesting).   This figure shows the RMSE for the outer domain (36 km) and the five high-resolution (12 km) two-way nested domains for the May case   The domains represented by the traces are the Outer Domain (heavy solid), Domain A (heavy dotted), Domain B (dashed), Domain C (solid), Domain D (dotted), and Domain E (dash-dot).

the downstream (Domain A) and upstream (Domains C to E) domains exhibited an oscillatory nature relative to Domain B (the control) throughout the entire forecast period.   The upstream domains showed as much as six percent improvement relative to Domain B when cyclogenesis was in the verification zone between 84 and 120 hours.   In contrast, the upstream domains displayed as much as five percent degradation relative to Domain B beyond 120 hours.   The results were inconclusive in showing whether there is an optimal placement of the windward lateral boundary

Figure 57   Two-way nested domain placement comparison (wind speed) for the May case over a 950/150 mb layer. This figure compares the placement of the five high-resolution (12 km) two-way nested domains for the May case using normalized RMSE where the control value is from Domain B. The domains represented by the traces are Domain A (solid), Domain B (heavy dotted), Domain C (dotted), Domain D (dashed), and Domain E (dash-dot).

for wind speed. Similar patterns were seen for the 950/700 mb and 500/200 mb layers.

4.3.2.5   *Wind Direction.*   Figure 58 shows January wind direction RMSE for the outer domain and the five two-way nested domains over a 950/150 mb layer. This graph indicates that the RMSE was oscillatory as it increased with time and there was minimal divergence in the various solutions of the nested domain. Figure 59 shows the statistical comparison (wind direction) of the five
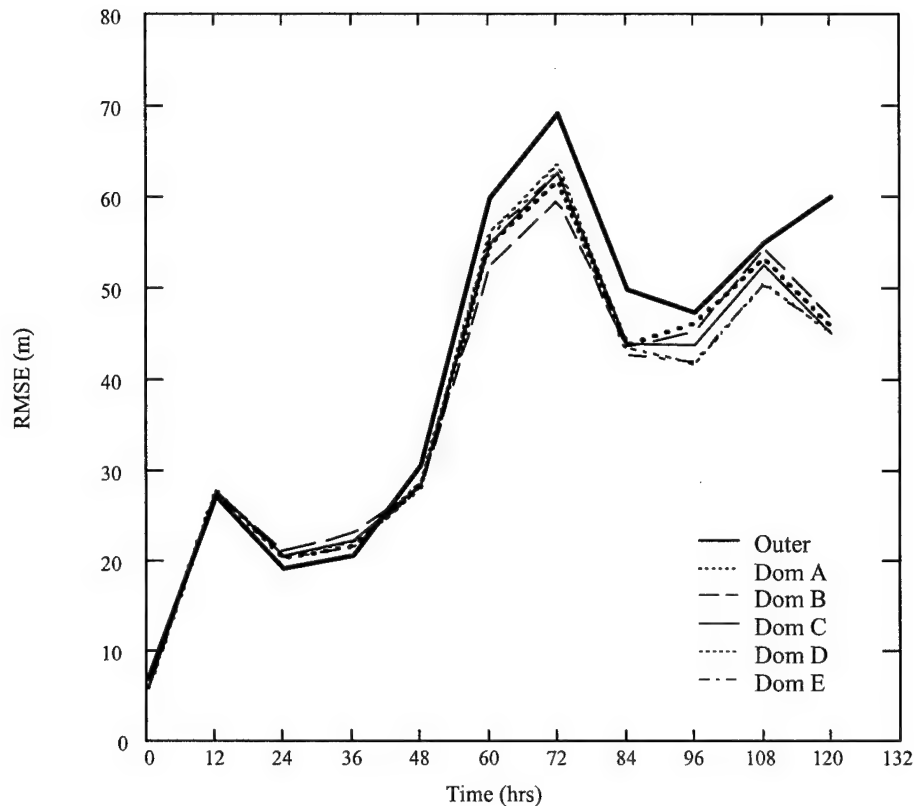
Figure 58   Wind direction RMSE for the January case over a 950/150 mb layer (two-way nesting).   This figure shows the RMSE for the outer domain (36 km) and the five high-resolution (12 km) two-way nested domains for the January case The domains represented by the traces are the Outer Domain (heavy solid), Domain A (heavy dotted), Domain B (dashed), Domain C (solid), Domain D (dotted), and Domain E (dash-dot).

two-way nested domains for the January case over a 950/150 mb layer.   As seen from the graph, both the downstream (Domain A) and upstream (Domains C to E) domains oscillated between five percent improvement and five percent degradation relative to Domain B (the control) during the entire forecast period.   The results were inconclusive in showing whether there is an optimal placement of the windward lateral boundary for wind direction.   Similar patterns were seen for the 950/700 mb and 500/200 mb layers.

Figure 60 shows May wind direction RMSE for the outer domain and the five

Figure 59   Two-way nested domain placement comparison (wind direction) for the January case over a 950/150 mb layer. This figure compares the placement of the five high-resolution (12 km) two-way nested domains for the January case using normalized RMSE where the control value is from Domain B. The domains represented by the traces are Domain A (solid), Domain B (heavy dotted), Domain C (dotted), Domain D (dashed), and Domain E (dash-dot).

two-way nested domains over a 950/150 mb layer.   This graph indicates that the RMSE was extremely oscillatory as it increased with time and the various nested domain solutions were sporadically divergent.   Figure 61 shows the statistical comparison (wind direction) of the five two-way nested domains for the May case over a 950/150 mb layer.   This case showed similar results to the January case.   As seen from the graph, both the downstream (Domain A) and upstream (Domains C to E) domains exhibited marginal improvements relative to Domain B (the control) during first 132 hours of the forecast period.   At 144 hours, the upstream domain
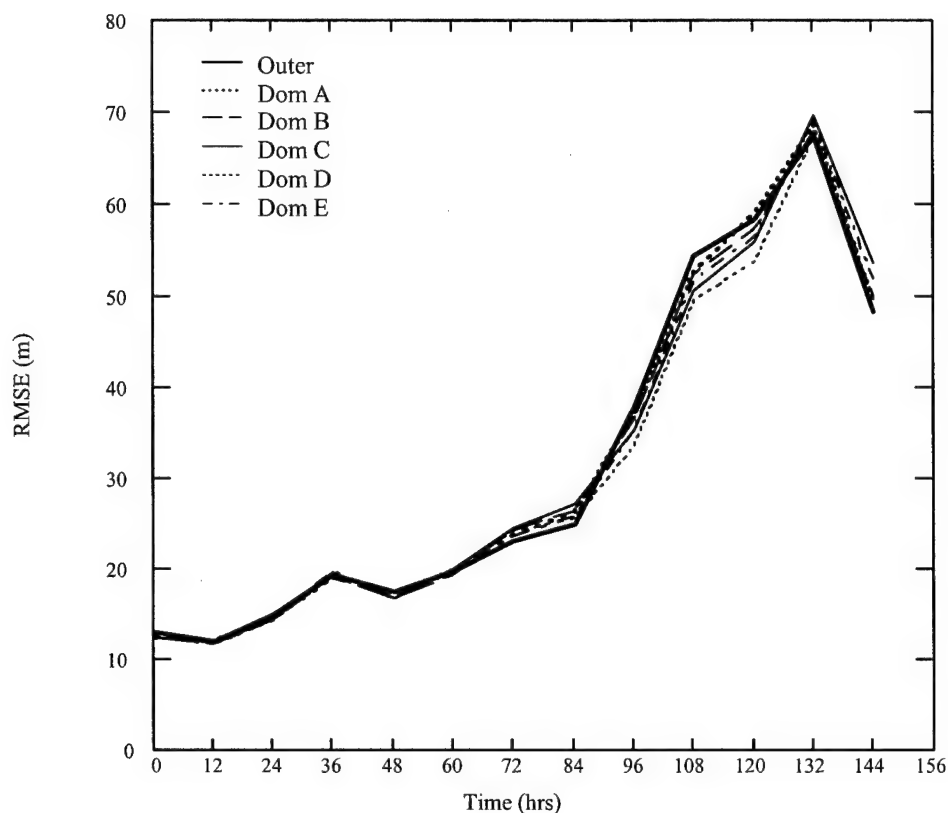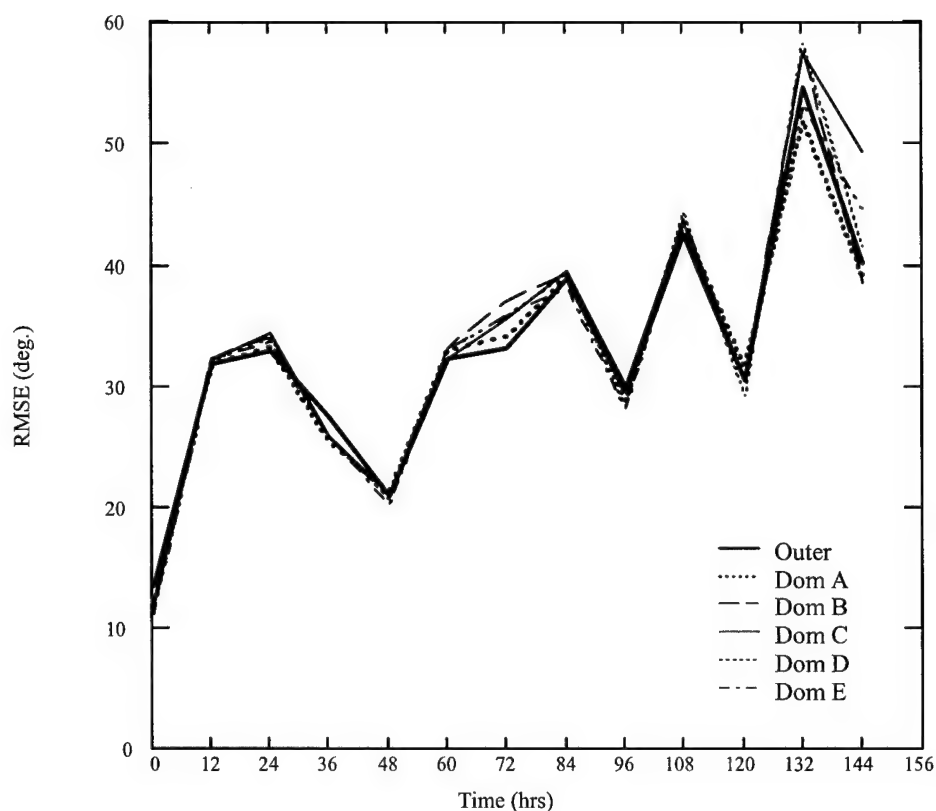
Figure 60   Wind direction RMSE for the May case over a 950/150 mb layer (two-way nesting).   This figure shows the RMSE for the outer domain (36 km) and the five high-resolution (12 km) two-way nested domains for the May case The domains represented by the traces are the Outer Domain (heavy solid), Domain A (heavy dotted), Domain B (dashed), Domain C (solid), Domain D (dotted), and Domain E (dash-dot).

showed sharp degradation: 25 percent for Domain C, 15 percent for Domain E, and 8 percent for Domain D. The results were inconclusive in showing whether there is an optimal placement of the windward lateral boundary for wind direction. Similar patterns were seen for the 950/700 mb and 500/200 mb layers.

4.3.2.6 Summary.   The findings presented in this subsection indicated that the placement of the windward lateral boundary over strong topographic features for two-way nesting substantially impacted the model's forecast veracity for the geopotential height and temperature fields.   In general, the results indicated

79
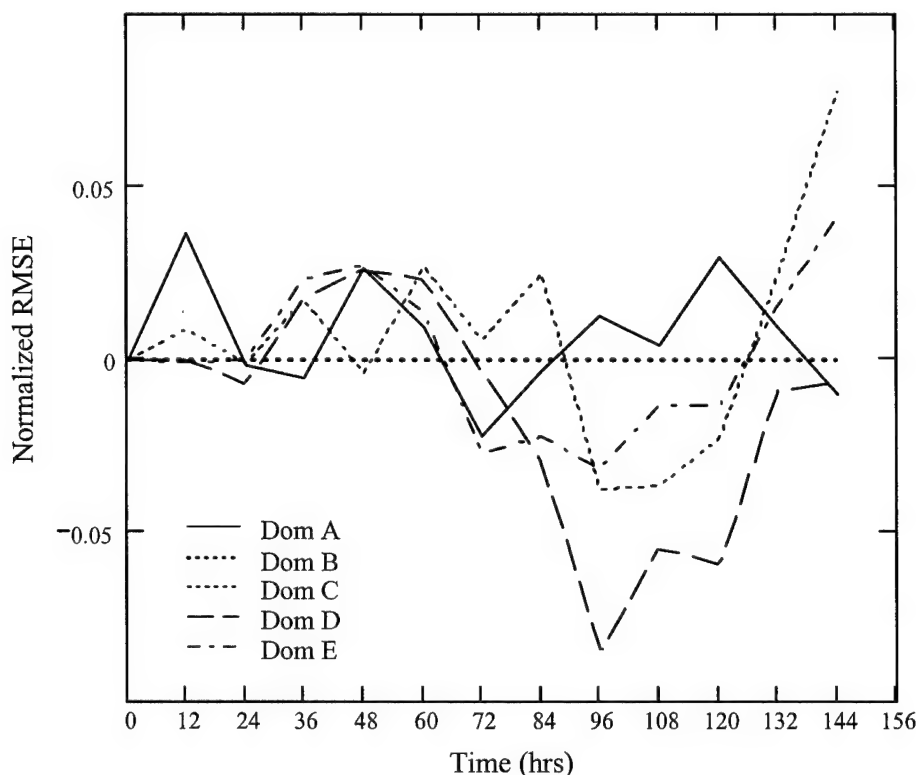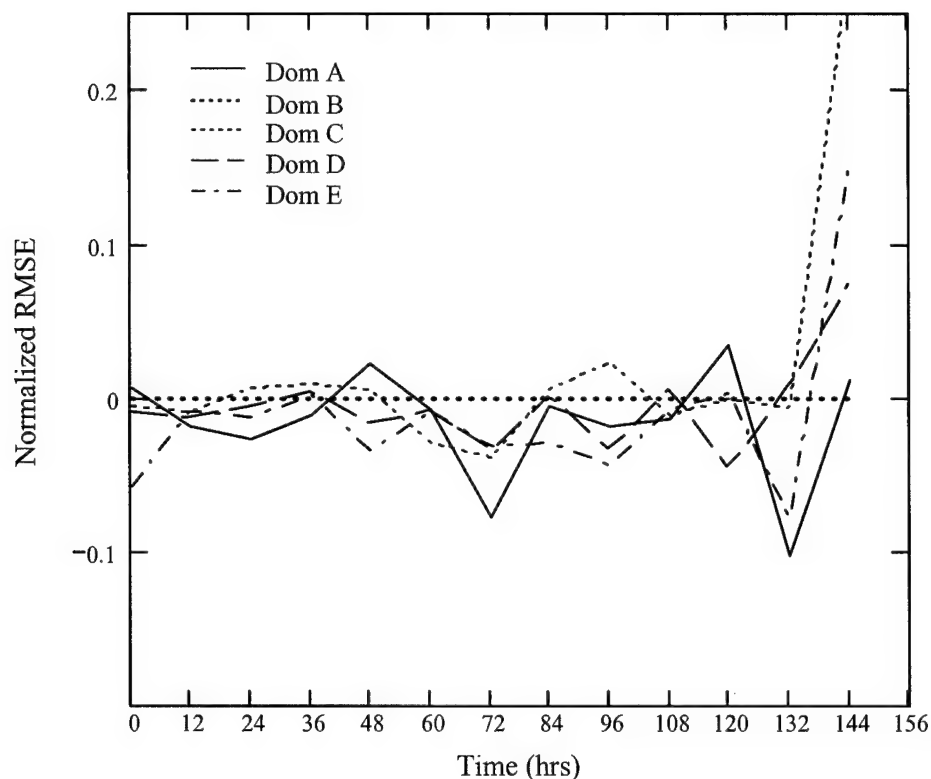
Figure 61   Two-way nested domain placement comparison (wind direction) for the May case over a 950/150 mb layer. This figure compares the placement of the five high-resolution (12 km) two-way nested domains for the May case using normalized RMSE where the control value is from Domain B. The domains represented by the traces are Domain A (solid), Domain B (heavy dotted), Domain C (dotted), Domain D (dashed), and Domain E (dash-dot).

a reduction in the RMSE (or forecast improvement) as the model grid was moved upstream of the mountain's tallest peaks; however, the results indicated a limit to how far the grid should be moved upstream. Overall, the results suggested the model produced the best forecast for a placement of the windward lateral boundary between Domain D and E. Since the tallest peaks of the Rocky Mountains are at about 106° longitude (windward boundary of Domain B), it can be concluded (in this study) that a placement of the windward lateral boundary 5-8° longitude up-

stream from the mountain's tallest peaks yielded the most accurate model forecast for two-way nesting.

4.3.3   Findings for One-way Nesting.

4.3.3.1   General Discussion.   The plots in this subsection are standardized with time (in hours) along the abscissa, and RMSE or normalized RMSE along the ordinate. Normalized RMSE is either positive, negative, or zero. The zero line represents the control value which has been chosen as Domain B for each plot. A negative value represents a decrease in the RMSE, or improvement in the model's forecast, and vice versa. Each trace represents the model domain denoted in the key and was generated using the RMSE calculation for each verification time during the forecast period. It should also be noted that the resulting percentages of these normalized plots must be compared to the actual RMSE to quantify the decrease or increase in error (relative to domain B). Statistical plots have been generated for three layers in the atmosphere: 950/150 mb, 950/700 mb, and 500/200 mb where verification was computed every 25 mb throughout the layer.

4.3.3.2   Geopotential Height.   Figure 62 shows January geopotential height RMSE for the outer domain and the five one-way nested domains over a 950/150 mb layer (entire troposphere). This graph indicates that the RMSE generally increased with time and there was minimal divergence in the various nested domain solutions. Figure 62 should be used in conjunction with the next figure to obtain the actual decrease or increase of RMSE relative to Domain B. Figure 63 shows the statistical comparison (geopotential height) of the five one-way nested domains for the January case over a 950/150 mb layer (33 verification levels). As seen from the graph, both the downstream (Domain A) and upstream (Domains C to E) domains oscillate between 3.5 percent degradation and 9 percent improvement relative to Domain B (the control) during the first 48 hours of the forecast period.

81
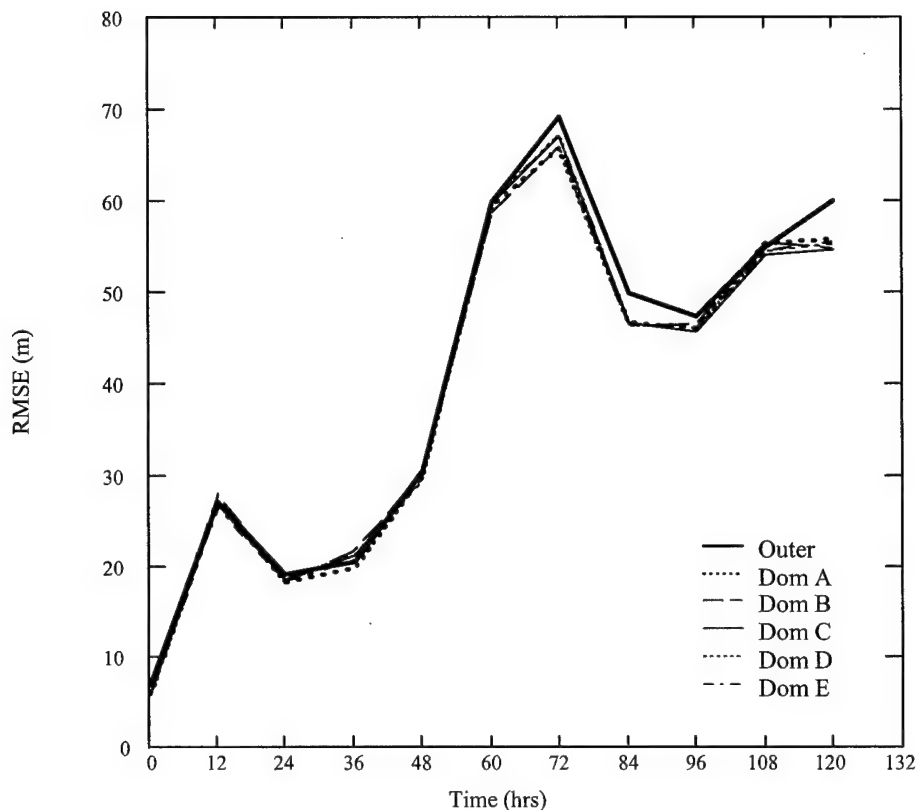
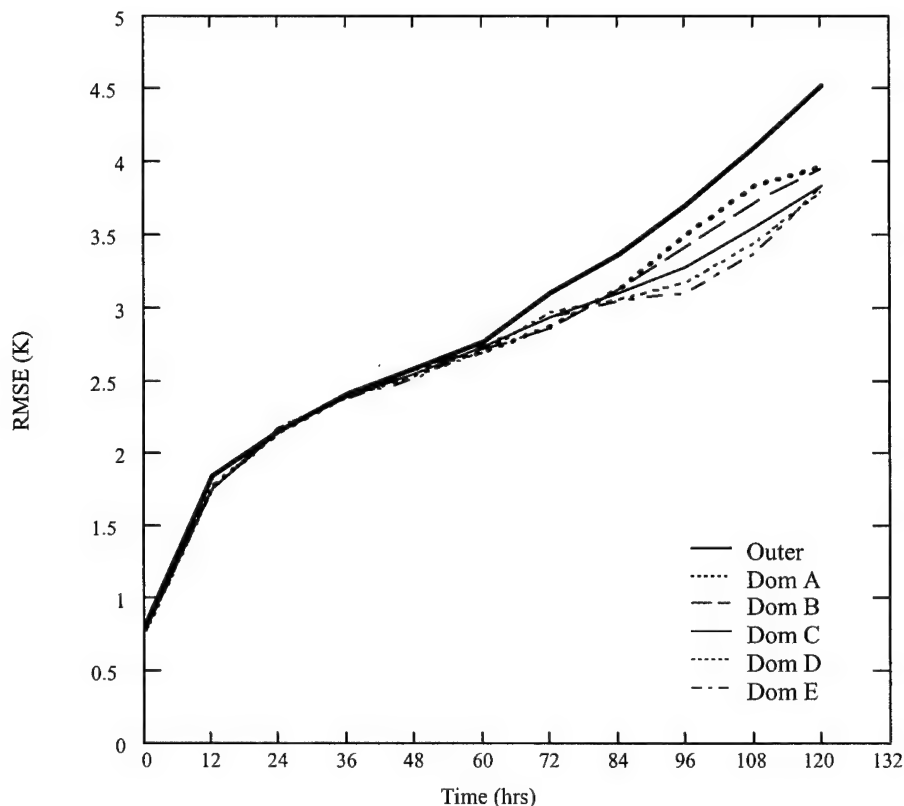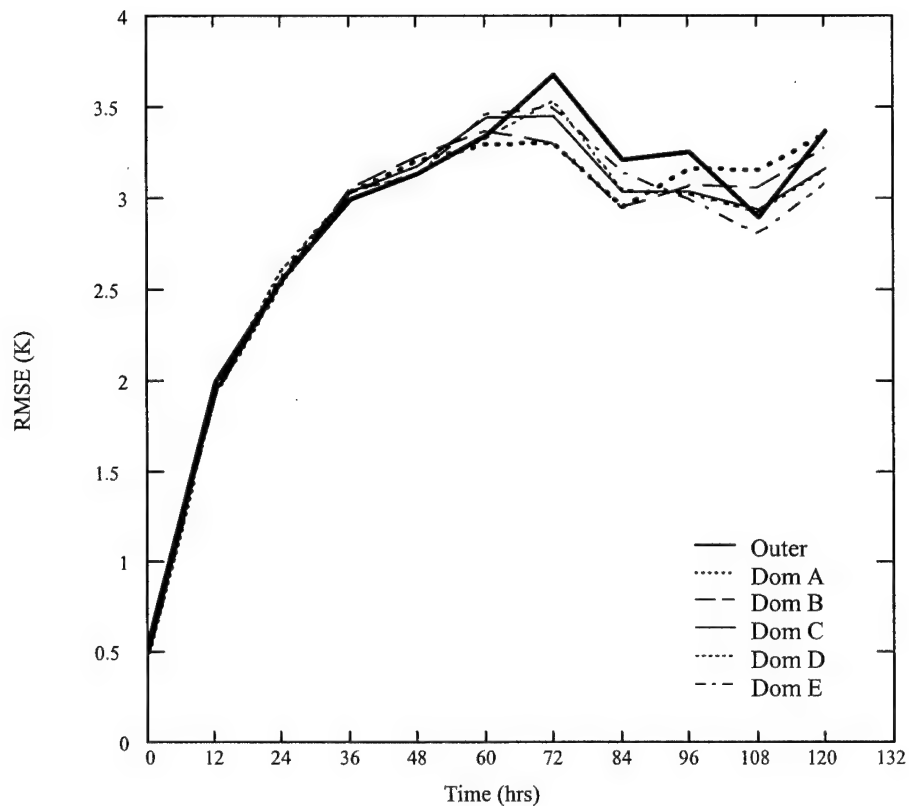Figure 62   Geopotential height RMSE for the January case over a 950/150 mb layer
(one-way nesting).   This figure shows the RMSE for the outer domain
(36 km) and the five high-resolution (12 km) one-way nested domains for
the January case The domains represented by the traces are the Outer
Domain (heavy solid), Domain A (heavy dotted), Domain B (dashed),
Domain C (solid), Domain D (dotted), and Domain E (dash-dot).

Beyond the 48 hr forecast, the solutions for the various domains remain very simi-
lar. The most significant geopotential height improvement relative to Domain B was
shown by the downstream domain at 36 hours. Overall, no significant conclusions
can be drawn about windward boundary placement based on these results. Similar
patterns were seen for the 950/700 mb and 500/200 mb layers.

Figure 64 shows May geopotential height RMSE for the outer domain and the
five one-way nested domains over a 950/150 mb layer. This graph indicates that the
RMSE increased slowly during the first 84 hours than more rapidly with time. The
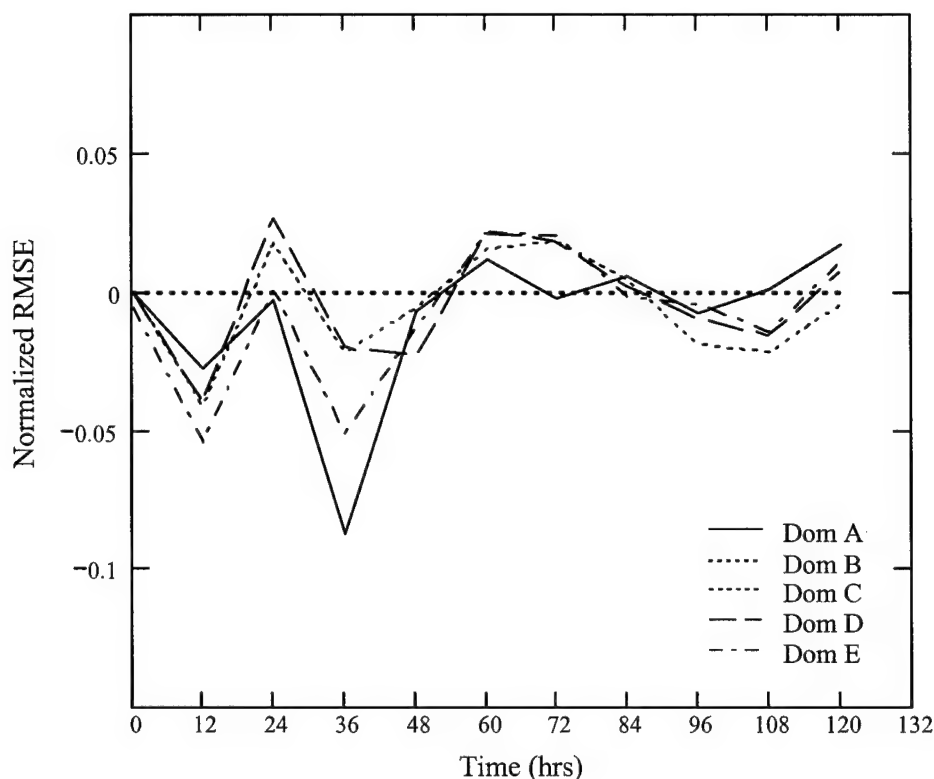
Figure 63   One-way nested domain placement comparison (geopotential height) for the January case over a 950/150 mb layer.   This figure compares the placement of the five high-resolution (12 km) one-way nested domains for the January case using normalized RMSE where the control value is from Domain B. The domains represented by the traces are Domain A (solid), Domain B (heavy dotted), Domain C (dotted), Domain D (dashed), and Domain E (dash-dot).

solutions of the nested domains showed minimal divergence.   Figure 65 shows the statistical comparison (geopotential height) of the five one-way nested domains for the May case over a 950/150 mb layer.   As seen from the graph, both the downstream (Domain A) and upstream (Domains C to E) domains oscillated between 5.5 percent improvement and 6 percent degradation relative to Domain B (the control) during the entire forecast period.   The results were inconclusive in showing whether there is an optimal placement of the windward lateral boundary for geopotential height. Similar patterns were seen for the 950/700 mb and 500/200 mb layers.
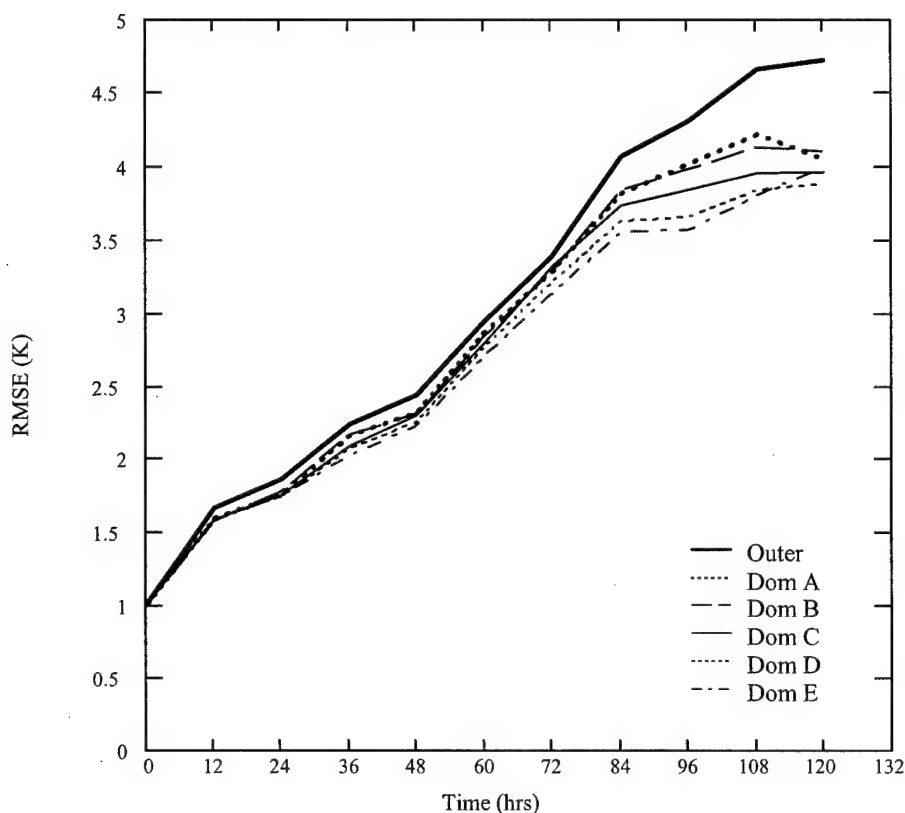
83
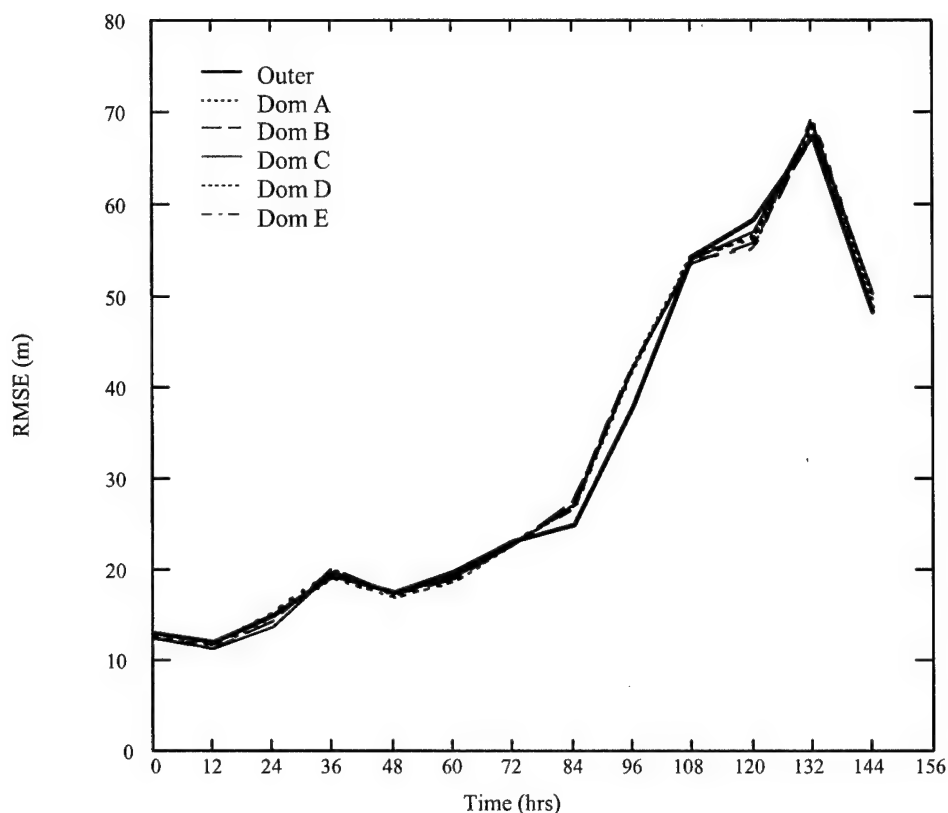
Figure 64   Geopotential height RMSE for the May case over a 950/150 mb layer
(one-way nesting). This figure shows the RMSE for the outer domain
(36 km) and the five high-resolution (12 km) one-way nested domains
for the May case The domains represented by the traces are the Outer
Domain (heavy solid), Domain A (heavy dotted), Domain B (dashed),
Domain C (solid), Domain D (dotted), and Domain E (dash-dot).

4.3.3.3   Temperature.   Figure 66 shows January temperature RMSE
for the outer domain and the five one-way nested domains over a 950/150 mb layer.
This graph indicates that the RMSE steadily increased with time and the various
nested domain solutions began to diverge after 12 hours. Figure 67 shows the statis-
tical comparison (temperature) of the five one-way nested domains for the January
case over a 950/150 mb layer. As seen from the graph, both the downstream (Do-
main A) and upstream (Domains C to E) domains yielded as much as five percent
improvement relative to Domain B (the control) during the first 48 hours of the
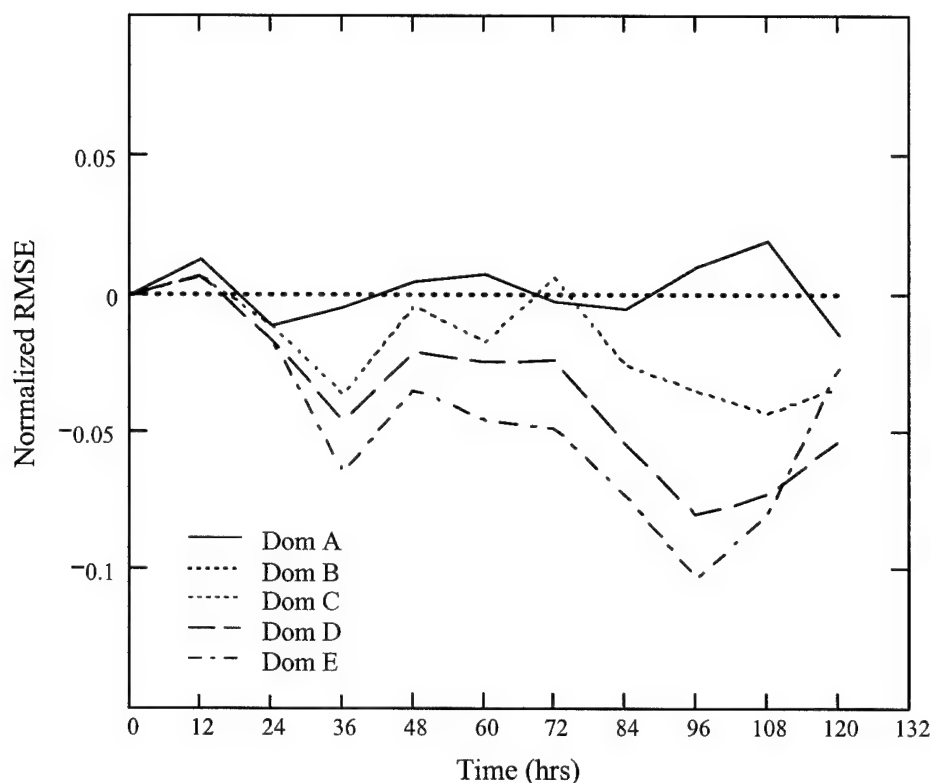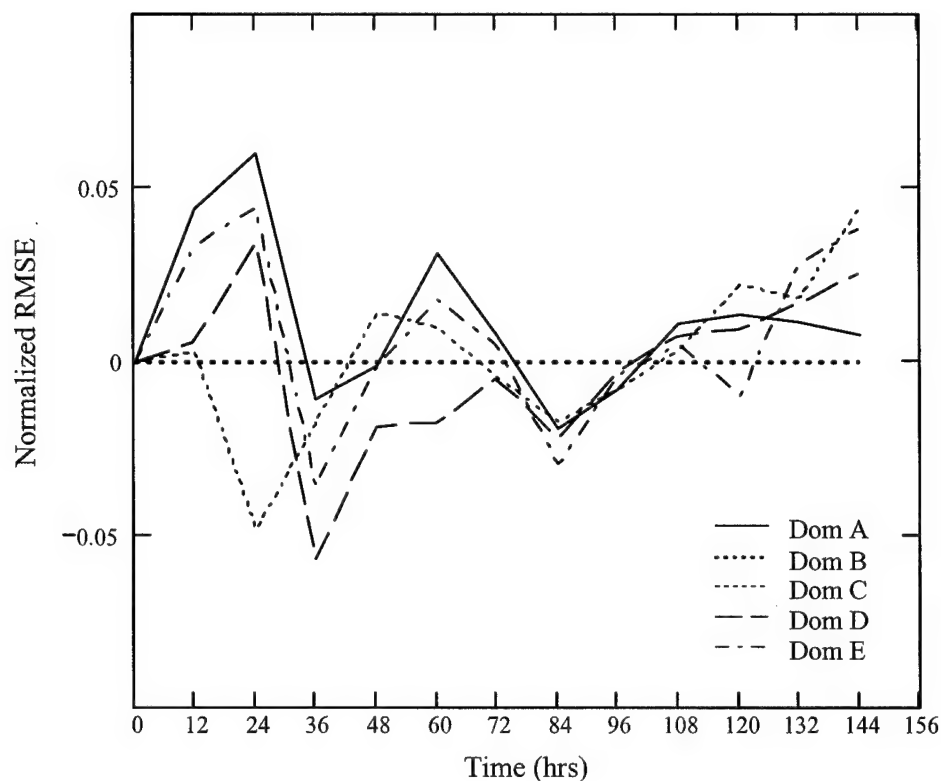
Figure 65   One-way nested domain placement comparison (geopotential height) for the May case over a 950/150 mb layer. This figure compares the placement of the five high-resolution (12 km) one-way nested domains for the May case using normalized RMSE where the control value is from Domain B. The domains represented by the traces are Domain A (solid), Domain B (heavy dotted), Domain C (dotted), Domain D (dashed), and Domain E (dash-dot).

forecast period. Beyond the 60 hr forecast, both the downstream and upstream domains showed a similar solution to Domain B. Improvement relative to Domain B increased as the windward boundary was moved farther upstream (i.e., Domains C, D and E). As with geopotential height, the downstream domain yielded the most significant temperature improvement at 24 hours. However, no significant conclusions can be drawn about windward boundary placement based on these results. Similar patterns were seen for the 950/700 mb and 500/200 mb layers.

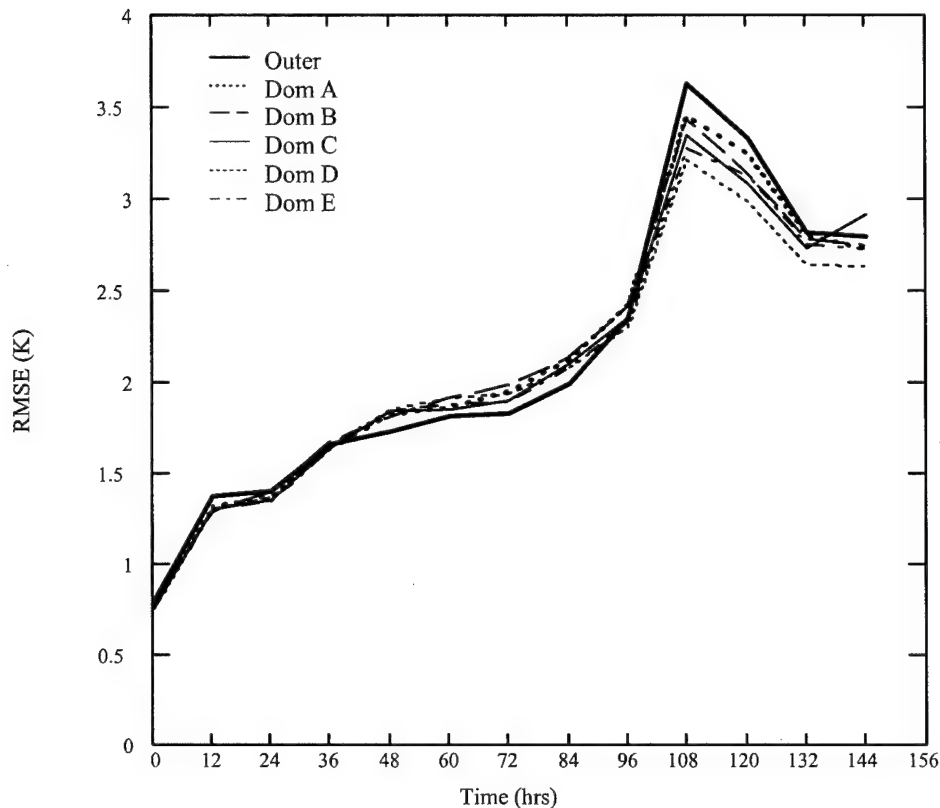Figure 68 shows May temperature RMSE for the outer domain and the five
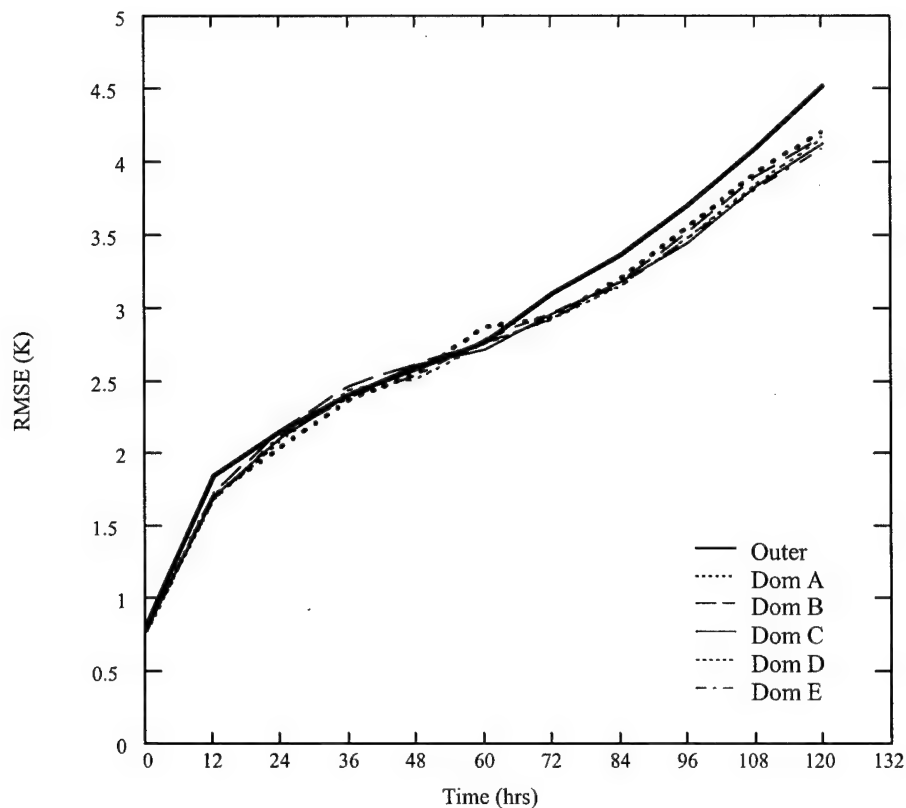
Figure 66   Temperature RMSE for the January case over a 950/150 mb layer (one-way nesting).   This figure shows the RMSE for the outer domain (36 km) and the five high-resolution (12 km) one-way nested domains for the January case The domains represented by the traces are the Outer Domain (heavy solid), Domain A (heavy dotted), Domain B (dashed), Domain C (solid), Domain D (dotted), and Domain E (dash-dot).

one-way nested domains over a 950/150 mb layer.   This graph indicates that the RMSE slowly increased with time until 84 hour when the error increase rapidly. Divergence was seen in the solutions of the nested domains sporadically throughout the entire forecast period.   Figure 69 shows the statistical comparison (temperature) of the five one-way nested domains for the May case over a 950/150 mb layer (33 verification levels).   As seen from the graph, both the downstream (Domain A) and upstream (Domains C to E) domains oscillated between 4 percent improvement and 6.5 percent degradation relative to Domain B (the control) during the entire
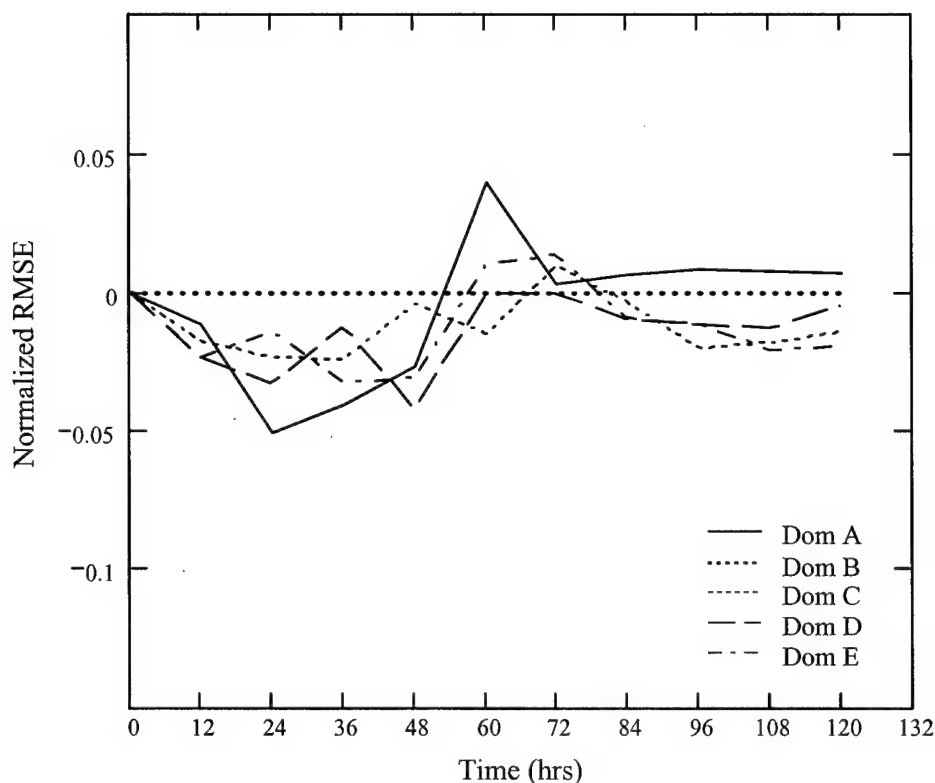
Figure 67   One-way nested domain placement comparison (temperature) for the January case over a 950/150 mb layer. This figure compares the placement of the five high-resolution (12 km) one-way nested domains for the January case using normalized RMSE where the control value is from Domain B. The domains represented by the traces are Domain A (solid), Domain B (heavy dotted), Domain C (dotted), Domain D (dashed), and Domain E (dash-dot).

forecast period. As with geopotential height, the results were again inconclusive in showing whether there is an optimal placement of the windward lateral boundary for geopotential height. Similar patterns were seen for the 950/700 mb and 500/200 mb layers.

4.3.3.4   Wind Speed.   Figure 70 shows January wind speed RMSE for the outer domain and the five one-way nested domains over a 950/150 mb layer. This graph indicates that the RMSE generally increased with time with minimal
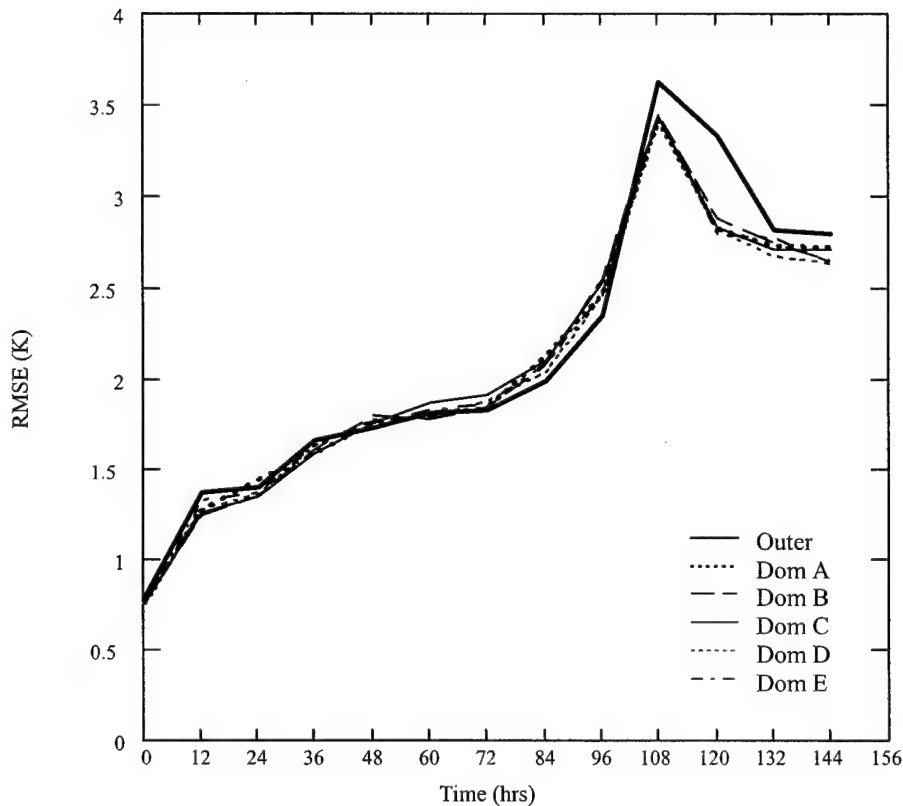
Figure 68 Temperature RMSE for the May case over a 950/150 mb layer (one-way nesting). This figure shows the RMSE for the outer domain (36 km) and the five high-resolution (12 km) one-way nested domains for the May case The domains represented by the traces are the Outer Domain (heavy solid), Domain A (heavy dotted), Domain B (dashed), Domain C (solid), Domain D (dotted), and Domain E (dash-dot).

divergence in the various solutions of the nested domains. Figure 71 shows the statistical comparison (wind speed) of the five one-way nested domains for the January case over a 950/150 mb layer (33 verification levels). As seen from the graph, both the downstream (Domain A) and upstream (Domains C to E) domains yield as much as twelve percent improvement relative to Domain B (the control) during the first 24 hours of the forecast period. Beyond the 24 hr forecast, both the downstream and upstream domains showed a similar solution to Domain B. In contrast to the previous forecast fields, Domains D and E yielded the most significant wind speed
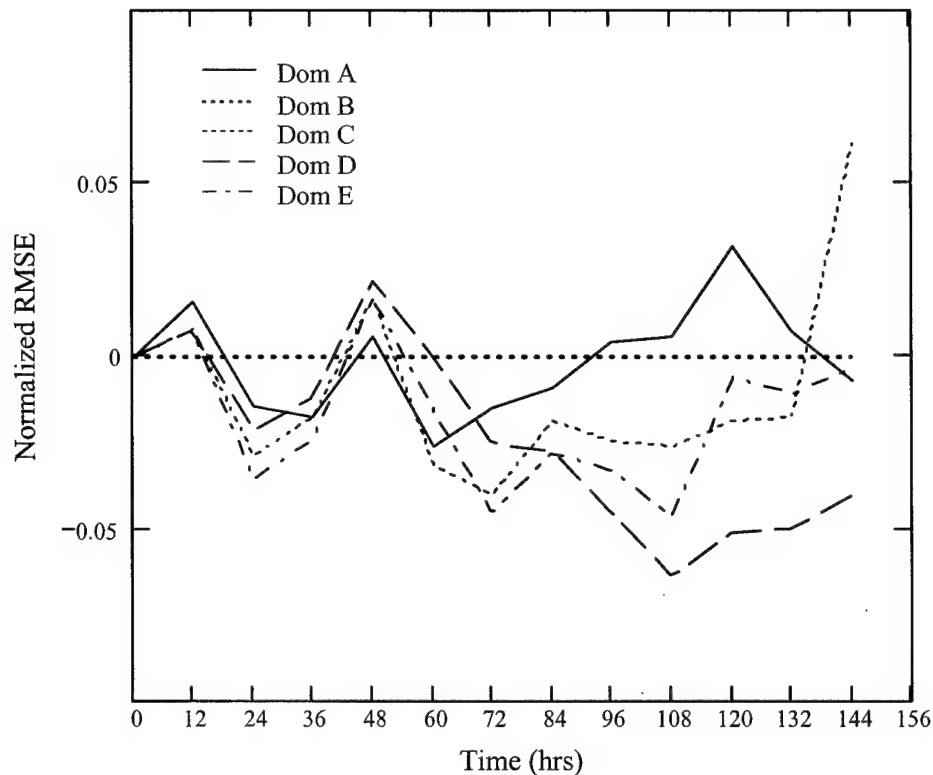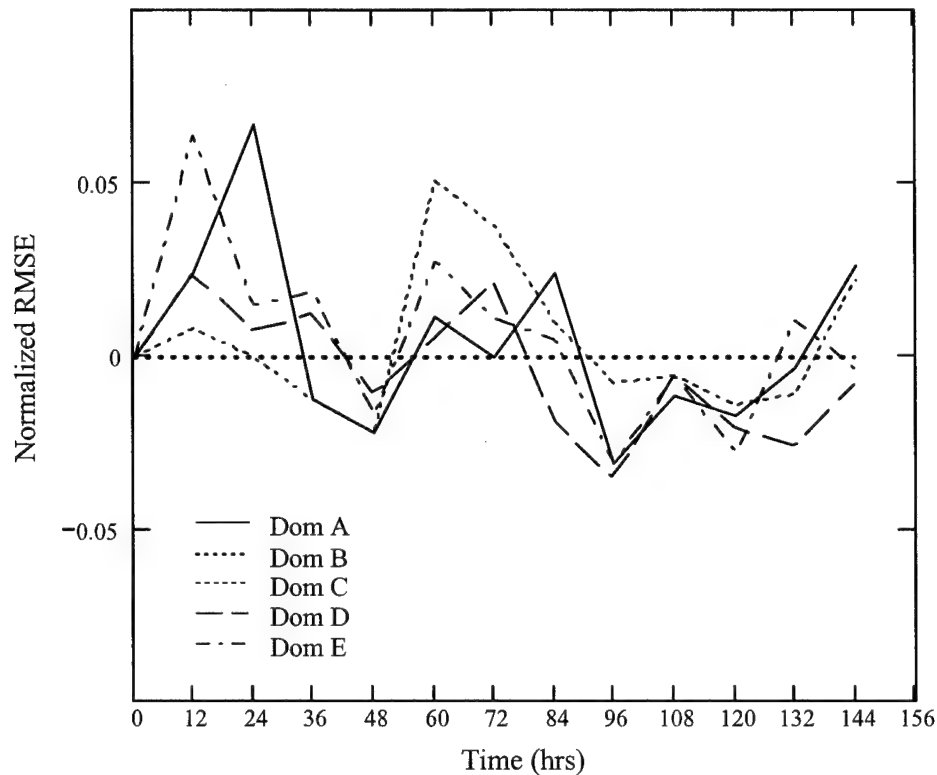
Figure 69   One-way nested domain placement comparison (temperature) for the May case over a 950/150 mb layer. This figure compares the placement of the five high-resolution (12 km) one-way nested domains for the May case using normalized RMSE where the control value is from Domain B. The domains represented by the traces are Domain A (solid), Domain B (heavy dotted), Domain C (dotted), Domain D (dashed), and Domain E (dash-dot).

improvement at 12 hours. However, no significant conclusions can be drawn about windward boundary placement based on these results. Similar patterns were seen for the 950/700 mb and 500/200 mb layers.

Figure 72 shows May wind speed RMSE for the outer domain and the five one-way nested domains over a 950/150 mb layer. This graph indicates that the RMSE generally increased with time, except at 72 hours where a spike in the error occurred. The most significant divergence of the nested domain solutions was seen after 84 hours. Figure 73 shows the statistical comparison (wind speed) of the five
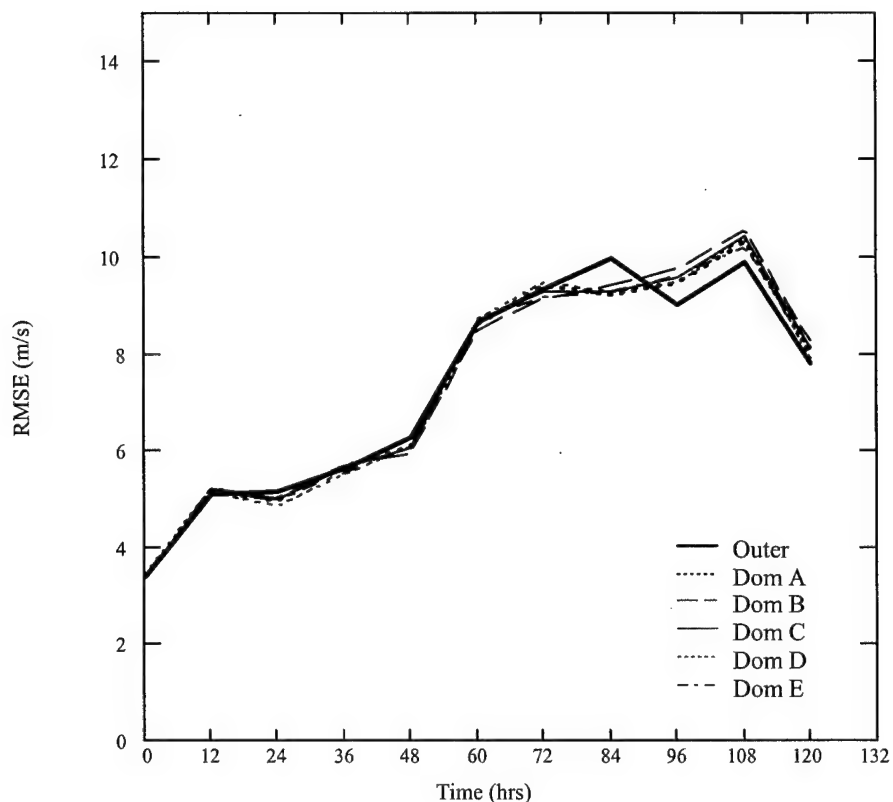
89
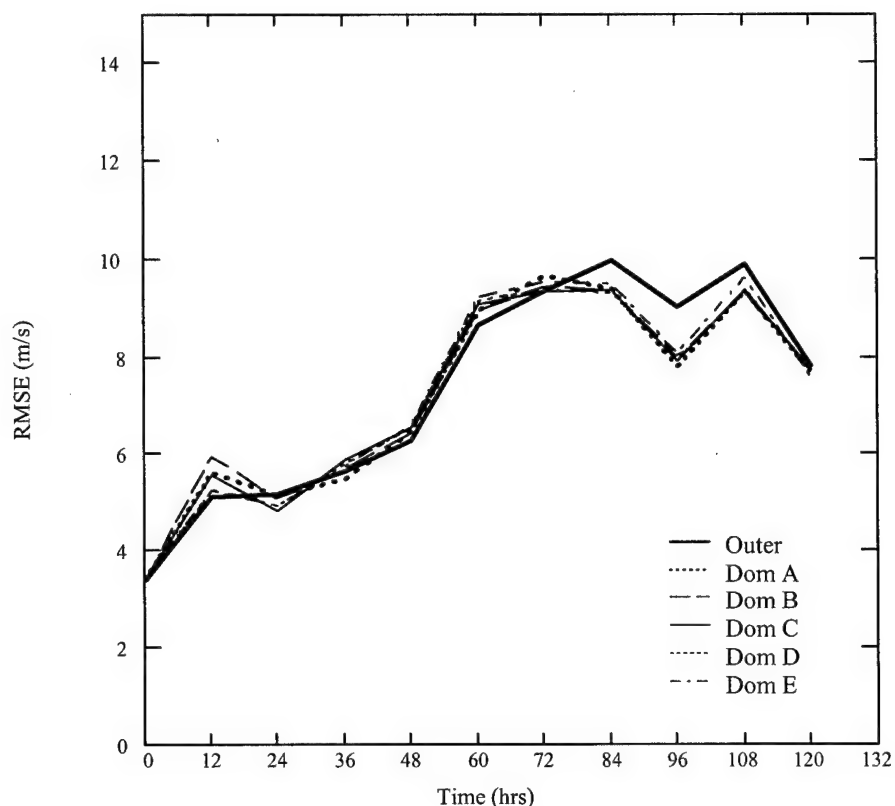
Figure 70   Wind speed RMSE for the January case over a 950/150 mb layer (one-way nesting). This figure shows the RMSE for the outer domain (36 km) and the five high-resolution (12 km) one-way nested domains for the January case The domains represented by the traces are the Outer Domain (heavy solid), Domain A (heavy dotted), Domain B (dashed), Domain C (solid), Domain D (dotted), and Domain E (dash-dot).

one-way nested domains for the May case over a 950/150 mb layer. As seen from the graph, both the downstream (Domain A) and upstream (Domains C to E) domains exhibited an oscillatory nature relative to Domain B (the control) throughout the entire forecast period. The upstream domains showed as much as 3.5 percent improvement and 7 percent degradation relative to Domain B. The downstream domain ranged from 5 percent improvement to 4.5 degradation relative to Domain B. The results were inconclusive in showing whether there is an optimal placement
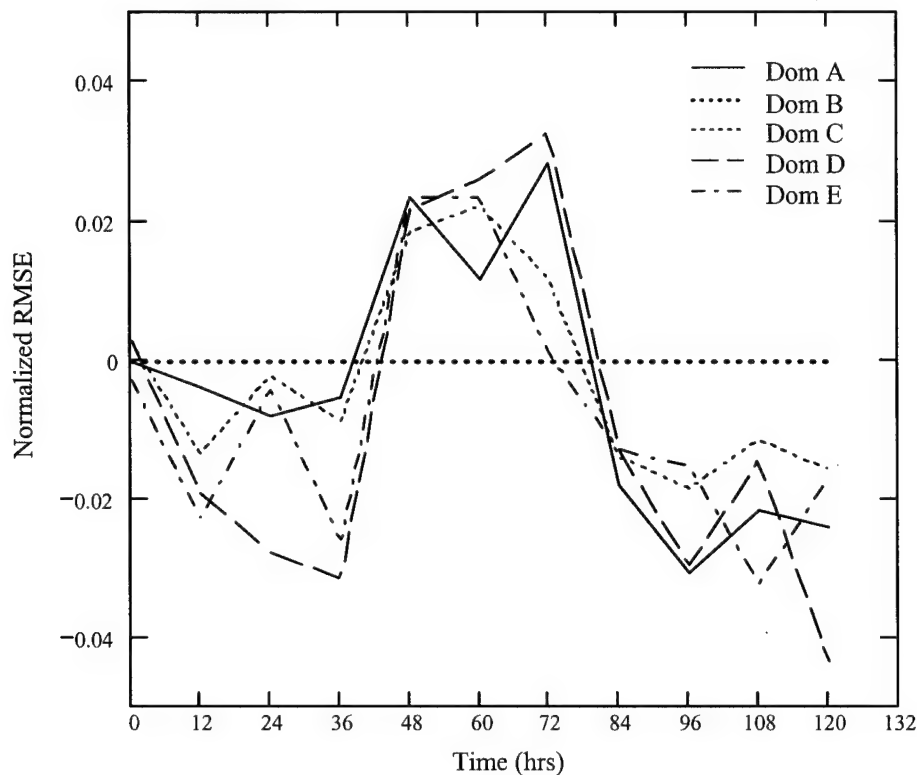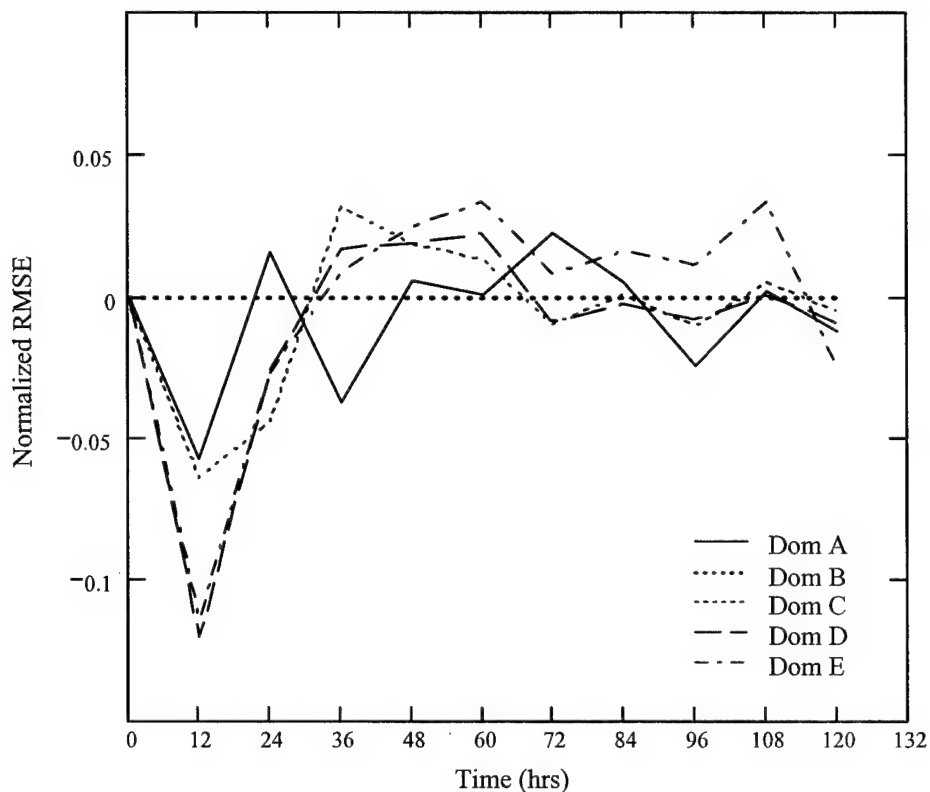
Figure 71   One-way nested domain placement comparison (wind speed) for the
             January case over a 950/150 mb layer. This figure compares the place-
             ment of the five high-resolution (12 km) one-way nested domains for
             the January case using normalized RMSE where the control value is
             from Domain B. The domains represented by the traces are Domain
             A (solid), Domain B (heavy dotted), Domain C (dotted), Domain D
             (dashed), and Domain E (dash-dot).

of the windward lateral boundary for wind speed.   Similar patterns were seen for
the 950/700 mb and 500/200 mb layers.

    4.3.3.5   Wind Direction.   Figure 74 shows January wind direction
RMSE for the outer domain and the five one-way nested domains over a 950/150 mb
layer. This graph indicates that the RMSE generally increased with time, except at
12 hours where a spike in the error occurred. Divergence was seen in the solutions of
the various nested domains throughout the entire forecast period. Figure 75 shows

91
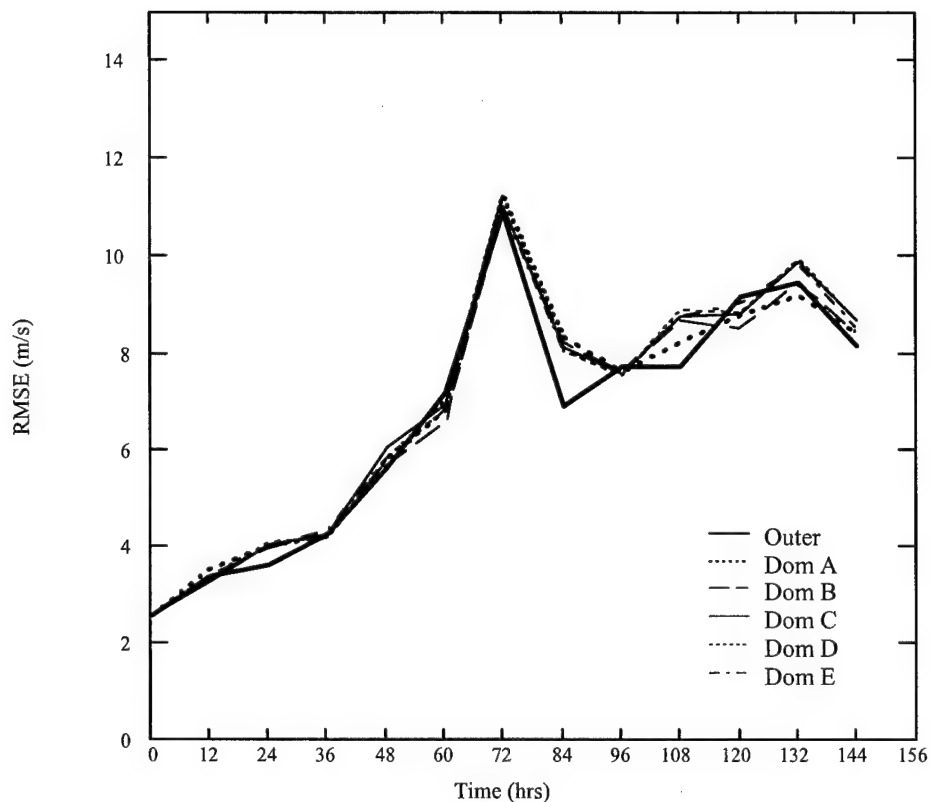
Figure 72   Wind speed RMSE for the May case over a 950/150 mb layer (one-way nesting).   This figure shows the RMSE for the outer domain (36 km) and the five high-resolution (12 km) one-way nested domains for the May case   The domains represented by the traces are the Outer Domain (heavy solid), Domain A (heavy dotted), Domain B (dashed), Domain C (solid), Domain D (dotted), and Domain E (dash-dot).

the statistical comparison (wind direction) of the five one-way nested domains for the January case over a 950/150 mb layer.   As seen from the graph, the upstream (Domains C to E) domains oscillated between 7.5 percent improvement and 5 percent degradation relative to Domain B (the control) during the entire forecast period.   In contrast, the downstream domain (Domain A) yielded a similar solution to Domain B, except for a period with as much as 6.5 percent improvement between 36 and 48 hours.   However, no significant conclusions can be drawn about windward boundary
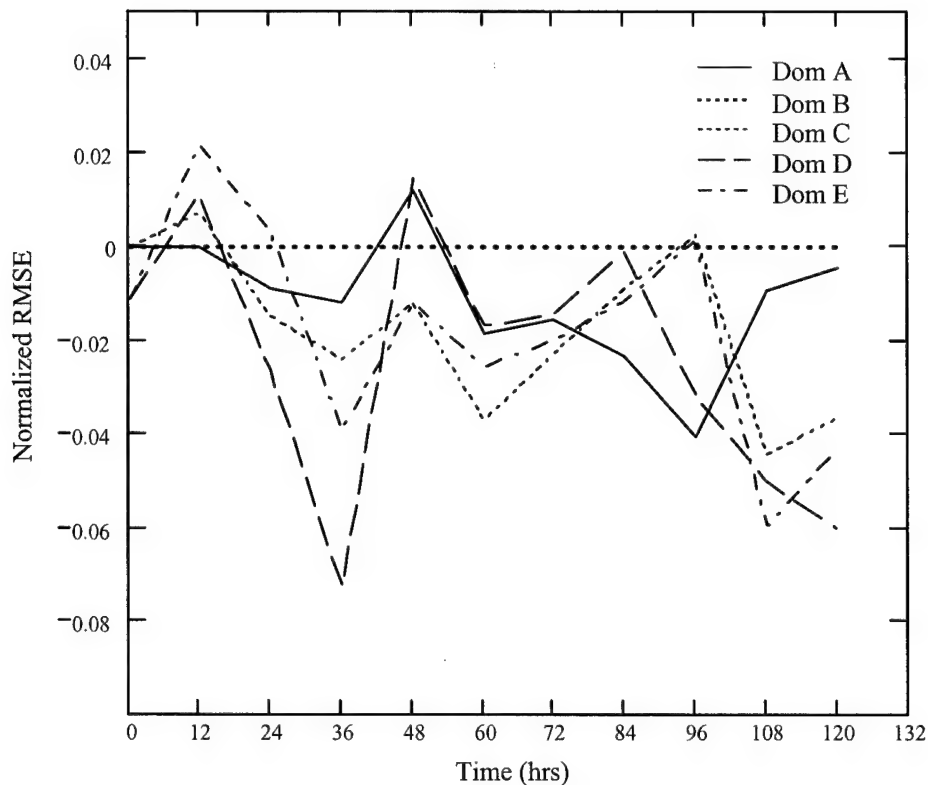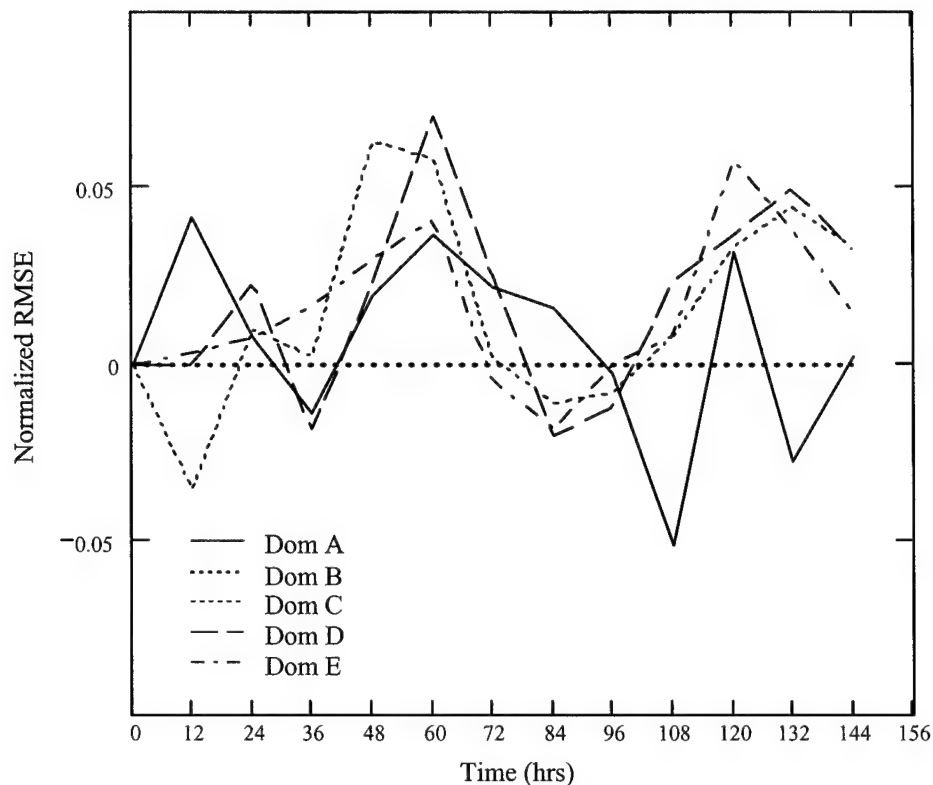
Figure 73   One-way nested domain placement comparison (wind speed) for the May case over a 950/150 mb layer. This figure compares the placement of the five high-resolution (12 km) one-way nested domains for the May case using normalized RMSE where the control value is from Domain B. The domains represented by the traces are Domain A (solid), Domain B (heavy dotted), Domain C (dotted), Domain D (dashed), and Domain E (dash-dot).

placement based on these results. Similar patterns were seen for the 950/700 mb and 500/200 mb layers.

Figure 76 shows May wind direction RMSE for the outer domain and the five one-way nested domains over a 950/150 mb layer. This graph indicates that the RMSE was extremely oscillatory as it increased with time and the various nested domain solutions were sporadically divergent. Figure 77 shows the statistical comparison (wind direction) of the five one-way nested domains for the May case over a 950/150 mb layer. As seen from the graph, both the downstream (Domain A) and
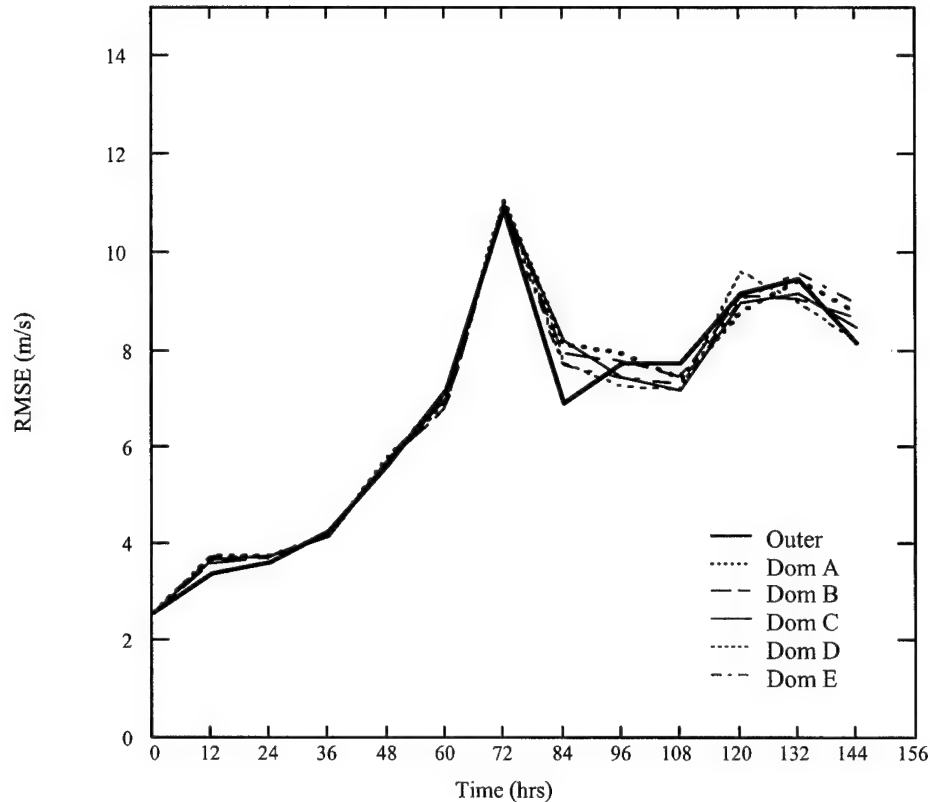
93
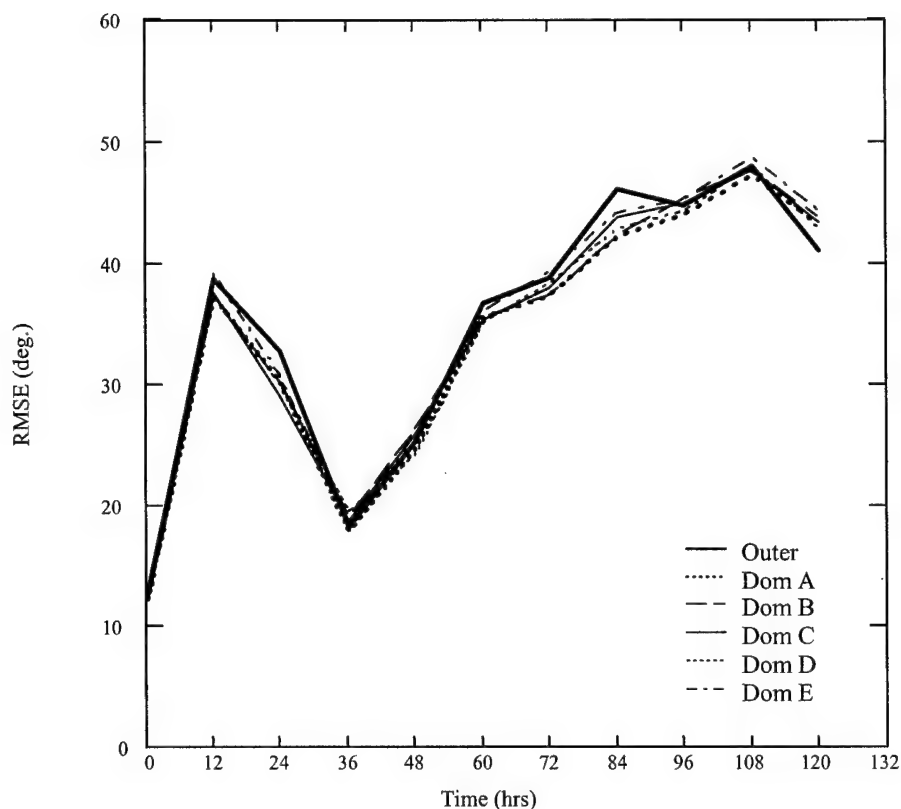
Figure 74   Wind direction RMSE for the January case over a 950/150 mb layer
(one-way nesting).   This figure shows the RMSE for the outer domain
(36 km) and the five high-resolution (12 km) one-way nested domains for
the January case The domains represented by the traces are the Outer
Domain (heavy solid), Domain A (heavy dotted), Domain B (dashed),
Domain C (solid), Domain D (dotted), and Domain E (dash-dot).

upstream (Domains C to E) domains oscillated between twelve percent improve-
ment and ten percent degradation relative to Domain B (the control) during the
entire forecast period.   The results were inconclusive in showing whether there is
an optimal placement of the windward lateral boundary for wind direction.   Similar
patterns were seen for the 950/700 mb and 500/200 mb layers.

4.3.3.6 Summary.   The findings presented in this subsection indi-
cated that the placement of the windward lateral boundary over strong topographic
features for one-way nesting impacted the model's forecast veracity inconsistently
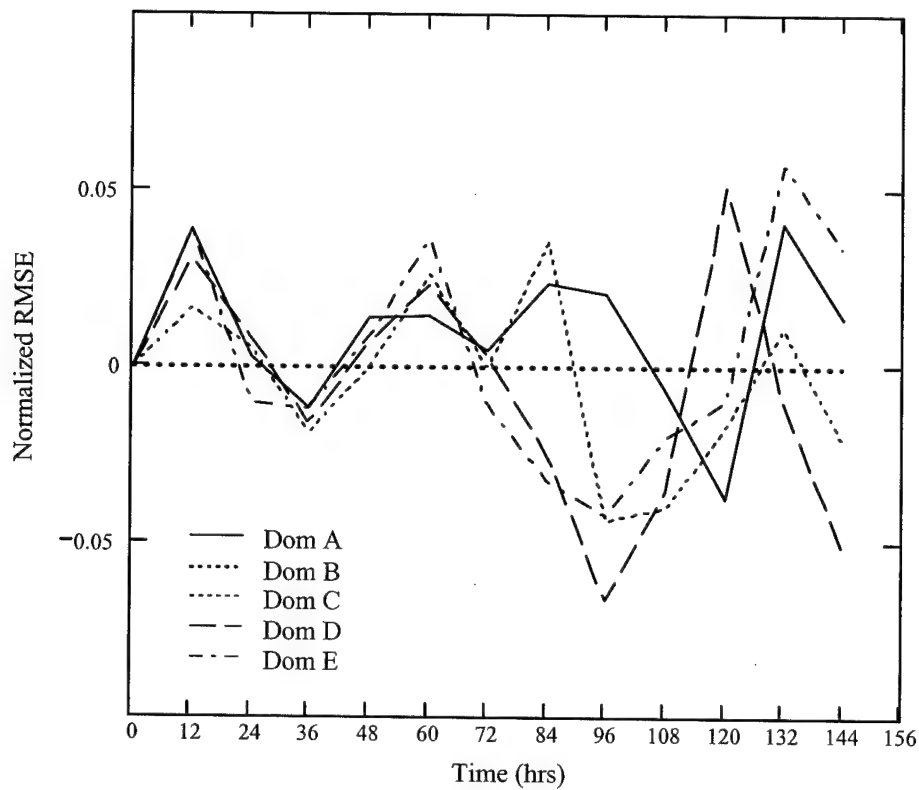
94
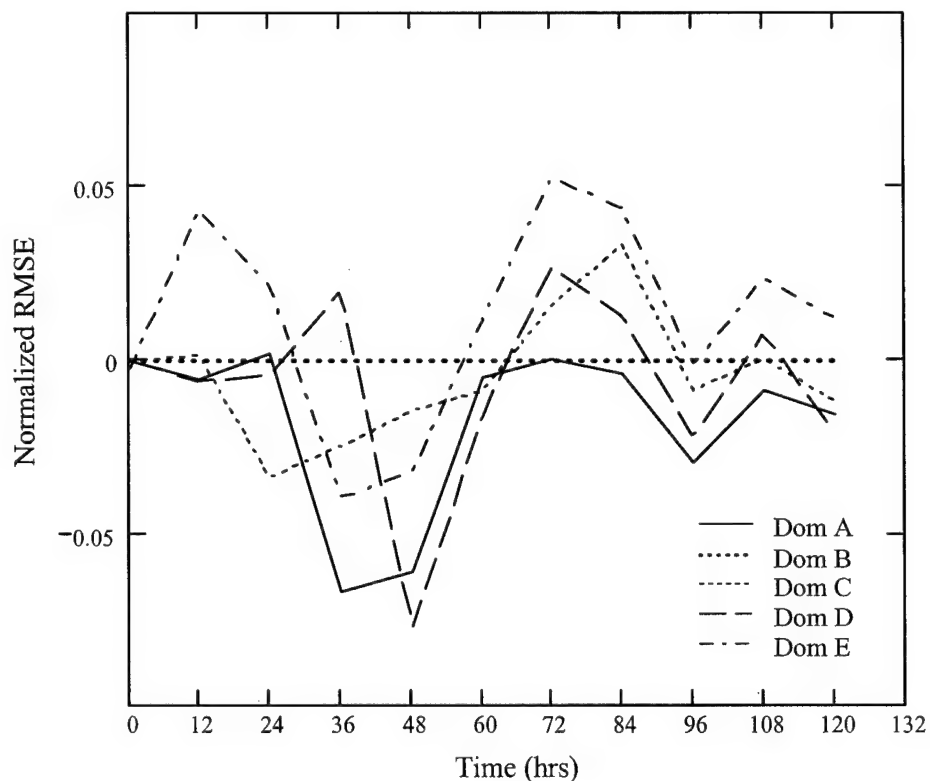
Figure 75   One-way nested domain placement comparison (wind direction) for the January case over a 950/150 mb layer. This figure compares the placement of the five high-resolution (12 km) one-way nested domains for the January case using normalized RMSE where the control value is from Domain B. The domains represented by the traces are Domain A (solid), Domain B (heavy dotted), Domain C (dotted), Domain D (dashed), and Domain E (dash-dot).

among the various forecast fields. In general, the oscillatory nature of the various nested domain solutions (relative to Domain B) showed little correlation to the known cyclogenetic events within the verification zone. Therefore, no sound conclusions can be drawn on the best placement of the windward lateral boundary in regions of strong topographic influence for one-way nesting.
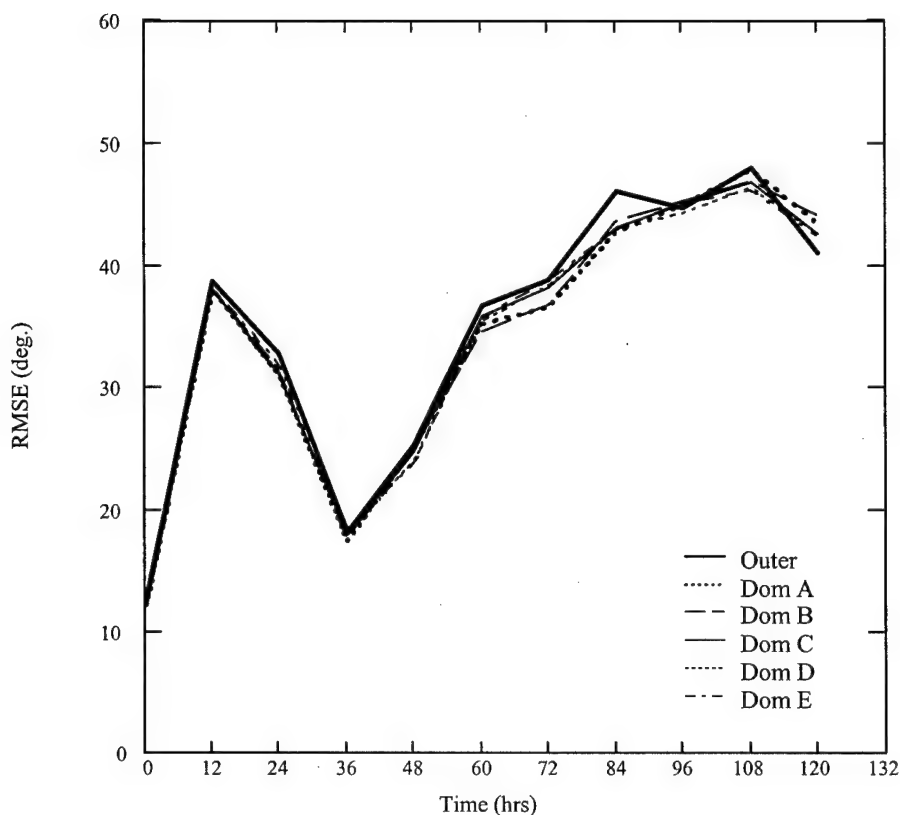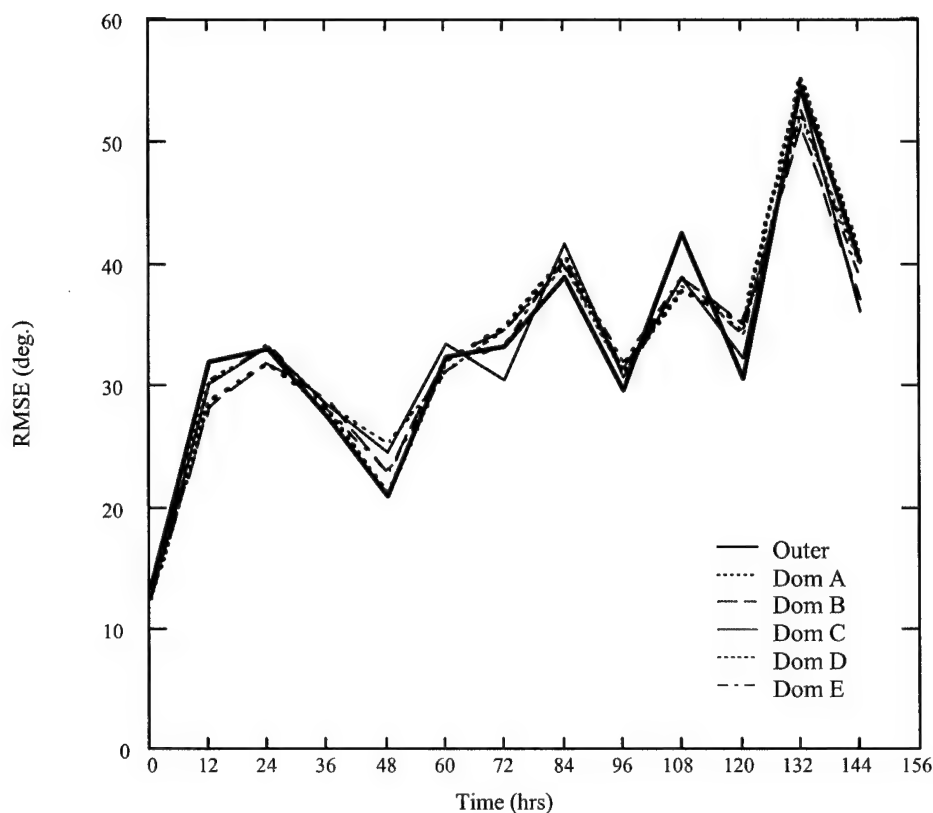
Figure 76   Wind direction RMSE for the May case over a 950/150 mb layer (one-way nesting).   This figure shows the RMSE for the outer domain (36 km) and the five high-resolution (12 km) one-way nested domains for the May case   The domains represented by the traces are the Outer Domain (heavy solid), Domain A (heavy dotted), Domain B (dashed), Domain C (solid), Domain D (dotted), and Domain E (dash-dot).

4.4   High Resolution versus Low Resolution

4.4.1   General Discussion.   An additional question, stated in Chapter 1, addressed the following issue: Is the paradigm that finer grid resolution always improves a models forecast correct?   This section explored this issue by employing RMSE calculations on the model output for each of the domain configurations discussed in Chapter 3.   The meteorological variables that were examined to address the posed question are geopotential height, temperature, wind speed, wind direction, and precipitation.
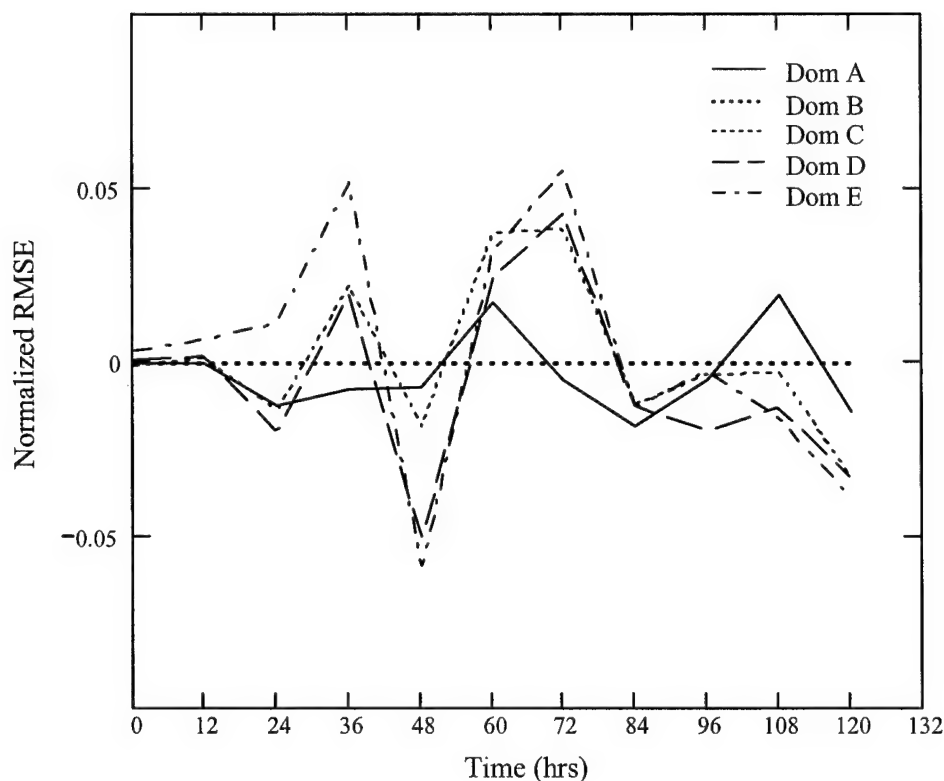
96
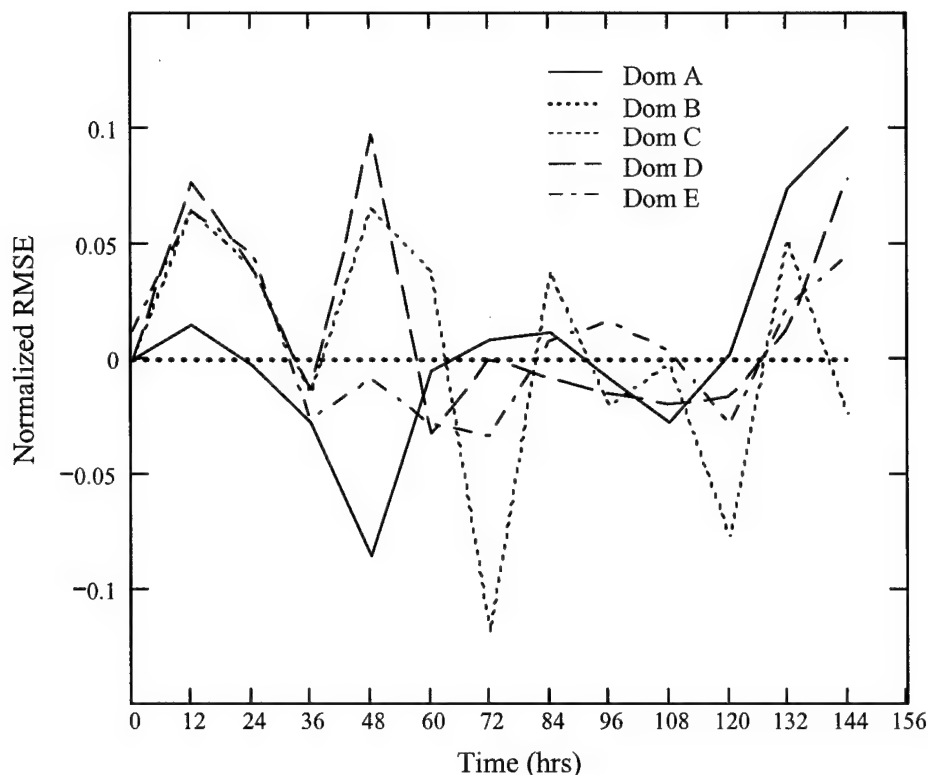
Figure 77   One-way nested domain placement comparison (wind direction) for the May case over a 950/150 mb layer. This figure compares the placement of the five high-resolution (12 km) one-way nested domains for the May case using normalized RMSE where the control value is from Domain B. The domains represented by the traces are Domain A (solid), Domain B (heavy dotted), Domain C (dotted), Domain D (dashed), and Domain E (dash-dot).

In this section, the statistical plots have been normalized to provide a more meaningful representation of the results. Normalization allows direct comparison of the high-resolution domain forecasts to those provided by the lower resolution (36 km) domain. The plots are standardized with time (in hours) along the abscissa and normalized RMSE along the ordinate. Normalized RMSE is either positive, negative, or zero. The zero line represents the control value which has been chosen as the independently run 36 km low-resolution (outer) domain. A negative value represents a decrease in the RMSE, or improvement in the model's forecast, and vice

versa. Each trace represents the model domain denoted in the key and was generated using the RMSE calculation for each verification time during the forecast period. It should also be noted that the resulting percentages of these normalized plots must be compared to the actual RMSE in the tables of Appendices A and B (some of the RMSE graphs were presented in the previous section) to quantify the decrease or increase in error relative to the low-resolution domain. Statistical plots have been generated for the 950/150 mb layer (where verification was computed every 25 mb throughout the layer) since it best represents the three-dimensional veracity of the various high-resolution model domains relative to the lower resolution grid.

The significant surface cyclogenetic events the reader should be aware of while viewing the statistical plots for the January case are as follows: the first cyclone entered the verification zone through the western boundary 36 hours into the forecast period, and the second cyclone reached its maximum intensity in the east portion of the verification zone 108 hours into the forecast period. A significant surface cyclogenetic event to be aware of for the May case is the entrance of a cyclone through the southwestern boundary of the verification zone 84 hours into the forecast period. The results in this section are presented by meteorological variable since significant differences in the findings exists between variables.

4.4.2 Geopotential Height. The first meteorological variable discussed is geopotential height. Figure 78 shows the statistical comparison of the five two-way nested 12 km resolution domains to the 36 km resolution domain for geopotential height over a 950/150 mb layer (January case). As seen from the graph, the two-way nested domains provided 14 percent improvement to the analysis relative to the low-resolution domain (the control); however, the geopotential height was degraded by 5 to 12 percent through the 36 hr forecast. After the entrance of the first surface cyclone through the western boundary of the verification zone 36 hours into the forecast, the two-way nested domains showed consistent improvement over the 36 km resolution domain. The geopotential height typical improved by 5 to 14 percent
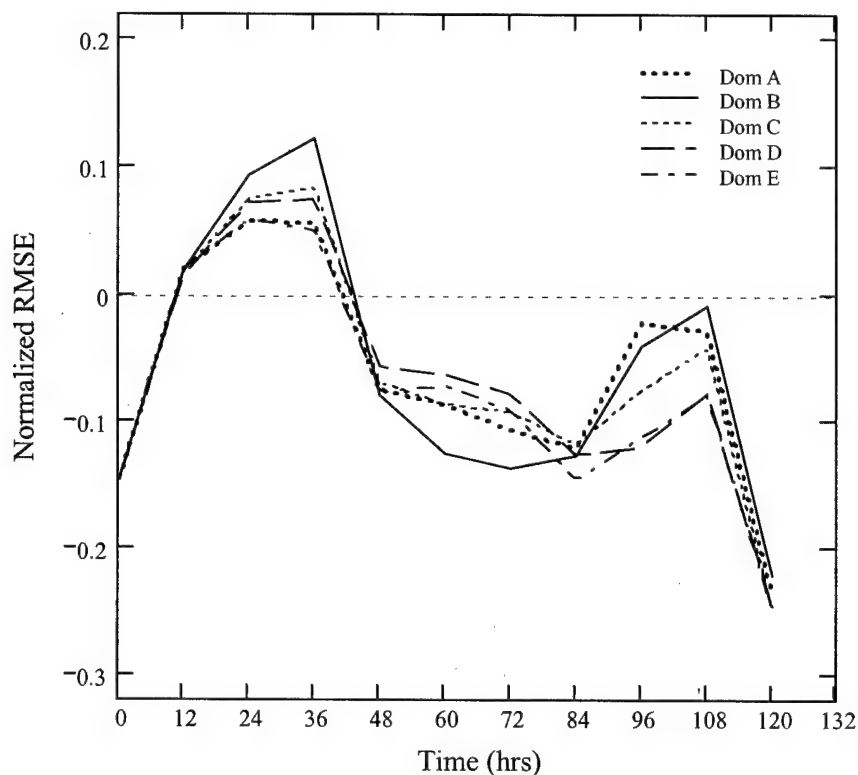
Figure 78   Normalized RMSE for geopotential height over a two-way nested 950/150 mb layer (January case). This figure compares the normalized geopotential height RMSE for the five high-resolution (12 km) two-way nested domains of the January case with the lower resolution (36 km) domain. The domains represented by the traces are Domain A (heavy dotted), Domain B (solid), Domain C (dotted), Domain D (dashed), and Domain E (dash-dot).

(relative to the low-resolution domain) from the 48 hr through 96 hr forecast. The second peak in the graph was found to be associated with the approximate time the second cyclone reached maximum intensity at the 108 hr forecast. As the second cyclone weakened and moved eastward out of the verification zone 120 hours into the forecast, the two-way nested domains provided up to 24 percent improvement to the forecasted geopotential height relative to the 36 km resolution domain. Figure 79 shows the statistical comparison of the five one-way nested 12 km resolution domains to the 36 km resolution domain for geopotential height over a 950/150 mb layer

99
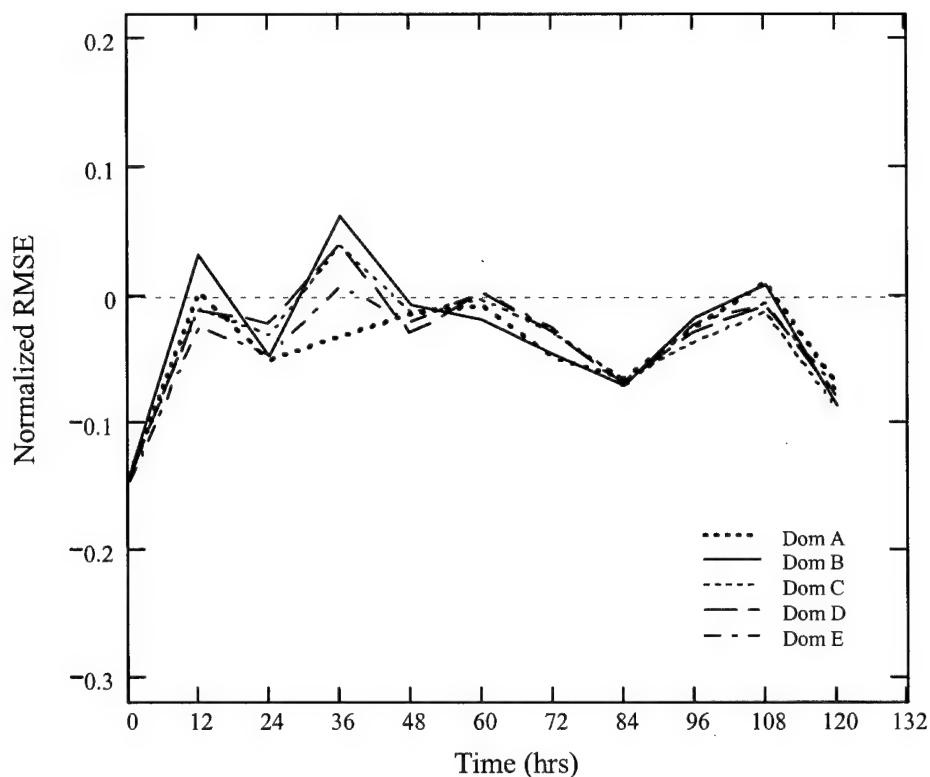
Figure 79   Normalized RMSE for geopotential height over a one-way nested
            950/150 mb layer (January case). This figure compares the normalized
            geopotential height RMSE for the five high-resolution (12 km) one-way
            nested domains of the January case with the lower resolution (36 km)
            domain. The domains represented by the traces are Domain A (heavy
            dotted), Domain B (solid), Domain C (dotted), Domain D (dashed),
            and Domain E (dash-dot).

(January case). As seen from the graph, the one-way nested domains provided 14

percent improvement to the analysis relative to the low-resolution domain; however,

the improvement in the geopotential height was decreased to less than 3 percent

during the spin-up period of the model (first 12 hours of the forecast). From the 12

hr to 36 hr forecast, the one-way nested domains displayed an oscillatory nature with

results ranging from five percent improvement to five percent degradation (relative

to the low-resolution domain). Beyond the 36 hr forecast, the one-way nested

domains improved the geopotential height by zero to eight percent over the 36 km

100
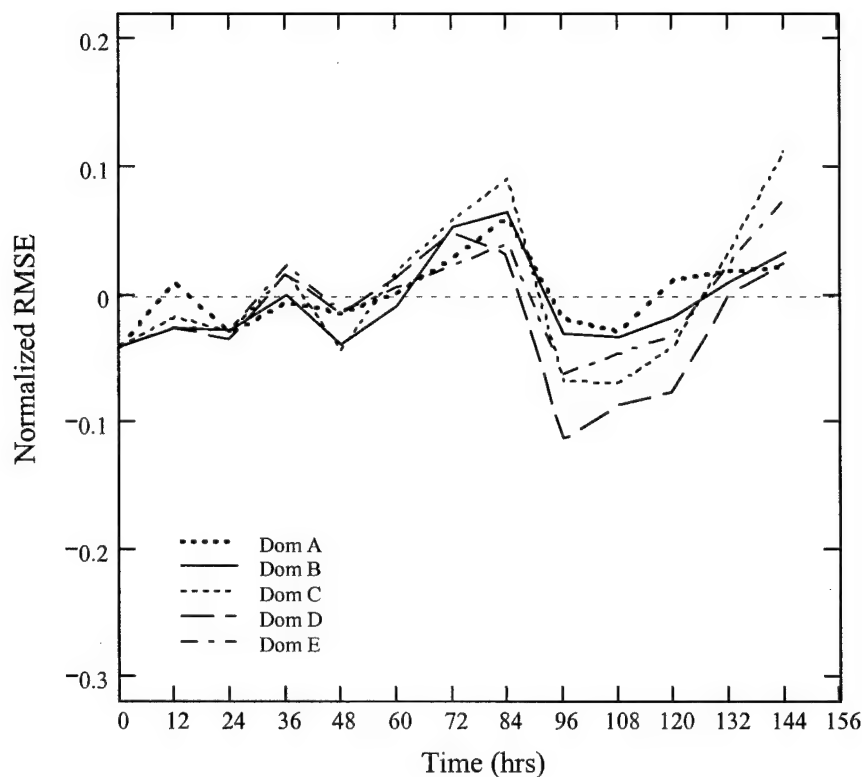
Figure 80   Normalized RMSE for geopotential height over a two-way nested
             950/150 mb layer (May case).   This figure compares the normalized
             geopotential height RMSE for the five high-resolution (12 km) two-way
             nested domains of the May case with the lower resolution (36 km) do-
             main.   The domains represented by the traces are Domain A (heavy
             dotted), Domain B (solid), Domain C (dotted), Domain D (dashed),
             and Domain E (dash-dot).

resolution domain.   It should be noted that the one-way nested domains produced

the most accurate forecast when surface cyclogenesis in the verification zone was

weak or absent, as shown in Table 3 of Appendix A.

Figure 80 shows the statistical comparison of the five two-way nested 12 km

resolution domains to the 36 km resolution domain for geopotential height over

a 950/150 mb layer (May case).   As seen from the graph, the two-way nested

domains provided four percent improvement to the analysis relative to the low-

resolution domain; however, the geopotential height showed an oscillatory degrading

101

trend through the 84 hr forecast. The forecasts of the two-way nested domains typically ranged from four percent improvement to five percent degradation, and up to nine percent degradation was seen by the 84 hr forecast (relative to the low-resolution domain). After the surface cyclone entered the southwestern boundary of the verification zone 84 hours into the forecast, the two-way nested domains showed up to twelve percent improvement over the 36 km resolution domain. As the cyclone weakened over the northern portion of the verification zone during the final 24 hours of the forecast period, the 36 km resolution domain again produced the superior forecast. Figure 81 shows the statistical comparison of the five one-way nested 12 km resolution domains to the 36 km resolution domain for geopotential height over a 950/150 mb layer (May case). As seen from the graph, the one-way nested domains provided four percent improvement to the analysis relative to the low-resolution domain; however, geopotential height oscillated between improvement and degradation for the remainder of the forecast period. The one-way nested domains typically ranged from five percent improvement to five percent degradation through the 84 hr forecast (relative to the low-resolution domain). As the surface cyclone entered the southwestern boundary of the verification zone 84 hours into the forecast and reached its maximum intensity near the 96 hr point, the geopotential height was degraded by ten to twelve percent when compared to the 36 km resolution domain. Beyond the 96 hr forecast, the one-way nested domains exhibited an oscillation between four percent improvement and four percent degradation relative to the 36 km resolution domain.

In summary, the results indicate the two-way nested 12 km resolution domain yields a substantial improvement in the model's geopotential height forecast over the independently run 36 km resolution domain during the period when ageostrophic motions in the atmosphere are generally large (e.g., cyclogenesis in the domain). However, the results also indicate the two-way nested domain is of little benefit, and can in fact degrade the forecast, during periods when the atmosphere tends toward
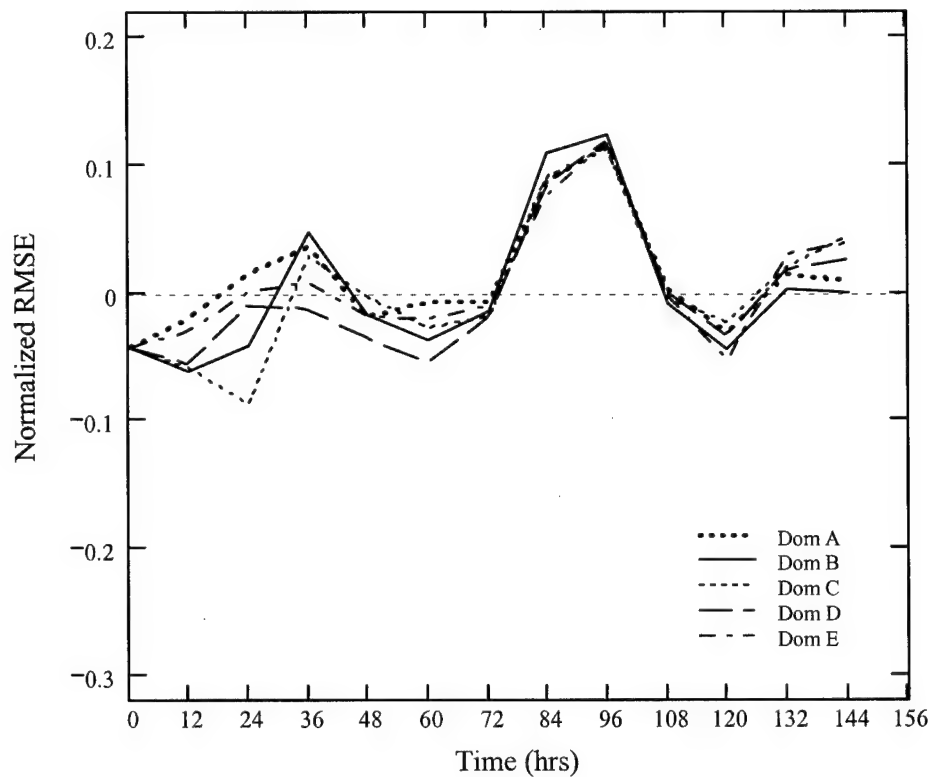
Figure 81   Normalized RMSE for geopotential height over a one-way nested
             950/150 mb layer (May case).   This figure compares the normalized
             geopotential height RMSE for the five high-resolution (12 km) one-way
             nested domains of the May case with the lower resolution (36 km) do-
             main.   The domains represented by the traces are Domain A (heavy
             dotted), Domain B (solid), Domain C (dotted), Domain D (dashed),
             and Domain E (dash-dot).

geostrophic balance.   This was evident in the May case where cyclogenesis was
absent from the verification zone during the first 84 hours of the forecast.   For the
one-way nested 12 km resolution domain, the results indicate the best geopotential
height forecast is produced when cyclogenesis is weak or nonexistent.   However,
improvements in the model's forecast over the 36 km resolution domain are often
marginal.   It was evident from both case studies that strong cyclogenesis generally
limited the forecast improvement one-way nested domains provided when compared
to the 36 km resolution domain, and usually degrades it.
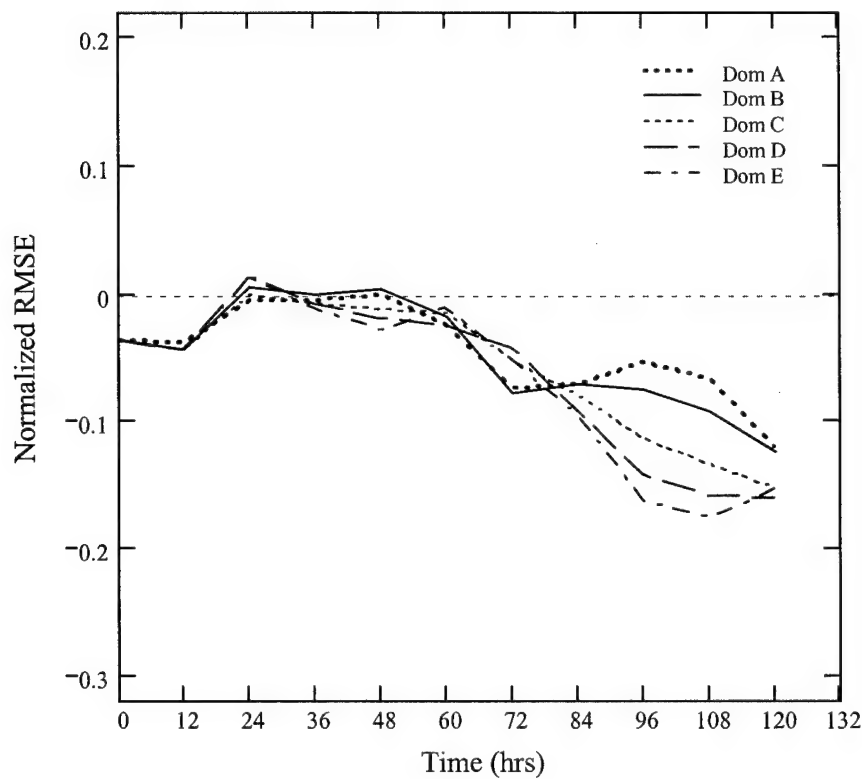
Figure 82   Normalized RMSE for temperature over a two-way nested 950/150 mb layer (January case).   This figure compares the normalized temperature RMSE for the five high-resolution (12 km) two-way nested domains of the January case with the lower resolution (36 km) domain.   The domains represented by the traces are Domain A (heavy dotted), Domain B (solid), Domain C (dotted), Domain D (dashed), and Domain E (dash-dot).

4.4.3   Temperature.   Next, temperature will be discussed.   Figure 82 shows the statistical comparison of the five two-way nested 12 km resolution domains to the 36 km resolution domain for temperature over a 950/150 mb layer (January case).   As seen from the graph, the two-way nested domains provided 3.5 percent improvement to the analysis and 12 hr forecast relative to the low-resolution domain (the control). From the 24 hr to 48 hr forecast, the two-way nested domains provided little or no improvement over the 36 km resolution domain.   Twelve hours after the first surface cyclone entered the verification zone through the western boundary (48 hour point),

104
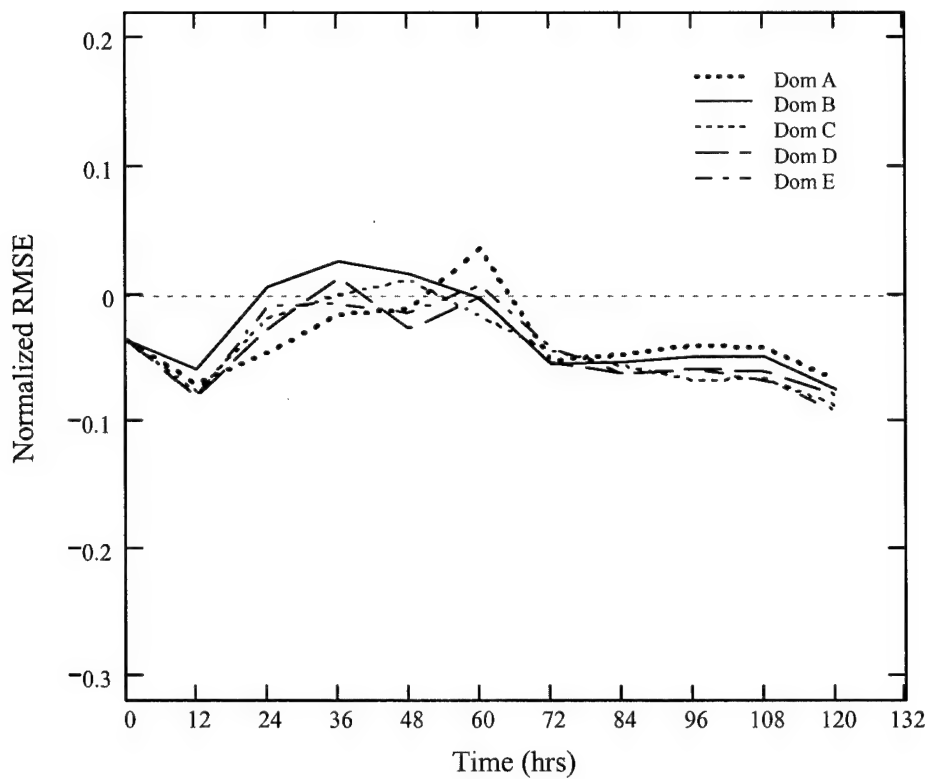
Figure 83   Normalized RMSE for temperature over a one-way nested 950/150 mb layer (January case). This figure compares the normalized temperature RMSE for the five high-resolution (12 km) one-way nested domains of the January case with the lower resolution (36 km) domain. The domains represented by the traces are Domain A (heavy dotted), Domain B (solid), Domain C (dotted), Domain D (dashed), and Domain E (dash-dot).

the forecasted temperature of the two-way nested domains consistently improved when compared to the low-resolution domain. The two-way nested domains provided up to 18 percent improvement in the forecasted temperature (relative to the low-resolution domain) between the 60 hr and 120 hr forecasts. Figure 83 shows the statistical comparison of the five one-way nested 12 km resolution domains to the 36 km resolution domain for temperature over a 950/150 mb layer (January case). As seen from the graph, the one-way nested domains provided 3.5 percent improvement to the analysis and up to an 8 percent improvement to the 12 hr forecast relative to
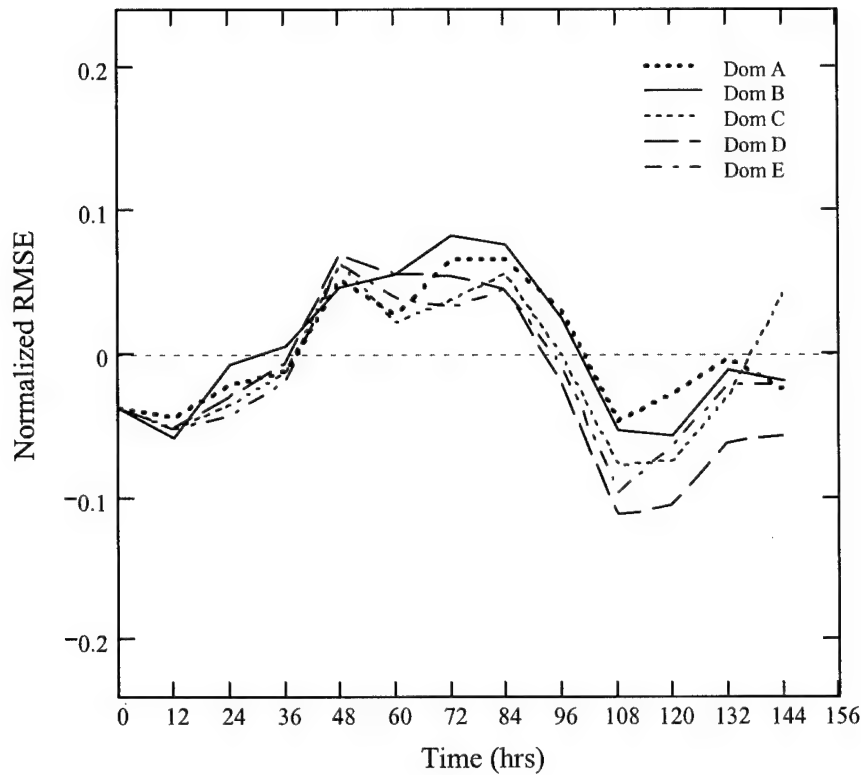
Figure 84   Normalized RMSE for temperature over a two-way nested 950/150 mb
layer (May case).   This figure compares the normalized temperature
RMSE for the five high-resolution (12 km) two-way nested domains of
the May case with the lower resolution (36 km) domain.   The domains
represented by the traces are Domain A (heavy dotted), Domain B
(solid), Domain C (dotted), Domain D (dashed), and Domain E (dash-
dot).

the low-resolution domain.   From the 24 hr to 60 hr forecast, the one-way nested

domains offered little or no improvement to the temperature provided by the 36 km

resolution domain.   Again, the performances of the one-way nested domains were

poor during the period of maximum intensity for the first cyclone.   Beyond the 60

hr forecast, the one-way nested domains offered a four to eight percent improvement

over the temperature provided by the 36 km resolution domain.

Figure 84 shows the statistical comparison of the five two-way nested 12 km

resolution domains to the 36 km resolution domain for temperature over a 950/150

106
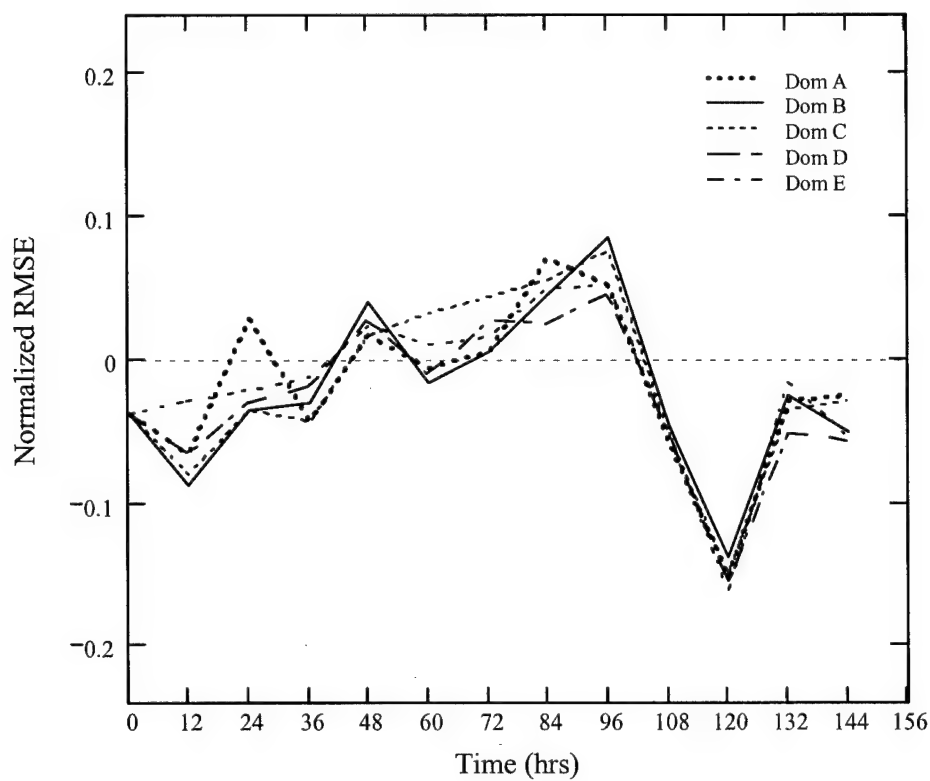
Figure 85   Normalized RMSE for temperature over a one-way nested 950/150 mb
layer (May case).   This figure compares the normalized temperature
RMSE for the five high-resolution (12 km) one-way nested domains of
the May case with the lower resolution (36 km) domain. The domains
represented by the traces are Domain A (heavy dotted), Domain B
(solid), Domain C (dotted), Domain D (dashed), and Domain E (dash-
dot).

mb layer (May case). As seen from the graph, the two-way nested domains provided

four to five percent improvement to the analysis and 12 hr forecast relative to the

low-resolution domain; however, the temperature showed a degrading trend from the

12 hr to 84 hr forecast. The forecasted temperature was degraded by nine percent

(relative to the low-resolution domain) when the surface cyclone entered the south-

western boundary of the verification zone 84 hours into the forecast. Beyond the 84

hr forecast, the two-way nested domains offered up to eleven percent improvement

in the temperature over the 36 km resolution domain. Figure 85 shows the statis-

tical comparison of the five one-way nested 12 km resolution domains to the 36 km resolution domain for temperature over a 950/150 mb layer (May case). As seen from the graph, the one-way nested domains provided four percent improvement to the analysis and up to nine percent improvement to the 12 hr forecast relative to the low-resolution domain. From the 12 hr to 96 hr forecast, the one-way nested domains showed a degrading trend when compared to the low-resolution domain. By the 96 hr forecast (approximate time of surface cyclones maximum intensity), the temperature was degraded by nine percent when compared to the forecast of the 36 km resolution domain. Beyond the 96 hour point, the one-way nested domains typically improved the forecast by 2 to 5 percent (relative to the low-resolution domain), except for the 120 hr forecast which was improved by as much as 16 percent.

In summary, the results indicate the two-way nested 12 km resolution domain yields a substantial improvement in the model's temperature forecast veracity over the independently run 36 km resolution domain during the period when ageostrophic motions in the atmosphere are generally large. Again, the results also indicate the two-way nested domain is of little benefit, and can in fact degrade the forecast, during periods when the atmosphere tends toward geostrophic balance. This was evident in both case studies where cyclogenesis was absent from the verification zone. For the one-way nested 12 km resolution domain, the results indicate the best temperature forecast (relative to the low-resolution domain) is produced when cyclogenesis is weak or in the eastern portion of the verification zone. However, improvements in the model's forecast over the 36 km resolution domain are generally limited to about five percent. It was evident in both case studies that one-way nesting temperature improvements lag the maximum intensity of surface cyclogenesis by at least 12 hours.

4.4.4 Wind Speed. Wind speed will be examined in this subsection. Figure 86 shows the statistical comparison of the five two-way nested 12 km resolution domains to the 36 km resolution domain for wind speed over a 950/150 mb layer (January case). As seen from the graph, the two-way nested domains provided
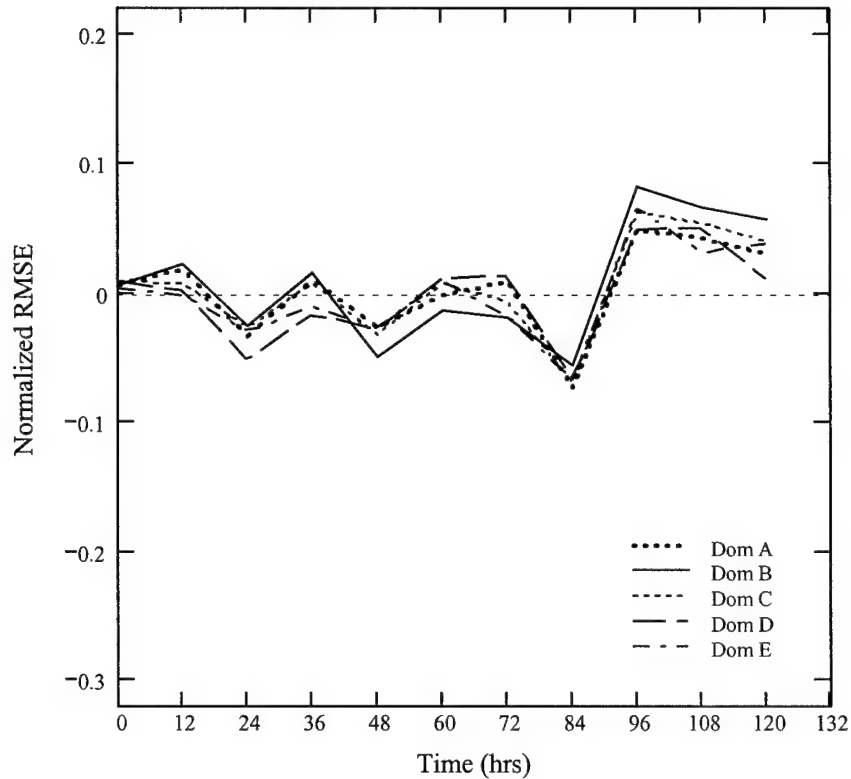
Figure 86   Normalized RMSE for wind speed over a two-way nested 950/150 mb layer (January case). This figure compares the normalized wind speed RMSE for the five high-resolution (12 km) two-way nested domains of the January case with the lower resolution (36 km) domain. The domains represented by the traces are Domain A (heavy dotted), Domain B (solid), Domain C (dotted), Domain D (dashed), and Domain E (dash-dot).

wind speed forecasts which were oscillatory in nature when compared to the low-resolution domain (the control). From the analysis to the 72 hr forecast, the two-way nested domains oscillated between up to five percent improvement and two percent degradation relative to the 36 km resolution domain. After the 72 hr forecast, the oscillation became larger ranging between up to seven percent improvement and eight percent degradation (relative to the low-resolution domain). There appeared to be no apparent association between the relative RMSE and the significant surface cyclogenetic events. Figure 87 shows the statistical comparison of the five one-way

109
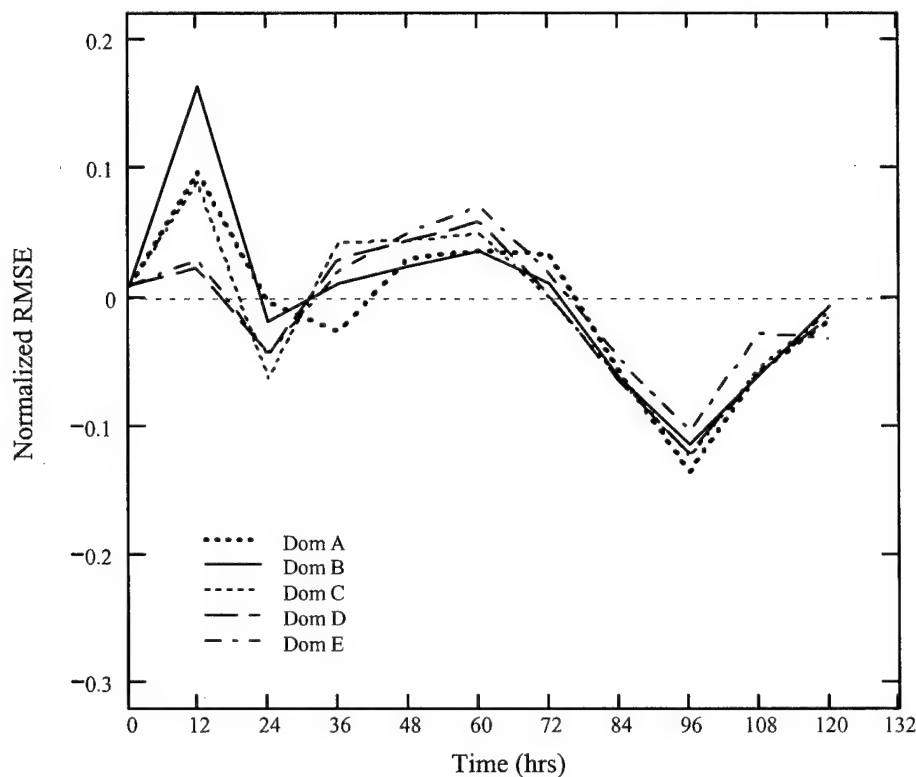
Figure 87   Normalized RMSE for wind speed over a one-way nested 950/150 mb
layer (January case). This figure compares the normalized wind speed
RMSE for the five high-resolution (12 km) one-way nested domains
of the January case with the lower resolution (36 km) domain. The
domains represented by the traces are Domain A (heavy dotted), Do-
main B (solid), Domain C (dotted), Domain D (dashed), and Domain
E (dash-dot).

nested 12 km resolution domains to the 36 km resolution domain for wind speed
over a 950/150 mb layer (January case). As seen from the graph, the one-way
nested domains provided wind speed forecasts which were oscillatory in nature when
compared to the low-resolution domain. The one-way nested domains oscillated
between up to 16 percent degradation and 14 percent improvement (relative to the
low-resolution domain) throughout the 120 hour forecast period. There appeared
to be no apparent association between the relative RMSE and the significant surface
cyclogenetic events.

110
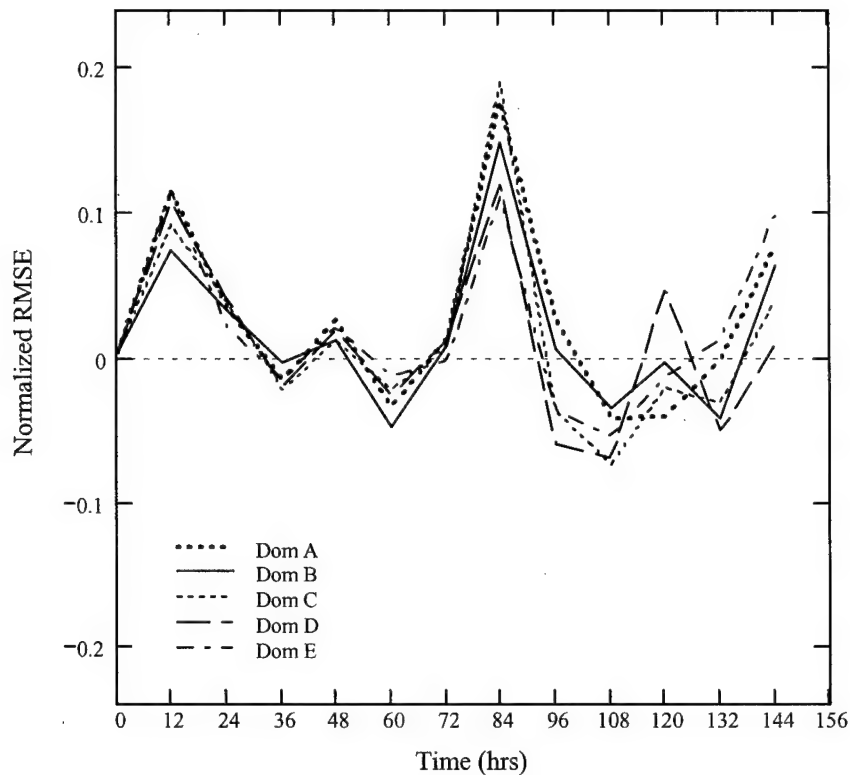
Figure 88   Normalized RMSE for wind speed over a two-way nested 950/150 mb layer (May case).   This figure compares the normalized wind speed RMSE for the five high-resolution (12 km) two-way nested domains of the May case with the lower resolution (36 km) domain.   The domains represented by the traces are Domain A (heavy dotted), Domain B (solid), Domain C (dotted), Domain D (dashed), and Domain E (dash-dot).

Figure 88 shows the statistical comparison of the five two-way nested 12 km resolution domains to the 36 km resolution domain for wind speed over a 950/150 mb layer (May case).   As seen from the graph, the two-way nested domains provided wind speed forecasts which were oscillatory in nature when compared to the low-resolution domain.   The two-way nested domains oscillated between up to 19 percent degradation and 7 percent improvement (relative to the low-resolution domain) throughout the 144 hour forecast period.   There appeared to be minimal association between the relative RMSE and the significant surface cyclogenetic event, except

111
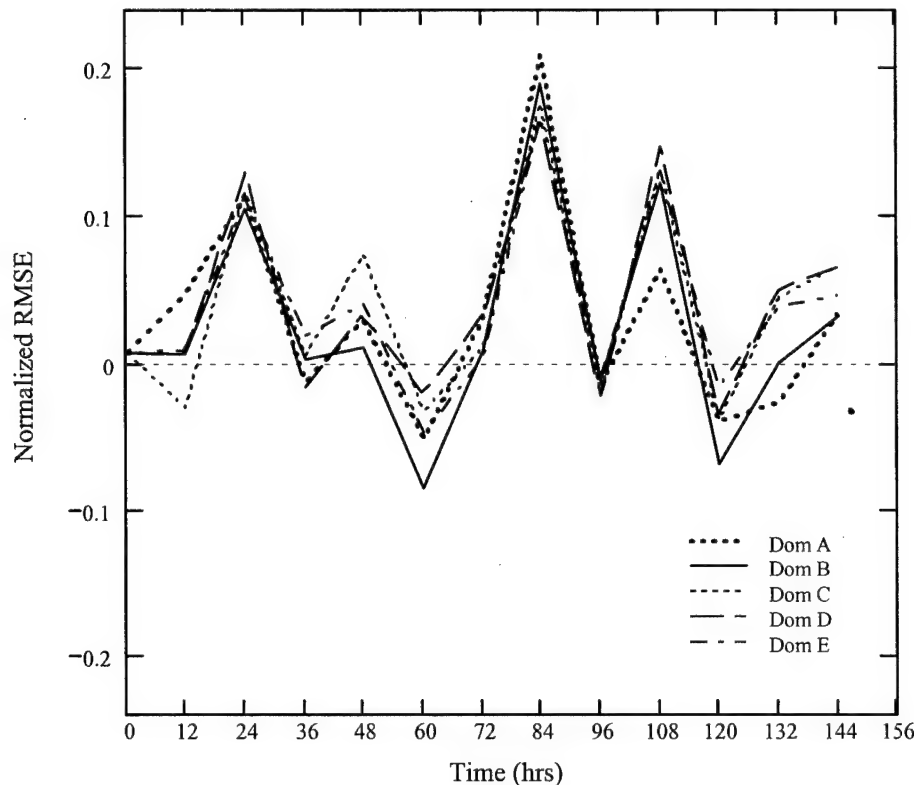
Figure 89   Normalized RMSE for wind speed over a one-way nested 950/150 mb
layer (May case).   This figure compares the normalized wind speed
RMSE for the five high-resolution (12 km) one-way nested domains of
the May case with the lower resolution (36 km) domain. The domains
represented by the traces are Domain A (heavy dotted), Domain B
(solid), Domain C (dotted), Domain D (dashed), and Domain E (dash-
dot).

the maximum degradation coincided with the cyclone entering the verification zone

through the southwestern boundary at the 84 hour point. Figure 89 shows the sta-

tistical comparison of the five one-way nested 12 km resolution domains to the 36 km

resolution domain for wind speed over a 950/150 mb layer (May case). As seen from

the graph, the one-way nested domains provided wind speed forecasts which were

oscillatory in nature when compared to the low-resolution domain.   The one-way

nested domains oscillated between up to 21.5 percent degradation and 8.5 percent

improvement (relative to the low-resolution domain) throughout the 144 hour fore-

112

cast period. There appeared to be minimal association between the relative RMSE and the significant surface cyclogenetic event, except the maximum degradation coincided with the cyclone entering the verification zone through the southwestern boundary at the 84 hour point.

In summary, the results indicate neither the two-way nested nor one-way nested 12 km resolution domains yield a wind speed forecast which is clearly superior that of the independently run 36 km resolution domain. In fact, the two types of nested domains can produce degraded results when averaged over the entire forecast period (this can be illustrated by summing each row of Table 51 in Appendix B). This degradation is most likely to occur when cyclogenesis is absent from the domain.

4.4.5 Wind Direction. Wind direction will be examined in this subsection. Figure 90 shows the statistical comparison of the five two-way nested 12 km resolution domains to the 36 km resolution domain for wind direction over a 950/150 mb layer (January case). As seen from the graph, the two-way nested domains provided wind direction forecasts which were oscillatory in nature when compared to the low-resolution domain (the control). From the analysis to the 108 hr forecast, the two-way nested domains generally oscillated between zero and six percent improvement over the 36 km resolution domain. After the 108 hr forecast (or maximum intensity of the second surface cyclone), the two-way nested domains degraded the wind direction forecast by as much as 7.5 percent (relative to the low-resolution domain). There appeared to be minimal association between the relative RMSE and the significant surface cyclogenetic events, except the degrading trend after the second surface cyclone reached its maximum intensity over the eastern portion of the verification zone. Figure 91 shows the statistical comparison of the five one-way nested 12 km resolution domains to the 36 km resolution domain for wind direction over a 950/150 mb layer (January case). As seen from the graph, the one-way nested domains provided wind direction forecasts which were oscillatory in nature when compared to the low-resolution domain. The one-way nested domains oscil-

113
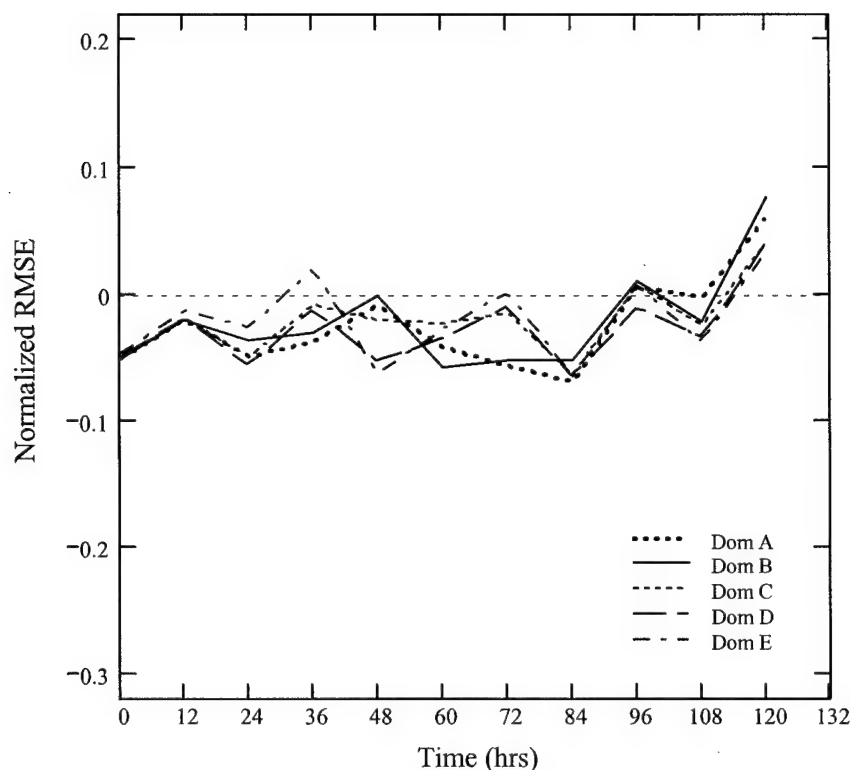
Figure 90   Normalized RMSE for wind direction over a two-way nested 950/150 mb layer (January case). This figure compares the normalized wind direction RMSE for the five high-resolution (12 km) two-way nested domains of the January case with the lower resolution (36 km) domain. The domains represented by the traces are Domain A (heavy dotted), Domain B (solid), Domain C (dotted), Domain D (dashed), and Domain E (dash-dot).

lated between up to 11 percent improvement and 7.5 percent degradation (relative to the low-resolution domain) throughout the 120 hour forecast period. There appeared to be minimal association between the relative RMSE and the significant surface cyclogenetic events, except the degrading trend when the first surface cyclone entered the western boundary and after the second surface cyclone reached its maximum intensity over the eastern portion of the verification zone.

Figure 92 shows the statistical comparison of the five two-way nested 12 km resolution domains to the 36 km resolution domain for wind direction over a 950/150

114
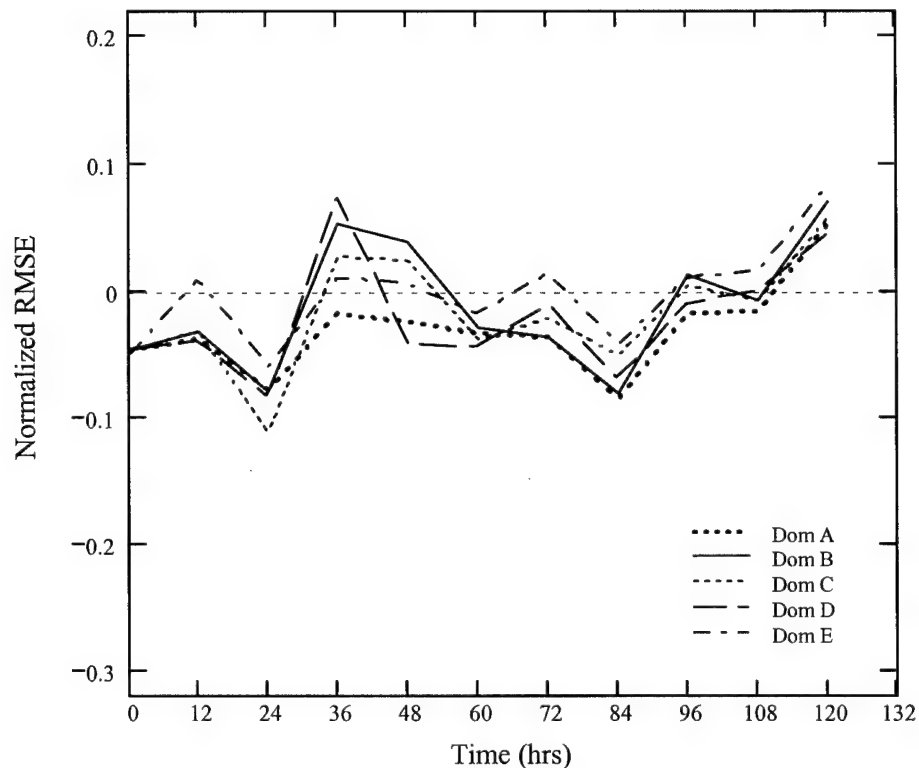
Figure 91   Normalized RMSE for wind direction over a one-way nested 950/150 mb layer (January case).   This figure compares the normalized wind direction RMSE for the five high-resolution (12 km) one-way nested domains of the January case with the lower resolution (36 km) domain. The domains represented by the traces are Domain A (heavy dotted), Domain B (solid), Domain C (dotted), Domain D (dashed), and Domain E (dash-dot).

mb layer (May case).   As seen from the graph, the two-way nested domains provided wind direction forecasts which were oscillatory in nature when compared to the low-resolution domain.   The two-way nested domains generally oscillated between up to 7.5 percent improvement and 12 percent degradation (relative to the low-resolution domain) throughout the 144 hour forecast period.   There appeared to be minimal association between the relative RMSE and the significant surface cyclogenetic event, except possibly a temporary dampening of the forecast's oscillatory nature when the cyclone entered the southwestern boundary of the verification zone.   Figure

115
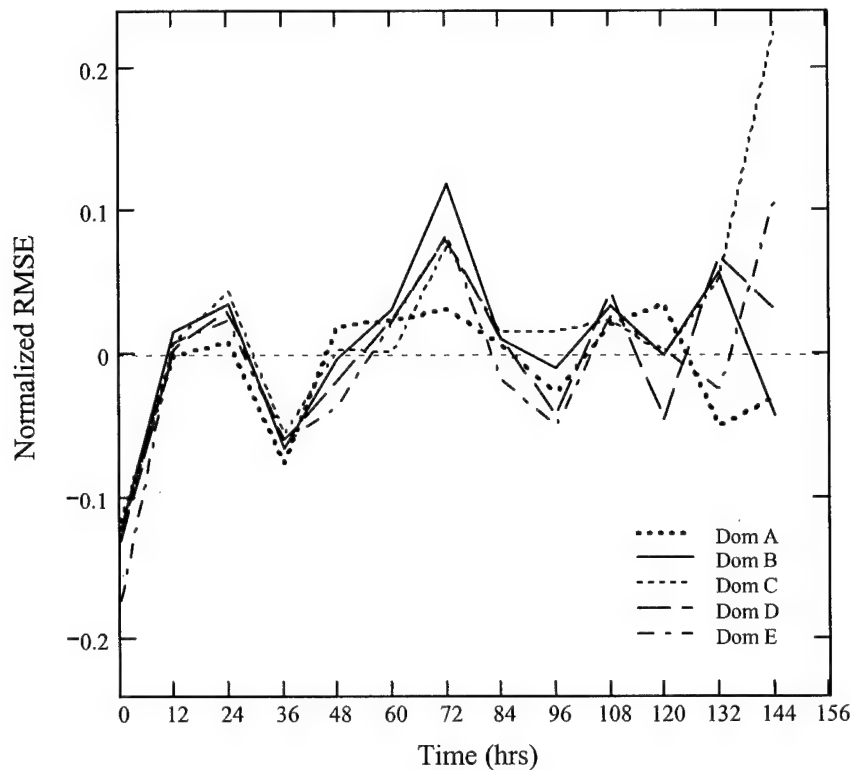
Figure 92   Normalized RMSE for wind direction over a two-way nested 950/150 mb layer (May case). This figure compares the normalized wind direction RMSE for the five high-resolution (12 km) two-way nested domains of the May case with the lower resolution (36 km) domain. The domains represented by the traces are Domain A (heavy dotted), Domain B (solid), Domain C (dotted), Domain D (dashed), and Domain E (dash-dot).

93 shows the statistical comparison of the five one-way nested 12 km resolution domains to the 36 km resolution domain for wind direction over a 950/150 mb layer (May case). As seen from the graph, the one-way nested domains provided wind direction forecasts which were extremely oscillatory in nature when compared to the low-resolution domain. The one-way nested domains oscillated between up to 11.5 percent improvement and 20 percent degradation (relative to the low-resolution domain) throughout the 144 hour forecast period. There appeared to be no apparent association between the relative RMSE and the significant surface cyclogenetic event.

116
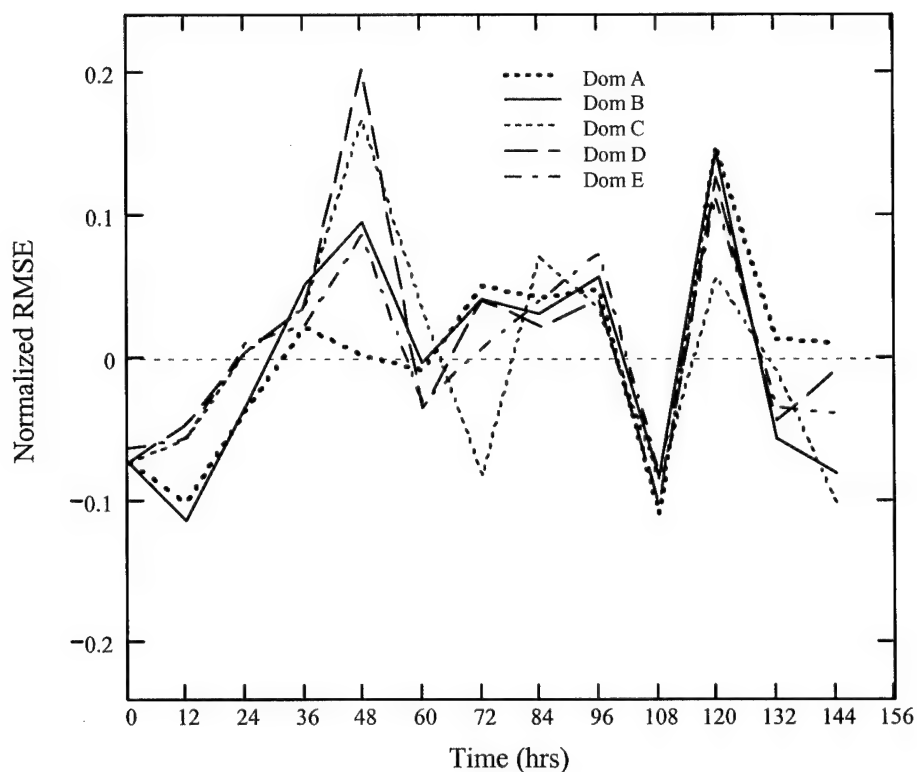
Figure 93   Normalized RMSE for wind direction over a one-way nested 950/150 mb layer (May case). This figure compares the normalized wind direction RMSE for the five high-resolution (12 km) one-way nested domains of the May case with the lower resolution (36 km) domain. The domains represented by the traces are Domain A (heavy dotted), Domain B (solid), Domain C (dotted), Domain D (dashed), and Domain E (dash-dot).

In summary, the results indicate both the two-way nested and the one-way nested 12 km resolution domains yield a marginal improvement to the model's wind direction forecast over the independently run 36 km resolution domain when surface cyclogenesis is present in the domain early in the forecast period. In contrast, the two types of nested domains yield an inferior forecast when cyclogenesis is absent from the domain, as indicated by the May case study.
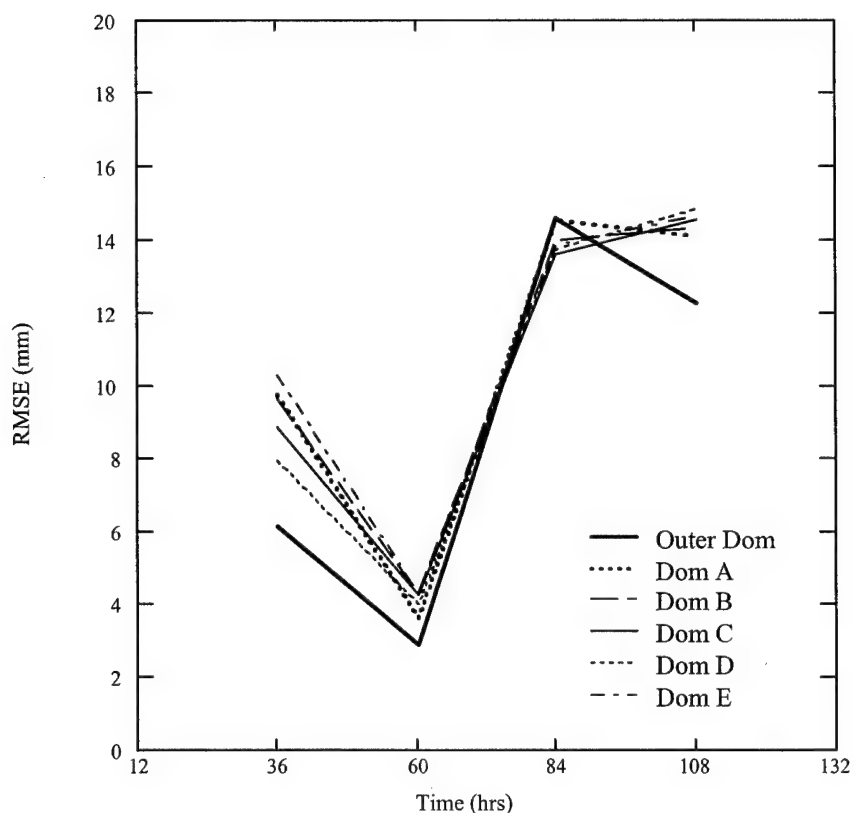
Figure 94   Precipitation RMSE for two-way nesting (January case).   This figure
shows the 24 hr cumulative precipitation RMSE for the outer domain
(36 km) and the five high-resolution (12 km) two-way nested domains for
the January case The domains represented by the traces are the Outer
Domain (heavy solid), Domain A (heavy dotted), Domain B (dashed),
Domain C (solid), Domain D (dotted), and Domain E (dash-dot).

4.4.6   Precipitation.   The final parameter to be examined is precipitation.
Figure 94 shows January 24 hr cumulative precipitation RMSE for the 36 km resolu-
tion domain and the five two-way nested 12 km resolution domains.   It is apparent
from the graph that the low-resolution (outer) domain yielded the best forecast for
all times except the 84 hr forecast.   Figure 94 should be used in conjunction with the
next figure to determine the actual differences between the low-resolution forecast
and the various high-resolution forecasts.   Figure 95 shows the statistical comparison
of the five two-way nested 12 km resolution domains to the 36 km resolution domain

118
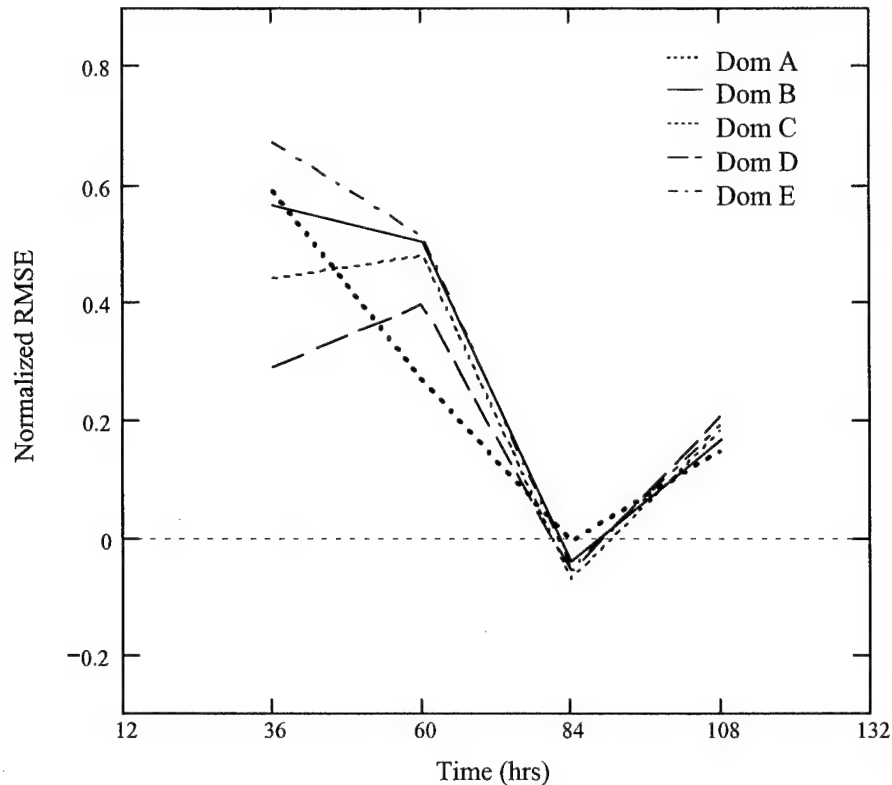
Figure 95   Normalized precipitation RMSE for two-way nesting (January case). This figure compares the normalized 24 hr cumulative precipitation RMSE for the five high-resolution (12 km) two-way nested domains of the January case with the lower resolution (36 km) domain. The domains represented by the traces are Domain A (heavy dotted), Domain B (solid), Domain C (dotted), Domain D (dashed), and Domain E (dash-dot).

for 24 hr cumulative precipitation (January case). This graph suggests that the two-way nested domains provided precipitation forecasts which were generally inferior to those of the 36 km resolution domain. The two-way nested domains degraded the model's forecast by as much as 67 percent for three of the four verification times. Only for the 84 hr forecast was the forecasted precipitation improved by a marginal five percent relative to the low-resolution domain. Figure 96 shows January 24 hr cumulative precipitation RMSE for the 36 km resolution domain and the five one-way nested 12 km resolution domains. It can be seen from the graph that most of

119
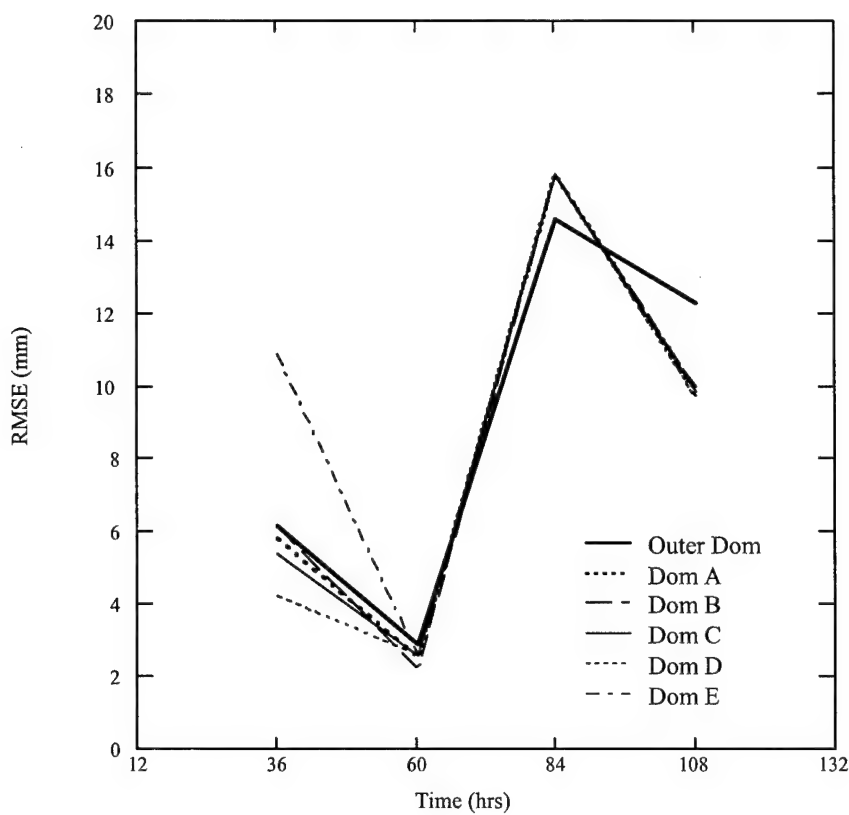
Figure 96   Precipitation RMSE for one-way nesting (January case).   This figure
shows the 24 hr cumulative precipitation RMSE for the outer domain
(36 km) and the five high-resolution (12 km) one-way nested domains for
the January case The domains represented by the traces are the Outer
Domain (heavy solid), Domain A (heavy dotted), Domain B (dashed),
Domain C (solid), Domain D (dotted), and Domain E (dash-dot).

the high-resolution one-way nested domains yielded the best forecast for all times
except the 84 hr forecast.   Figure 96 should be used in conjunction with the next
figure to determine the actual differences between the low-resolution forecast and
the various high-resolution forecasts.   Figure 97 shows the statistical comparison of
the five one-way nested 12 km resolution domains to the 36 km resolution domain
for 24 hr cumulative precipitation (January case).   This graph suggests that the
one-way nested domains provided precipitation forecasts which were generally supe-
rior to those of the 36 km resolution domain. The one-way nested domains generally
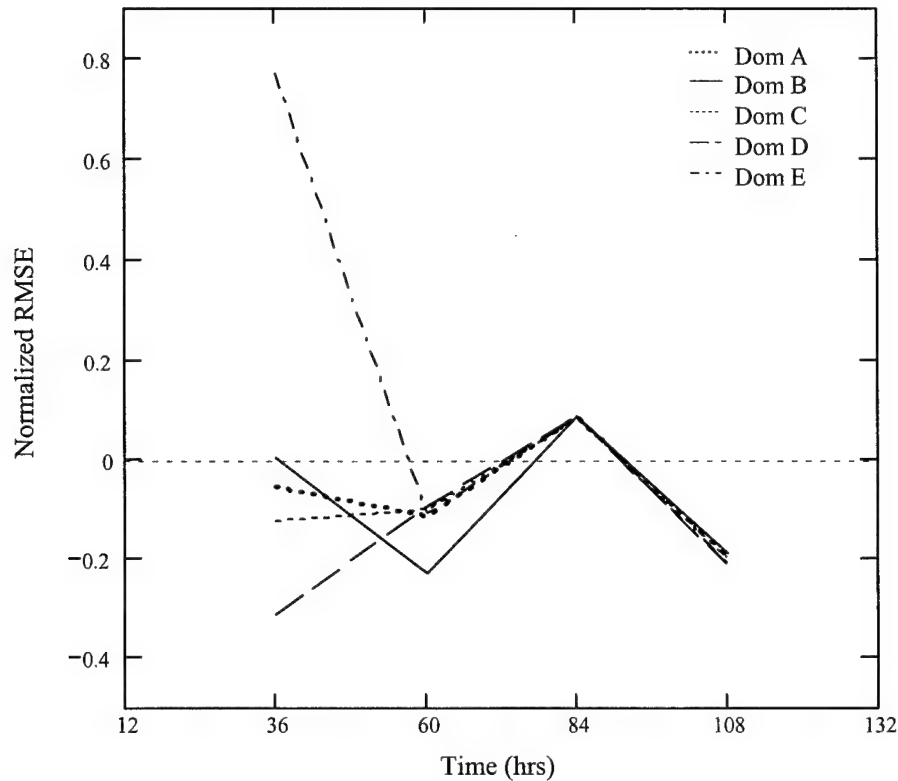
Figure 97   Normalized precipitation RMSE for one-way nesting (January case). This figure compares the normalized 24 hr cumulative precipitation RMSE for the five high-resolution (12 km) one-way nested domains of the January case with the lower resolution (36 km) domain. The domains represented by the traces are Domain A (heavy dotted), Domain B (solid), Domain C (dotted), Domain D (dashed), and Domain E (dash-dot).

improved the model's forecast by as much as 30 percent for three of the four verification times. Only for the 84 hr forecast was the forecasted precipitation degraded by about nine percent relative to the low-resolution domain.

Figures 98 through 100 show the 84 hr 15 January 1995 forecast of 24 hour cumulative precipitation for the 36 km resolution domain, 12 km resolution two-way nested domain, and 12 km resolution one-way nested domain, respectively. Although the Figures 94 through 97 suggest (on average) less than three millimeters of variation in the precipitation between the various grids at 84 hours, the contours plots in

121
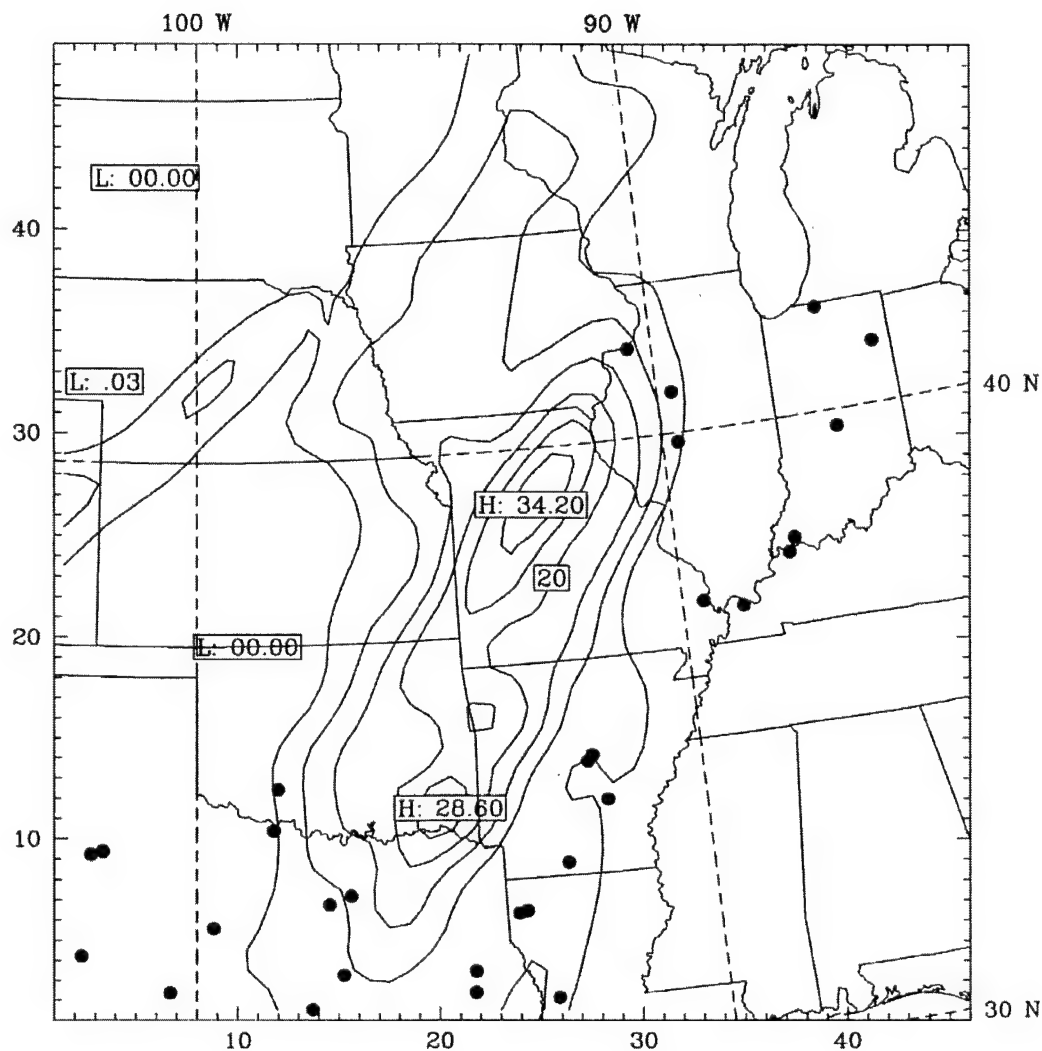
Figure 98   Precipitation for 84 hr 15 January 1995 forecast of the 36 km resolution domain. This chart shows the 24 hr cumulative precipitation forecast by the model's outer domain. The contours are in five millimeter intervals. The dots (•) show the locations used for grid-to-station verification. The coordinates are labeled in both grid point space and latitude/longitude.
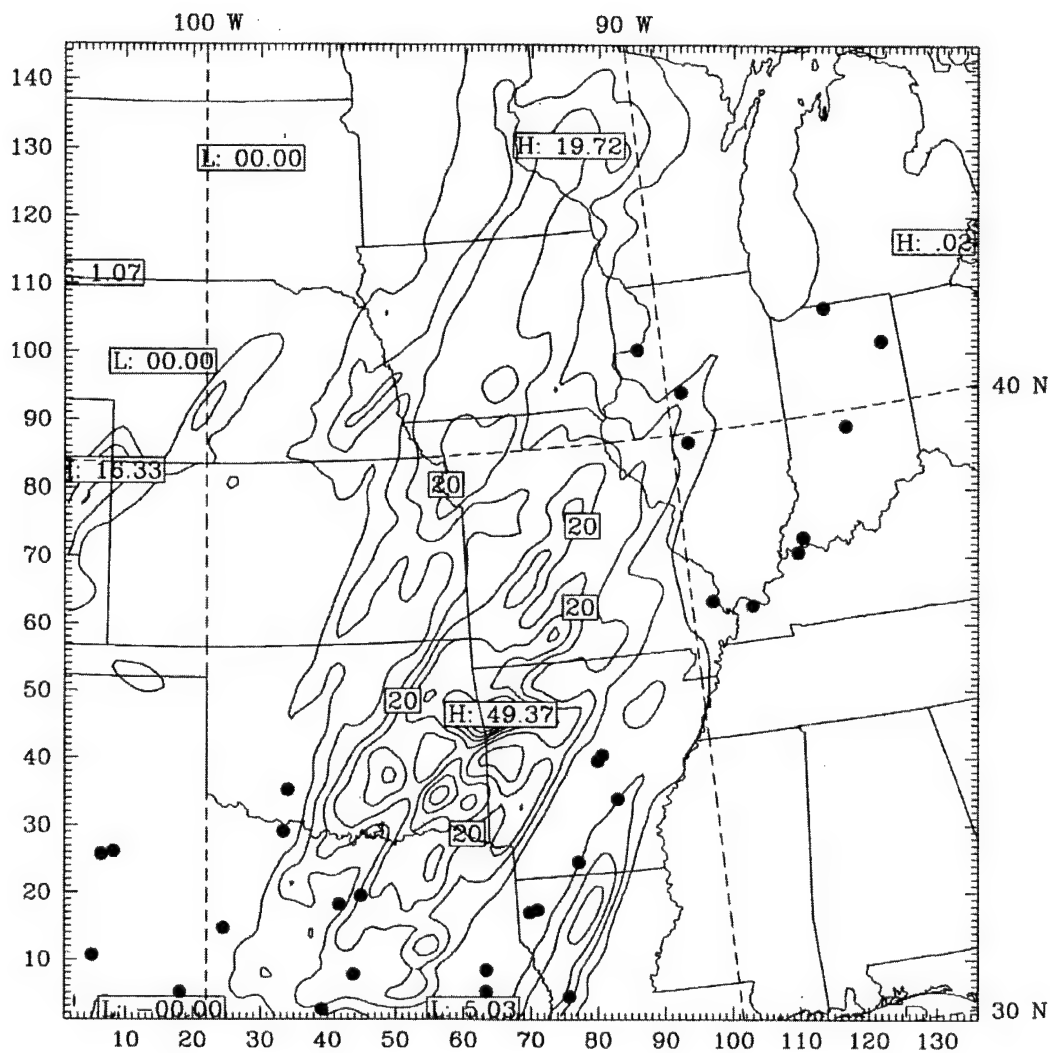
Figure 99   Precipitation for 84 hr 15 January 1995 forecast of the 12 km resolution
two-way nested domain. This chart shows the 24 hr cumulative precipi-
tation forecast by the model's two-way nested Domain D. The contours
are in five millimeter intervals. The dots (•) show the locations used for
grid-to-station verification. The coordinates are labeled in both grid
point space and latitude/longitude.
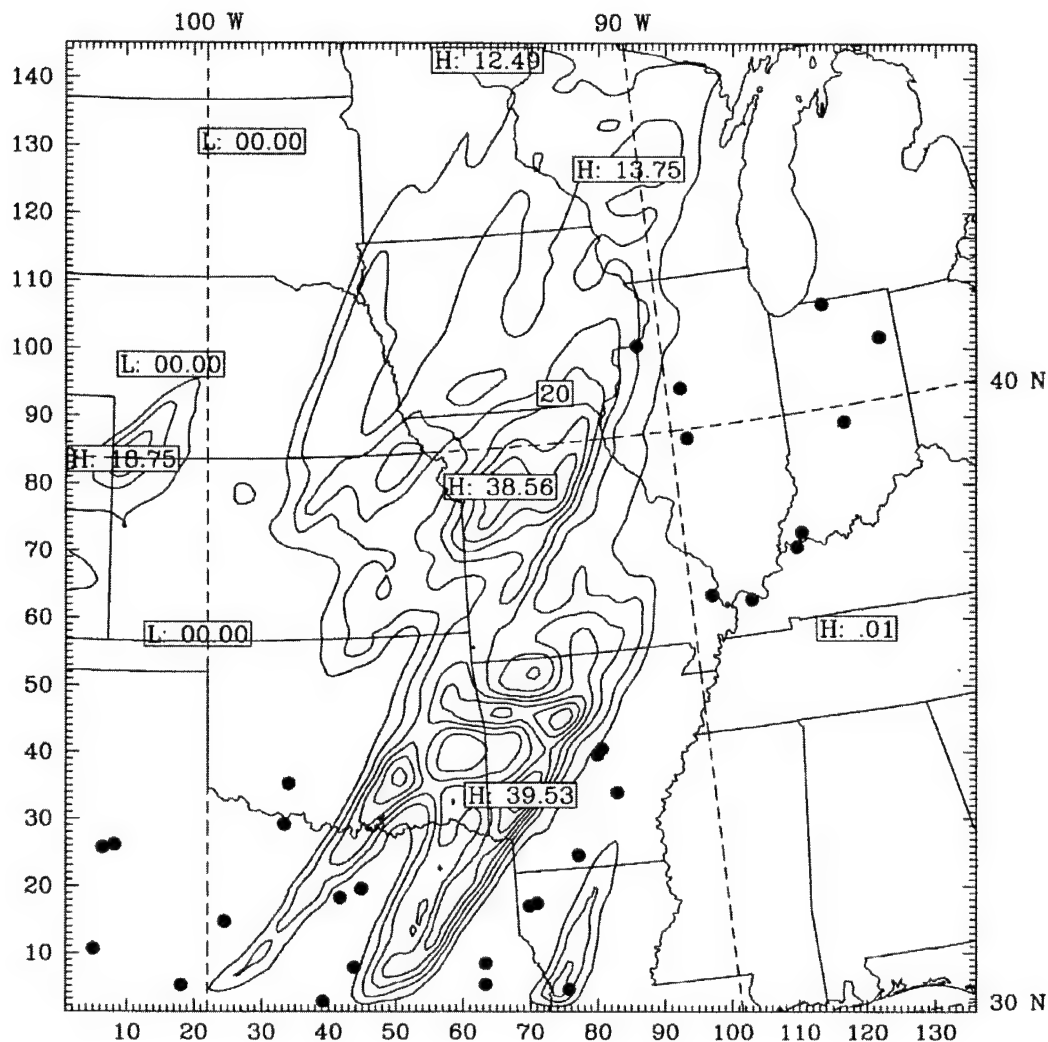
Figure 100   Precipitation for 84 hr 15 January 1995 forecast of the 12 km resolution one-way nested domain. This chart shows the 24 hr cumulative precipitation forecast by the model's one-way nested Domain D. The contours are in five millimeter intervals. The dots (•) show the locations used for grid-to-station verification. The coordinates are labeled in both grid point space and latitude/longitude.
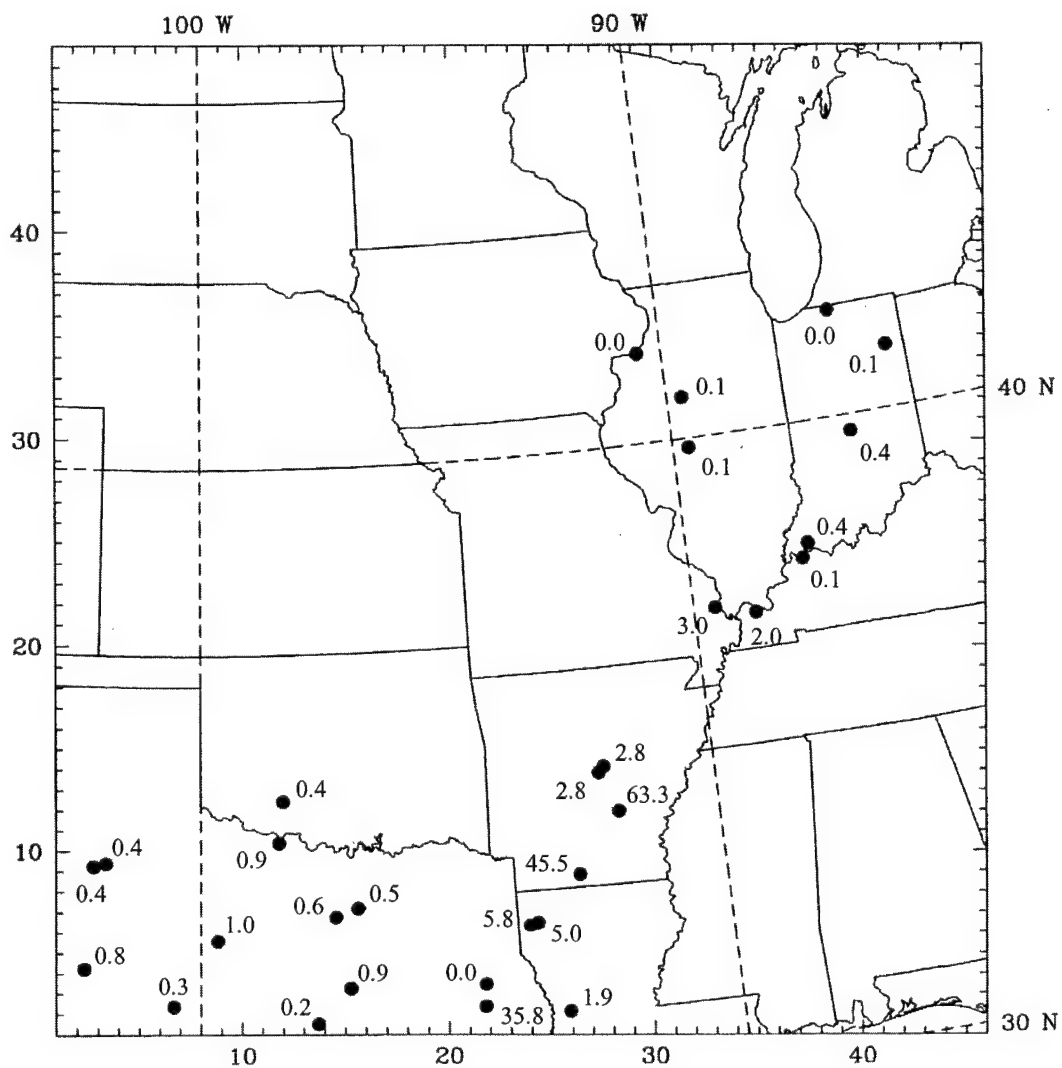
Figure 101   Observed precipitation at 1200 UTC 18 January 1995.   This chart displays the observed 24 hr cumulative precipitation (in millimeters) measured at the locations indicated by the dots (•).   Trace amounts of precipitation are labeled as zero.   The coordinates are labeled in both grid point space and latitude/longitude.

Figures 98 through 100 indicate that small scale detail and precipitation amounts differed considerably between grids. Figure 101 shows the observed precipitation (in millimeter) at 1200 UTC 18 January 1995. In general, these observations suggest that all three model grids over-forecasted the 24 hr cumulative precipitation amounts and may have a phase error (i.e., precipitation too far west). In addition, the contours show that the high resolution (12 km) nested grids were more accurate in their attempt to depict the heaviest band of observed precipitation extending from eastern Texas into southeastern Arkansas.

Figure 102 shows May 24 hr cumulative precipitation RMSE for the 36 km resolution domain and the five two-way nested 12 km resolution domains. It can be seen from the graph that the high-resolution two-way nested domains generally yielded the best forecast for all times except the 36 hr forecast. Figure 102 should be used in conjunction with the next figure to determine the actual differences between the low-resolution forecast and the various high-resolution forecasts. Figure 103 shows the statistical comparison of the five two-way nested 12 km resolution domains to the 36 km resolution domain for 24 hr cumulative precipitation (May case). This graph suggests that the two-way nested domains provided precipitation forecasts which were generally superior to those of the 36 km resolution domain for the 60 hr forecast and beyond. The two-way nested domains improved the model's forecast by as much as 41 percent for three of the four verification times. However, the 36 hr forecast of precipitation was degraded by about 140 percent relative to the low-resolution domain. Figure 104 shows May 24 hr cumulative precipitation RMSE for the 36 km resolution domain and the five one-way nested 12 km resolution domains. It is apparent from the graph that the low-resolution (outer) domain generally yielded the best forecast for all times except the 132 hr forecast. Figure 104 should be used in conjunction with the next figure to determine the actual differences between the low-resolution forecast and the various high-resolution forecasts. Figure 105 shows the statistical comparison of the five one-way nested 12 km resolution domains to the
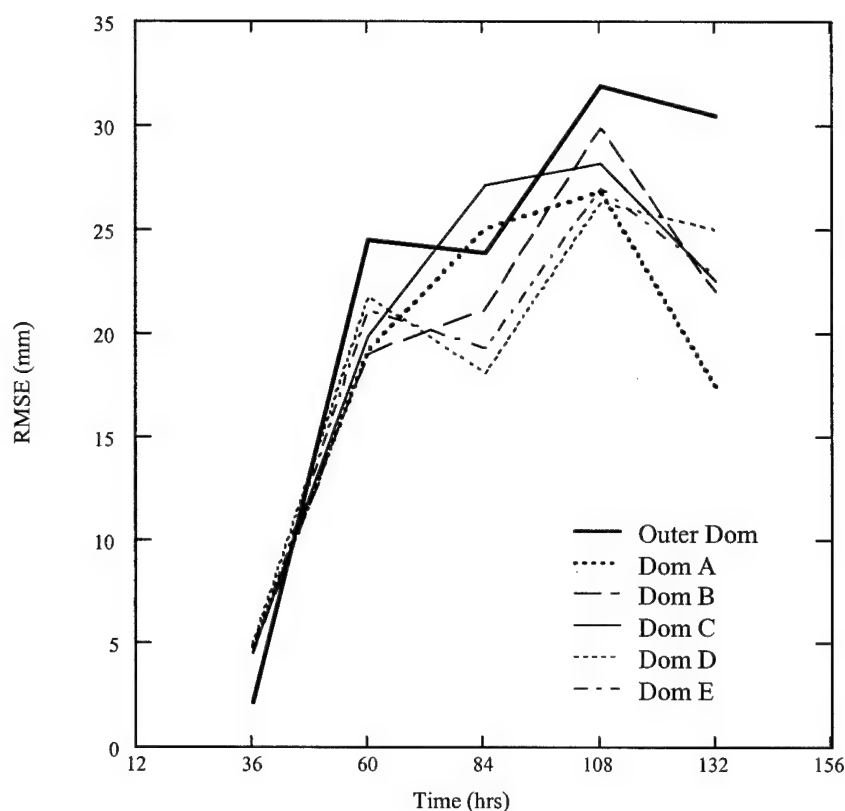
Figure 102   Precipitation RMSE for two-way nesting (May case).   This figure shows the 24 hr cumulative precipitation RMSE for the outer domain (36 km) and the five high-resolution (12 km) two-way nested domains for the May case The domains represented by the traces are the Outer Domain (heavy solid), Domain A (heavy dotted), Domain B (dashed), Domain C (solid), Domain D (dotted), and Domain E (dash-dot).

36 km resolution domain for 24 hr cumulative precipitation (May case). This graph suggests that the one-way nested domains provided precipitation forecasts which were generally inferior to those of the 36 km resolution domain. The one-way nested domains degraded the model's veracity by as much as 143 percent for three of the four verification times. Only for the 132 hr forecast was the forecasted precipitation improved by about 30 percent relative to the low-resolution domain.

Figures 106 through 108 show the 36 hr 4 May 1995 forecast of 24 hour cumulative precipitation for the 36 km resolution domain, 12 km resolution two-way
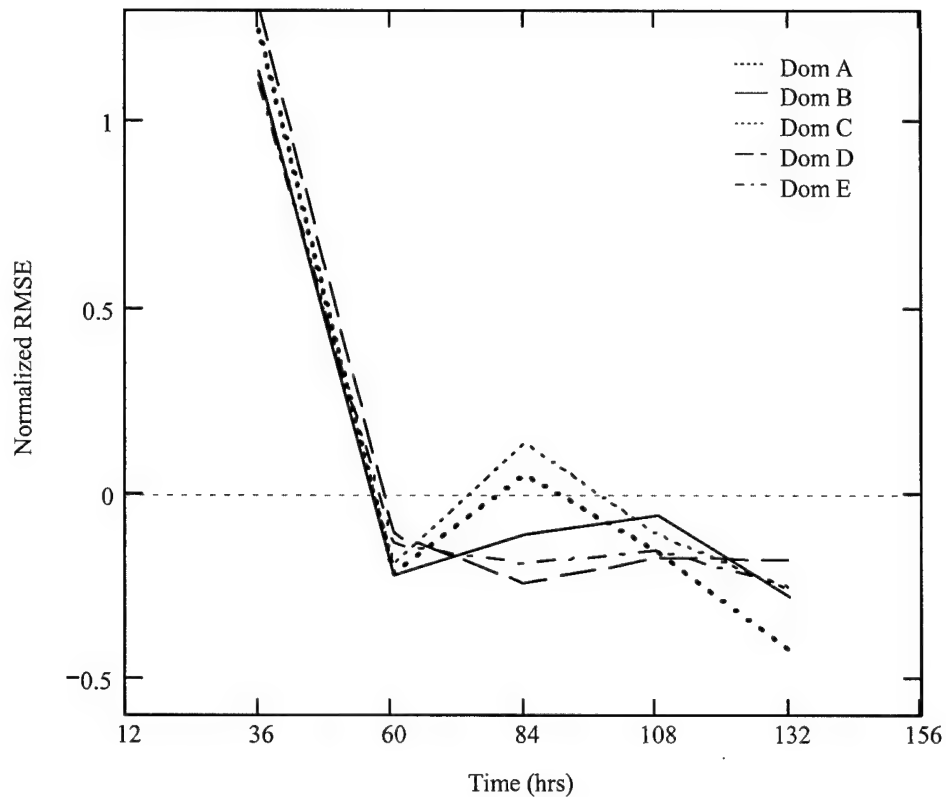
Figure 103   Normalized precipitation RMSE for two-way nesting (May case). This figure compares the normalized 24 hr cumulative precipitation RMSE for the five high-resolution (12 km) two-way nested domains of the May case with the lower resolution (36 km) domain. The domains represented by the traces are Domain A (heavy dotted), Domain B (solid), Domain C (dotted), Domain D (dashed), and Domain E (dash-dot).

nested domain, and 12 km resolution one-way nested domain, respectively. Figures 102 through 105 suggest (on average) the 36 hr precipitation error for the high-resolution nested grids was double that of the low-resolution grid during a period of light precipitation. This finding is consistent with the contour plots in Figures 106 to 108 which show a doubling of the precipitation amounts along the southern and eastern boundaries of the verification zone for the two nested grids. Figure 109 shows the observed precipitation (in millimeter) at 1200 UTC 5 May 1995. In general, these observations suggest that all three model grids over-forecasted the 24
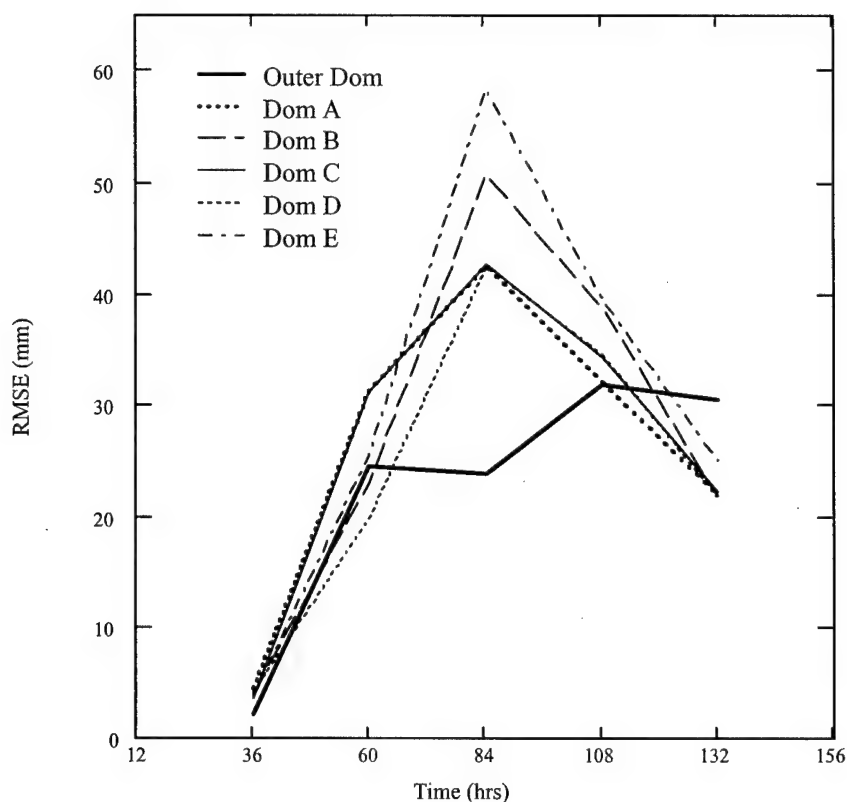
Figure 104   Precipitation RMSE for one-way nesting (May case). This figure shows
the 24 hr cumulative precipitation RMSE for the outer domain (36 km)
and the five high-resolution (12 km) one-way nested domains for the
May case The domains represented by the traces are the Outer Domain
(heavy solid), Domain A (heavy dotted), Domain B (dashed), Domain
C (solid), Domain D (dotted), and Domain E (dash-dot).

hr cumulative precipitation amounts along the southern and eastern boundary of the
verification zone.

Figures 110 through 112 show the 108 hr 4 May 1995 forecast of 24 hour cu-
mulative precipitation for the 36 km resolution domain, 12 km resolution two-way
nested domain, and 12 km resolution one-way nested domain, respectively.   Fig-
ures 102 through 105 suggest (on average) less than eight millimeters of variation
in the precipitation between the various grids at 108 hours.   In contrast, the con-
tour plots in Figures 106 to 108 show a similar precipitation pattern between the
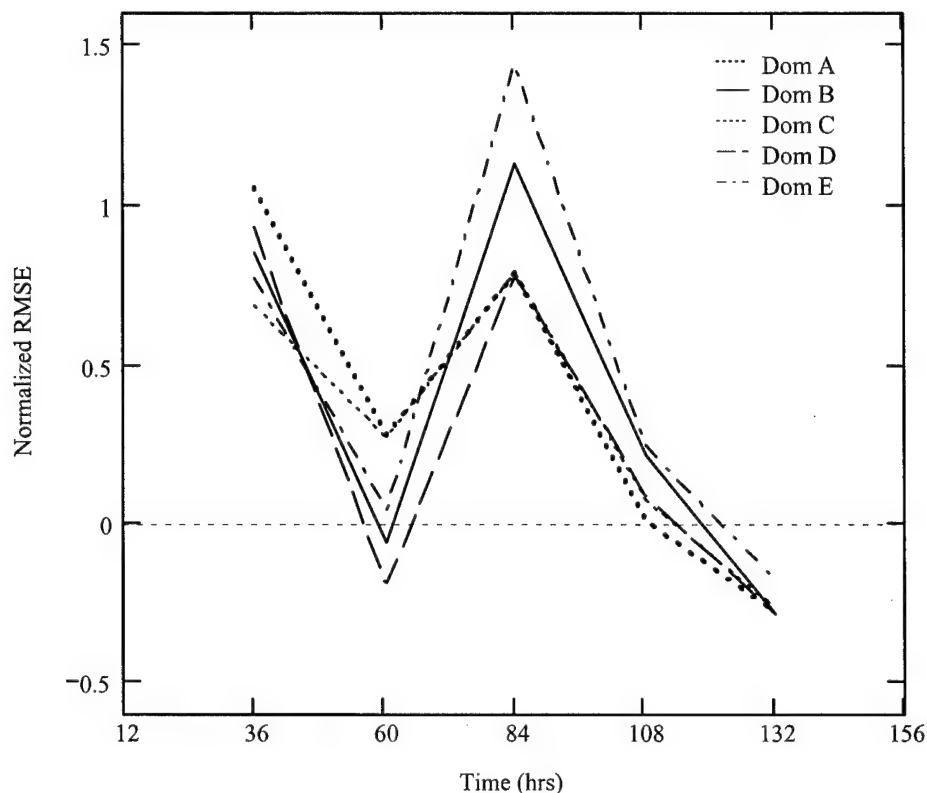
Figure 105   Normalized precipitation RMSE for one-way nesting (May case). This
figure compares the normalized 24 hr cumulative precipitation RMSE
for the five high-resolution (12 km) one-way nested domains of the
May case with the lower resolution (36 km) domain.   The domains
represented by the traces are Domain A (heavy dotted), Domain B
(solid), Domain C (dotted), Domain D (dashed), and Domain E (dash-
dot).

low-resolution grid and the high-resolution grid two-way nested grid, while the pre-
cipitation amounts for the high-resolution one-way nested grid were about 60 percent
greater.   Figure 113 shows the observed precipitation (in millimeter) at 1200 UTC
8 May 1995.   In general, these observations suggest that all three model grids had
minimal phase error; however, the 24 hr cumulative precipitation amounts were ex-
tremely over-forecasted by the model.

In summary, the results are generally limited by the paucity of a dense rain
gauge network to capture the spatial inhomogeneous distribution of precipitation.

130
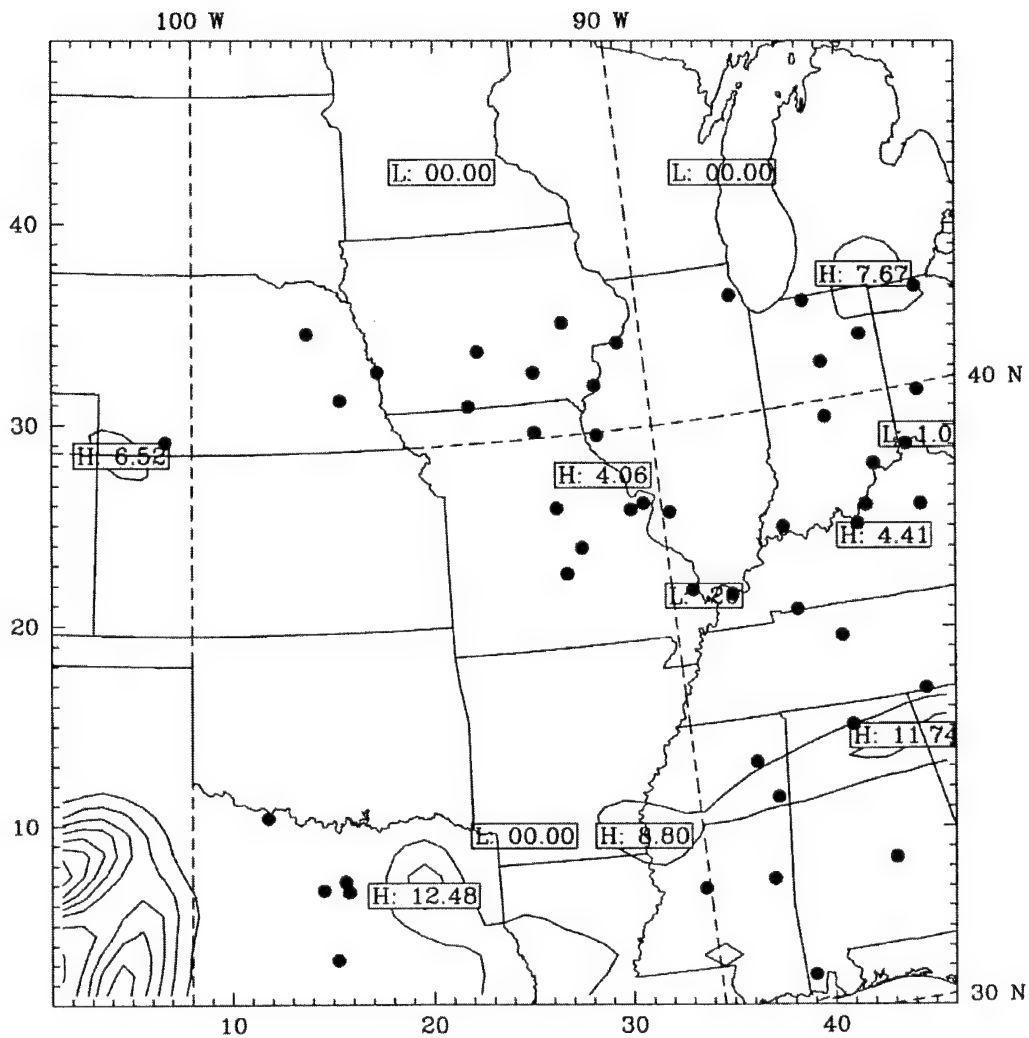
Figure 106   Precipitation for 36 hr 4 May 1995 forecast of the 36 km resolution
domain.   This chart shows the 24 hr cumulative precipitation forecast
by the model's outer domain.   The contours are in five millimeter
intervals.   The dots (•) show the locations used for grid-to-station
verification.   The coordinates are labeled in both grid point space and
latitude/longitude.

100 W 90 W

H: 1.5

H: 2.0

L: 000.0

H: 1.7

H: 14.1

H: 2.1

5.3

L: 000.0

40 N

H: 9.0

L: 8

L: .

H: 12.2

L: 000.0

H: 20.1

H: 22.6

H: 18.2

H: 7.1

H: 130.6

30 N

140 130 120 110 100 90 80 70 60 50 40 30 20 10

10 20 30 40 50 60 70 80 90 100 110 120 130
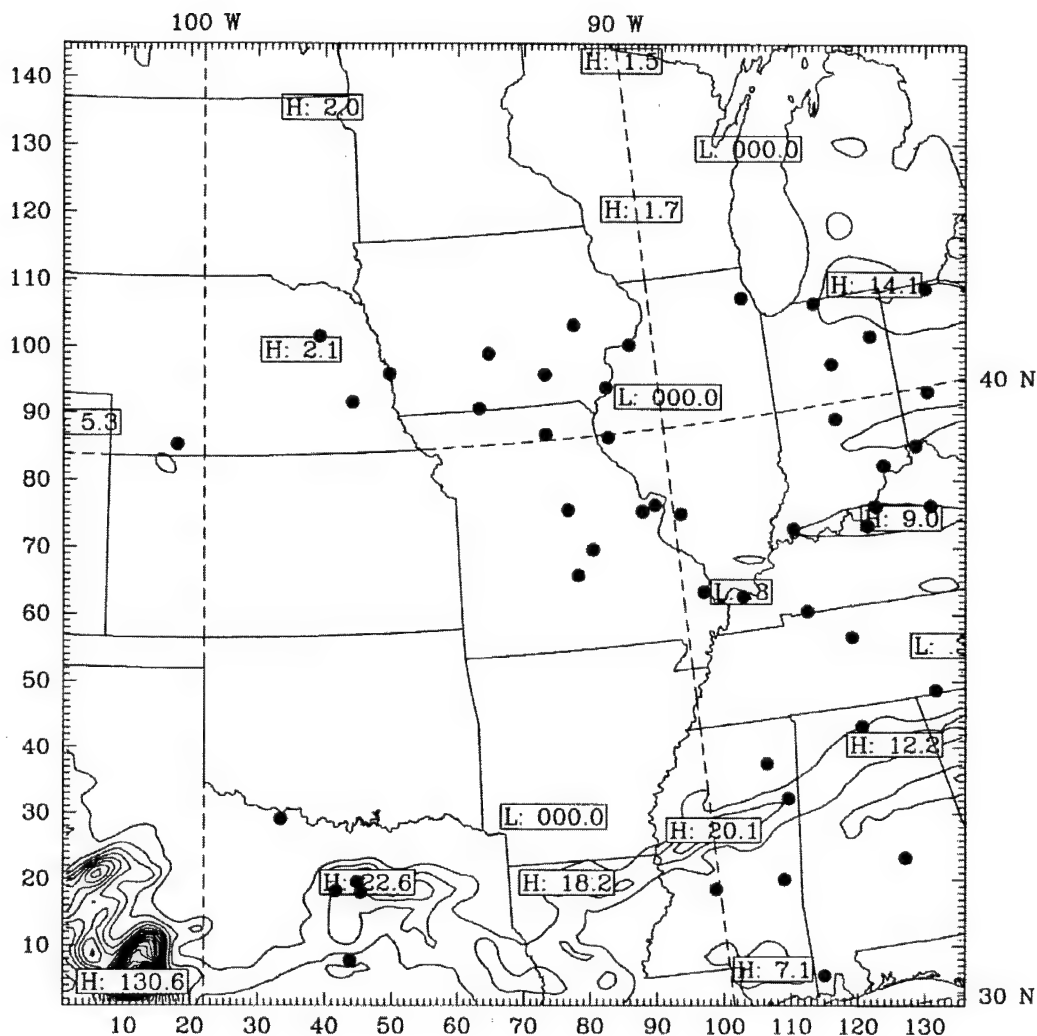
Figure 107   Precipitation for 36 hr 4 May 1995 forecast of the 12 km resolution two-way nested domain.   This chart shows the 24 hr cumulative precipitation forecast by the model's two-way nested Domain D.   The contours are in five millimeter intervals. The dots (•) show the locations used for grid-to-station verification. The coordinates are labeled in both grid point space and latitude/longitude.
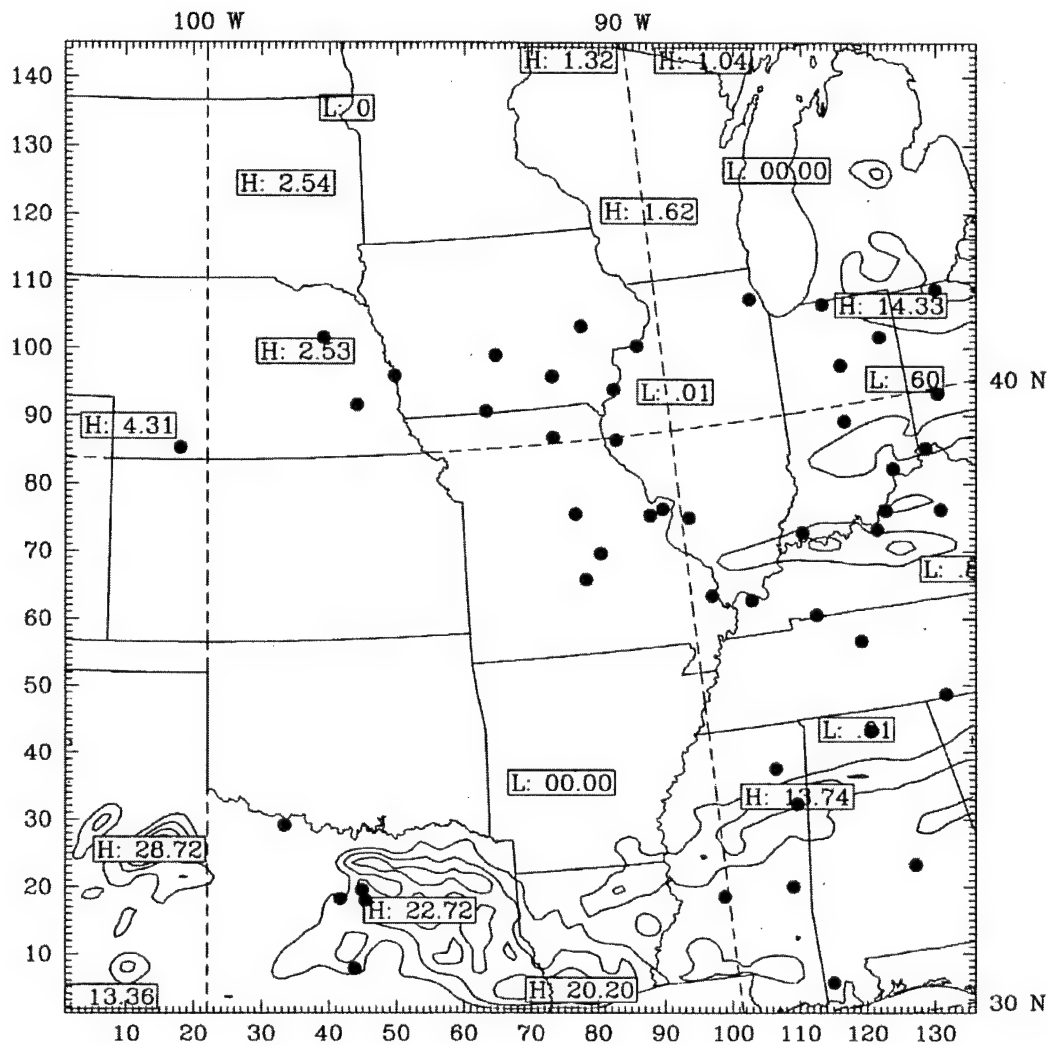
Figure 108   Precipitation for 36 hr 4 May 1995 forecast of the 12 km resolution one-way nested domain. This chart shows the 24 hr cumulative precipitation forecast by the model's one-way nested Domain D. The contours are in five millimeter intervals. The dots (•) show the locations used for grid-to-station verification. The coordinates are labeled in both grid point space and latitude/longitude.
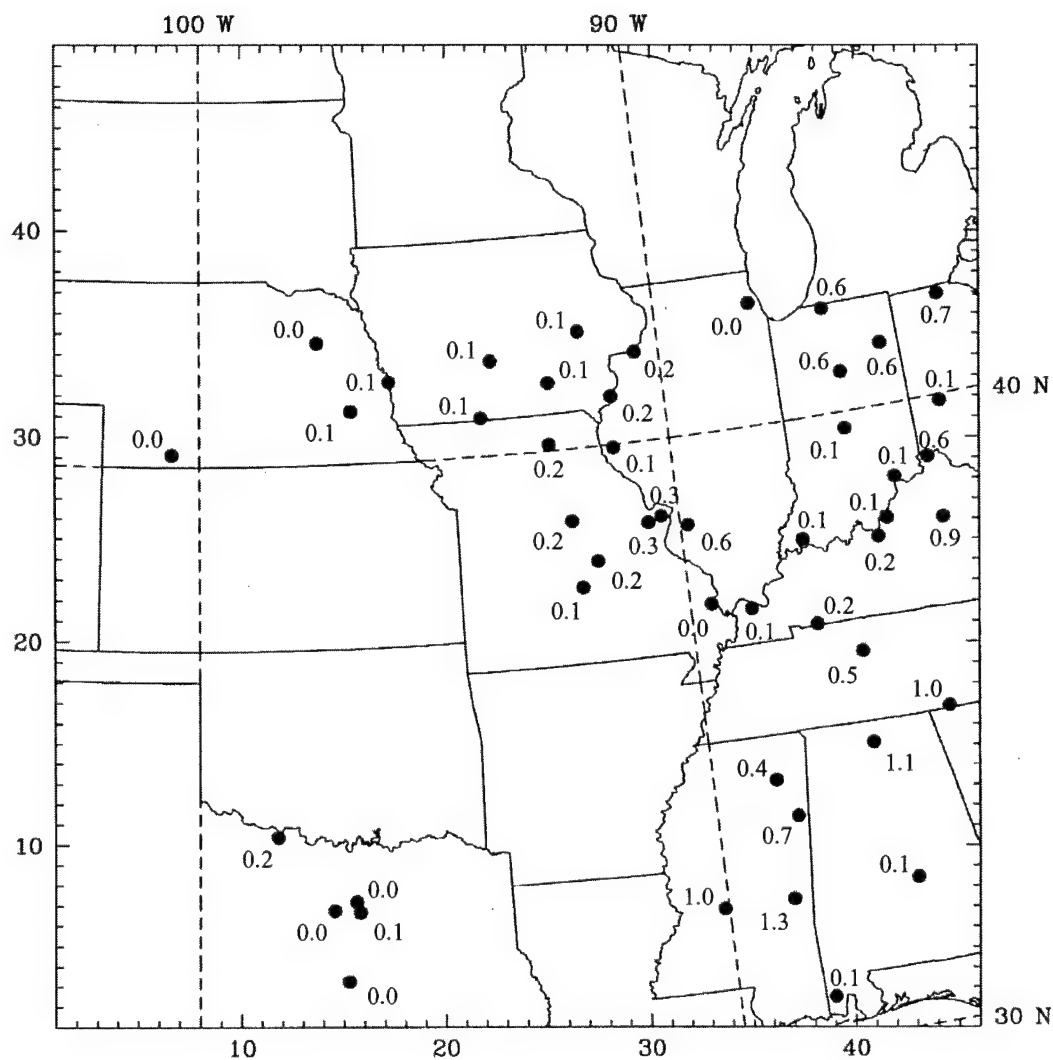
Figure 109   Observed precipitation at 1200 UTC 5 May 1995. This chart displays
the observed 24 hr cumulative precipitation (in millimeters) measured
at the locations indicated by the dots (•). Trace amounts of precip-
itation are labeled as zero. The coordinates are labeled in both grid
point space and latitude/longitude.
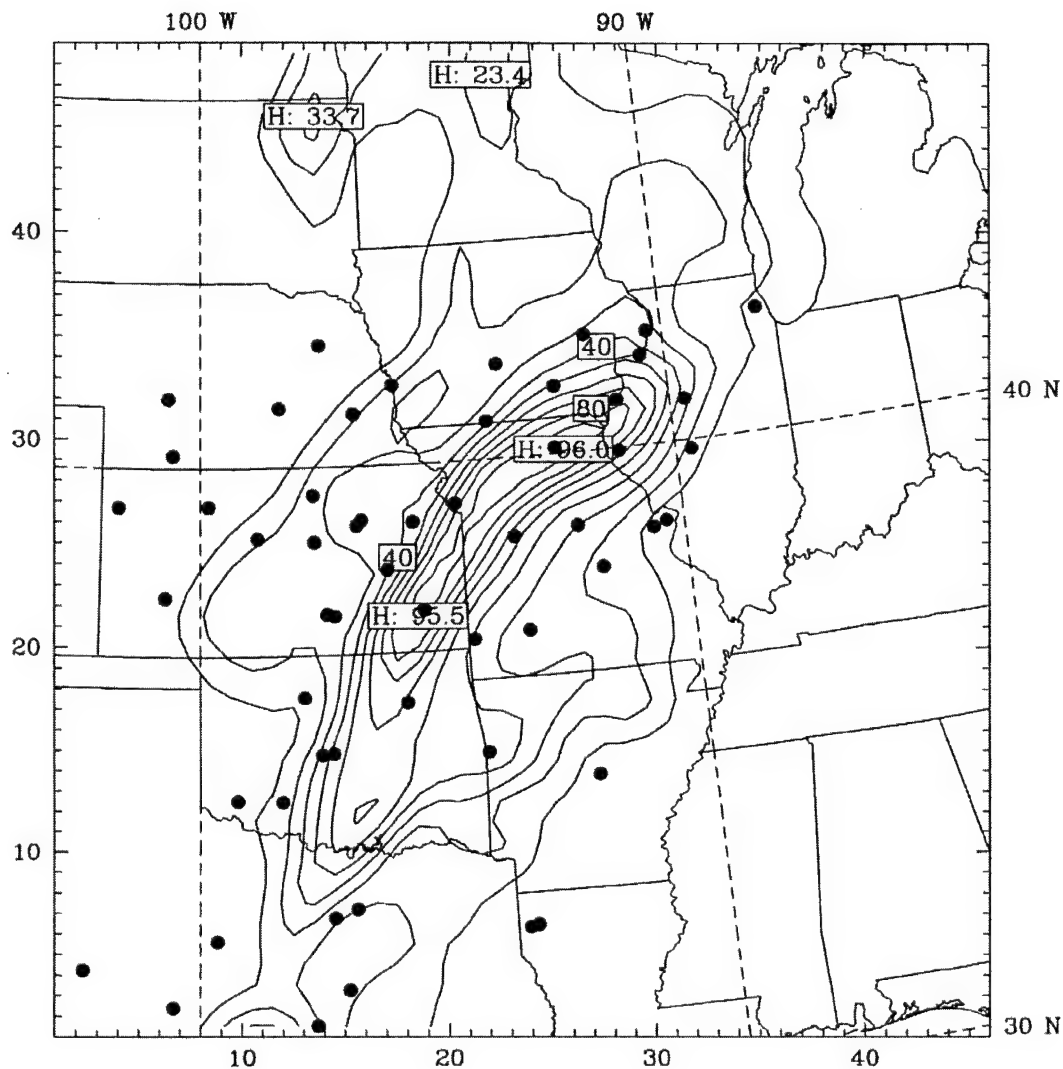
Figure 110   Precipitation for 108 hr 4 May 1995 forecast of the 36 km resolution
domain. This chart shows the 24 hr cumulative precipitation forecast
by the model's outer domain.   The contours are in five millimeter
intervals.   The dots (•) show the locations used for grid-to-station
verification. The coordinates are labeled in both grid point space and
latitude/longitude.
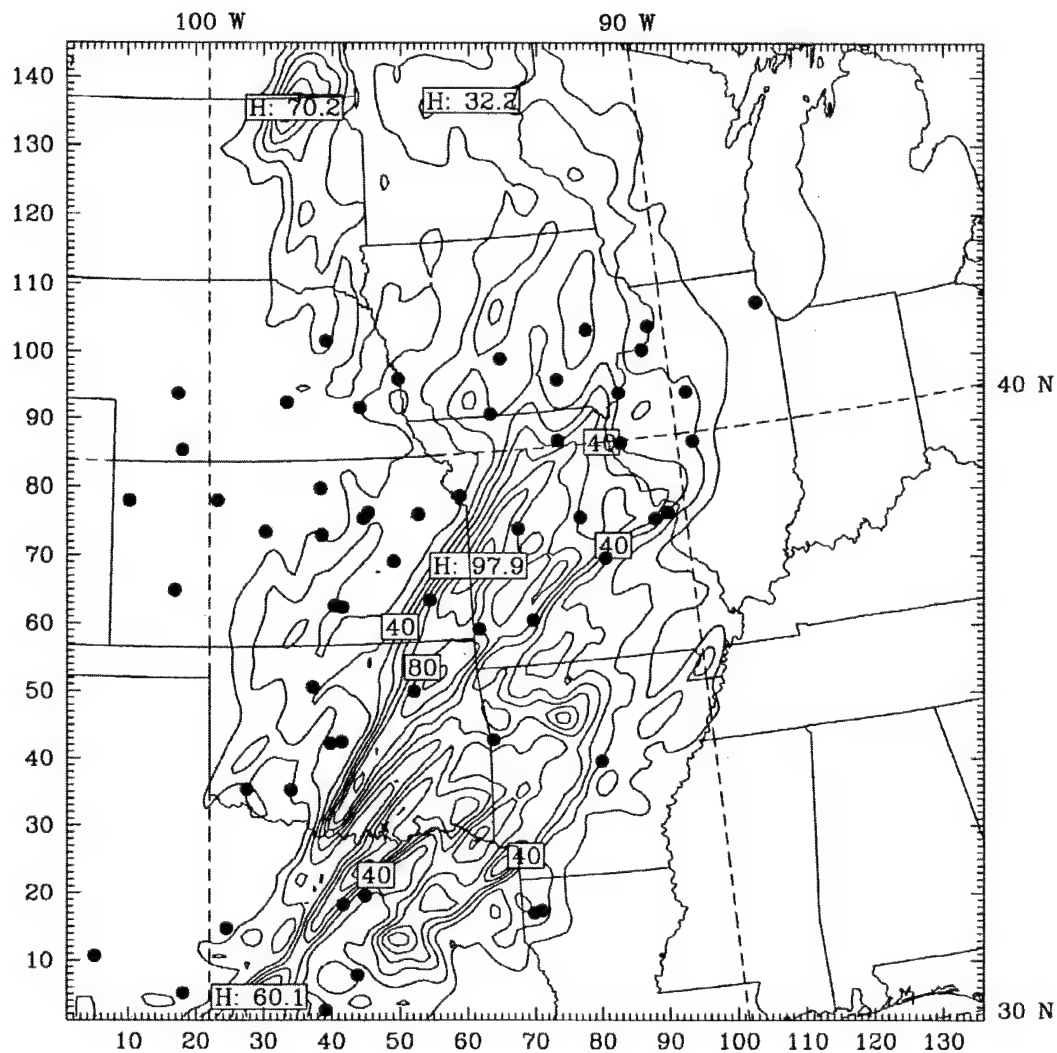
Figure 111   Precipitation for 108 hr 4 May 1995 forecast of the 12 km resolution
two-way nested domain. This chart shows the 24 hr cumulative pre-
cipitation forecast by the model's two-way nested Domain D. The
contours are in five millimeter intervals. The dots (•) show the loca-
tions used for grid-to-station verification. The coordinates are labeled
in both grid point space and latitude/longitude.
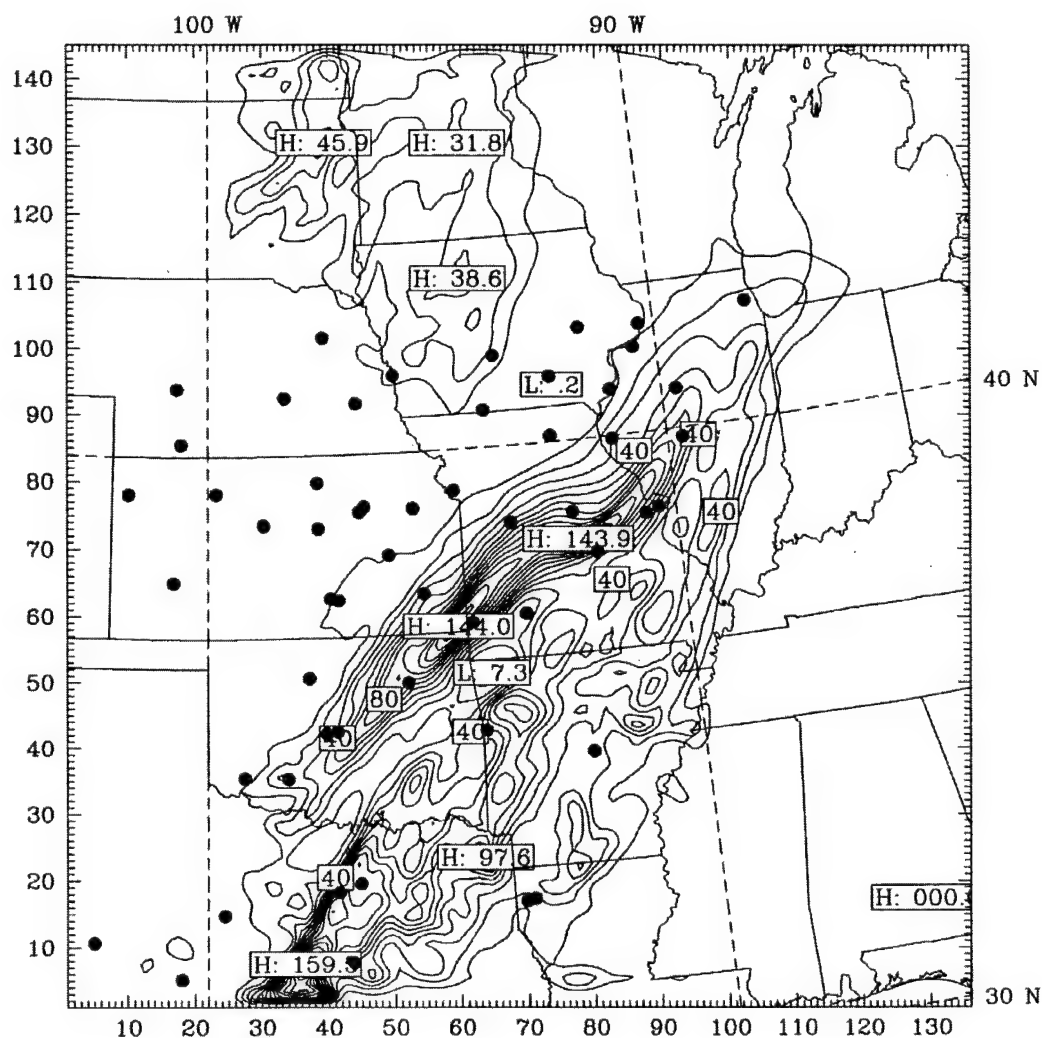
Figure 112　Precipitation for 108 hr 4 May 1995 forecast of the 12 km resolution one-way nested domain. This chart shows the 24 hr cumulative precipitation forecast by the model's one-way nested Domain D. The contours are in five millimeter intervals. The dots (•) show the locations used for grid-to-station verification. The coordinates are labeled in both grid point space and latitude/longitude.
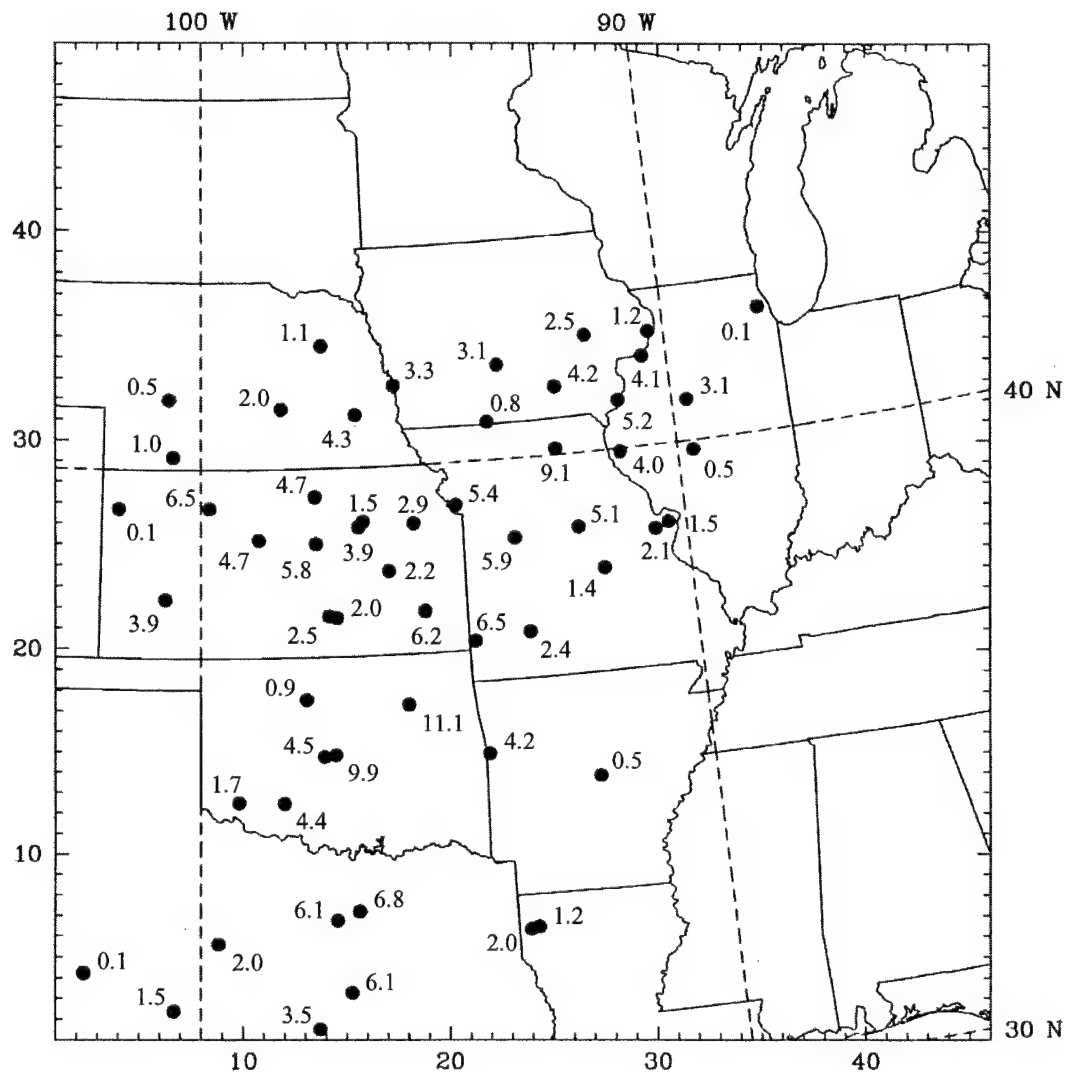
Figure 113   Observed precipitation at 1200 UTC 8 May 1995. This chart displays
the observed 24 hr cumulative precipitation (in millimeters) measured
at the locations indicated by the dots (•).   Trace amounts of precip-
itation are labeled as zero.   The coordinates are labeled in both grid
point space and latitude/longitude.

However, the results suggest that the low-resolution grid can provide a better forecast during periods of little precipitation. This finding is consistent with previous research by White et al. (22: 1999). In their research, it was concluded that light precipitation events were best depicted by a low-resolution grid, while heavy precipitation events were best depicted by a high-resolution grid. In addition, the results suggest that the model had a tendency to over-forecast precipitation amounts as forecast time was extended.

4.5 Two-way Nesting versus One-way Nesting

4.5.1 General Discussion. The final question, stated in Chapter 1, attempted to shed light on the controversy over whether one-way or two-way nested model grids provide the superior forecast. This section explored this controversy by employing RMSE calculations on the model output for each of the domain configurations discussed in Chapter 3. The meteorological variables that were examined to address the posed question are geopotential height and temperature. The wind speed, wind direction, and precipitation fields have been eliminated from this section, since previous sections have shown that these variables are prone to oscillatory behavior and may prove to be unreliable in answering the current question. In addition, the May case study will not be shown, because the nested domains provided limited improvement over the 36 km resolution grid due to the lack of cyclogenesis during the first 84 hour of the forecast period.

In this section, the statistical plots have been normalized to provide a more meaningful representation of the results. Normalization allows direct comparison of the high-resolution domain forecasts to those provided by the lower resolution (36 km) domain. The plots are standardized with time (in hours) along the abscissa and normalized RMSE along the ordinate. Normalized RMSE is either positive, negative, or zero. The zero line represents the control value which has been chosen as the independently run 36 km low-resolution domain. A negative value represents

139

a decrease in the RMSE, or improvement in the model's forecast, and vice versa. The 36 km resolution domain was chosen as the standard, since the superiority of one nesting type over another is meaningless if it cannot provide improvement over its lower resolution (36 km) host domain. Each trace represents the model nesting type denoted in the key and was generated using the RMSE calculation for each verification time during the forecast period. Statistical plots have been generated for the 950/150 mb layer (where verification was computed every 25 mb throughout the layer) since it best represents the three-dimensional veracity of the various model nested domains. The percentages discussed in this section are the differences in relative RMSE between the two types of nesting, and not relative to the 36 km resolution domain.

The significant surface cyclogenetic events the reader should be aware of while viewing the statistical plots for the January case are as follows: the first cyclone entered the verification zone through the western boundary 36 hours into the forecast period, and the second cyclone reached its maximum intensity in the east portion of the verification zone 108 hours into the forecast period. For clarity, the results in this section have been presented for individual nested grid locations (i.e., Domains A, B, C, D, and E).

4.5.2 Findings. The first meteorological variable to be discussed is geopotential height. Figure 114 shows the statistical comparison of two-way nesting to one-way nesting for geopotential height in Domain A (January case). As seen from the graph, the one-way nested domain provided up to a 10.5 percent improvement over the two-way nested domain during the first 36 hours of the forecast period. After the 36 hr forecast, the two-way nested domain provided a superior forecast when compared to the one-way nested domain. The forecasted geopotential height was improved by as much as 16.5 percent over the forecast of the one-way nesting. Figure 115 shows the statistical comparison of two-way nesting to one-way nesting for geopotential height in Domain B (January case). As seen from the graph, the

140
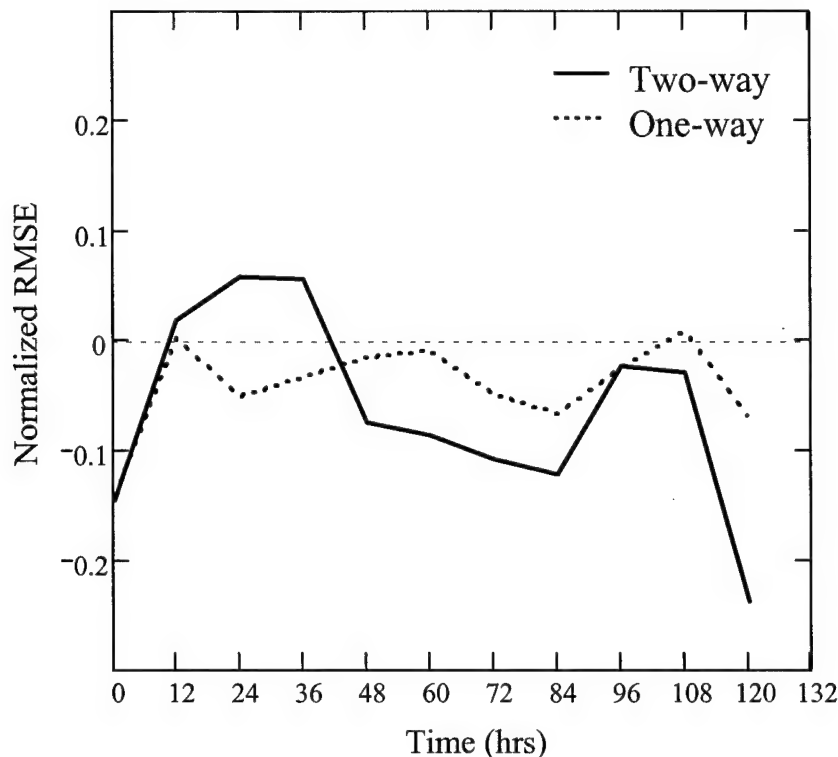
Figure 114   Domain A normalized geopotential height RMSE for nesting type comparison (January case). This figure compares two-way and one-way nesting using normalized geopotential height RMSE over a 950/150 mb layer where the control value is provided by the lower resolution (36 km) domain. The solid trace represents the two-way nested domain and dotted trace represents the one-way nested domain.

one-way and two-way nested domains are comparable for the analysis and the 12 hr forecast. For the 24 hr and 36 hr forecasts, the one-way nested domain provided up to a 13.5 percent improvement over the two-way nested domain. After the 36 hr forecast, the two-way nested domain provided a superior forecast when compared to the one-way nested domain. The forecasted geopotential height was improved by as much as 14 percent over the forecast of the one-way nesting. Figure 116 shows the statistical comparison of two-way nesting to one-way nesting for geopotential height in Domain C (January case). As seen from the graph, the one-way nested domain provided up to a 13.5 percent improvement over the two-way nested domain during
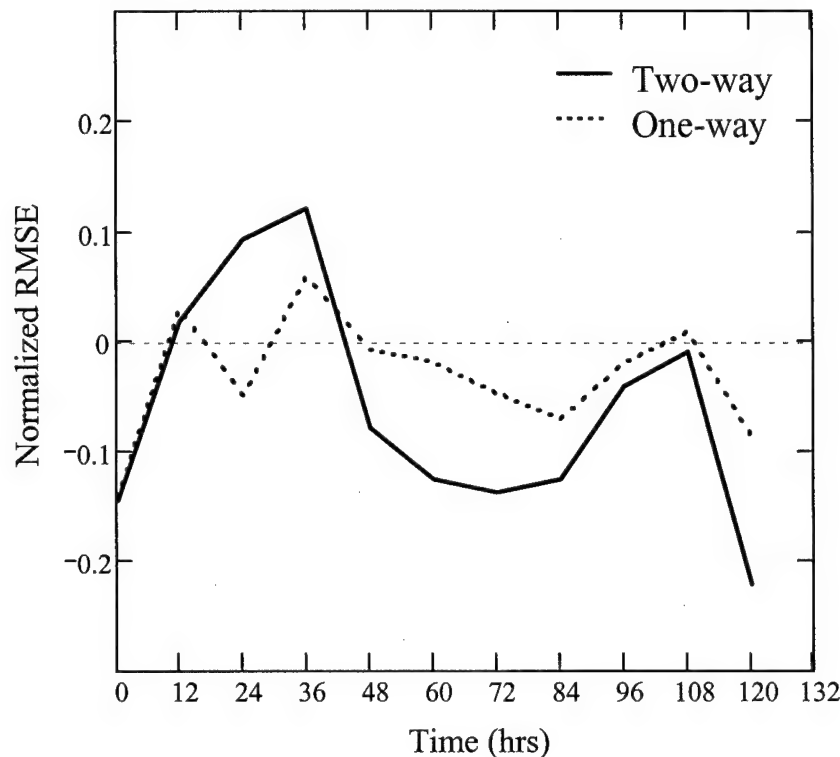
Figure 115   Domain B normalized geopotential height RMSE for nesting type comparison (January case).   This figure compares two-way and one-way nesting using normalized geopotential height RMSE over a 950/150 mb layer where the control value is provided by the lower resolution (36 km) domain.   The solid trace represents the two-way nested domain and dotted trace represents the one-way nested domain.

the first 36 hours of the forecast period. After the 36 hr forecast, the two-way nested domain provided a superior forecast when compared to the one-way nested domain. The forecasted geopotential height was improved by as much as 17 percent over the forecast of the one-way nesting.   Figure 117 shows the statistical comparison of two-way nesting to one-way nesting for geopotential height in Domain D (January case).   As seen from the graph, the one-way nested domain provided up to a 9.5 percent improvement over the two-way nested domain during the first 36 hours of the forecast period.   After the 36 hr forecast, the two-way nested domain provided a superior forecast when compared to the one-way nested domain.   The forecasted
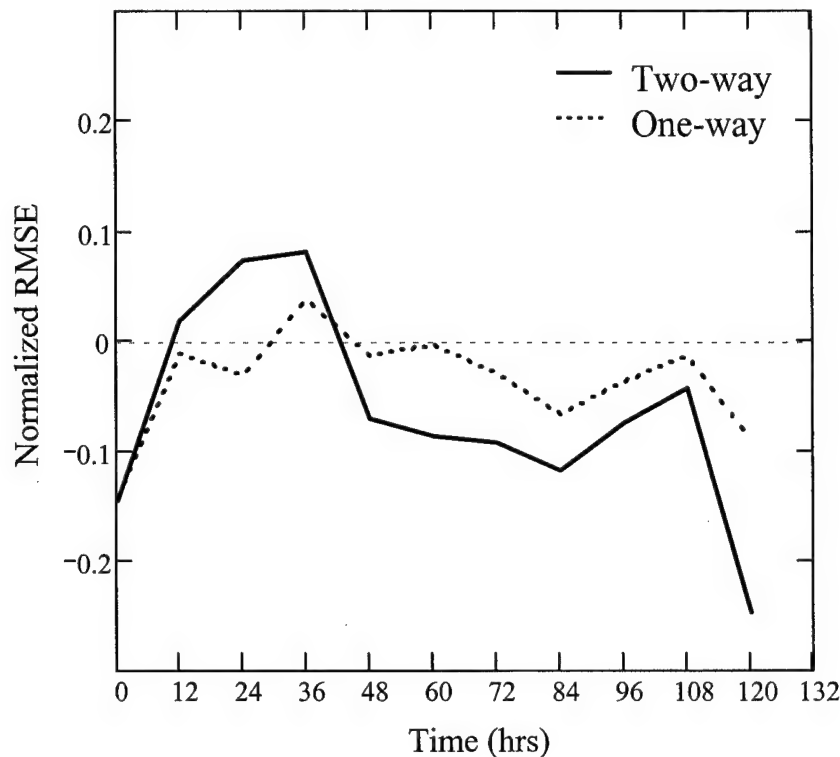
Figure 116   Domain C normalized geopotential height RMSE for nesting type comparison (January case).   This figure compares two-way and one-way nesting using normalized geopotential height RMSE over a 950/150 mb layer where the control value is provided by the lower resolution (36 km) domain.   The solid trace represents the two-way nested domain and dotted trace represents the one-way nested domain.

geopotential height was improved by as much as 17.5 percent over the forecast of the one-way nesting.   Figure 118 shows the statistical comparison of two-way nesting to one-way nesting for geopotential height in Domain E (January case).   As seen from the graph, the one-way nested domain provided up to ten percent improvement over the two-way nested domain during the first 36 hours of the forecast period.   After the 36 hr forecast, the two-way nested domain provided a superior forecast when compared to the one-way nested domain.   The forecasted geopotential height was improved by as much as 17.5 percent over the forecast of the one-way nesting.

Now, the temperature forecasts will be discussed.   Figure 119 shows the statis-
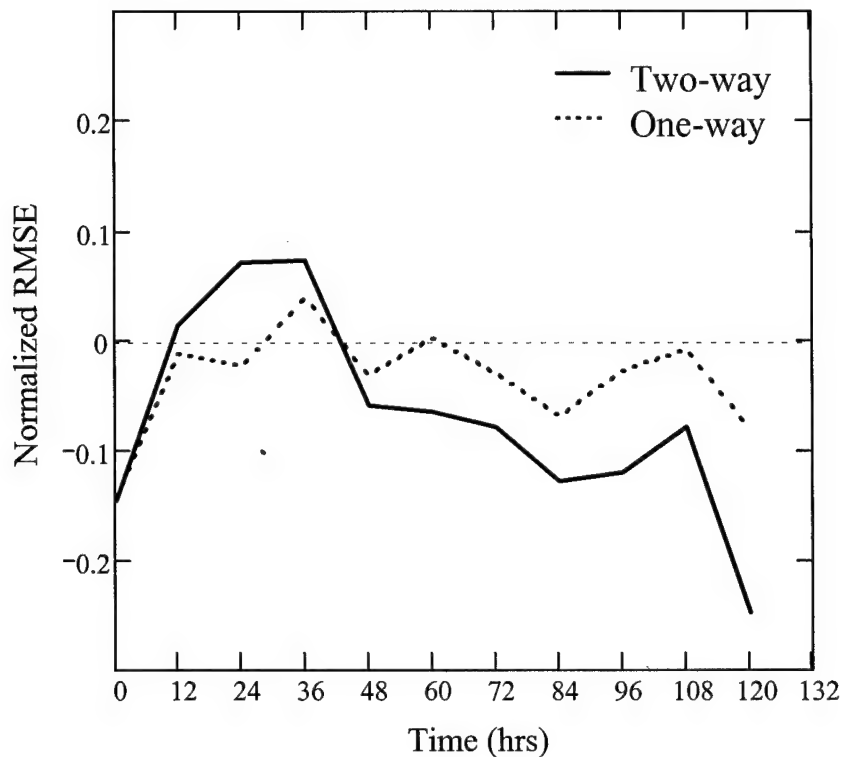
Figure 117   Domain D normalized geopotential height RMSE for nesting type comparison (January case).   This figure compares two-way and one-way nesting using normalized geopotential height RMSE over a 950/150 mb layer where the control value is provided by the lower resolution (36 km) domain.   The solid trace represents the two-way nested domain and dotted trace represents the one-way nested domain.

tical comparison of two-way nesting to one-way nesting for temperature in Domain A (January case).   As seen from the graph, the one-way nested domain provided up to 4.5 percent improvement over the two-way nested domain during the first 48 hours of the forecast period.   After the 48 hr forecast, the two-way nested domain provided a superior forecast when compared to the one-way nested domain.   The forecasted temperature was improved by as much as 6.5 percent over the forecast of the one-way nesting.   Figure 120 shows the statistical comparison of two-way nesting to one-way nesting for temperature in Domain B (January case).   As seen from the graph, the one-way nested domain provided up to 1.5 percent improvement over the

144
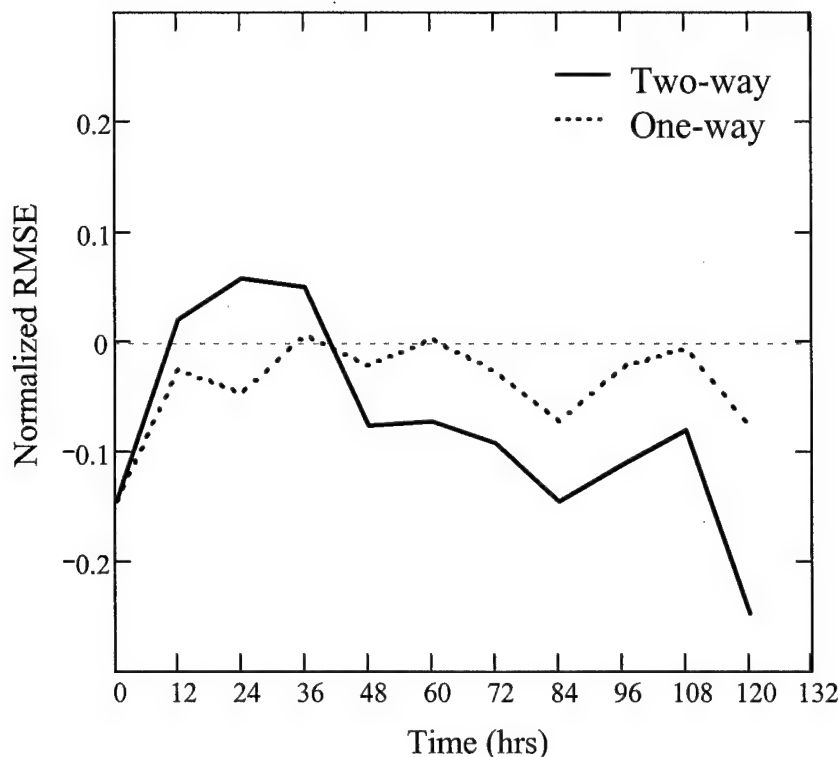
Figure 118   Domain E normalized geopotential height RMSE for nesting type comparison (January case).   This figure compares two-way and one-way nesting using normalized geopotential height RMSE over a 950/150 mb layer where the control value is provided by the lower resolution (36 km) domain.   The solid trace represents the two-way nested domain and dotted trace represents the one-way nested domain.

two-way nested domain during the first 12 hours of the forecast period. For the 24 hr forecast, both types of nesting produced a temperature forecast consistent with the 36 km resolution domain. After the 24 hr forecast, the two-way nested domain provided a superior forecast when compared to the one-way nested domain. The forecasted temperature was improved by as much as five percent over the forecast of the one-way nesting. Figure 121 shows the statistical comparison of two-way nesting to one-way nesting for temperature in Domain C (January case). As seen from the graph, the one-way nested domain provided up to 3.5 percent improvement over the two-way nested domain during the first 24 hours of the forecast period. After
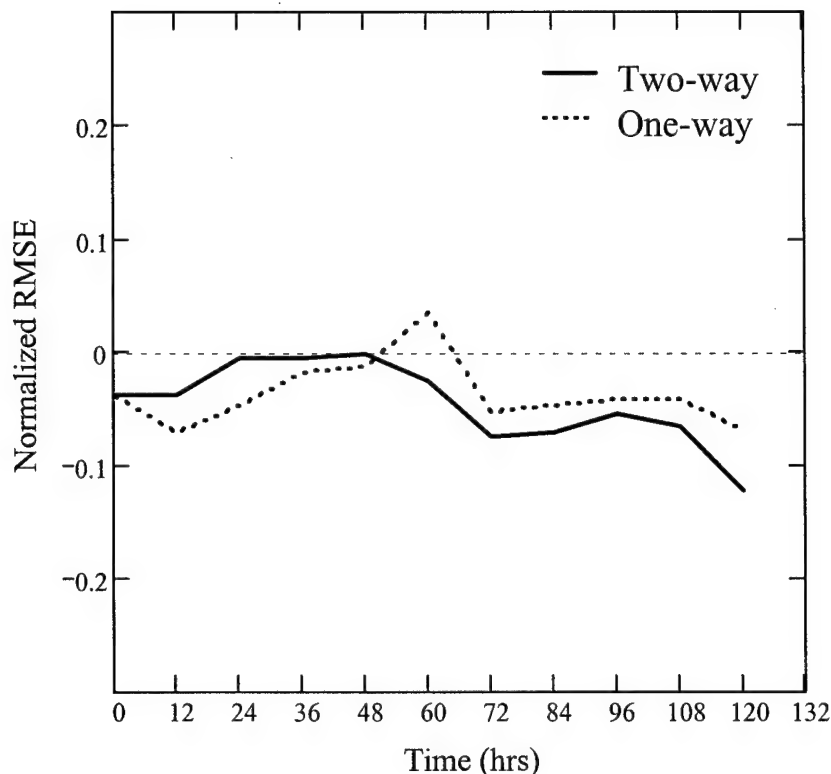
Figure 119   Domain A normalized temperature RMSE for nesting type comparison (January case).   This figure compares two-way and one-way nesting using normalized temperature RMSE over a 950/150 mb layer where the control value is provided by the lower resolution (36 km) domain. The solid trace represents the two-way nested domain and dotted trace represents the one-way nested domain.

the 24 hr forecast, the two-way nested domain provided a superior forecast when compared to the one-way nested domain, except for the 60 hr forecast for which they were equivalent.   The forecasted temperature was improved by as much as 7.5 percent over the forecast of the one-way nesting.   Figure 122 shows the statistical comparison of two-way nesting to one-way nesting for temperature in Domain D (January case).   As seen from the graph, the one-way nested domain provided up to 3.5 percent improvement over the two-way nested domain during the first 24 hours of the forecast period.   After the 24 hr forecast, the two-way nested domain provided a superior forecast when compared to the one-way nested domain, except for the 48

146
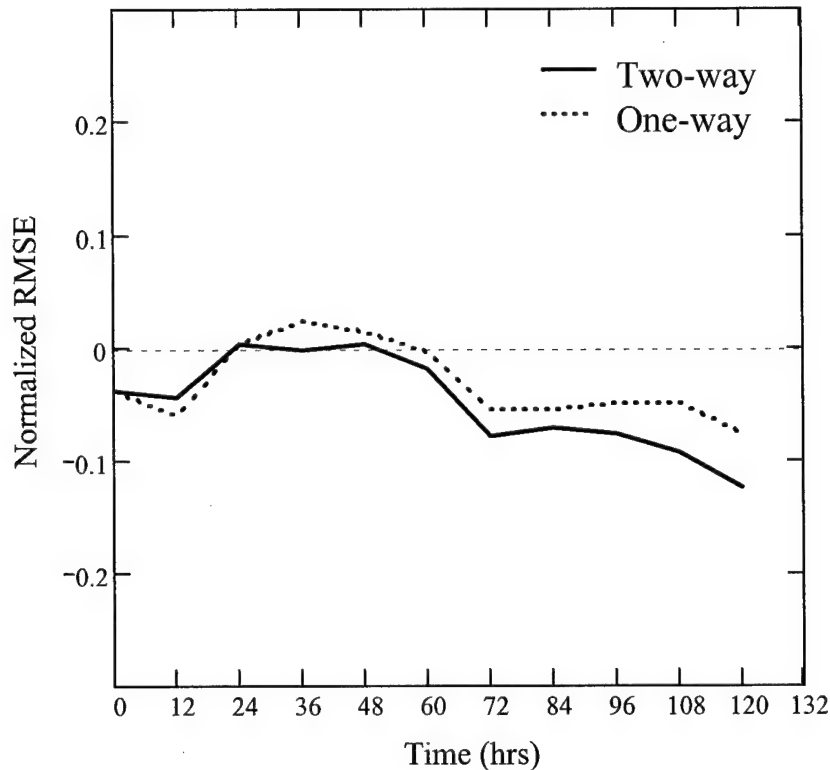
Figure 120   Domain B normalized temperature RMSE for nesting type comparison (January case). This figure compares two-way and one-way nesting using normalized temperature RMSE over a 950/150 mb layer where the control value is provided by the lower resolution (36 km) domain. The solid trace represents the two-way nested domain and dotted trace represents the one-way nested domain.

hr and 72 hr forecasts for which they were nearly equivalent. The forecasted temperature was improved by as much as ten percent over the forecast of the one-way nesting. Figure 123 shows the statistical comparison of two-way nesting to one-way nesting for temperature in Domain E (January case). As seen from the graph, the one-way nested domain provided up to 3.5 percent improvement over the two-way nested domain during the first 24 hours of the forecast period. After the 24 hr forecast, the two-way nested domain provided a superior forecast when compared to the one-way nested domain. The forecasted temperature was improved by as much as 10.5 percent over the forecast of the one-way nesting.
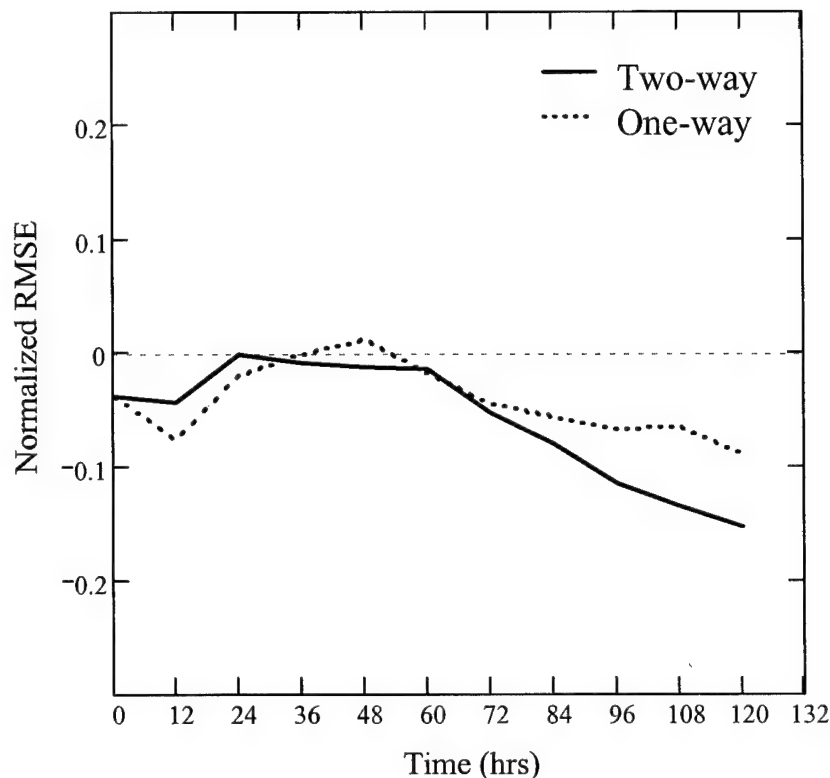
Figure 121   Domain C normalized temperature RMSE for nesting type comparison
(January case).   This figure compares two-way and one-way nesting
using normalized temperature RMSE over a 950/150 mb layer where
the control value is provided by the lower resolution (36 km) domain.
The solid trace represents the two-way nested domain and dotted trace
represents the one-way nested domain.

In summary, it must be reiterated that the first surface cyclone entered the ver-
ification zone through the western boundary about 36 hours into the forecast period.
First (having stated this observation), the results clearly indicate a one-way nested
domain provides the superior forecast during the early portion of the forecast period
in the absence of cyclogenesis. However, the May case study showed that, if the ab-
sence of cyclogenesis persists well into the forecast period, any forecast improvement
offered by a one-way nested domain over the two-way nesting is eventually negated
by the superior forecast of the lower resolution (36 km) host domain (see example in
Figure 124). If surface cyclogenesis is absent, it can be concluded that one-way nest-
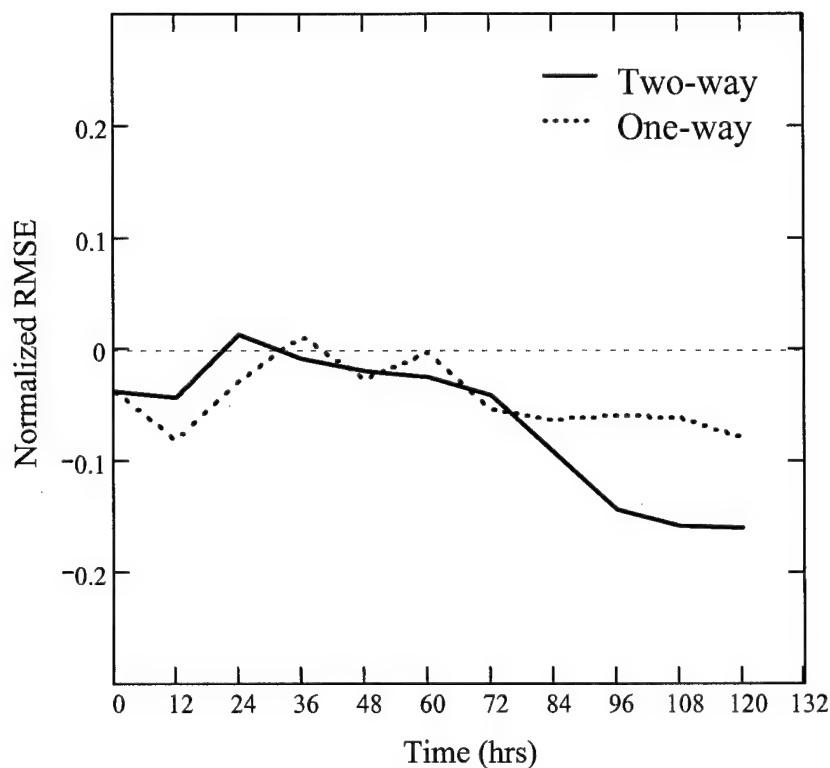
Figure 122   Domain D normalized temperature RMSE for nesting type comparison (January case). This figure compares two-way and one-way nesting using normalized temperature RMSE over a 950/150 mb layer where the control value is provided by the lower resolution (36 km) domain. The solid trace represents the two-way nested domain and dotted trace represents the one-way nested domain.

ing will provide a superior forecast during the first 36 hours of the forecast period. Secondly, it is obvious from the results that a two-way nested domain will provide the superior forecast when strong cyclogenesis is present in the forecast region. The ageostrophic circulations associated with cyclogenesis are evidently handled better through the feedback mechanism provided by two-way nesting.
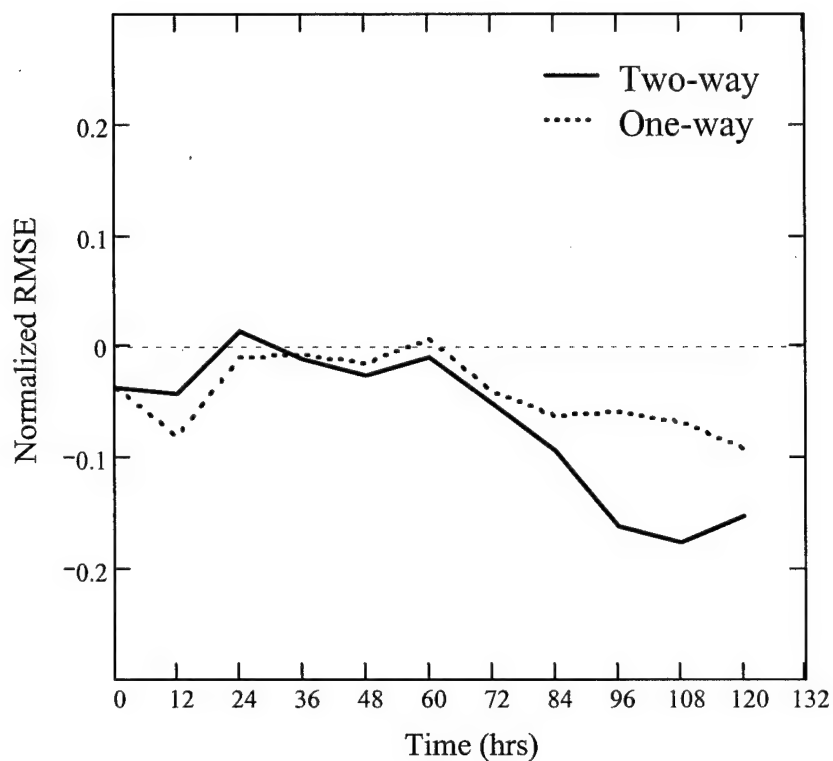
Figure 123   Domain E normalized temperature RMSE for nesting type comparison (January case).   This figure compares two-way and one-way nesting using normalized temperature RMSE over a 950/150 mb layer where the control value is provided by the lower resolution (36 km) domain. The solid trace represents the two-way nested domain and dotted trace represents the one-way nested domain.
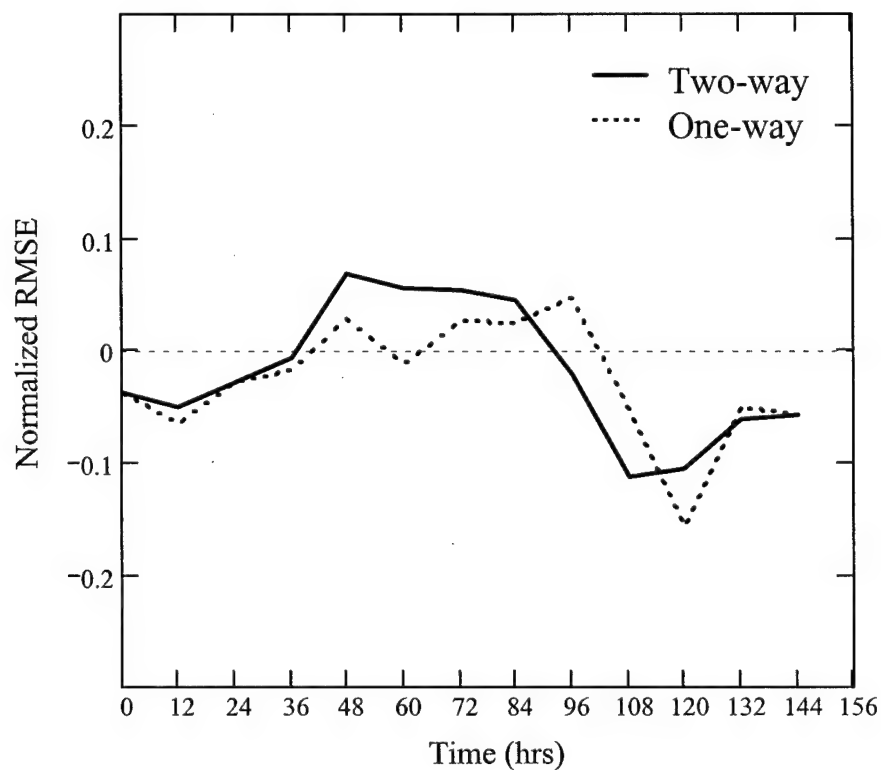
Figure 124   Domain D normalized temperature RMSE for nesting type comparison (May case). This figure compares two-way and one-way nesting using normalized temperature RMSE over a 950/150 mb layer where the control value is provided by the lower resolution (36 km) domain. The solid trace represents the two-way nested domain and dotted trace represents the one-way nested domain.

151

V. Conclusions and Recommendations

5.1 Overview

This chapter begins by presenting the major conclusions drawn from the results of the current research. Next, it offers recommendations to the modeling community based on the findings of the specific topics address in this document. Lastly, suggestions for future research topics are offered.

5.2 Conclusions

Numerical weather prediction is not an exact science; therefore, it is plagued with many uncertainties when it comes to model configuration. Although the results were occasionally muddled by oscillatory behavior in the forecast fields, useful information has been gleaned from this research. The conclusions that follow address the three questions posed in Chapter 1.

First, the placement of the windward lateral boundary for a two-way nested domain had a significant impact on the veracity of the model's forecast, as was clearly shown by the findings in Chapter 4. In general, the results indicate an optimum placement (in this study) of the model's western boundary 5-8° longitude upstream from the tallest peaks of the mountain yielded the most accurate forecast on average. Unlike two-way nesting, the optimum placement of the windward lateral boundary for a one-way nested domain was inconclusive.

Next, the paradigm that high resolution grids always improve a model's veracity over forecasts generated by lower resolution grids appears to be flawed. In the case of certain meteorological variables, such as geopotential height and temperature, this paradigm was found to be accurate for a two-way nested domain when cyclogenesis was present in the model grid. A one-way nested domain also offered improvement to the lower resolution geopotential height and temperature forecasts provided cyclogenesis was weak or nonexistent. In contrast, the results indicate

this paradigm is sometimes flawed when cyclogenetic events are absent during an extended portion the forecast period. Under these circumstances, the high resolution domains (for both one-way and two-way nesting) produced an inferior forecast beyond approximately 36 hours. In addition, wind speed, wind direction, and precipitation were more accurately forecasted on average by the low-resolution domain in this study. The reader is reminded that these results apply to an independently run lower resolution domain, since the forecast of the lower resolution (host) domain for two-way nesting tends toward that of the nested domain for the region of the nest.

Finally, the results indicate a two-way nested domain generated more accurate geopotential height and temperature forecasts than one-way nesting when strong ageostrophic motions (i.e., cyclogenesis) were present in the troposphere. In addition, the results show a one-way nested domain provided the most accurate geopotential height and temperature forecasts during the first 36 hours of the forecast period provided cyclogenesis was absent from the model grid. The conclusions on two-way versus one-way nesting are vividly clear from the plots of the five different domain locations presented in Chapter 4.

5.3 Recommendations

Based on the findings of this research, there are four recommendations: (1) future research on mesoscale models needs to include a greater number of sensitivity studies to increase current knowledge on how topography and various weather scenarios affect the forecast veracity; (2) two-way nested model domains should be used instead of one-way nesting in region where strong synoptic forcing is generally present, such as the midlatitudes; (3) the windward boundary of two-way nested domains need to be placed approximately 5-8° of longitude upstream of the tallest peaks of a mountain range to improve the model's forecast accuracy; and (4) the use

of high-resolution model grids in tropical regions of the world needs to be studied to determine their usefulness in light of the added computational costs.

These recommendations apply to the modeling community as a whole, but are of greater importance to the United States Air Force (USAF). One organizational-specific recommendation concerns the USAF: the Air Force Weather Agency (AFWA) needs to embrace a program that involves active research in the use of mesoscale models. The extensive use of the mesoscale models by AFWA throughout numerous parts of the world has generated the need for sensitivity studies to better understand how to optimize its performance and detail its limitations. The employment of active research in AFWA will yield great benefits in the realm of optimizing current model output and streamlining computational cost by identifying regions of the world where high resolution is of limited benefit.

5.4 Future Research

Since a limited number of sensitivity studies have been conducted on mesoscale models to date, a tremendous number of possible research topics exist. Four topics that will yield benefits to the operations of the USAF are listed: (1) the placement of the mesoscale model's lateral boundaries needs to be studied in other regions of the world using a similar method to that employed by this research to determine the optimum placement of nested windows with respect to orography; (2) the usefulness of finer resolution model grids in tropical locations, where limited synoptic forcing exists, needs to be explored to determine if computational resources are being exploited in a useful manner; (3) the impacts of two-way nesting on the host grid need to explored outside of the nested region, especially downstream from the nested domain, (4) sensitivity studies exploring the increase of vertical grid resolution need to be conducted to assess the benefits/impacts on the model's output.

154

Appendix A. January Root Mean Square Error Tables

This appendix contains the root mean square error (RMSE) data from the January 1995 case study. The tables in this appendix are as follows: Tables 3 through 10 contain the geopotential height RMSE, Tables 11 through 18 contain the temperature RMSE, Tables 19 through 26 contain wind speed RMSE, and Tables 27 through 34 contain wind direction RMSE. The following layers were calculated in 25 mb increments for each meteorological variable listed above: 950/150 mb, 950/700 mb, and 500/200 mb. The individual levels calculated for each variable listed above include 925, 850, 700, 500, 300 mb.

All tables in this appendix have been standardized with units for the RMSE values listed in the title of the table. The date/time group is listed across the top row covering the period from 0000 UTC 15 January 1995 to 0000 UTC 20 January 1995 in 12 hour intervals. The model domain numbers are found along the left margin, or first column. The domains are listed in the following order: independently run 36 km resolution outer domain (1), Domain A using 12 km resolution two-way nesting (2A), Domain B using 12 km resolution two-way nesting (2B), Domain C using 12 km resolution two-way nesting (2C), Domain D using 12 km resolution two-way nesting (2D), Domain E using 12 km resolution two-way nesting (2E), Domain A using 12 km resolution one-way nesting (A), Domain B using 12 km resolution one-way nesting (B), Domain C using 12 km resolution one-way nesting (C), Domain D using 12 km resolution one-way nesting (D), and Domain E using 12 km resolution one-way nesting (E). See Chapter 3 of this document for the placement of Domains A through E.

155

Table 3   Geopotential Height (m) RMSE, 950/150 mb (Case: January 1995)

#	15/00	15/12	16/00	16/12	17/00	17/12	18/00	18/12	19/00	19/12	20/00
					Date/Time (UTC)						
1	6.79	27.17	19.13	20.48	30.44	59.82	69.03	49.80	47.24	54.79	59.89
2A	5.80	27.70	20.23	21.62	28.16	54.65	61.65	43.75	46.19	53.21	45.64
2B	5.80	27.68	20.91	22.97	28.04	52.36	59.56	43.51	45.31	54.33	46.64
2C	5.80	27.66	20.55	22.17	28.33	54.66	62.64	43.94	43.72	52.45	45.00
2D	5.80	27.57	20.50	21.99	28.69	56.03	63.64	43.48	41.60	50.48	45.06
2E	5.80	27.71	20.25	21.51	28.12	55.51	62.74	42.57	41.93	50.42	45.10
A	5.83	27.24	18.17	19.83	30.01	59.34	65.67	46.54	46.05	55.32	55.69
B	5.83	28.00	18.22	21.73	30.21	58.66	65.81	46.28	46.38	55.25	54.73
C	5.83	26.87	18.55	21.26	30.05	59.61	67.01	46.50	45.51	54.07	54.52
D	5.83	26.90	18.71	21.30	29.53	59.95	67.05	46.37	45.96	54.40	55.16
E	5.80	26.49	18.24	20.63	29.82	59.95	67.17	46.22	46.18	54.47	55.36

Table 4   Geopotential Height (m) RMSE, 950/700 mb (Case: January 1995)

#	15/00	15/12	16/00	16/12	17/00	17/12	18/00	18/12	19/00	19/12	20/00
					Date/Time (UTC)						
1	4.58	24.72	13.90	16.72	30.60	39.50	42.39	32.36	46.24	43.04	36.56
2A	4.21	24.62	12.87	15.43	28.17	36.58	39.10	31.67	46.21	37.27	22.06
2B	4.21	24.67	13.22	16.01	27.56	34.91	38.92	33.25	44.43	35.79	22.51
2C	4.21	24.79	13.35	16.14	28.51	36.90	39.39	31.75	43.86	34.59	20.71
2D	4.21	25.09	13.32	16.31	29.36	38.07	40.35	32.36	42.43	34.47	20.78
2E	4.21	25.19	13.24	16.27	29.18	37.96	39.70	31.37	42.87	33.88	20.50
A	4.47	24.16	14.41	16.63	31.28	37.73	39.56	26.95	44.67	42.62	31.89
B	4.48	24.34	13.81	17.16	30.93	39.12	40.07	26.55	45.05	42.94	30.78
C	4.48	23.89	13.27	16.28	30.82	41.06	40.95	26.98	44.36	42.04	30.78
D	4.48	24.15	13.30	16.25	29.77	41.65	41.40	27.87	45.37	42.98	31.68
E	4.40	24.28	13.07	15.50	30.94	41.25	40.53	28.19	44.95	42.75	32.56

Table 5   Geopotential Height (m) RMSE, 500/200 mb (Case: January 1995)

#	Date/Time (UTC)										
	15/00	15/12	16/00	16/12	17/00	17/12	18/00	18/12	19/00	19/12	20/00
1	7.63	28.06	23.46	25.47	49.95	76.24	78.90	57.93	43.43	57.64	68.64
2A	6.43	28.54	24.68	27.52	46.11	69.10	70.08	48.79	42.93	58.62	54.13
2B	6.42	28.42	25.34	28.93	45.27	66.16	67.53	47.80	42.52	60.39	54.48
2C	6.42	28.30	24.83	27.50	46.51	69.26	71.60	49.55	41.65	59.33	53.96
2D	6.42	27.90	24.68	27.16	47.36	71.09	72.59	49.78	40.62	57.52	55.24
2E	6.42	28.08	24.45	26.44	45.82	70.30	71.73	48.69	40.46	57.28	54.82
A	6.38	27.96	21.22	24.62	48.94	75.53	75.07	54.61	42.97	59.12	65.63
B	6.38	29.09	21.58	27.23	49.96	74.12	74.93	54.68	42.96	59.08	65.68
C	6.38	27.72	22.18	27.22	49.60	75.28	76.57	54.82	41.90	58.02	65.55
D	6.38	27.63	22.69	27.00	50.24	75.45	76.41	54.69	42.56	58.13	66.08
E	6.38	27.01	22.23	26.27	50.73	76.07	77.01	54.28	43.11	58.33	66.03

Table 6   Geopotential Height (m) RMSE, 925 mb (Case: January 1995)

#	Date/Time (UTC)										
	15/00	15/12	16/00	16/12	17/00	17/12	18/00	18/12	19/00	19/12	20/00
1	7.06	24.61	21.86	30.79	37.85	37.07	39.85	32.52	42.52	36.49	23.81
2A	6.18	23.85	20.33	29.60	35.49	34.96	36.69	30.67	42.19	31.78	21.04
2B	6.18	24.04	20.30	29.37	34.77	33.47	37.71	32.39	40.52	31.57	23.90
2C	6.18	24.19	20.64	29.35	35.60	34.01	36.85	31.04	40.32	30.07	21.78
2D	6.18	24.53	20.96	29.75	36.80	35.99	37.65	32.23	39.57	29.78	20.26
2E	6.19	24.67	20.76	29.40	36.52	35.27	36.50	30.70	39.94	29.29	21.10
A	6.29	23.48	22.26	31.35	38.16	36.01	36.71	27.40	40.50	35.09	20.07
B	6.31	23.59	21.70	31.47	38.24	37.45	36.49	26.37	40.79	35.36	19.91
C	6.31	23.38	20.88	30.03	39.54	39.85	39.51	27.75	39.93	34.71	20.05
D	6.31	23.66	21.27	29.32	37.95	39.72	37.97	28.29	41.13	35.86	20.36
E	6.27	23.85	20.61	29.45	39.08	39.50	38.10	28.68	40.70	35.67	21.34

Table 7   Geopotential Height (m) RMSE, 850 mb (Case: January 1995)

| # | Date/Time (UTC) | | | | | | | | | | |
#	15/00	15/12	16/00	16/12	17/00	17/12	18/00	18/12	19/00	19/12	20/00
1	5.42	23.48	15.77	26.54	34.99	39.54	41.57	33.78	43.43	40.12	30.51
2A	5.02	23.08	14.36	25.29	32.49	37.00	38.62	32.19	42.77	33.17	17.81
2B	5.03	23.22	14.30	25.40	31.45	35.53	39.22	33.54	41.03	31.71	18.92
2C	5.03	23.36	14.75	25.42	32.53	36.85	39.13	32.09	40.56	30.71	17.54
2D	5.03	23.63	15.06	25.83	33.92	38.52	40.02	33.05	39.40	30.89	17.32
2E	5.03	23.77	14.87	25.29	33.42	38.40	39.01	31.62	39.59	30.33	17.27
A	5.15	22.85	16.04	27.31	36.01	38.38	38.55	28.48	41.75	38.99	25.84
B	5.16	22.99	15.73	27.13	35.84	39.59	38.24	27.45	41.90	39.01	24.55
C	5.16	22.66	14.38	25.94	37.47	41.80	40.36	28.50	41.09	38.32	24.79
D	5.16	22.91	14.99	25.22	35.35	41.91	39.79	29.13	42.15	39.13	25.60
E	5.11	23.21	14.41	26.05	36.36	41.27	39.70	29.38	41.70	38.87	26.64

Table 8   Geopotential Height (m) RMSE, 700 mb (Case: January 1995)

| # | Date/Time (UTC) | | | | | | | | | | |
#	15/00	15/12	16/00	16/12	17/00	17/12	18/00	18/12	19/00	19/12	20/00
1	4.25	21.84	9.34	14.75	31.37	47.94	50.12	34.28	40.81	41.03	40.19
2A	4.03	21.84	9.55	14.71	28.96	44.62	45.96	32.97	40.35	35.59	22.45
2B	4.03	21.81	9.70	15.61	27.99	43.20	46.23	34.80	38.90	33.01	21.16
2C	4.03	21.88	9.30	15.33	29.45	44.79	46.76	33.00	37.82	32.33	19.90
2D	4.03	22.04	9.24	15.13	30.36	46.37	47.98	33.45	36.02	32.30	21.09
2E	4.04	22.13	9.40	14.82	30.06	46.51	47.05	32.34	36.55	31.45	20.17
A	4.17	21.60	9.83	14.98	33.81	47.27	47.34	30.32	40.73	41.48	35.98
B	4.17	21.69	9.47	15.51	33.07	47.91	47.71	29.34	40.48	41.61	35.05
C	4.17	21.19	9.70	15.73	33.39	48.46	49.68	30.46	39.97	40.62	34.69
D	4.17	21.45	9.38	14.69	32.31	49.81	49.48	29.93	40.32	41.33	35.73
E	4.12	21.54	9.20	15.30	32.75	49.49	49.31	31.30	40.10	41.03	36.03

Table 9   Geopotential Height (m) RMSE, 500 mb (Case: January 1995)

#	15/00	15/12	16/00	16/12	17/00	17/12	18/00	18/12	19/00	19/12	20/00
					Date/Time (UTC)						
1	5.50	25.64	17.99	21.28	40.36	54.24	60.04	37.50	44.18	53.06	68.70
2A	4.35	26.11	18.95	22.74	37.79	49.13	53.45	34.45	44.27	51.57	46.59
2B	4.34	25.92	19.22	23.81	37.54	47.08	52.60	36.09	42.59	49.73	42.95
2C	4.34	25.88	18.98	22.83	37.87	50.18	54.99	34.92	41.34	49.19	43.00
2D	4.34	25.56	18.77	22.45	39.05	51.92	56.26	35.64	40.62	48.61	45.95
2E	4.33	25.78	18.81	21.94	37.73	52.04	56.11	34.81	40.11	47.62	44.62
A	4.29	25.74	16.71	19.87	41.31	55.01	56.29	33.87	44.60	54.35	63.29
B	4.28	26.52	17.73	22.72	41.55	53.72	57.41	34.73	45.23	54.94	63.13
C	4.28	25.68	19.05	23.49	41.49	55.43	59.00	33.84	42.74	53.51	62.67
D	4.28	25.35	18.85	22.82	41.73	55.24	58.64	33.42	43.59	54.09	64.40
E	4.25	24.38	18.41	22.78	42.29	55.84	59.90	34.39	44.15	53.90	64.27

Table 10   Geopotential Height (m) RMSE, 300 mb (Case: January 1995)

#	15/00	15/12	16/00	16/12	17/00	17/12	18/00	18/12	19/00	19/12	20/00
					Date/Time (UTC)						
1	7.01	28.94	27.47	30.78	52.97	84.13	82.48	56.28	32.86	55.24	73.62
2A	5.49	29.47	28.84	33.67	48.86	76.47	72.58	44.71	35.10	58.53	61.52
2B	5.48	29.37	29.50	35.56	48.23	73.52	69.51	42.73	34.36	60.31	62.29
2C	5.48	29.17	28.92	33.55	49.82	76.87	74.88	46.72	34.00	60.14	62.61
2D	5.48	28.59	28.73	32.96	50.57	78.90	76.46	47.79	33.69	58.68	63.98
2E	5.48	28.76	28.35	32.07	49.11	78.19	75.65	46.77	34.00	58.63	63.54
A	5.37	29.37	24.62	30.23	51.88	83.01	78.22	51.46	33.47	57.87	72.16
B	5.38	31.13	24.99	33.33	52.65	81.15	77.78	51.35	33.20	57.72	72.57
C	5.38	29.14	24.98	33.22	52.02	82.53	80.13	52.70	33.28	56.76	72.70
D	5.38	29.54	25.68	32.61	52.79	83.17	80.44	52.47	33.50	56.77	72.60
E	5.38	28.43	24.80	31.37	53.60	83.75	80.83	51.62	34.24	57.29	72.51

Table 11   Temperature (K) RMSE, 950/150 mb (Case: January 1995)

#	Date/Time (UTC)										
	15/00	15/12	16/00	16/12	17/00	17/12	18/00	18/12	19/00	19/12	20/00
1	0.81	1.84	2.15	2.41	2.58	2.77	3.10	3.37	3.70	4.10	4.52
2A	0.78	1.77	2.14	2.40	2.58	2.70	2.87	3.13	3.50	3.83	3.97
2B	0.78	1.76	2.16	2.41	2.59	2.72	2.86	3.13	3.42	3.72	3.96
2C	0.78	1.76	2.15	2.39	2.55	2.73	2.94	3.10	3.28	3.55	3.83
2D	0.78	1.76	2.18	2.39	2.53	2.70	2.97	3.06	3.17	3.45	3.80
2E	0.78	1.76	2.18	2.38	2.51	2.74	2.94	3.05	3.10	3.38	3.83
A	0.78	1.71	2.05	2.37	2.55	2.87	2.94	3.21	3.55	3.93	4.21
B	0.78	1.73	2.16	2.47	2.62	2.76	2.93	3.19	3.52	3.90	4.18
C	0.78	1.70	2.11	2.41	2.61	2.72	2.96	3.18	3.45	3.83	4.12
D	0.78	1.69	2.09	2.44	2.51	2.76	2.93	3.16	3.48	3.85	4.16
E	0.78	1.69	2.13	2.39	2.54	2.79	2.97	3.16	3.48	3.82	4.10

Table 12   Temperature (K) RMSE, 950/700 mb (Case: January 1995)

#	Date/Time (UTC)										
	15/00	15/12	16/00	16/12	17/00	17/12	18/00	18/12	19/00	19/12	20/00
1	0.56	1.99	2.55	2.99	3.13	3.34	3.67	3.21	3.25	2.89	3.36
2A	0.50	1.93	2.54	3.03	3.20	3.29	3.30	2.95	3.16	3.15	3.35
2B	0.50	1.92	2.55	3.05	3.23	3.37	3.30	2.94	3.07	3.05	3.28
2C	0.50	1.94	2.54	3.03	3.17	3.44	3.45	3.03	3.03	2.93	3.16
2D	0.50	1.94	2.61	3.03	3.13	3.33	3.53	3.04	3.02	2.92	3.15
2E	0.50	1.94	2.58	3.04	3.12	3.46	3.50	3.14	2.99	2.80	3.08
A	0.49	1.85	2.48	2.96	3.04	3.55	3.36	3.04	3.02	2.94	3.49
B	0.49	1.88	2.66	3.10	3.17	3.35	3.52	3.06	3.00	3.03	3.56
C	0.49	1.89	2.56	3.05	3.15	3.22	3.59	3.07	2.97	2.94	3.45
D	0.49	1.89	2.51	3.06	2.96	3.31	3.55	3.09	3.03	3.02	3.49
E	0.49	1.80	2.54	3.01	3.09	3.33	3.60	3.05	3.03	3.01	3.43

160

Table 13   Temperature (K) RMSE, 500/200 mb (Case: January 1995)

#	15/00	15/12	16/00	16/12	17/00	17/12	18/00	18/12	19/00	19/12	20/00
					Date/Time (UTC)						
1	1.02	1.67	1.86	2.24	2.44	2.95	3.39	4.07	4.31	4.66	4.72
2A	1.02	1.60	1.76	2.16	2.32	2.87	3.29	3.82	4.02	4.22	4.05
2B	1.02	1.58	1.78	2.17	2.31	2.85	3.30	3.84	3.98	4.14	4.11
2C	1.02	1.59	1.76	2.09	2.30	2.80	3.32	3.74	3.84	3.96	3.97
2D	1.02	1.59	1.75	2.07	2.26	2.78	3.22	3.63	3.66	3.84	3.89
2E	1.02	1.59	1.75	2.03	2.23	2.72	3.14	3.56	3.57	3.81	4.00
A	1.02	1.59	1.64	2.16	2.34	2.91	3.41	3.98	4.19	4.60	4.44
B	1.02	1.61	1.70	2.19	2.44	2.87	3.28	3.97	4.15	4.54	4.38
C	1.02	1.54	1.72	2.21	2.41	2.87	3.26	3.86	4.08	4.52	4.41
D	1.02	1.53	1.70	2.17	2.43	2.88	3.20	3.85	4.12	4.51	4.37
E	1.02	1.56	1.72	2.19	2.42	2.92	3.23	3.88	4.15	4.50	4.37

Table 14   Temperature (K) RMSE, 925 mb (Case: January 1995)

#	15/00	15/12	16/00	16/12	17/00	17/12	18/00	18/12	19/00	19/12	20/00
					Date/Time (UTC)						
1	0.57	2.34	2.80	3.55	3.28	4.47	3.58	4.13	3.28	4.32	3.62
2A	0.46	2.25	2.87	3.55	3.24	4.26	3.35	4.09	3.43	4.26	3.71
2B	0.46	2.24	2.86	3.53	3.38	4.39	3.34	4.01	3.40	4.09	3.72
2C	0.46	2.25	2.89	3.58	3.43	4.56	3.69	4.13	3.28	4.07	3.52
2D	0.46	2.26	2.85	3.54	3.34	4.33	3.62	4.08	3.31	3.98	3.39
2E	0.46	2.27	2.83	3.57	3.35	4.62	3.64	4.31	3.16	3.81	3.38
A	0.48	2.11	2.75	3.45	3.22	4.86	3.44	4.10	3.39	4.26	3.78
B	0.48	2.14	2.84	3.53	3.12	4.42	3.40	4.19	3.30	4.22	3.63
C	0.48	2.18	2.89	3.48	3.07	4.17	3.35	3.91	3.28	4.20	3.56
D	0.48	2.18	2.91	3.62	3.19	4.21	3.32	4.02	3.44	4.36	3.60
E	0.48	2.10	2.93	3.51	3.27	4.35	3.42	3.96	3.37	4.36	3.59

161

Table 15   Temperature (K) RMSE, 850 mb (Case: January 1995)

#	15/00	15/12	16/00	16/12	17/00	17/12	18/00	18/12	19/00	19/12	20/00
				Date/Time (UTC)							
1	0.75	2.42	4.06	4.34	3.78	4.01	4.32	3.91	3.78	2.58	4.45
2A	0.63	2.34	4.07	4.35	3.78	3.85	3.98	3.51	3.48	3.07	4.14
2B	0.63	2.33	4.13	4.39	3.80	3.81	3.97	3.56	3.42	3.01	4.05
2C	0.63	2.35	4.13	4.20	3.86	3.90	3.99	3.56	3.49	2.89	3.87
2D	0.63	2.33	4.25	4.24	3.71	3.92	4.05	3.65	3.49	2.76	3.78
2E	0.63	2.34	4.17	4.18	3.81	3.96	4.10	3.57	3.56	2.80	3.77
A	0.61	2.18	3.97	4.11	3.61	4.05	3.95	3.73	3.38	2.76	4.46
B	0.61	2.12	4.21	4.34	3.85	3.87	4.15	3.55	3.30	2.91	4.54
C	0.61	2.21	4.25	4.27	4.03	4.05	4.11	3.79	3.30	2.78	4.43
D	0.61	2.20	4.06	4.17	3.67	4.16	3.97	3.61	3.32	2.95	4.49
E	0.61	2.14	3.93	4.24	3.65	3.98	4.16	3.70	3.39	2.82	4.43

Table 16   Temperature (K) RMSE, 700 mb (Case: January 1995)

#	15/00	15/12	16/00	16/12	17/00	17/12	18/00	18/12	19/00	19/12	20/00
				Date/Time (UTC)							
1	0.50	1.33	1.96	2.74	3.05	1.53	3.10	1.91	2.27	1.96	1.99
2A	0.44	1.31	1.91	2.83	3.08	1.61	2.70	1.69	2.20	2.25	2.06
2B	0.44	1.29	1.85	2.84	3.20	1.59	2.74	1.80	2.08	2.20	2.03
2C	0.44	1.30	1.93	2.83	3.07	1.61	2.87	1.71	2.11	2.12	2.06
2D	0.44	1.29	1.91	2.80	3.06	1.66	2.93	1.78	2.18	2.21	2.23
2E	0.44	1.28	1.93	2.69	3.07	1.66	2.94	1.68	2.09	1.98	2.13
A	0.45	1.27	1.96	2.83	3.15	1.80	2.60	1.61	1.99	2.00	2.04
B	0.45	1.34	1.95	2.96	3.22	1.76	2.70	1.72	2.11	2.15	2.21
C	0.45	1.31	1.88	2.95	3.17	1.60	2.79	1.77	2.06	2.12	2.11
D	0.45	1.28	1.82	2.74	3.01	1.62	2.84	1.85	2.06	2.08	2.06
E	0.45	1.29	1.96	2.83	3.12	1.79	2.87	1.79	2.01	2.11	2.04

Table 17   Temperature (K) RMSE, 500 mb (Case: January 1995)

#	15/00	15/12	16/00	16/12	17/00	17/12	18/00	18/12	19/00	19/12	20/00
1	0.44	1.05	1.25	1.43	1.40	2.96	2.56	2.49	2.85	3.20	3.21
2A	0.38	1.03	1.21	1.40	1.37	2.72	2.38	2.12	2.90	3.17	3.28
2B	0.38	1.04	1.23	1.45	1.43	2.65	2.35	2.08	2.78	3.10	3.27
2C	0.38	1.05	1.26	1.49	1.47	2.64	2.52	2.15	2.97	3.14	3.34
2D	0.38	1.03	1.28	1.54	1.52	2.61	2.56	2.22	2.92	3.15	3.43
2E	0.38	1.02	1.29	1.49	1.46	2.61	2.48	2.22	2.94	3.18	3.47
A	0.38	0.88	1.01	1.38	1.30	2.80	2.35	2.05	2.89	3.01	3.22
B	0.38	0.98	1.08	1.36	1.47	2.74	2.25	2.11	2.81	2.99	3.30
C	0.38	0.97	1.14	1.31	1.45	2.73	2.35	2.20	2.89	2.95	3.33
D	0.38	0.97	1.20	1.47	1.58	2.77	2.36	2.16	3.02	2.96	3.38
E	0.38	0.93	1.20	1.37	1.54	2.80	2.44	2.18	2.98	3.00	3.33

Table 18   Temperature (K) RMSE, 300 mb (Case: January 1995)

#	15/00	15/12	16/00	16/12	17/00	17/12	18/00	18/12	19/00	19/12	20/00
1	1.00	1.64	2.53	1.93	2.36	3.37	4.45	5.14	4.46	4.98	4.23
2A	1.01	1.52	2.46	1.84	2.29	3.36	4.49	4.99	4.15	4.50	3.50
2B	1.01	1.49	2.51	1.85	2.29	3.39	4.52	5.03	4.20	4.45	3.60
2C	1.01	1.48	2.44	1.78	2.25	3.36	4.55	4.89	3.99	4.25	3.37
2D	1.01	1.51	2.44	1.78	2.18	3.31	4.37	4.74	3.80	4.13	3.27
2E	1.01	1.51	2.47	1.75	2.13	3.21	4.27	4.70	3.79	4.13	3.37
A	1.04	1.51	2.33	1.97	2.34	3.43	4.65	5.14	4.34	4.98	3.95
B	1.04	1.58	2.26	1.90	2.42	3.40	4.50	5.16	4.31	4.96	3.95
C	1.04	1.56	2.36	1.87	2.39	3.42	4.46	4.98	4.08	4.86	3.93
D	1.04	1.51	2.37	1.83	2.36	3.42	4.36	4.99	4.31	4.90	3.99
E	1.04	1.56	2.45	1.84	2.38	3.48	4.36	5.08	4.31	4.86	3.92

Table 19   Wind Speed (m/s) RMSE, 950/150 mb (Case: January 1995)

#	15/00	15/12	16/00	16/12	17/00	17/12	18/00	18/12	19/00	19/12	20/00
					Date/Time (UTC)						
1	3.40	5.12	5.15	5.63	6.27	8.64	9.34	9.97	9.02	9.90	7.81
2A	3.42	5.21	4.98	5.69	6.10	8.62	9.42	9.24	9.46	10.32	8.05
2B	3.42	5.23	5.02	5.72	5.96	8.52	9.16	9.41	9.76	10.55	8.25
2C	3.43	5.16	5.01	5.67	6.07	8.71	9.27	9.28	9.58	10.43	8.12
2D	3.43	5.13	4.88	5.54	6.09	8.74	9.46	9.29	9.47	10.40	7.89
2E	3.41	5.11	5.00	5.57	6.10	8.72	9.17	9.29	9.61	10.21	8.11
A	3.43	5.61	5.13	5.48	6.46	8.95	9.64	9.39	7.80	9.33	7.67
B	3.43	5.95	5.05	5.69	6.42	8.94	9.43	9.34	7.99	9.31	7.76
C	3.43	5.57	4.83	5.87	6.54	9.06	9.34	9.35	7.91	9.36	7.72
D	3.43	5.23	4.92	5.79	6.54	9.14	9.35	9.32	7.93	9.32	7.69
E	3.43	5.27	4.92	5.74	6.58	9.24	9.51	9.49	8.08	9.62	7.56

Table 20   Wind Speed (m/s) RMSE, 950/700 mb (Case: January 1995)

#	15/00	15/12	16/00	16/12	17/00	17/12	18/00	18/12	19/00	19/12	20/00
					Date/Time (UTC)						
1	0.89	2.87	3.46	3.24	4.34	6.88	6.89	7.90	7.33	8.24	6.01
2A	0.88	2.79	3.36	3.27	4.23	6.94	6.86	7.56	7.80	8.30	6.27
2B	0.88	2.79	3.39	3.31	4.18	7.07	6.97	7.74	8.13	8.38	6.30
2C	0.88	2.81	3.34	3.23	4.13	6.81	6.81	7.67	8.15	8.01	6.07
2D	0.87	2.82	3.30	3.07	4.24	6.95	6.87	7.73	7.87	7.96	5.92
2E	0.87	2.85	3.40	3.18	4.13	6.89	6.83	7.65	8.14	7.88	6.03
A	0.89	2.74	3.53	3.11	4.54	6.63	6.75	7.46	6.38	8.14	5.87
B	0.89	2.73	3.51	3.33	4.49	6.84	6.54	7.40	6.82	8.04	5.92
C	0.89	2.70	3.41	3.20	4.57	7.07	6.47	7.57	6.52	8.02	5.78
D	0.89	2.73	3.37	3.02	4.30	7.14	6.64	7.57	6.66	7.89	5.72
E	0.89	2.69	3.22	3.20	4.56	7.23	6.95	7.60	6.75	8.25	5.65

164

Table 21   Wind Speed (m/s) RMSE, 500/200 mb (Case: January 1995)

#	15/00	15/12	16/00	16/12	17/00	17/12	18/00	18/12	19/00	19/12	20/00
1	4.11	6.52	6.79	7.20	9.67	9.86	10.78	10.48	11.03	11.75	10.36
2A	4.13	6.67	6.62	7.23	9.43	9.62	10.62	9.80	11.63	12.26	10.08
2B	4.14	6.71	6.71	7.32	9.42	9.44	10.15	10.03	11.85	12.68	9.96
2C	4.14	6.58	6.69	7.22	9.44	9.89	10.58	9.71	11.64	12.78	9.78
2D	4.15	6.57	6.46	7.08	9.51	9.97	10.78	9.71	11.60	12.79	9.61
2E	4.14	6.56	6.54	7.13	9.45	9.89	10.57	9.66	11.69	12.59	9.90
A	4.14	7.30	6.76	7.21	9.92	10.59	11.05	10.10	9.97	10.91	10.15
B	4.14	7.87	6.49	7.36	10.09	10.10	10.86	10.01	9.86	10.95	10.11
C	4.14	7.20	6.24	7.63	10.30	10.03	10.72	10.17	9.88	11.04	10.05
D	4.14	6.80	6.40	7.40	10.12	10.16	10.76	10.05	9.84	11.10	10.11
E	4.14	6.98	6.34	7.28	10.18	10.23	10.87	10.32	10.03	11.21	9.72

Date/Time (UTC)

Table 22   Wind Speed (m/s) RMSE, 925 mb (Case: January 1995)

#	15/00	15/12	16/00	16/12	17/00	17/12	18/00	18/12	19/00	19/12	20/00
1	0.81	3.08	2.96	3.91	3.07	6.41	8.28	6.27	6.29	8.07	5.15
2A	0.84	2.94	3.04	3.77	3.02	6.85	7.88	6.47	7.32	7.59	4.20
2B	0.84	2.95	2.97	3.80	3.33	6.73	8.24	6.79	7.57	7.86	4.12
2C	0.84	2.94	2.97	3.83	3.63	6.44	8.01	6.61	7.52	8.05	4.38
2D	0.84	2.95	2.82	3.76	3.45	6.81	8.27	6.48	7.13	7.68	4.28
2E	0.84	2.94	2.90	3.68	3.34	6.31	8.06	6.70	7.27	7.89	4.46
A	0.84	2.89	2.99	3.98	2.97	6.31	7.88	5.93	6.00	7.46	5.03
B	0.84	2.92	2.64	3.78	3.13	6.79	7.50	5.85	6.33	7.66	4.95
C	0.84	2.82	2.67	3.81	3.01	6.61	7.78	5.67	5.97	7.38	4.92
D	0.84	2.76	2.55	3.60	2.94	6.38	7.74	5.75	6.31	7.36	5.05
E	0.84	2.95	2.72	3.66	2.91	6.63	8.03	5.73	6.28	7.57	4.91

Date/Time (UTC)

Table 23   Wind Speed (m/s) RMSE, 850 mb (Case: January 1995)

#	Date/Time (UTC)										
	15/00	15/12	16/00	16/12	17/00	17/12	18/00	18/12	19/00	19/12	20/00
1	0.43	3.52	4.40	4.41	5.40	5.83	6.79	7.49	7.05	8.46	6.29
2A	0.43	3.35	4.41	4.52	5.16	5.88	7.54	7.33	7.33	8.65	5.40
2B	0.43	3.33	4.32	4.83	5.11	5.96	7.59	7.42	7.61	8.33	5.57
2C	0.43	3.36	4.18	4.71	5.15	5.95	7.32	7.33	7.72	8.10	5.35
2D	0.44	3.37	4.12	4.47	4.99	6.00	7.32	7.56	7.38	8.12	5.64
2E	0.45	3.46	3.90	4.63	4.94	5.93	7.38	7.51	7.64	8.08	5.45
A	0.45	2.86	4.57	4.39	5.42	6.12	6.99	7.66	6.71	8.10	5.61
B	0.45	3.36	4.25	4.89	5.42	6.42	6.40	7.74	6.78	7.99	5.48
C	0.45	3.46	4.28	4.42	5.68	6.65	6.76	7.96	6.66	7.92	5.43
D	0.45	3.58	4.14	4.52	4.63	6.74	6.79	7.84	6.56	7.70	5.55
E	0.44	3.51	3.89	4.26	5.20	6.47	7.27	7.85	6.66	8.06	5.27

Table 24   Wind Speed (m/s) RMSE, 700 mb (Case: January 1995)

#	Date/Time (UTC)										
	15/00	15/12	16/00	16/12	17/00	17/12	18/00	18/12	19/00	19/12	20/00
1	0.76	3.04	3.39	4.76	3.81	8.87	6.52	9.57	7.81	7.10	6.71
2A	0.72	3.04	3.30	4.54	3.83	9.01	6.18	8.89	7.90	7.14	7.55
2B	0.72	3.01	3.66	4.99	3.68	8.99	6.62	8.96	8.23	7.04	7.41
2C	0.72	2.97	3.24	4.84	4.02	9.00	6.35	8.89	8.38	7.00	7.19
2D	0.70	2.93	3.03	4.89	4.17	8.43	6.42	8.96	8.06	6.78	7.07
2E	0.69	2.92	3.71	4.96	4.32	8.83	6.14	8.93	8.20	6.88	7.26
A	0.76	2.56	2.97	5.13	4.50	8.00	6.45	7.88	6.37	7.43	6.53
B	0.76	2.44	3.10	5.55	4.63	8.27	6.37	7.73	6.46	6.96	6.97
C	0.76	2.42	3.16	4.62	4.55	8.78	5.72	7.94	6.55	7.13	6.73
D	0.76	2.51	2.80	4.67	4.97	8.35	5.81	8.12	6.71	6.93	6.60
E	0.76	2.58	3.29	4.72	4.73	8.63	6.40	8.17	6.60	7.57	6.46

166

Table 25   Wind Speed (m/s) RMSE, 500 mb (Case: January 1995)

#	15/00	15/12	16/00	16/12	17/00	17/12	18/00	18/12	19/00	19/12	20/00
					Date/Time (UTC)						
1	1.72	4.25	3.96	5.83	6.92	6.78	8.71	8.56	9.70	11.18	8.65
2A	1.73	4.13	3.83	6.62	6.77	6.81	8.85	7.42	9.92	10.94	8.59
2B	1.73	4.10	3.91	6.19	6.74	6.99	8.56	7.94	10.18	11.15	8.04
2C	1.73	3.89	4.13	6.63	6.92	7.57	8.47	7.58	10.13	11.64	8.00
2D	1.73	4.04	3.81	6.07	7.07	7.38	8.89	7.29	9.86	11.86	8.10
2E	1.71	4.05	3.84	5.98	7.08	7.57	8.56	7.48	9.90	11.87	8.47
A	1.78	4.35	4.28	5.73	7.47	6.78	8.85	8.24	8.43	8.80	8.58
B	1.78	4.69	4.83	6.17	7.32	7.81	7.94	8.21	8.35	8.99	8.52
C	1.78	4.68	4.93	6.09	7.50	7.24	7.60	8.15	8.70	9.42	8.34
D	1.78	4.55	4.71	6.34	7.43	7.53	7.56	7.86	8.88	9.44	8.48
E	1.78	4.76	4.11	6.05	7.30	7.38	7.66	8.31	8.79	9.51	7.97

Table 26   Wind Speed (m/s) RMSE, 300 mb (Case: January 1995)

#	15/00	15/12	16/00	16/12	17/00	17/12	18/00	18/12	19/00	19/12	20/00
					Date/Time (UTC)						
1	3.13	6.46	7.09	8.98	8.06	10.57	10.74	10.50	10.81	10.17	7.49
2A	3.07	6.64	6.87	8.95	8.10	10.01	10.55	9.59	12.02	11.09	8.01
2B	3.09	6.74	7.06	9.36	7.91	9.75	9.79	10.08	11.98	11.77	8.96
2C	3.08	6.55	6.92	9.37	8.11	10.37	10.43	9.56	11.86	11.70	8.83
2D	3.09	6.46	6.67	9.20	8.06	10.56	11.09	9.62	11.92	11.86	8.21
2E	3.05	6.45	6.74	9.26	8.05	10.54	10.44	9.55	11.87	11.33	8.22
A	3.06	8.06	7.11	9.14	8.25	11.28	10.94	9.94	10.40	10.43	7.56
B	3.06	9.03	6.46	9.30	8.55	10.75	10.88	10.02	10.18	10.70	7.47
C	3.06	8.09	6.22	9.71	8.10	10.75	10.78	10.07	10.35	10.45	7.54
D	3.06	7.17	6.52	9.35	7.98	10.74	10.84	10.24	10.31	10.21	7.49
E	3.06	7.19	6.88	9.06	8.10	11.07	11.30	10.75	10.59	10.55	7.47

Table 27   Wind Direction (deg.) RMSE, 950/150 mb (Case: January 1995)

#	15/00	15/12	16/00	16/12	17/00	17/12	18/00	18/12	19/00	19/12	20/00
					Date/Time (UTC)						
1	12.79	38.76	32.76	18.20	25.33	36.75	38.77	46.09	44.78	48.05	40.99
2A	12.15	37.95	31.16	17.51	25.09	35.19	36.59	42.87	45.00	47.90	43.46
2B	12.15	37.97	31.56	17.65	25.27	34.60	36.77	43.66	45.22	46.98	44.09
2C	12.14	38.03	31.13	18.04	24.81	35.90	38.19	43.14	45.07	46.85	42.63
2D	12.16	38.04	30.93	17.99	23.98	35.46	38.35	43.08	44.34	46.38	42.62
2E	12.19	38.22	31.92	18.57	23.77	35.72	38.80	43.09	45.11	46.22	42.36
A	12.19	37.29	30.22	17.88	24.69	35.51	37.36	42.17	44.02	47.24	43.14
B	12.19	37.49	30.16	19.17	26.31	35.69	37.35	42.33	45.36	47.66	43.83
C	12.19	37.53	29.14	18.70	25.93	35.37	37.93	43.74	44.96	47.67	43.31
D	12.19	37.26	30.02	19.55	24.26	35.13	38.36	42.86	44.35	48.03	42.88
E	12.16	39.11	30.81	18.41	25.47	36.11	39.30	44.18	45.29	48.78	44.36

Table 28   Wind Direction (deg.) RMSE, 950/700 mb (Case: January 1995)

#	15/00	15/12	16/00	16/12	17/00	17/12	18/00	18/12	19/00	19/12	20/00
					Date/Time (UTC)						
1	14.37	44.78	47.23	22.80	39.93	58.56	56.20	69.18	62.91	56.84	34.35
2A	12.88	44.18	44.68	21.14	39.31	55.75	53.64	63.42	62.64	54.27	39.25
2B	12.88	44.12	45.72	21.07	39.61	54.53	53.72	64.08	62.01	52.44	38.27
2C	12.86	44.36	45.13	21.68	38.92	56.93	54.88	64.30	61.75	52.20	34.24
2D	12.91	44.02	44.57	21.95	37.49	56.22	55.23	64.89	60.38	51.91	34.42
2E	12.90	44.24	45.64	22.69	37.22	56.75	56.03	64.10	61.56	51.68	34.32
A	12.94	41.58	38.73	21.49	38.65	55.34	53.81	63.35	61.72	53.82	38.70
B	12.94	41.24	38.10	22.05	41.55	55.87	53.75	63.82	63.70	54.89	39.81
C	12.94	43.08	37.60	21.98	40.83	55.43	55.91	66.77	62.68	54.82	41.14
D	12.94	43.55	37.88	22.61	37.87	55.27	56.92	65.15	62.38	55.54	39.15
E	12.85	45.90	42.94	22.12	39.79	56.68	57.99	67.32	63.38	56.25	40.64

Table 29   Wind Direction (deg.) RMSE, 500/200 mb (Case: January 1995)

#	15/00	15/12	16/00	16/12	17/00	17/12	18/00	18/12	19/00	19/12	20/00
1	10.58	26.88	14.41	15.37	13.70	30.04	23.62	25.76	29.97	45.22	39.53
2A	10.36	26.51	14.13	15.04	13.73	28.97	25.86	25.34	31.06	46.17	40.90
2B	10.35	26.57	14.20	15.75	13.44	28.90	26.66	26.62	32.12	46.00	42.81
2C	10.33	26.49	13.35	15.90	12.75	29.41	25.48	24.09	31.94	46.09	42.72
2D	10.31	26.90	13.53	15.88	12.75	30.54	25.77	24.08	32.37	45.50	42.17
2E	10.30	26.79	13.34	15.98	12.70	30.16	26.92	23.65	32.10	45.66	41.55
A	10.44	25.06	16.36	14.81	14.02	30.14	24.56	21.98	30.99	45.63	40.17
B	10.44	25.96	16.60	17.53	14.14	30.89	23.96	23.29	30.87	45.37	40.44
C	10.44	24.77	15.72	16.40	14.52	31.08	26.99	23.32	31.01	45.53	38.48
D	10.44	22.87	14.71	17.06	14.23	29.88	23.75	22.12	30.69	45.66	39.30
E	10.44	26.02	16.36	16.31	14.28	30.97	23.94	25.29	30.91	46.29	40.46

Table 30   Wind Direction (deg.) RMSE, 925 mb (Case: January 1995)

#	15/00	15/12	16/00	16/12	17/00	17/12	18/00	18/12	19/00	19/12	20/00
1	10.25	40.88	40.38	34.90	48.19	72.77	75.03	83.37	71.96	60.94	45.87
2A	10.28	42.08	35.07	29.86	48.43	71.24	73.59	80.90	70.77	59.71	49.44
2B	10.27	42.46	39.08	31.10	48.90	72.87	72.78	82.35	68.86	55.52	51.76
2C	10.28	42.16	34.98	31.90	45.01	74.91	75.15	80.42	70.04	52.24	49.63
2D	10.31	41.99	29.93	31.98	41.09	71.33	74.16	80.91	66.92	55.39	49.15
2E	9.80	41.38	29.42	32.42	41.31	72.92	75.38	79.79	70.86	53.94	50.92
A	10.60	33.95	41.30	30.70	43.74	68.70	73.58	80.66	76.15	55.22	44.41
B	10.60	34.50	27.87	31.66	54.37	67.41	71.88	80.96	78.40	57.27	42.58
C	10.60	36.45	30.41	29.90	50.86	69.80	75.39	82.92	75.35	56.44	44.20
D	10.60	36.88	28.26	29.15	43.87	69.49	76.28	80.72	75.74	58.16	42.04
E	10.07	36.02	28.20	30.44	50.62	71.71	75.84	83.01	77.50	59.57	45.41

Table 31   Wind Direction (deg.) RMSE, 850 mb (Case: January 1995)

#	15/00	15/12	16/00	16/12	17/00	17/12	18/00	18/12	19/00	19/12	20/00
					Date/Time (UTC)						
1	17.14	38.68	52.19	33.82	46.14	62.40	57.08	74.00	56.54	60.77	35.31
2A	16.91	41.38	48.46	33.29	43.80	59.54	57.27	65.47	58.73	48.09	43.68
2B	16.78	41.93	48.99	34.18	42.62	57.88	57.43	66.52	57.69	48.05	42.49
2C	16.49	42.20	48.06	34.38	43.54	61.81	55.09	66.82	55.63	45.51	28.07
2D	16.18	40.91	50.08	33.19	41.16	61.05	56.38	66.48	56.74	46.44	28.73
2E	15.02	40.72	49.66	34.16	40.76	62.37	55.87	66.31	59.55	46.69	26.93
A	17.77	36.08	39.93	31.14	43.02	60.94	56.69	65.14	52.89	55.73	38.90
B	17.77	35.82	47.05	36.40	59.16	64.86	55.35	66.00	55.71	56.80	39.49
C	17.77	40.55	38.90	34.63	45.60	63.52	64.02	69.89	56.44	58.74	39.88
D	17.77	39.76	40.37	30.74	42.56	62.81	63.52	67.40	55.64	60.25	38.08
E	17.79	45.82	52.89	32.36	42.49	64.13	64.27	69.68	55.49	59.38	40.20

Table 32   Wind Direction (deg.) RMSE, 700 mb (Case: January 1995)

#	15/00	15/12	16/00	16/12	17/00	17/12	18/00	18/12	19/00	19/12	20/00
					Date/Time (UTC)						
1	7.59	49.12	40.79	12.29	15.77	43.97	41.59	51.59	48.12	26.98	23.67
2A	7.00	36.63	41.31	13.12	16.31	42.31	38.10	46.52	46.05	32.43	23.32
2B	7.02	36.47	41.29	12.91	16.47	45.72	38.12	45.50	46.93	33.72	23.80
2C	7.01	36.14	41.21	13.18	18.17	37.61	38.09	48.03	47.79	33.42	24.81
2D	7.05	35.94	41.77	12.12	18.73	45.57	39.20	48.08	47.03	32.75	24.69
2E	7.19	37.10	41.58	14.02	17.44	47.54	37.00	48.00	48.39	32.33	26.21
A	6.99	44.91	28.97	11.82	15.07	42.04	38.30	46.99	45.80	28.22	27.20
B	6.99	43.13	29.53	13.22	15.11	43.88	35.13	47.63	47.37	28.39	27.78
C	6.99	41.57	36.19	12.03	17.80	41.27	39.98	48.50	45.61	27.98	26.31
D	6.99	43.21	34.81	14.91	16.77	44.13	37.23	49.66	45.56	28.02	26.79
E	6.99	50.30	42.07	12.11	14.67	50.48	41.44	48.82	46.79	28.12	27.21

Table 33   Wind Direction (deg.) RMSE, 500 mb (Case: January 1995)

#	15/00	15/12	16/00	16/12	17/00	17/12	18/00	18/12	19/00	19/12	20/00
1	14.06	47.37	10.02	14.49	16.55	36.32	30.97	37.08	35.59	29.45	33.99
2A	14.07	44.90	11.30	14.57	16.60	33.01	28.29	37.90	37.04	28.36	32.35
2B	14.05	44.86	11.68	14.23	15.32	32.71	29.21	37.50	38.58	28.42	38.12
2C	13.97	44.32	11.40	15.45	14.46	37.57	28.12	33.83	37.45	28.41	42.75
2D	13.90	46.04	11.37	14.26	14.47	41.97	30.65	36.52	37.70	26.98	43.19
2E	13.77	45.95	10.75	14.49	14.73	40.15	29.33	33.40	36.87	26.89	44.78
A	13.85	31.13	12.38	16.91	16.88	35.06	32.22	32.01	35.67	31.50	38.54
B	13.85	37.68	13.39	16.36	16.37	37.87	32.36	32.64	36.64	31.45	36.81
C	13.85	32.37	12.36	17.27	17.74	38.11	42.17	32.05	36.15	32.01	34.25
D	13.85	29.83	10.15	16.39	16.42	34.45	34.32	30.02	34.18	31.64	35.14
E	13.85	45.33	11.10	15.24	17.22	37.50	31.78	37.01	36.21	33.28	38.07

Date/Time (UTC)

Table 34   Wind Direction (deg.) RMSE, 300 mb (Case: January 1995)

#	15/00	15/12	16/00	16/12	17/00	17/12	18/00	18/12	19/00	19/12	20/00
1	7.55	13.10	14.53	11.38	12.77	22.33	15.92	17.27	15.39	47.11	44.42
2A	7.30	13.46	15.18	12.64	12.74	21.94	15.92	17.22	14.72	48.56	46.05
2B	7.27	13.63	15.14	13.28	12.75	21.82	16.65	18.33	15.09	45.56	45.63
2C	7.22	13.78	14.42	12.58	12.47	21.73	16.78	17.92	14.57	45.27	44.39
2D	7.14	13.58	14.07	12.72	12.62	21.41	16.64	17.74	15.03	47.31	43.71
2E	7.02	13.44	13.81	12.83	12.18	21.20	16.66	17.72	14.85	45.11	43.65
A	7.24	13.29	15.04	10.73	12.89	22.99	16.79	15.54	18.58	51.05	43.20
B	7.24	13.63	16.53	14.11	13.09	22.78	16.12	15.96	18.15	49.96	42.66
C	7.24	12.13	15.83	12.93	13.35	23.06	15.77	15.66	17.30	49.71	40.92
D	7.24	10.55	14.86	12.57	13.25	22.67	15.42	15.53	17.23	49.68	41.29
E	7.24	11.21	17.18	11.78	13.07	23.40	16.02	16.54	17.51	49.97	44.24

Date/Time (UTC)

171

Appendix B. May Root Mean Square Error Tables

This appendix contains the root mean square error (RMSE) data from the May 1995 case study. The tables in this appendix are as follows: Tables 35 through 42 contain the geopotential height RMSE, Tables 43 through 50 contain the temperature RMSE, Tables 51 through 58 contain wind speed RMSE, and Tables 59 through 66 contain wind direction RMSE. The following layers were calculated in 25 mb increments for each meteorological variable listed above: 950/150 mb, 950/700 mb, and 500/200 mb. The individual levels calculated for each variable listed above include 925, 850, 700, 500, 300 mb.

All tables in this appendix have been standardized with units for the RMSE values listed in the title of the table. The date/time group is listed across the top row covering the period from 0000 UTC 4 May 1995 to 0000 UTC 10 May 1995 in 12 hour intervals. The model domain numbers are found along the left margin, or first column. The domains are listed in the following order: independently run 36 km resolution outer domain (1), Domain A using 12 km resolution two-way nesting (2A), Domain B using 12 km resolution two-way nesting (2B), Domain C using 12 km resolution two-way nesting (2C), Domain D using 12 km resolution two-way nesting (2D), Domain E using 12 km resolution two-way nesting (2E), Domain A using 12 km resolution one-way nesting (A), Domain B using 12 km resolution one-way nesting (B), Domain C using 12 km resolution one-way nesting (C), Domain D using 12 km resolution one-way nesting (D), and Domain E using 12 km resolution one-way nesting (E). See Chapter 3 of this document for the placement of Domains A through E.

Table 35   Geopotential Height (m) RMSE, 950/150 mb (Case: May 1995)

#	4/00	4/12	5/00	5/12	6/00	6/12	7/00	7/12	8/00	8/12	9/00	9/12	10/00
1	12.82	11.92	14.85	19.17	17.39	19.58	23.09	24.83	37.86	54.26	58.26	67.29	48.20
2A	12.30	12.03	14.40	19.04	17.14	19.59	23.74	26.32	37.14	52.64	58.89	68.52	49.22
2B	12.30	11.61	14.43	19.15	16.70	19.41	24.29	26.41	36.68	52.42	57.20	67.90	49.74
2C	12.30	11.71	14.41	19.48	16.63	19.93	24.43	27.07	35.28	50.48	55.87	69.54	53.62
2D	12.30	11.61	14.33	19.48	17.14	19.86	24.21	25.61	33.55	49.54	53.77	67.28	49.42
2E	12.30	11.60	14.43	19.59	17.16	19.67	23.62	25.81	35.49	51.72	56.43	68.92	51.82
A	12.27	11.67	15.08	19.84	17.06	19.43	22.92	26.99	42.15	54.38	56.42	68.18	48.59
B	12.27	11.18	14.23	20.06	17.08	18.84	22.74	27.53	42.50	53.79	55.67	67.41	48.21
C	12.27	11.21	13.54	19.70	17.32	19.03	22.64	27.05	42.14	53.98	56.91	68.64	50.34
D	12.27	11.24	14.71	18.90	16.77	18.50	22.64	26.92	42.37	54.21	56.20	68.53	49.45
E	12.27	11.55	14.86	19.34	17.06	19.18	22.84	26.70	42.32	54.06	55.12	69.28	50.08

Table 36   Geopotential Height (m) RMSE, 950/700 mb (Case: May 1995)

#	4/00	4/12	5/00	5/12	6/00	6/12	7/00	7/12	8/00	8/12	9/00	9/12	10/00
1	4.28	8.54	5.69	10.03	12.65	16.97	12.41	15.35	29.81	37.69	31.93	45.61	37.82
2A	3.70	8.23	5.99	10.56	13.76	17.48	12.08	13.82	26.99	34.39	33.41	49.35	40.26
2B	3.70	7.88	6.01	10.37	12.64	17.22	11.53	14.41	26.97	34.00	32.11	46.82	39.64
2C	3.70	7.74	6.10	10.74	12.90	17.33	11.60	15.19	25.11	32.43	32.26	49.20	41.67
2D	3.70	7.56	6.11	10.72	13.09	17.75	12.82	13.95	25.13	32.21	31.20	47.20	39.61
2E	3.70	7.63	6.15	10.33	13.05	17.29	11.96	14.27	26.74	32.53	31.17	48.54	41.69
A	3.66	8.18	6.82	11.03	12.72	16.00	10.51	15.60	31.62	34.96	35.62	47.91	39.62
B	3.66	7.96	6.71	10.75	12.35	14.82	10.00	16.64	32.39	34.03	35.37	46.68	38.44
C	3.66	8.06	6.15	10.26	11.54	14.17	10.25	15.62	31.97	35.03	37.13	48.87	40.76
D	3.66	7.87	5.69	10.48	11.67	14.81	10.02	15.79	33.29	33.73	35.94	49.43	40.58
E	3.66	8.10	5.70	10.23	11.57	16.00	10.82	15.81	32.08	33.60	36.57	49.77	41.34

173

Table 37   Geopotential Height (m) RMSE, 500/200 mb (Case: May 1995)

#	4/00	4/12	5/00	5/12	6/00	6/12	7/00	7/12	8/00	8/12	9/00	9/12	10/00
					Date/Time (UTC)								
1	16.54	15.28	22.84	23.70	21.06	29.11	34.79	33.67	58.77	84.67	90.99	85.99	54.77
2A	15.62	15.37	22.03	23.68	20.34	28.28	34.90	34.80	59.11	84.08	91.51	86.47	55.34
2B	15.62	15.18	21.98	23.57	19.89	28.75	35.97	35.03	57.48	83.16	89.28	86.83	56.41
2C	15.62	15.53	22.37	24.08	19.91	30.02	36.36	35.70	56.25	81.47	89.28	89.78	61.55
2D	15.62	15.51	22.34	24.30	20.61	29.81	35.69	34.28	54.01	79.71	86.30	86.26	56.35
2E	15.62	15.56	22.57	24.45	20.64	29.34	35.35	34.99	56.50	82.86	89.71	88.05	58.20
A	15.59	13.58	21.54	24.36	20.64	29.98	34.24	35.92	62.56	89.09	87.21	86.20	54.90
B	15.59	13.28	21.05	24.79	20.85	28.24	34.26	36.96	63.49	88.61	85.99	85.10	55.42
C	15.59	13.94	20.25	24.46	21.40	29.27	33.85	37.90	63.53	88.33	86.89	86.40	57.04
D	15.59	14.05	22.35	23.38	20.80	28.25	34.01	37.42	63.63	88.07	87.00	85.93	55.88
E	15.59	14.43	22.48	24.01	21.13	29.31	34.13	37.51	64.03	88.52	85.30	87.04	56.33

Table 38   Geopotential Height (m) RMSE, 925 mb (Case: May 1995)

#	4/00	4/12	5/00	5/12	6/00	6/12	7/00	7/12	8/00	8/12	9/00	9/12	10/00
					Date/Time (UTC)								
1	4.95	8.87	4.92	13.43	17.25	23.22	14.94	22.16	35.47	42.03	37.52	43.71	34.97
2A	4.02	8.75	4.88	15.01	18.55	24.15	14.48	20.97	32.92	39.36	39.94	48.14	37.09
2B	4.01	8.28	4.77	14.67	17.72	23.35	13.99	21.16	32.03	38.30	36.37	46.42	35.74
2C	4.01	8.22	4.85	15.36	17.83	23.28	13.35	21.27	30.93	37.88	37.62	46.71	35.57
2D	4.01	8.07	4.79	15.05	18.12	23.81	16.02	20.80	29.68	37.18	36.97	45.29	35.71
2E	4.01	8.07	4.86	14.74	17.13	23.27	14.41	20.93	31.80	37.90	36.61	45.71	35.12
A	4.09	8.28	6.04	13.72	17.13	21.79	12.40	22.13	36.64	39.46	39.83	47.35	36.89
B	4.08	8.07	6.39	12.04	17.54	20.10	12.44	22.87	36.33	38.66	38.94	45.98	37.03
C	4.08	8.14	5.82	11.86	16.86	20.49	12.38	23.54	36.35	40.41	40.80	48.18	38.44
D	4.08	7.98	4.74	12.21	15.62	20.35	10.89	23.07	36.67	39.39	40.73	49.50	39.08
E	4.09	8.01	4.87	11.82	17.86	22.05	12.73	22.67	36.15	39.47	41.70	49.05	38.95

174

Table 39   Geopotential Height (m) RMSE, 850 mb (Case: May 1995)

#	4/00	4/12	5/00	5/12	6/00	6/12	7/00	7/12	8/00	8/12	9/00	9/12	10/00
						Date/Time (UTC)							
1	3.74	7.46	4.00	12.50	16.11	20.34	11.75	19.84	33.81	44.20	38.38	48.06	38.63
2A	3.19	7.12	4.30	13.30	17.37	20.65	11.44	17.98	31.23	42.08	41.13	51.91	40.50
2B	3.19	6.79	4.28	12.85	16.20	20.00	10.69	18.88	30.54	40.82	37.99	49.58	39.20
2C	3.19	6.68	4.58	13.73	16.90	20.04	10.59	19.16	29.38	40.27	39.26	51.08	41.03
2D	3.19	6.51	4.57	13.38	16.84	20.35	12.33	17.88	28.86	39.29	38.08	49.38	39.58
2E	3.19	6.57	4.67	13.05	15.94	19.87	11.30	18.34	30.51	40.21	37.97	49.93	40.25
A	3.15	7.19	5.34	12.31	16.64	19.05	9.39	20.09	35.23	41.99	40.10	50.33	40.13
B	3.15	6.72	5.36	11.36	16.49	17.33	8.69	21.06	35.45	41.54	39.38	49.54	39.45
C	3.15	6.80	4.82	11.49	15.55	17.22	9.16	20.94	35.19	43.01	41.39	51.40	41.60
D	3.15	6.69	4.07	10.72	15.10	17.64	8.51	20.97	35.96	41.85	40.86	52.30	41.49
E	3.14	6.88	4.10	10.85	16.01	18.88	9.59	20.58	35.18	42.08	41.76	52.45	41.94

Table 40   Geopotential Height (m) RMSE, 700 mb (Case: May 1995)

#	4/00	4/12	5/00	5/12	6/00	6/12	7/00	7/12	8/00	8/12	9/00	9/12	10/00
						Date/Time (UTC)							
1	3.74	6.52	8.58	8.87	9.31	15.54	12.32	20.11	33.06	48.80	44.80	53.59	42.74
2A	3.37	6.23	9.18	8.58	9.81	15.41	11.92	19.29	32.05	48.67	47.02	56.80	45.15
2B	3.36	6.54	9.40	8.55	8.94	14.80	12.05	19.83	31.82	47.03	44.94	54.91	43.80
2C	3.36	6.49	9.72	8.70	9.28	15.06	11.53	19.81	30.22	46.49	46.05	57.35	47.54
2D	3.36	6.53	9.83	8.59	9.28	15.27	12.90	18.03	30.30	45.30	43.58	55.05	44.30
2E	3.36	6.62	9.90	8.64	9.13	14.79	12.36	19.55	31.84	46.29	44.29	56.47	46.60
A	3.29	6.84	9.17	9.17	9.14	14.77	11.15	20.79	35.99	46.76	46.48	56.36	44.01
B	3.29	6.60	8.75	9.14	8.58	13.98	11.36	22.67	36.22	47.41	46.84	55.22	42.38
C	3.29	6.53	8.21	9.05	8.08	12.45	11.56	22.37	36.00	48.24	47.56	55.90	44.53
D	3.29	6.64	8.43	8.54	8.27	13.14	11.82	22.64	37.24	47.23	46.91	56.65	44.48
E	3.29	7.35	9.01	8.72	7.97	13.41	12.25	22.71	36.35	48.14	47.91	57.63	45.33

Table 41   Geopotential Height (m) RMSE, 500 mb (Case: May 1995)

#	4/00	4/12	5/00	5/12	6/00	6/12	7/00	7/12	8/00	8/12	9/00	9/12	10/00
						Date/Time (UTC)							
1	6.60	10.74	15.87	10.48	10.10	17.29	20.71	25.22	44.94	63.30	64.05	63.48	42.71
2A	5.58	9.79	15.43	10.23	9.85	16.58	20.16	26.96	44.38	62.84	65.42	64.18	45.22
2B	5.58	10.34	15.39	10.96	9.95	16.59	21.05	27.48	44.49	61.77	63.82	64.04	44.34
2C	5.58	10.18	15.99	10.66	9.85	16.85	20.69	27.02	42.38	60.37	64.51	68.12	50.02
2D	5.58	10.35	16.14	10.75	10.16	17.68	21.13	25.49	41.32	57.49	62.04	66.15	46.53
2E	5.58	10.29	16.50	10.60	10.23	17.26	21.55	28.06	43.15	60.39	63.22	66.44	48.27
A	5.51	8.28	15.44	9.73	10.23	17.15	20.72	25.97	47.66	63.02	63.74	65.00	43.96
B	5.51	8.55	14.50	10.49	10.46	17.64	20.95	28.46	47.44	62.32	63.38	64.26	42.79
C	5.51	9.57	13.11	10.39	10.99	15.70	21.27	29.49	47.68	63.21	64.18	66.07	46.22
D	5.51	10.21	14.91	9.15	10.21	15.71	20.93	28.14	48.74	62.11	64.48	66.76	45.89
E	5.52	10.96	16.24	10.37	10.83	15.23	21.22	28.58	48.24	62.87	64.09	67.11	46.20

Table 42   Geopotential Height (m) RMSE, 300 mb (Case: May 1995)

#	4/00	4/12	5/00	5/12	6/00	6/12	7/00	7/12	8/00	8/12	9/00	9/12	10/00
						Date/Time (UTC)							
1	19.80	19.70	28.87	29.08	26.77	29.70	34.12	38.90	69.59	102.3	107.9	95.52	54.15
2A	18.57	18.82	27.68	28.91	25.86	28.00	33.12	39.27	70.46	101.2	108.0	96.87	54.47
2B	18.57	18.97	27.79	28.90	25.93	28.40	34.01	39.60	68.22	100.7	105.7	97.33	56.92
2C	18.57	19.42	28.12	29.35	25.51	29.96	34.85	40.59	67.00	98.24	105.3	100.3	62.88
2D	18.57	19.50	28.02	29.77	26.38	29.85	34.26	39.36	63.97	97.39	101.5	96.01	56.34
2E	18.56	19.58	28.35	29.86	26.71	29.12	33.98	39.74	67.25	100.8	106.1	98.99	58.93
A	18.51	16.16	25.79	30.06	26.56	31.20	32.87	42.27	74.03	107.9	101.4	96.04	54.33
B	18.52	15.80	25.03	30.24	27.08	28.35	32.35	42.68	75.78	107.7	100.7	94.59	55.30
C	18.52	16.75	25.23	29.77	27.74	30.41	31.80	43.22	75.35	106.9	101.5	96.35	56.31
D	18.52	17.14	28.39	28.90	27.08	28.93	31.90	43.49	75.13	107.2	101.6	95.55	55.10
E	18.51	17.40	27.38	29.49	27.43	30.81	32.28	43.36	75.94	107.7	99.44	96.85	55.90

Table 43 — Temperature (K) RMSE, 950/150 mb (Case: May 1995)

#	Date/Time (UTC)												
	4/00	4/12	5/00	5/12	6/00	6/12	7/00	7/12	8/00	8/12	9/00	9/12	10/00
1	0.79	1.37	1.40	1.66	1.73	1.81	1.83	1.99	2.35	3.62	3.33	2.81	2.79
2A	0.76	1.31	1.37	1.64	1.82	1.86	1.95	2.12	2.42	3.45	3.24	2.80	2.72
2B	0.76	1.29	1.39	1.67	1.81	1.91	1.98	2.14	2.41	3.43	3.14	2.78	2.74
2C	0.76	1.30	1.35	1.64	1.84	1.85	1.90	2.10	2.35	3.34	3.08	2.73	2.91
2D	0.76	1.30	1.36	1.65	1.85	1.91	1.93	2.08	2.30	3.21	2.98	2.64	2.63
2E	0.76	1.30	1.34	1.63	1.84	1.88	1.89	2.08	2.33	3.27	3.12	2.75	2.73
A	0.76	1.28	1.44	1.59	1.76	1.80	1.84	2.13	2.47	3.41	2.82	2.73	2.72
B	0.76	1.25	1.35	1.61	1.80	1.78	1.84	2.08	2.55	3.45	2.87	2.74	2.65
C	0.76	1.26	1.35	1.59	1.76	1.87	1.91	2.10	2.53	3.43	2.83	2.71	2.71
D	0.76	1.28	1.36	1.63	1.78	1.79	1.88	2.04	2.46	3.43	2.81	2.67	2.63
E	0.76	1.33	1.37	1.64	1.77	1.83	1.86	2.09	2.47	3.43	2.79	2.77	2.64

Table 44 — Temperature (K) RMSE, 950/700 mb (Case: May 1995)

#	Date/Time (UTC)												
	4/00	4/12	5/00	5/12	6/00	6/12	7/00	7/12	8/00	8/12	9/00	9/12	10/00
1	0.59	1.16	1.48	1.83	1.59	1.94	1.90	1.95	2.25	2.76	3.32	2.73	2.85
2A	0.50	1.24	1.52	1.88	1.71	2.04	2.09	2.00	2.37	2.65	3.25	2.74	2.77
2B	0.50	1.21	1.52	1.87	1.65	2.07	2.08	2.10	2.33	2.74	3.19	2.72	2.70
2C	0.50	1.25	1.50	1.84	1.67	1.93	1.96	1.99	2.29	2.63	3.21	2.79	3.19
2D	0.50	1.25	1.52	1.90	1.69	2.02	2.06	2.10	2.27	2.57	3.12	2.65	2.72
2E	0.51	1.25	1.48	1.81	1.66	2.02	1.98	2.05	2.40	2.62	3.27	2.83	2.93
A	0.51	1.11	1.60	1.85	1.70	1.85	1.90	2.15	2.39	2.54	3.07	2.63	2.75
B	0.51	1.14	1.52	1.79	1.71	1.81	1.90	2.08	2.47	2.48	3.22	2.67	2.51
C	0.51	1.19	1.52	1.76	1.75	1.91	2.08	2.15	2.51	2.51	3.09	2.61	2.75
D	0.51	1.16	1.49	1.77	1.72	1.87	2.00	2.06	2.49	2.58	3.10	2.54	2.62
E	0.51	1.21	1.55	1.81	1.68	1.88	1.99	2.17	2.51	2.51	3.18	2.64	2.64

Table 45   Temperature (K) RMSE, 500/200 mb (Case: May 1995)

#	4/00	4/12	5/00	5/12	6/00	6/12	7/00	7/12	8/00	8/12	9/00	9/12	10/00
						Date/Time (UTC)							
1	0.85	1.41	1.47	1.53	1.71	1.74	1.89	1.97	2.79	4.43	3.86	3.11	2.89
2A	0.84	1.34	1.42	1.51	1.73	1.78	1.99	2.24	2.81	4.23	3.72	3.14	2.84
2B	0.84	1.33	1.45	1.47	1.70	1.89	2.10	2.23	2.78	4.24	3.66	3.10	2.89
2C	0.84	1.32	1.40	1.50	1.79	1.91	2.05	2.22	2.64	4.15	3.59	2.93	2.77
2D	0.84	1.32	1.38	1.48	1.81	1.94	1.98	2.11	2.65	4.06	3.49	2.74	2.63
2E	0.84	1.32	1.39	1.49	1.85	1.86	1.96	2.12	2.69	4.11	3.66	2.93	2.64
A	0.84	1.34	1.41	1.42	1.61	1.86	1.91	2.25	2.83	4.24	3.47	3.02	2.82
B	0.84	1.30	1.36	1.54	1.71	1.78	2.01	2.24	3.00	4.24	3.50	2.96	2.79
C	0.84	1.29	1.33	1.57	1.60	1.92	1.97	2.26	2.92	4.17	3.52	2.98	2.79
D	0.84	1.32	1.41	1.54	1.64	1.82	1.96	2.21	2.85	4.18	3.49	2.91	2.74
E	0.84	1.37	1.39	1.54	1.69	1.89	1.94	2.25	2.91	4.23	3.46	3.00	2.73

Table 46   Temperature (K) RMSE, 925 mb (Case: May 1995)

#	4/00	4/12	5/00	5/12	6/00	6/12	7/00	7/12	8/00	8/12	9/00	9/12	10/00
						Date/Time (UTC)							
1	0.33	1.08	1.59	2.01	1.49	1.10	2.02	1.24	2.61	3.40	4.78	4.19	4.27
2A	0.19	1.25	1.70	2.12	1.63	1.28	2.26	1.70	2.45	2.99	4.15	4.08	4.04
2B	0.19	1.23	1.70	2.17	1.50	1.24	2.17	1.73	2.66	3.15	4.15	3.86	4.06
2C	0.19	1.31	1.67	2.09	1.90	1.24	2.09	2.04	2.32	2.96	4.19	3.81	4.95
2D	0.19	1.30	1.67	2.09	1.59	1.22	2.30	1.79	2.32	2.84	4.10	3.84	4.10
2E	0.19	1.30	1.63	2.09	1.63	1.21	2.16	1.70	2.68	3.00	4.42	3.93	4.30
A	0.21	1.25	1.90	2.24	1.70	1.21	1.86	1.57	3.08	3.02	4.21	3.58	4.01
B	0.21	1.28	1.77	2.27	1.73	1.16	2.04	1.79	3.15	2.61	4.46	3.52	3.56
C	0.21	1.34	1.73	2.18	1.55	1.17	2.31	1.64	3.16	2.76	4.08	3.75	4.02
D	0.21	1.21	1.67	2.14	1.67	1.10	2.28	1.62	3.24	3.05	4.55	3.61	3.71
E	0.21	1.32	1.74	2.13	1.53	1.16	2.10	1.74	3.24	2.69	4.39	3.79	3.79

Table 47   Temperature (K) RMSE, 850 mb (Case: May 1995)

#	4/00	4/12	5/00	5/12	6/00	6/12	7/00	7/12	8/00	8/12	9/00	9/12	10/00
					Date/Time (UTC)								
1	0.67	1.04	1.42	1.87	1.95	2.44	2.65	2.30	2.24	2.98	3.27	2.82	2.83
2A	0.53	1.15	1.49	2.03	1.96	2.62	2.62	2.69	2.27	3.04	2.95	3.03	3.19
2B	0.53	1.13	1.45	1.93	2.03	2.53	2.81	2.41	2.15	2.92	3.07	2.82	3.01
2C	0.53	1.13	1.46	1.93	1.90	2.43	2.57	2.48	2.19	2.96	3.06	3.35	3.24
2D	0.53	1.15	1.44	1.94	2.03	2.54	2.95	2.53	1.98	2.90	2.93	3.01	2.97
2E	0.53	1.15	1.47	1.90	2.03	2.54	2.80	2.37	2.23	2.91	3.08	3.16	3.31
A	0.51	1.05	1.40	1.77	2.08	2.38	2.66	2.28	2.59	2.86	3.16	3.05	2.89
B	0.51	1.03	1.55	1.59	1.98	2.44	2.80	2.69	2.29	3.15	3.32	2.99	2.73
C	0.51	1.13	1.49	1.63	1.96	2.47	2.91	2.49	2.33	2.79	3.12	2.65	2.81
D	0.51	1.14	1.50	1.69	1.96	2.36	2.83	2.54	2.36	2.75	3.33	2.83	2.80
E	0.51	1.18	1.53	1.71	2.06	2.45	3.02	2.51	2.43	2.96	3.26	2.82	2.86

Table 48   Temperature (K) RMSE, 700 mb (Case: May 1995)

#	4/00	4/12	5/00	5/12	6/00	6/12	7/00	7/12	8/00	8/12	9/00	9/12	10/00
					Date/Time (UTC)								
1	0.43	1.18	1.34	1.81	1.30	1.49	2.08	2.28	1.89	2.63	2.34	1.53	1.40
2A	0.38	1.17	1.35	1.93	1.43	1.27	2.21	2.45	2.10	2.54	2.38	1.47	1.39
2B	0.38	1.10	1.29	1.90	1.39	1.37	2.25	2.70	2.22	2.71	2.46	1.47	1.27
2C	0.38	1.15	1.30	1.93	1.37	1.35	2.11	2.62	2.25	2.60	2.43	1.57	1.43
2D	0.38	1.18	1.39	1.94	1.34	1.59	2.37	2.56	2.18	2.52	2.36	1.61	1.41
2E	0.38	1.15	1.30	1.89	1.43	1.60	2.30	2.57	2.17	2.70	2.41	1.72	1.35
A	0.37	0.83	1.51	1.79	1.36	1.22	2.12	2.52	1.81	2.35	2.26	1.47	1.42
B	0.37	0.92	1.34	1.63	1.25	1.19	1.95	2.39	1.84	2.38	2.26	1.48	1.31
C	0.37	1.00	1.34	1.98	1.44	1.16	2.19	2.56	1.97	2.48	2.09	1.54	1.28
D	0.37	1.04	1.37	1.29	1.24	1.20	2.20	2.49	1.82	2.47	2.20	1.63	1.39
E	0.38	1.07	1.40	1.46	1.31	1.22	2.04	2.63	1.94	2.46	2.30	1.58	1.33

Table 49   Temperature (K) RMSE, 500 mb (Case: May 1995)

#	Date/Time (UTC)												
#	4/00	4/12	5/00	5/12	6/00	6/12	7/00	7/12	8/00	8/12	9/00	9/12	10/00
1	0.42	0.80	0.97	0.87	0.95	1.19	1.51	1.60	2.08	3.72	3.74	2.35	2.25
2A	0.40	0.91	0.98	0.97	0.94	0.97	1.45	1.69	2.14	3.71	3.66	2.28	2.22
2B	0.40	0.86	0.95	0.96	0.88	1.10	1.36	1.61	1.93	3.66	3.32	2.29	2.20
2C	0.40	0.88	0.98	0.85	0.87	1.19	1.34	1.59	1.92	3.67	3.40	2.25	2.22
2D	0.40	0.88	0.98	0.89	0.93	1.15	1.40	1.63	1.87	3.55	3.51	2.03	2.12
2E	0.40	0.91	0.97	0.95	1.09	1.14	1.47	1.61	2.00	3.49	3.52	2.21	2.10
A	0.40	0.73	0.97	0.83	0.88	1.15	1.25	1.67	2.20	3.75	3.32	2.07	2.28
B	0.40	0.75	1.02	0.94	0.83	1.10	1.32	1.35	2.30	3.85	3.07	2.22	2.24
C	0.40	0.75	0.87	0.99	0.89	1.41	1.28	1.72	2.30	3.83	3.10	2.12	2.16
D	0.40	0.73	1.04	0.79	0.96	1.30	1.29	1.50	2.18	3.62	3.15	2.09	2.11
E	0.40	0.79	1.00	0.81	0.92	1.42	1.27	1.61	2.36	3.62	3.02	2.34	2.16

Table 50   Temperature (K) RMSE, 300 mb (Case: May 1995)

#	Date/Time (UTC)												
#	4/00	4/12	5/00	5/12	6/00	6/12	7/00	7/12	8/00	8/12	9/00	9/12	10/00
1	0.20	0.85	1.19	1.49	2.00	1.34	1.67	1.78	2.00	2.85	2.45	2.55	2.42
2A	0.21	0.93	1.22	1.50	1.94	1.26	1.90	1.91	2.04	2.78	2.41	2.61	2.39
2B	0.21	0.88	1.22	1.37	1.78	1.35	2.06	1.90	2.04	2.83	2.35	2.26	2.39
2C	0.21	0.90	1.19	1.47	1.94	1.47	2.10	1.99	2.05	2.74	2.35	2.20	2.10
2D	0.21	0.92	1.18	1.40	1.94	1.52	1.92	1.71	2.14	2.70	2.31	2.14	2.07
2E	0.21	0.91	1.19	1.40	1.93	1.40	1.89	1.76	2.16	3.02	2.52	2.03	2.22
A	0.21	0.81	1.25	1.30	1.77	1.40	2.07	1.95	1.96	2.62	2.49	2.39	2.30
B	0.21	0.94	1.17	1.49	1.88	1.19	2.07	1.90	2.17	2.50	2.75	2.31	2.41
C	0.21	0.93	1.17	1.40	1.65	1.41	2.08	1.95	2.07	2.51	2.53	2.16	2.31
D	0.21	0.89	1.27	1.51	1.70	1.37	2.07	1.94	2.12	2.46	2.36	2.09	2.17
E	0.21	0.90	1.26	1.47	1.76	1.31	2.05	2.05	2.08	2.55	2.55	2.26	2.16

Table 51   Wind Speed (m/s) RMSE, 950/150 mb (Case: May 1995)

#	Date/Time (UTC)												
	4/00	4/12	5/00	5/12	6/00	6/12	7/00	7/12	8/00	8/12	9/00	9/12	10/00
1	2.54	3.36	3.60	4.23	5.64	7.17	10.87	6.90	7.72	7.73	9.15	9.44	8.14
2A	2.55	3.75	3.73	4.17	5.79	6.93	11.02	8.12	7.93	7.41	8.78	9.42	8.78
2B	2.55	3.61	3.72	4.22	5.71	6.83	10.97	7.93	7.77	7.46	9.12	9.05	8.66
2C	2.55	3.67	3.74	4.14	5.71	7.01	10.97	8.21	7.43	7.16	8.96	9.15	8.47
2D	2.55	3.72	3.75	4.15	5.75	6.99	11.00	7.73	7.25	7.20	9.59	8.96	8.21
2E	2.55	3.75	3.68	4.17	5.76	7.08	10.85	7.67	7.44	7.31	9.03	9.57	8.95
A	2.56	3.52	4.01	4.18	5.81	6.80	11.21	8.34	7.61	8.23	8.79	9.19	8.42
B	2.56	3.38	3.98	4.24	5.70	6.56	10.97	8.21	7.63	8.68	8.52	9.45	8.40
C	2.56	3.26	4.02	4.25	6.06	6.94	10.99	8.12	7.57	8.75	8.80	9.87	8.68
D	2.56	3.38	4.07	4.16	5.83	7.02	11.24	8.04	7.54	8.88	8.83	9.92	8.67
E	2.56	3.39	4.01	4.31	5.87	6.83	10.92	8.06	7.63	8.75	9.01	9.81	8.52

Table 52   Wind Speed (m/s) RMSE, 950/700 mb (Case: May 1995)

#	Date/Time (UTC)												
	4/00	4/12	5/00	5/12	6/00	6/12	7/00	7/12	8/00	8/12	9/00	9/12	10/00
1	1.62	2.51	2.81	3.68	2.32	3.85	11.97	4.37	5.01	6.78	5.07	6.78	6.25
2A	1.60	3.10	2.78	3.50	2.60	3.69	12.02	4.61	5.09	5.84	5.58	7.41	7.02
2B	1.60	3.03	2.83	3.60	2.40	3.88	11.92	4.37	4.70	6.14	5.52	6.37	6.74
2C	1.59	3.09	2.91	3.56	2.52	3.71	11.98	4.77	4.41	5.89	5.09	6.81	6.45
2D	1.59	3.10	2.92	3.56	2.67	3.86	11.99	4.36	4.84	5.83	5.27	6.58	6.25
2E	1.58	3.10	2.90	3.67	2.59	3.81	11.94	4.42	5.05	5.92	5.35	7.32	7.29
A	1.60	3.21	3.05	3.68	2.60	3.59	12.07	4.93	4.32	7.40	5.54	7.25	6.53
B	1.60	2.83	2.91	3.93	2.35	3.61	12.04	4.82	4.37	8.33	5.56	6.55	6.46
C	1.60	2.87	2.88	4.08	2.38	4.14	11.98	5.14	4.51	8.11	5.65	6.93	6.64
D	1.60	2.86	2.93	3.62	2.38	3.52	12.07	4.80	4.92	8.86	5.89	7.24	6.54
E	1.60	2.94	3.00	3.63	2.29	3.71	11.75	4.85	4.82	8.57	6.08	7.22	6.54

181

Table 53   Wind Speed (m/s) RMSE, 500/200 mb (Case: May 1995)

	Date/Time (UTC)												
#	4/00	4/12	5/00	5/12	6/00	6/12	7/00	7/12	8/00	8/12	9/00	9/12	10/00
1	3.34	3.72	4.32	5.31	7.55	9.69	10.50	9.27	11.21	14.75	12.40	10.38	8.55
2A	3.36	4.09	4.40	5.16	7.89	9.95	10.68	10.39	11.83	14.65	12.00	10.19	8.95
2B	3.36	3.94	4.38	5.29	7.56	10.22	10.72	10.17	11.79	14.65	12.08	9.96	9.02
2C	3.36	4.02	4.40	5.18	7.70	10.39	10.63	10.25	11.41	14.52	12.21	10.06	9.15
2D	3.36	4.05	4.35	5.21	7.82	10.68	10.77	10.04	10.90	14.41	12.71	9.89	8.92
2E	3.36	4.13	4.27	5.20	7.73	10.33	10.57	10.09	11.24	14.58	12.04	10.38	9.15
A	3.38	3.88	4.87	4.99	7.77	9.87	10.96	10.21	11.79	14.26	11.81	10.03	8.85
B	3.38	3.76	4.83	5.06	7.90	9.33	10.79	10.11	11.23	14.35	11.47	10.54	8.91
C	3.38	3.57	4.70	5.06	8.39	9.75	10.74	10.22	11.15	14.50	11.88	11.25	9.03
D	3.38	3.75	4.91	4.92	8.16	9.84	11.07	10.21	11.05	14.69	11.98	10.91	9.04
E	3.38	3.83	4.74	5.36	8.23	9.52	10.79	10.48	11.42	14.10	12.04	10.98	8.90

Table 54   Wind Speed (m/s) RMSE, 925 mb (Case: May 1995)

	Date/Time (UTC)												
#	4/00	4/12	5/00	5/12	6/00	6/12	7/00	7/12	8/00	8/12	9/00	9/12	10/00
1	0.98	2.64	2.06	1.78	1.59	3.27	4.08	4.49	5.45	6.61	4.95	6.48	3.63
2A	0.88	3.07	2.10	1.98	1.92	3.07	3.82	4.57	4.38	5.11	4.73	6.73	4.15
2B	0.88	3.00	2.25	2.19	1.76	3.04	3.53	3.57	4.13	5.84	4.68	5.89	3.64
2C	0.88	3.06	2.23	2.01	1.72	3.15	4.06	5.08	4.18	5.73	5.10	6.24	4.11
2D	0.88	3.07	2.27	2.05	1.86	3.38	3.65	3.77	4.28	5.87	4.41	6.08	4.02
2E	0.88	2.97	2.13	2.07	1.71	3.11	3.75	3.62	4.12	5.50	4.23	6.83	4.41
A	0.87	3.01	1.89	2.17	1.89	2.77	4.55	4.96	4.97	7.57	4.26	7.07	3.84
B	0.87	2.76	1.85	2.18	1.80	3.13	4.55	5.07	4.84	9.45	4.92	6.35	3.53
C	0.87	2.88	1.84	2.19	1.71	3.64	3.58	5.73	4.53	8.12	3.79	6.74	3.68
D	0.87	2.90	1.87	2.08	1.71	3.06	3.75	4.81	4.88	9.78	5.69	7.07	4.04
E	0.87	3.08	1.85	1.93	1.79	2.70	3.97	4.91	5.41	9.66	5.25	6.97	3.80

Table 55   Wind Speed (m/s) RMSE, 850 mb (Case: May 1995)

#	4/00	4/12	5/00	5/12	6/00	6/12	7/00	7/12	8/00	8/12	9/00	9/12	10/00
						Date/Time (UTC)							
1	0.74	2.88	2.48	2.94	2.16	3.45	4.71	4.81	4.54	7.39	6.71	6.90	5.49
2A	0.72	3.01	2.23	2.83	2.22	3.77	4.45	4.90	4.69	6.89	6.94	7.55	5.88
2B	0.71	2.97	2.29	2.89	2.13	4.24	4.43	5.06	4.23	7.67	6.60	6.86	5.90
2C	0.72	3.03	2.31	3.02	2.17	4.14	4.50	4.84	4.10	6.69	6.22	7.55	5.87
2D	0.72	3.06	2.32	2.93	2.27	3.42	4.36	4.58	4.59	6.71	6.22	7.36	5.35
2E	0.72	3.06	2.34	3.09	2.19	3.93	4.08	4.71	4.78	7.35	7.07	7.80	6.34
A	0.73	3.26	2.37	2.58	2.31	3.58	4.51	5.30	3.69	7.87	7.12	7.76	5.72
B	0.73	2.91	2.29	2.75	2.36	3.72	4.32	4.80	3.59	8.74	7.29	6.71	5.89
C	0.73	2.88	2.18	2.74	2.12	4.47	3.98	4.90	4.02	8.31	7.32	7.05	5.82
D	0.73	2.83	2.34	2.90	2.05	3.89	4.36	4.92	4.55	9.07	7.78	7.40	6.11
E	0.73	2.84	2.35	2.95	2.03	4.05	4.66	4.89	4.64	9.06	7.79	7.70	6.00

Table 56   Wind Speed (m/s) RMSE, 700 mb (Case: May 1995)

#	4/00	4/12	5/00	5/12	6/00	6/12	7/00	7/12	8/00	8/12	9/00	9/12	10/00
						Date/Time (UTC)							
1	1.54	2.92	2.62	3.69	3.67	5.61	12.25	6.17	4.93	7.01	6.58	8.15	8.61
2A	1.47	3.44	2.97	3.48	4.02	5.47	12.56	5.59	5.21	6.23	6.90	8.62	9.56
2B	1.47	3.30	2.98	3.62	3.61	5.00	12.34	5.45	4.73	6.52	6.86	8.15	9.18
2C	1.47	3.36	3.09	3.64	4.06	4.91	12.31	5.94	4.59	6.75	7.15	8.67	8.89
2D	1.46	3.37	3.06	3.67	4.09	5.64	12.48	5.88	4.47	6.81	7.34	8.35	8.82
2E	1.44	3.35	3.10	3.52	3.97	5.20	12.46	5.93	4.98	6.72	7.23	9.74	10.42
A	1.49	3.37	3.05	4.08	4.30	4.11	12.49	5.04	4.73	7.13	7.10	8.06	8.88
B	1.49	3.08	3.01	4.41	4.22	3.91	12.42	5.97	5.02	6.97	6.63	8.14	8.56
C	1.49	3.05	3.16	4.32	4.85	4.02	12.65	5.69	4.86	7.91	6.98	7.96	9.09
D	1.49	3.08	3.34	3.98	4.22	4.95	12.62	4.95	5.19	7.39	6.88	8.68	8.94
E	1.49	3.18	3.40	3.80	4.21	4.91	11.98	5.70	4.59	7.69	7.23	8.15	9.13

Table 57 Wind Speed (m/s) RMSE, 500 mb (Case: May 1995)

#	4/00	4/12	5/00	5/12	6/00	6/12	7/00	7/12	8/00	8/12	9/00	9/12	10/00
1	1.16	2.78	3.85	3.22	6.27	7.51	4.77	6.60	10.41	9.50	8.83	8.36	8.14
2A	1.17	2.96	4.24	3.19	6.50	6.90	4.92	7.03	9.95	10.10	8.44	8.39	8.76
2B	1.17	2.89	4.04	3.34	6.16	7.03	5.04	6.49	10.12	9.32	8.31	8.26	9.08
2C	1.15	2.85	4.01	3.23	6.12	7.69	5.25	6.75	10.01	9.04	8.21	8.06	8.99
2D	1.14	2.92	4.18	3.46	5.75	7.18	5.35	6.48	9.15	9.09	8.88	7.33	8.88
2E	1.15	2.91	3.83	3.43	5.62	6.89	5.18	6.95	9.53	9.10	8.87	8.29	9.32
A	1.14	2.85	3.79	3.70	6.43	6.85	5.83	5.23	10.36	9.05	8.17	8.44	8.67
B	1.14	2.87	4.38	3.44	6.93	7.04	5.33	5.96	9.28	9.64	8.20	9.10	7.62
C	1.14	2.68	4.55	3.35	7.36	7.21	5.12	6.05	9.57	8.82	8.08	9.27	9.15
D	1.14	2.69	4.01	3.41	6.97	6.86	5.64	6.18	9.14	9.36	8.14	9.23	9.04
E	1.14	2.92	3.80	3.82	7.15	6.56	5.43	6.88	9.49	9.35	8.55	9.26	9.03

Table 58 Wind Speed (m/s) RMSE, 300 mb (Case: May 1995)

#	4/00	4/12	5/00	5/12	6/00	6/12	7/00	7/12	8/00	8/12	9/00	9/12	10/00
1	7.45	3.29	4.37	5.38	6.73	9.68	8.36	9.10	8.27	15.86	15.56	13.01	9.83
2A	7.57	3.37	4.21	5.09	6.99	10.50	8.02	10.84	9.70	16.00	14.91	13.35	9.84
2B	7.57	3.39	4.48	5.25	6.99	10.17	7.98	10.81	9.31	16.20	14.96	12.84	9.77
2C	7.56	3.31	4.46	5.03	7.18	10.47	7.84	10.65	8.72	16.19	15.21	13.33	10.03
2D	7.56	3.34	4.39	5.16	7.63	10.92	8.53	10.99	8.62	16.66	15.07	13.55	9.71
2E	7.56	3.33	4.24	5.09	7.36	10.78	7.95	10.75	9.21	16.13	15.05	13.46	9.84
A	7.54	3.93	5.14	5.62	7.20	10.46	8.61	10.19	9.67	16.29	15.29	12.38	10.09
B	7.54	3.99	4.30	5.41	7.46	9.66	7.90	10.42	9.95	16.05	14.02	13.50	10.45
C	7.54	3.97	4.14	5.19	8.27	10.12	8.53	10.04	9.00	16.69	15.14	14.02	9.57
D	7.54	4.05	5.01	4.69	7.78	10.83	8.49	10.33	9.70	16.65	15.03	14.01	9.98
E	7.54	4.06	4.72	5.59	7.97	10.15	8.41	10.39	9.70	16.43	15.12	14.30	9.52

184

Table 59   Wind Direction (deg.) RMSE, 950/150 mb (Case: May 1995)

#	Date/Time (UTC)
	4/00	4/12	5/00	5/12	6/00	6/12	7/00	7/12	8/00	8/12	9/00	9/12	10/00
1	13.51	31.97	33.04	27.51	21.00	32.34	33.18	38.91	29.65	42.48	30.58	54.54	40.24
2A	11.94	31.93	33.31	25.43	21.41	33.12	34.21	39.16	28.85	43.37	31.66	51.77	39.02
2B	11.85	32.48	34.21	25.71	20.93	33.34	37.08	39.31	29.38	43.94	30.57	57.67	38.54
2C	11.80	32.23	34.48	25.98	21.06	32.40	35.68	39.55	30.11	43.48	30.59	57.36	49.32
2D	11.75	32.12	34.08	25.85	20.60	33.13	35.85	39.40	28.40	44.28	29.19	58.24	41.48
2E	11.18	32.27	33.80	25.79	20.23	33.08	35.94	38.22	28.14	43.65	30.68	53.21	44.48
A	12.51	28.74	31.84	28.12	21.03	32.07	34.84	40.58	31.07	37.85	35.09	55.24	40.68
B	12.51	28.33	31.93	28.92	23.01	32.25	34.54	40.13	31.32	38.91	35.03	51.43	36.99
C	12.51	30.16	33.19	28.50	24.51	33.46	30.45	41.66	30.69	38.84	32.30	54.09	36.09
D	12.51	30.50	33.19	28.52	25.26	31.17	34.55	39.80	30.86	38.16	34.45	52.09	39.90
E	12.66	30.15	33.39	28.17	22.82	31.33	33.41	40.46	31.84	39.06	34.05	52.62	38.66

Table 60   Wind Direction (deg.) RMSE, 950/700 mb (Case: May 1995)

#	Date/Time (UTC)
	4/00	4/12	5/00	5/12	6/00	6/12	7/00	7/12	8/00	8/12	9/00	9/12	10/00
1	16.62	44.11	50.75	42.42	25.90	46.77	46.30	49.72	38.77	55.72	31.92	52.86	38.85
2A	14.56	42.86	51.07	38.12	27.80	48.39	46.80	49.81	37.21	57.02	33.78	50.09	34.80
2B	14.35	43.99	52.84	38.90	26.62	47.73	51.76	48.27	37.49	57.44	31.13	60.25	43.30
2C	14.22	43.70	53.30	38.69	26.28	46.40	48.07	49.07	39.01	58.65	30.40	57.62	43.64
2D	14.09	43.47	52.57	38.35	25.74	47.21	49.04	49.05	36.35	61.01	28.92	64.03	43.49
2E	12.49	43.60	51.87	38.38	25.23	47.44	49.54	45.69	36.01	59.67	30.52	59.99	43.87
A	15.21	42.40	48.01	43.75	26.53	47.20	49.11	49.19	39.97	48.74	41.19	55.84	38.94
B	15.21	40.35	48.53	45.26	30.13	48.13	48.72	47.72	41.75	49.87	38.20	48.79	37.13
C	15.21	42.67	51.36	44.64	32.89	50.97	41.31	51.80	38.83	49.32	36.47	54.22	34.35
D	15.21	41.96	51.39	44.18	33.03	45.47	47.99	48.18	39.22	49.63	38.72	54.86	41.77
E	15.58	41.37	51.92	43.04	31.10	46.23	46.76	50.95	41.54	49.89	38.64	56.58	41.37

Table 61   Wind Direction (deg.) RMSE, 500/200 mb (Case: May 1995)

#	4/00	4/12	5/00	5/12	6/00	6/12	7/00	7/12	8/00	8/12	9/00	9/12	10/00
1	7.18	18.26	11.02	15.22	16.67	20.96	25.12	24.05	23.33	44.24	59.17	48.26	38.64
2A	7.28	19.38	11.63	14.77	16.38	19.91	26.17	23.77	23.37	40.91	58.80	45.63	37.97
2B	7.32	19.35	11.43	13.86	16.14	21.67	26.75	25.31	23.73	38.59	55.08	49.59	34.69
2C	7.28	19.26	11.84	14.96	16.63	20.68	27.15	24.74	23.66	35.54	57.20	50.47	49.59
2D	7.25	19.15	11.73	15.14	16.68	20.98	27.46	25.18	23.87	36.70	51.13	48.40	39.96
2E	7.13	19.37	11.91	14.82	16.51	21.62	26.16	24.86	23.24	36.71	56.55	43.28	40.92
A	7.14	12.97	11.18	13.56	16.63	20.47	25.06	26.14	24.91	41.84	58.04	49.14	36.79
B	7.14	15.27	11.15	15.12	16.11	20.62	24.93	26.82	24.99	41.59	56.86	45.69	34.69
C	7.14	17.40	10.98	14.53	16.84	19.70	24.29	26.21	25.31	41.15	58.91	46.57	34.22
D	7.14	18.51	11.67	13.74	16.26	20.78	25.70	26.58	25.57	44.49	58.86	43.25	34.58
E	7.14	18.47	11.31	14.88	14.86	20.69	25.43	26.69	25.13	42.54	57.81	42.41	33.78

Table 62   Wind Direction (deg.) RMSE, 925 mb (Case: May 1995)

#	4/00	4/12	5/00	5/12	6/00	6/12	7/00	7/12	8/00	8/12	9/00	9/12	10/00
1	6.43	51.48	64.75	42.39	14.78	47.72	49.16	33.55	33.11	58.69	47.57	54.27	36.03
2A	5.79	58.06	63.91	50.54	18.10	57.66	47.66	38.84	25.72	54.94	47.33	55.82	31.53
2B	5.78	52.06	64.40	48.57	16.25	52.69	51.43	34.36	29.04	50.32	62.01	65.07	40.16
2C	5.76	58.80	66.67	46.79	16.47	51.27	48.54	36.03	25.66	51.95	51.09	61.43	42.38
2D	5.76	60.05	64.90	48.13	16.20	51.32	46.62	37.22	25.81	50.62	61.77	66.44	26.19
2E	5.80	59.31	63.68	46.30	15.88	57.78	46.96	35.84	25.41	53.48	50.40	65.08	37.69
A	6.00	48.31	57.36	47.61	17.83	50.65	46.80	29.54	27.95	46.85	63.30	58.14	39.07
B	6.00	47.19	55.63	52.36	18.65	53.43	46.56	51.59	36.21	47.22	65.80	56.76	37.96
C	6.00	56.35	59.72	46.89	17.41	52.70	46.25	31.47	28.25	43.64	56.40	61.35	37.08
D	6.00	53.67	56.83	47.65	21.01	52.66	47.78	31.30	27.45	45.99	60.74	63.89	43.79
E	6.00	53.26	64.75	47.90	17.27	49.99	47.23	40.67	29.06	44.55	66.92	65.95	41.44

186

Table 63   Wind Direction (deg.) RMSE, 850 mb (Case: May 1995)

#	4/00	4/12	5/00	5/12	6/00	6/12	7/00	7/12	8/00	8/12	9/00	9/12	10/00
1	14.23	40.13	55.31	48.53	23.23	58.78	39.11	54.06	35.51	56.34	54.67	41.41	27.43
2A	14.11	37.80	64.37	27.30	24.86	63.78	41.86	49.37	30.59	59.64	65.29	35.35	27.59
2B	14.00	38.72	67.29	27.26	23.90	62.03	43.61	46.42	32.47	62.25	64.56	50.35	39.09
2C	13.98	38.38	66.76	26.56	23.08	60.35	41.02	48.32	31.99	56.46	66.10	49.18	33.31
2D	13.99	38.16	65.69	26.82	22.97	63.03	43.54	46.65	30.30	67.56	68.23	51.40	49.31
2E	13.90	38.26	65.75	25.46	24.93	61.11	41.49	43.31	31.68	63.35	58.43	49.03	45.85
A	14.74	39.61	56.85	41.46	28.17	61.75	44.62	45.13	38.63	57.41	56.74	42.48	31.28
B	14.74	38.46	57.68	42.73	27.48	63.53	44.88	44.29	41.76	60.06	53.65	40.36	22.29
C	14.74	38.03	68.13	41.92	38.36	58.97	38.18	48.20	37.53	57.17	55.11	41.30	24.99
D	14.74	38.73	64.68	40.11	31.67	62.48	40.59	47.43	39.32	57.43	59.06	43.28	49.23
E	14.72	38.99	61.56	46.36	28.45	62.92	40.11	52.07	44.19	58.28	56.53	45.79	32.45

Table 64   Wind Direction (deg.) RMSE, 700 mb (Case: May 1995)

#	4/00	4/12	5/00	5/12	6/00	6/12	7/00	7/12	8/00	8/12	9/00	9/12	10/00
1	6.87	36.18	21.42	29.46	25.51	21.89	31.77	51.74	36.52	57.71	54.19	53.78	54.43
2A	7.11	34.79	21.43	29.05	21.87	24.52	34.48	53.27	37.24	56.78	53.24	44.86	40.56
2B	7.10	34.37	20.62	32.13	24.19	25.20	34.72	53.19	36.48	59.93	56.90	55.69	36.56
2C	7.08	35.03	20.50	33.04	21.88	24.46	35.22	55.06	37.53	60.86	57.28	48.64	39.86
2D	7.05	34.94	20.54	32.31	23.86	25.33	34.74	52.41	36.44	62.08	53.59	60.69	32.24
2E	7.05	35.23	20.70	32.68	26.76	24.56	36.43	53.46	37.49	62.84	56.96	50.64	45.81
A	6.94	31.33	22.28	33.03	21.80	23.81	34.94	51.91	36.98	52.42	54.39	54.93	49.47
B	6.94	31.80	20.42	31.88	24.02	22.27	34.30	50.36	35.93	50.27	45.67	43.74	58.21
C	6.94	31.87	19.74	29.35	27.86	23.60	32.00	52.18	36.64	50.25	48.63	55.29	49.40
D	6.94	33.13	21.67	29.28	26.47	21.54	35.12	49.74	37.32	49.05	52.59	49.82	45.38
E	6.94	33.38	23.04	31.72	26.91	21.91	34.13	50.34	37.41	50.80	48.86	51.65	53.55

Table 65   Wind Direction (deg.) RMSE, 500 mb (Case: May 1995)

#	Date/Time (UTC)												
	4/00	4/12	5/00	5/12	6/00	6/12	7/00	7/12	8/00	8/12	9/00	9/12	10/00
1	6.97	12.33	12.92	15.18	22.27	26.74	18.63	27.32	21.72	57.12	66.70	51.23	26.14
2A	7.25	11.85	14.20	16.01	23.36	24.65	21.56	26.97	21.34	49.56	64.60	44.01	31.41
2B	7.33	12.13	13.72	14.51	23.55	27.73	22.89	29.44	20.79	44.09	55.42	48.77	19.05
2C	7.23	12.16	14.24	16.06	23.33	27.19	23.54	28.70	19.93	41.90	64.98	49.13	36.79
2D	7.18	12.33	13.94	16.05	22.73	27.04	24.02	30.84	20.19	41.47	60.29	49.88	32.45
2E	7.02	12.25	14.35	15.59	23.62	26.09	22.58	29.36	18.95	41.25	68.11	46.21	30.00
A	6.92	10.94	12.92	15.53	24.61	22.92	23.00	31.17	22.64	57.23	67.80	50.60	28.68
B	6.92	10.60	13.51	16.14	24.83	23.44	20.17	31.35	19.92	59.57	60.41	49.12	21.59
C	6.92	10.61	13.11	16.92	26.81	22.85	21.21	31.19	20.30	57.47	66.66	55.29	25.43
D	6.92	10.64	14.18	17.37	24.70	22.99	22.80	30.69	20.50	57.77	63.18	51.07	23.04
E	6.92	10.59	13.55	17.36	22.33	22.53	22.50	30.88	20.00	57.75	62.18	50.14	25.05

Table 66   Wind Direction (deg.) RMSE, 300 mb (Case: May 1995)

#	Date/Time (UTC)												
	4/00	4/12	5/00	5/12	6/00	6/12	7/00	7/12	8/00	8/12	9/00	9/12	10/00
1	7.84	13.64	8.11	12.60	14.06	12.40	30.63	23.09	23.09	38.10	53.88	52.22	43.26
2A	7.80	17.65	8.32	11.77	11.06	13.52	30.90	21.88	22.47	39.01	50.45	52.55	48.09
2B	7.84	17.59	8.07	10.64	13.44	15.62	31.27	23.06	22.33	38.91	45.53	54.33	42.38
2C	7.81	17.73	8.61	11.38	13.20	12.59	31.55	23.03	21.60	36.57	45.75	54.79	50.04
2D	7.78	17.57	8.43	11.46	13.32	13.16	32.03	21.68	22.40	36.49	33.98	36.63	39.74
2E	7.69	17.75	8.93	10.89	13.57	12.91	31.14	23.53	22.15	37.08	39.62	42.26	47.15
A	7.75	10.73	8.70	12.05	11.52	13.59	29.75	25.08	23.73	31.19	47.45	50.24	39.49
B	7.75	13.15	8.54	13.66	12.34	15.55	29.20	25.57	24.81	31.45	49.95	49.38	46.60
C	7.75	16.38	8.24	13.71	10.10	14.65	28.47	24.44	24.38	32.76	54.22	43.81	39.38
D	7.75	18.58	8.53	13.12	10.61	14.25	29.64	24.73	24.31	32.75	53.29	43.93	38.46
E	7.75	19.07	8.83	13.99	10.48	15.26	29.07	23.50	23.13	32.77	49.71	42.29	41.98

Appendix C. Precipitation Root Mean Square Error Tables

This appendix contains the root mean square error (RMSE) data for 24 hr cumulative precipitation. Table 67 contains the precipitation RMSE for the January case, while Table 68 contains the precipitation RMSE for the May case.

All tables in this appendix have been standardized with units for the RMSE values listed in the title of the table. The date/time group is listed across the top row covering the period from 1200 UTC 16 January 1995 to 1200 UTC 19 January 1995 in 24 hour intervals for the January case and the period from 1200 UTC 5 May 1995 to 1200 UTC 9 May 1995 in 24 hour intervals for the May case. The model domain numbers are found along the left margin, or first column. The domains are listed in the following order: independently run 36 km resolution outer domain (1), Domain A using 12 km resolution two-way nesting (2A), Domain B using 12 km resolution two-way nesting (2B), Domain C using 12 km resolution two-way nesting (2C), Domain D using 12 km resolution two-way nesting (2D), Domain E using 12 km resolution two-way nesting (2E), Domain A using 12 km resolution one-way nesting (A), Domain B using 12 km resolution one-way nesting (B), Domain C using 12 km resolution one-way nesting (C), Domain D using 12 km resolution one-way nesting (D), and Domain E using 12 km resolution one-way nesting (E). See Chapter 3 of this document for the placement of Domains A through E.

It should be noted that the first verification point is the 36 hr forecast of the model since two model forecast fields are needed and verification was conducted at 1200 UTC (e.g., verification at 1200 UTC 16 January 1995 requires the 24 hr and 36 hr forecasts valid at 0000 and 1200 UTC 16 January 1995, respectively). In addition, the representativeness of the RMSE values for 1200 UTC 16 January 1995 should be considered suspicious since only a limited number of observations were available to verify the forecast at this time.

Table 67   24 Hour Precipitation (mm) RMSE (Case: January 1995)

		Date/Time (UTC)		
#	16/12	17/12	18/12	19/12
1	6.135	2.855	14.595	12.259
2A	9.744	3.623	14.540	14.113
2B	9.617	4.296	13.995	14.345
2C	8.854	4.232	13.603	14.564
2D	7.939	3.993	13.737	14.855
2E	10.251	4.324	13.860	14.667
A	5.790	2.533	15.836	9.871
B	6.148	2.197	15.831	9.951
C	5.367	2.568	15.807	9.830
D	4.211	2.586	15.835	9.652
E	10.846	2.544	15.837	9.698

Table 68   24 Hour Precipitation (mm) RMSE (Case: May 1995)

		Date/Time (UTC)			
#	5/12	6/12	7/12	8/12	9/12
1	2.156	24.492	23.870	31.861	30.465
2A	4.837	19.184	25.075	26.809	17.436
2B	4.602	19.093	21.183	29.929	21.943
2C	4.582	19.845	27.116	28.221	22.500
2D	4.971	21.810	18.098	26.354	24.983
2E	4.537	21.108	19.340	26.993	22.750
A	4.420	31.306	42.668	32.130	21.986
B	3.996	23.007	50.708	38.806	21.786
C	3.642	31.135	42.694	34.333	22.253
D	4.163	19.801	42.542	34.650	21.797
E	3.817	25.618	58.259	39.609	25.043

Bibliography

1. Alpert, P., S. O. Krichak T. N. Krishnamurti U. Stein and M. Tsidulko. "The Relative Roles of Lateral Boundaries, Initial Conditions, and Topography in Mesoscale Simulations of Lee Cyclogenesis," *Journal of Applied Meteorology*, *35*:1091–1099 (1996).

2. Atkins, N. T., R. M. Wakimoto and C. L. Ziegler. "Observations of the Finescale Structure of a Dryline During VORTEX 95," *Monthly Weather Review, 126*:525–550 (1998).

3. Baumhefner, D. P. and D. J. Perkey. "Evaluation of Lateral Boundary Errors in a Limited-Domain Model," *Tellus, 34*:409–428 (1982).

4. Daley, R. *Atmospheric Data Analysis*. Cambridge University Press, 1996. 457 pp.

5. Djuric, D. *Weather Analysis*. Prentice Hall, 1994. 304 pp.

6. Gill, A. E. *Atmosphere-Ocean Dynamics*. International Geophysics Series, Volume 30, Academic Press, 1982. 662 pp.

7. Haltiner, G. J. and R. T. Williams. *Numerical Prediction and Dynamic Meteorology*. Wiley, 1980. 477 pp.

8. Holton, J. R. *An Introduction to Dynamic Meteorology* (Third Edition). International Geophysics Series, Volume 48, Academic Press, 1992. 511 pp.

9. James, I. N. *Introduction to Circulating Atmospheres*. Cambridge University Press, 1995. 422 pp.

10. Kocin P. J., P. N. Schumacher, R. F. Morales Jr. and L. W. Uccellini. "Overview of the 12-14 March 1993 Superstorm," *Bulletin of the American Meteorological Society, 76*:165 –182 (1995).

11. Martin, J. E. "The Structure and Evolution of a Continental Winter Cyclone. Part I: Frontal Structure and the Occlusion Process," *Monthly Weather Review, 126*:303–328 (1998).

12. Mesoscale and Microscale Meteorology Division, National Center for Atmospheric Research. *PSU/NCAR Mesoscale Modeling System Tutorial Class Notes and User's Guide: MM5 Modeling System Version II*, June 1999.

13. Perkey, D. J. and C. W. Kreitzberg. "A Time-Depedent Lateral Boundary Scheme for Limited-Area Primitive Equation Models," *Monthly Weather Review, 104*:744–755 (1976).

14. Pielke, R. A. *Mesoscale Meteorological Modeling*. Academic Press, 1984. 612 pp.

15. Stein, U. and P. Alpert. "Factor Separation in Numerical Simulations," *Journal of the Atmospheric Sciences*, *50*:2107–2115 (1993).

16. Stoelinga, M. T. *A User's Guide to Read/Interpolate/Plot (RIP): A Program for Visualizing PSU/NCAR Mesoscale Model Output*. University of Washington, October 1997.

17. Treadon, R. E. and R. A. Petersen. "Domain Size Sensitivity Experiments Using the NMC Eta Model." *13th Conference on Weather Analysis and Forecasting*. 176–177. American Meteorological Society, August 1993.

18. Uccellini L. W., P. J. Kocin, R. S. Schneider P. M. Stokols and R. A. Dorr. "Forecasting the 12-14 March 1993 Superstorm," *Bulletin of the American Meteorological Society*, *76*:183–199 (1995).

19. Vukicevic, T. and R. M. Errico. "The Influence of Artificial and Physical Factors Upon Predictability Estimates Using a Complex Limited-Area Model," *Monthly Weather Review*, *118*:1460–1482 (1990).

20. Vukicevic, T. and J. Paegle. "The Influence of One-Way Interacting Lateral Boundary Conditions Upon Predictability of Flow in Bounded Numerical Models," *Monthly Weather Review*, *117*:340–350 (1989).

21. Warner, T. T., R. A. Peterson and R. E. Treadon. "A Tutorial on Lateral Boundary Conditions as a Basic and Potentially Serious Limitation to Regional Numerical Weather Prediction," *Bulletin of the American Meteorological Society*, *78*:2599–2617 (1997).

22. White, B. G., J. Paegle W. J. Steenburgh J. D. Horel R. T. Swanson L. K. Cook D. J. Onton and J. G. Miles. "Short-Term Forecast Validation of Six Models," *Weather and Forecasting*, *14*:84–108 (1999).

23. Wilks, D. S. *Statistical Methods in the Atmospheric Sciences*. Academic Press, 1995. 467 pp.

24. Williamson, D. L. and G. L. Browning. "Formulation of the Lateral Boundary Conditions for the NCAR Limited-Area Model," *Journal of Applied Meteorology*, *13*:8–16 (1974).

25. Zhang, D., H. Chang N. L. Seaman T. T. Warner and J. M. Fritsch. "A Two-Way Interactive Nesting Procedure with Variable Terrain Resolution," *Monthly Weather Review*, *114*:1330–1339 (1986).

26. Zou, X. and Y. H. Kou. "Rainfall Assimilation Through an Optimal Control of Initial and Boundary Conditions in a Limited-Area Mesoscale Model," *Monthly Weather Review*, *124*:2859–2882 (1996).

Vita

Captain Robert A. Stenger was born on 3 February 1965, in Hamilton, Ohio. He graduated from Brookville High School in May 1983. He enlisted in the United States Air Force in February 1989. After completing basic military training, he attended technical training at Sheppard AFB, Texas. Upon graduating as an Aircraft Maintenance Specialist in May 1989, he was assigned to 438 OMS, McGuire AFB, New Jersey.

At McGuire AFB, he served in the Isochronal Inspection Branch where he directly supported the evacuation of 55 aircraft during Hurricane Hugo, ensured C-141B aircraft were fully mission capable during Operation Just Cause, and was directly involved with the success of more than 700 mission sorties during Operation Desert Shield/Storm. He was awarded an Associates Degree in Aircraft Systems Maintenance Technology from the Community College of the Air Force and graduated Summa Cum Laude with an Associates Degree in Engineering from Burlington County Community College, New Jersey, in December 1992.

In July 1992, he was selected to attend Texas A&M University under the AFIT Airman Education and Commissioning Program. He graduated Summa Cum Laude with a Baccalaureate Degree in Meteorology and was assigned to 24 WS, Howard AFB, Republic of Panama in December 1994. He attended Officer Training School en route to Panama before serving as Wing Weather Officer, USSouthCom Staff Weather Officer, USSouthCom Theater Weather Flight Commander, and Latin America Weather Operations Center Team OIC. In February 1998, he was selected to attend the AFIT Graduate Meteorology Program. Upon graduation from AFIT in March 2000, he will be assigned to HQ ACC at Langley AFB, Virginia.

He was married in June 1988 to the former Christy E. Smith of Gainesville, Texas. They have three children: Robert, Jr., Christopher, and Rebecca.

Permanent address: 8057 Oxford Pike
Brookville, IN 47012

REPORT DOCUMENTATION PAGE

1. AGENCY USE ONLY *(Leave blank)*	2. REPORT DATE	3. REPORT TYPE AND DATES COVERED
	March 2000	Master's Thesis

4. TITLE AND SUBTITLE
Sensitivity Studies on a Limited Area Mesoscale Model:
An Examination of Lateral Boundary Placement,
Grid Resolution and Nesting Type

5. FUNDING NUMBERS

6. AUTHOR(S)
Robert A. Stenger, Captain, USAF

7. PERFORMING ORGANIZATION NAME(S) AND ADDRESS(ES)
Air Force Institute of Technology
Graduate School of Engineering and Management (AFIT/EN)
2950 P Street, Building 640
WPAFB OH 45433-7765

8. PERFORMING ORGANIZATION REPORT NUMBER

AFIT/GM/ENP/00M-13

9. SPONSORING/MONITORING AGENCY NAME(S) AND ADDRESS(ES)
HQ AFWA/DNX
ATTN: Robert T. Williams, Jr., Capt, USAF
106 Peacekeeper Drive Ste 2N3
Offutt AFB, NE 68113-4039   DSN 271-3320

10. SPONSORING/MONITORING AGENCY REPORT NUMBER

11. SUPPLEMENTARY NOTES
Advisor: Lt Col Michael K. Walters, ENP, DSN: 785-3636, ext.4681

12a. DISTRIBUTION AVAILABILITY STATEMENT
APPROVED FOR PUBLIC RELEASE; DISTRIBUTION UNLIMITED.

12b. DISTRIBUTION CODE

13. ABSTRACT *(Maximum 200 words)*
With the advances of computer technology in recent years, limited area mesoscale models are being used to produce operational forecasts on a broader scale worldwide than ever before. The past limitations of computational resources have caused previous research efforts to focus more on model physics, thus creating a gap in the number of sensitivity studies conducted on these models. This research is intended to bridge a gap in the apparent paucity of sensitivity studies on the limited area model (LAM). The Pennsylvania State University/National Center for Atmospheric Research Mesoscale Model 5 was utilized to conduct sensitivity studies on lateral boundary placement in regions of strong topography, grid resolution and nesting type. This research has resulted in three significant findings: (1) optimally placing the windward lateral boundary of a LAM with respect to the tallest peaks of a strong orography increases the model's forecast veracity; (2) the paradigm that finer grid resolutions will always produce better forecasts is flawed when there is an absence of strong ageostrophic motions in the troposphere; and (3) two-way nesting will generally produce a more accurate forecast than one-way nesting when significant ageostrophic motions are present in the troposphere.

14. SUBJECT TERMS
MM5, Sensitivity Studies, Numerical Weather Prediction, Mesoscale Modeling, Limited Area Model, Lateral Boundary Placement, Grid Resolution, Nesting Type

15. NUMBER OF PAGES
213

16. PRICE CODE

17. SECURITY CLASSIFICATION OF REPORT	18. SECURITY CLASSIFICATION OF THIS PAGE	19. SECURITY CLASSIFICATION OF ABSTRACT	20. LIMITATION OF ABSTRACT
UNCLASSIFIED	UNCLASSIFIED	UNCLASSIFIED	UL